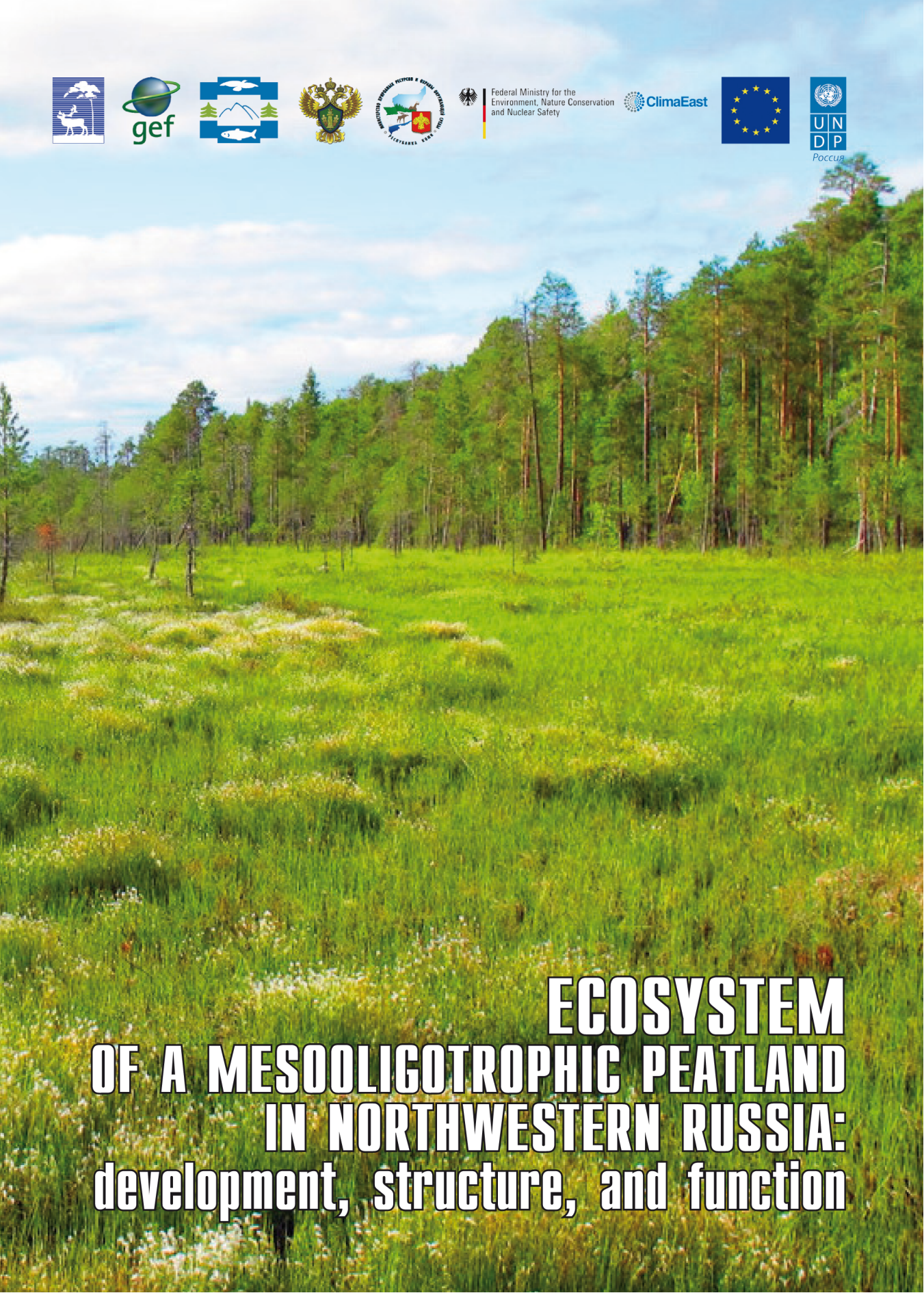
Federal Ministry for the
Environment, Nature Conservation
and Nuclear Safety
ClimaEast
UNDP
Россия
ECOSYSTEM
OF A MESOOLIGOTROPHIC PEATLAND
IN NORTHWESTERN RUSSIA:
development, structure, and function

ECOSYSTEM OF A MESOOLIGOTROPHIC PEATLAND IN NORTHWESTERN RUSSIA:

development, structure, and function

EDITED BY
S. Zagirova and J. Shneider

Syktyvkar 2016

УДК 574.5.556.56(470.1/2)

Ecosystem of a mesooligotrophic peatland in northwestern Russia: development, structure, and function. Syktyvkar. 2016. 172 p. (Komi Scientific Centre of the Ural Branch of the Russian Academy of Science)

The book provides data on a boreal mesoologotriphic peatland Medla-Pev-Nyur located in northwestern Russia. Research on the development of the peatland in Holocene and peat accumulation rates at different microforms are presented. Results of the studies on land cover and diversity of micromicetes in peat are reviewed. Another important topic of this book is turnover of greenhouse gases. We show results of carbon storage mapping and discuss CO_2 and CH_4 fluxes between peatland and atmosphere measured by different methods. Processes of methanogenesis and CH_4 oxidation in peat layer of different microforms in peatland Medla-Pev-Nyur are illuminated as well as diurnal and seasonal variations of energy and water balance of the peatland.

The book is addressed to professionals and students in the fields of biology, ecology and biogeochemistry.

Экосистема мезоолиготрофного болота на северо-западе России: эволюция, структура, функции. Сыктывкар, 2016. 172 с. (Коми научный центр УрО РАН).

В монографии представлены результаты исследований мезоолиготрофного болота Медла-Пэв-Нюр на северо-западе России. Приводятся данные о развитии болота в Голоцене и скорости накопления торфа в разных микроландшафтах. Содержится характеристика растительного покрова и разнообразия микромицетов в торфе. Обсуждаются результаты картирования запасов углерода и измерений обмена CO_2 и CH_4 между болотом и атмосферой, выполненные разными методами. Рассматриваются процессы метаногенеза и метаноокисления в слое торфа на разных участках болота, а также суточная и сезонная вариабельность показателей энергообмена в приземном слое атмосферы.

Книга предназначена для специалистов и студентов в области биологии, экологии и биогеохимии.

Reviewers
Doctor Evgeniya Golovatskaya
Doctor Andrey Sirin

Conservation and sustainable management of peatlands in Russia to minimize carbon emissions and help ecosystems to adapt to climate change.

Implemented under: UNDP/GEF project «Strengthening Protected Areas System of the Komi Republic to Conserve Virgine Forest Biodiversity in the Pechora River Headwaters Region» 00059042 in coopedration with Russian Academy of Sciences

UNDP partners with people at all levels of society to help build nations that can withstand crisis, and drive and sustain the kind of growth that improves the quality of life for everyone. On the ground in 177 countries and territories, we offer global perspective and local insight to help empower lives and build resilient nations. www.undp.org.

The GEF unites 182 countries in partnership with international institutions, nongovernmental organizations (NGOs), and the private sector to address global environmental issues while supporting national sustainable development initiatives. Today the GEF is the largest public funder of projects to improve the global environment. An independently operating financial organization, the GEF provides grants for projects related to biodiversity, climate change, international waters, land degradation, the ozone layer, and persistent organic pollutants. Since 1991, GEF has achieved a strong track record with developing countries and countries with economies in transition, providing $9.2 billion in grants and leveraging $40 billion in co-financing for over 2,700 projects in over 168 countries. www.thegef.org

ISBN 978-5-89606-562-3

CONTENTS

CONTRIBUTORS

Bärisch, Susanne
Greifswald Mire Center, Ellernholzstr. 1/3, 17489 Greifswald, Germany

Dorodnikov, Maxim
Department of Soil Science of Temperate Ecosystem, Faculty of Forest Sciences and Forest Ecology, Georg August University of Göttingen, Büsgenweg 2, D-37077 Göttingen, Germany

Forbrich, Inke
Institute of Botany and Landscape Ecology, Ernst Moritz Arndt University Greifswald, Soldmannstrasse 15, 17487 Greifswald, Germany; present affiliation at Marine Biological Laboratory, Ecosystem Centre, 7 MBL Rd., Woods Hole, USA

Gažovič, Michal
Institute of Botany and Landscape Ecology, Ernst Moritz Arndt University Greifswald, Soldmannstrasse 15, 17487 Greifswald, Germany; present affiliation at Department of Forest Ecology and Management, Swedish University of Agricultural Sciences, 901 83 Umee, Sweden

Goncharova, Nadejda
Institute of Biology, Komi Scientific Centre, Russian Academy of Sciences, Kommunisticheskaia ul. 28, 167982, Syktyvkar, Russia

Hugelius, Gustaf
Department of Physical Geography Stockholm University, S-10691 Stockholm, Sweden

Kanev, Vladimir
Institute of Biology, Komi Scientific Centre, Russian Academy of Sciences, Kommunisticheskaia ul. 28, 167982, Syktyvkar, Russia

Knoblauch, Christian
Institute of Soil Science, University of Hamburg, Allende-Platz 2, 20146 Hamburg, Germany

Kuhry, Peter
Department of Physical Geography, Stockholm University, S-10691 Stockholm, Sweden

Kutzbach, Lars
Institute of Soil Science, KlimaCampus, University of Hamburg, Allende-Platz 2, 20146 Hamburg, Germany

Miglovets, Mikhail
Institute of Biology, Komi Scientific Centre, Russian Academy of Sciences, Kommunisticheskaia ul. 28, 167982, Syktyvkar, Russia

Mikhailov, Oleg
Institute of Biology, Komi Scientific Centre, Russian Academy of Sciences, Kommunisticheskaia ul. 28, 167982, Syktyvkar, Russia

Kuusinen, Nea
Department of Forest Sciences, PO Box 27, 00014 University of Helsinki, Finland Pluchon, Nathalie Department of Forest Ecology and Management, Swedish University of Agricultural Sciences, SE-90183 Umea, Sweden

Runkle, Benjamin R.K.
Institute of Soil Science, Klima Campus, University of Hamburg, Allende-Platz 2, 20146 Hamburg, Germany

Schneider, Julia
Institute of Botany and Landscape Ecology, Ernst Moritz Arndt University Greifswald, Soldmannstrasse 15, 17487 Greifswald, Germany; present affiliation at Institute for Environmental Sciences, University of Koblenz-Landau, Fortstr. 7, 76829 Landau, Germany

Sivkov, Mikhail
Institute of Biology, Komi Scientific Centre, Russian Academy of Sciences, Kommunisticheskaia ul. 28, 167982, Syktyvkar, Russia

Sizonenko, Tatiana
Institute of Biology, Komi Scientific Centre, Russian Academy of Sciences, Kommunisticheskaia ul. 28, 167982, Syktyvkar, Russia

Susiluoto, Sanna
Department of Environmental Sciences, P.O. Box 27, 00014 University of Helsinki, Finland

Virtanen, Tarmo
Department of Environmental Sciences, P.O. Box 27, 00014 University of Helsinki, Finland

Wille, Christian
Institute of Soil Science, KlimaCampus, University of Hamburg, Allende-Platz 2, 20146 Hamburg, Germany

Wilmking, Martin
Institute of Botany and Landscape Ecology, Ernst Moritz Arndt University Greifswald, Soldmannstrasse 15, 17487 Greifswald, Germany

Wolf, Ulrike
Institute of Botany and Landscape Ecology, Ernst Moritz Arndt University Greifswald, Soldmannstrasse 15, 17487 Greifswald, Germany; present affiliation at Thünen Institute of Climate-Smart Agriculture, Bundesallee 50, 38116 Braunschweig, Germany

Wu, Jian
Institute of Applied Ecology, Chinese Academy of Sciences, 72 Wenhua Road, Shenyang, China

Zagirova, Svetlana
Institute of Biology, Komi Science Centre, Russian Academy of Sciences, Kommunisticheskaia ul. 28, 167982, Syktyvkar, Russia

PREFACE

Boreal peatland ecosystems cover 3% of the earth's land surface. Most of them are located in regions which were completely covered by glaciers 10-25 thousand years ago. In the rather short period since deglaciation peatlands have become widely established landscapes in northern hemisphere and contain now about 30 % of world's terrestrial soil carbon. Over the past two decades boreal peatlands have received considerable attention from researches in different countries, mainly due to ongoing climate change and its possible consequences for peatland ecosystem functions, including their abilities to regulate gas composition of the atmosphere. However, it remains uncertain how peatland ecosystem functions might change in a changing climate, demanding more complex research.

Peatlands occupy about 10 % of the territory of Komi Republic. Investigations of the peatlands begun in first half of XXth century and were caused by industrial and agricultural development of the region. Peatland's vegetation in the European North of Russia was studied by well known researches V.V. Tsinzerling, N.Ja. Katz, M.N. Nikonov, M.S. Boch, V.I. Vasilevich, T.K. Jurkovskaia. Today, in Komi Republic 110 bogs are protected natural areas and play an important role in preservation of the biological variety of the regional flora and fauna, stocks of carbon, and regulation of the hydrological conditions of northern rivers. At the same time, the ecosystem functions and the exchange of greenhouse gases and energy in the northern peatlands of Russia remain poorly studied. This book focuses on development, vegetation diversity and diversity of microorganisms, peat growth and microbial structure as well as carbon dioxide and methane exchange and variations of energy and water balance of the mesooligotrophic peatland Medla-Pev-Nyur which is located in middle taiga subzone in Komi Republic. The investigations were implemented by researches from the different countries in different years, including international projects CarboNorth (2006-2010) and UNDP-GEF (2008-2016).

Svetlana Zagirova and **Julia Schneider**

ПРЕДИСЛОВИЕ

Болотные экосистемы бореальной зоны занимают 3% поверхности суши. Большинство из них сформированы на территориях, которые 10-25 тыс. лет назад были полностью покрыты ледниками. За относительно короткий период времени после ледникового периода болота стали широко распространенными ландшафтами в северном полушарии, в которых сосредоточено около 30% запасов углерода почв. В последние два десятилетия изучению болот уделяют большое внимание во всем мире, и это связано, прежде всего, с изменением климата и возможными его последствиями для функционирования болотных экосистем, в том числе их способности регулировать газовый состав атмосферы. Однако в оценке экосистемных функций болот до сих пор остается много неопределенностей, требующих проведения комплексных исследований.

В Республике Коми торфяные болота занимают около 10% ее площади, их исследования были начаты в первой половине XX века в связи с необходимостью их промышленного и сельскохозяйственного освоения. В изучение разнообразия растительного покрова болотных систем на европейском Севере России значительный вклад внесли известные болотоведы В.В. Цинзерлинг, Н.Я. Кац, М.Н. Никонов, М.С. Боч, В.И. Василевич, Т.К. Юрковская. На сегодняшний день 110 болот в Республике Коми имеют статус особо охраняемых природных территорий, выполняющих важную роль в сохранении биологического разнообразия региональной флоры и фауны, запасов почвенного углерода, регулировании гидрологического режима северных рек. Вместе с тем, вопросы функционирования болотных экосистем, обмена веществ и энергии в них остаются слабо изученными в регионе. В представленной монографии обобщена информация об истории развития, разнообразии растительного покрова и почвенных микроорганизмов, скорости роста торфа, вариабельности потоков диоксида углерода и метана, энергообмена и водного обмена на мезоолиготрофном болоте Медла-Пэв-Нюр, расположенном в подзоне средней тайги на территории Республики Коми. Эти материалы были получены специалистами из разных стран в разные годы, в том числе в рамках выполнения международных проектов CarboNorth (2006-2010) и ПРООН/ГЭФ (2008-2016).

Светлана Загирова и **Юлия Шнайдер**

Chapter 1
PHYSICAL AND GEOGRAPHICAL CHARACTERISTICS OF THE STUDY AREA

The mesooligotrophic Medla-Pev-Nyur (Ust-Pojeg) peatland is common for middle taiga subzone (Fig. 1). It is located in the Syktyvdinsky region of the Komi Republic 1.4 km south-east of the Sludka village and 40 km north-west of the city of Syktyvkar (N 61°56′ E 50°13′). Its area is 2 790 ha with mean peat thickness of 1.4 m. The peatland occupies the second above-flood terrace with the Pozheg and Pychim Rivers as its water receivers (Peat Resources..., 2000).

Climate. The Medla-Pev-Nyur peatland belongs to the South-Western plain climatic region of the Komi Republic (The Atlas..., 1964). Mean annual temperature is +0.3...+1.0 °C. Mean temperature of the coldest year month (January) is −15...−16 and that of the warmest year month (July) +16...+17 °C. Snow cover forms approximately on October, 20, lasts for 165–175 days and melts on

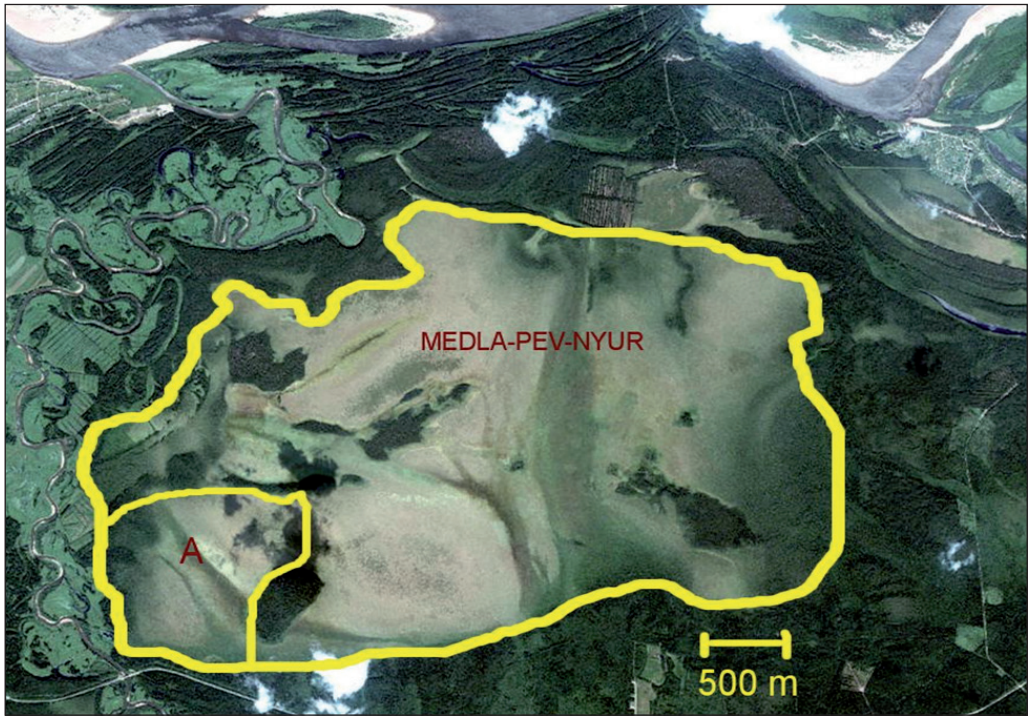

Fig. 1: The Medla-Pev-Nyur (Ust-Pojeg) peatland. A – study site. Satellite image (https://www.google.ru/maps/@61.9447616,50.283976,7891m/data=!3m1!1e3?hl).

May, 5. Mean snow cover height comprises about 60 cm. Frost-free period duration is 90-105 days. Vegetation period in the middle taiga zone lasts for about 158 days and ends in the II-III decades of September (Forests..., 1999). Active plant vegetation period includes 100-110 days. Mean annual sunshine duration is 1600 hours. Annual precipitation amount is 550-700 mm, among them 320-365 mm precipitate in warm period.

Air mass circulation plays a major role in climate formation at high latitudes. Within the period of 1850-2013, remarkable temperature fall in the Northern hemisphere was identified for 1875-1909 and 1946-1972 (Perevedentsev and Shantalinsky, 2014). By the authors, air temperature in subpolar regions rose by 2.38 °C for the last 37 years which is almost three times as more than that in the moderate climate zone. But since 2008, the climate warming tempo is gradually slowing down.

Air temperature and precipitation amount in the study area rose for the period of 1990-2012 (Fig. 2). In 1965-2012, mean annual temperature of atmospheric surface layer was higher by 0.4 °C and precipitation amount by 89 mm as compared with the first half of the former century. The differences were especially prominent in winter (Table 1). The sum of effective temperatures and number of days with positive air temperature also increased for the former one hundred years.

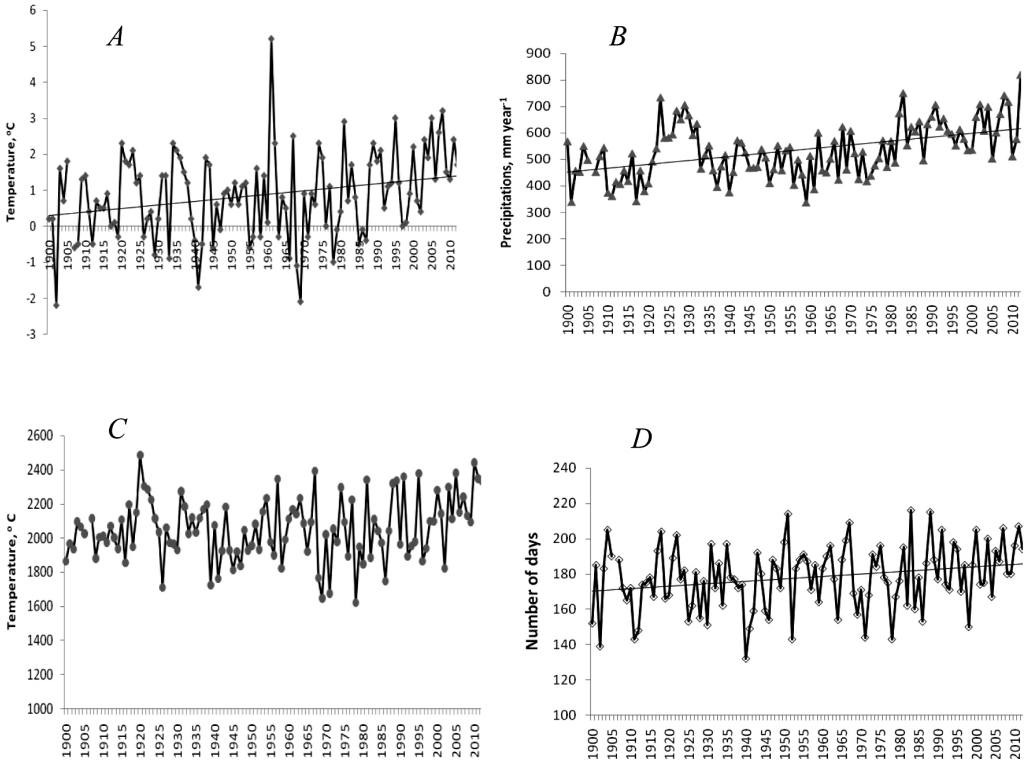

Fig. 2: Mean annual temperature (*A*), annual precipitation amount (*B*), sum of effective temperatures (*C*), and frost-free period duration (*D*) in Medla-Pev-Nyur region (by the Centre on Hydrometeorology and Environmental Monitoring of the Komi Republic for the Syktyvkar Meteorological Station, http://ib.komisc.ru/climat/index.php).

Table 1

Air temperature and precipitation amount dynamics for the period of 1900-2012 (by the Centre on Hydrometeorology and Environmental Monitoring of the Komi Republic for the Syktyvkar Meteorological Station, http://ib.komisc.ru/climat/index.php)

Parameter	1900-2012	1900-1964 (A)	1965-2012(B)
Mean annual temperature, °C	0.8	0.7	1.1
Mean summer temperature, °C	13.0	13.05	13.04
Mean winter temperature, °C	–13.7	–13.8	–13.5
Sum of effective temperatures (+ 5 °C and higher)	2056	2042	2074
Number of days with positive temperature	178	175	182
Annual precipitation amount, mm	534	497	586
Summer precipitation amount, mm	199	202	196
Winter precipitation amount, mm	78	64	97

Soils. The area belongs to the Vym-Vychegda okrug of typical podzols and peaty-podzolic-weakly gley illuvial-iron podzols (The Soil Atlas..., 2010). It lies northwards from the Vychegda River valley and is a weakly drained accumulative moraine plain. The most popular soil-forming rocks are two-layered deposits, thin sands, and sandy loams underlaid by moraine clay loams. There are water-ice and ancient-alluvial sandy plains along the Vychegda River and its right tributaries (the Vym River and the Vishera River). Upper peatlands are common for the Vym-Vychegda okrug. Peat stratigraphy in peatland Nedla-Pev-Nyur is given in Fig. 3.

Thick peat (240-245 cm) was identified on oligotrophic sites and poor peat (170-180 cm) - on mesotrophic and meso-eutrophic sites of the Medla-Pev-Nyur peatland. Peat thickness generally varied from 70 cm (forested peatland edge) to 245 cm (oligotrophic hummocks).

Oligotrophic hummock is remarkable through the deepest peat layer. Its lower horizons from 125 cm deep and before mineral part are transition-moor peat with decomposition degree of 30-40%. Upper horizon is raised magellanicum peat (Fig. 3) with low decomposition degree (5-15%). Oligotrophic hollow has a thick raised bog peat horizon (0-120 cm), transition-moor peat (120-180 cm). Peat decomposition degree varies with depth from 5 to 25% (5% each 20 cm), up to 30-35% at a 100-cm depth and remains so till mineral part.

Mesotrophic sedge-sphagnum hummock has its lower peat horizons composed of grassy and woody-grassy transition-moor peat dominated by cotton grass at a 70-150-cm depth. Raised bog peat is angustifolium peat. It is 0-70 cm thick which is less than raised bog peat thickness on oligotrophic sites.

Mesoeutrophic grassy-sphagnum swamp has the thinnest layer of raised bog peat (25 cm). This is related with running waters which wash out upper peat horizons. Peat decomposition degree is 15%. Transition-moor peat are 155 cm thick. All of them are grassy: woody-cotton grass peat at 25-100-cm depth, woody-grassy peat at 100-140 cm, and sedge-*Scheuchzeria* peat at 140-180 cm. Peat decomposition degree varies within 30-35%.

Anywhere, the deepest peat horizon is woody-*Scheuchzeria* peat which is gradually replaced by transition grassy-mossy and, finally, raised mossy peat. By the obtained data, peat formation developed by the following principle as forest-wet forest-mesooligotrophic peatland.

Stagnant waters are always highly acidic. The acidity varies during vegetation

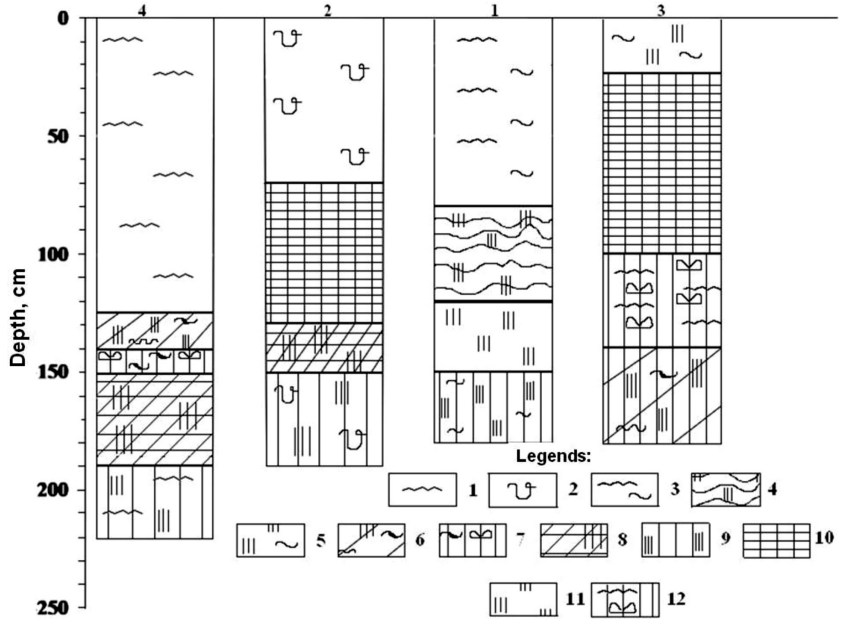

Fig. 3: Peat stratigraphy at the sites 1-4 (Miglovets, 2014). Peat types were identified by S.N. Tyuremnov et al. (1977) and R.N. Alekseeva (1988). Raised bog peat: 1 – magellanicum peat, 2 – angustifolium peat, 3 – sphagnum-swampy hollow, 4 – cotton grass-*Scheuchzeria*, 5 – *Scheuchzeria*-sphagnum. Transition moor: 6 – sedge-*Scheuchzeria*, 7 – woody-grassy-sphagnum, 8 – cotton grass-*Scheuchzeria*, 9 – woody-*Scheuchzeria*, 10 – woody-cotton grass, 11 – *Scheuchzeria*, 12 – woody-grassy. X-axis: 1 – oligotrophic hollow; 2 – mesotrophic dwarf shrub-sphagnum hummock, 3 – grassy-sphagnum running swamp, 4 – oligotrophic hummock.

period (Table 2). The *pH* water value at every study site increases in May-June and does not practically change afterwards. Low water acidity characterizes mesoeutrophic running swamp with the *pH* water value of 5.7 in summer. Swamp also has the highest content of water-dissolved organic carbon (Table 3).

This parameter visually rises in June for every study site. The discussed differences in content of water-dissolved organic carbon and water acidity value can be conditioned by water regime and qualitative (and quantitative) parameters of plant waste.

Vegetation. The study area is part of the European Taiga District, North-European Taiga Province, Kola-Pechora sub-Province (Vegetation..., 1980). Drained riverside slopes and interfluves are dominated by green-moss and

Table 2

Seasonal dynamics of pH water value at the study sites in 2011 year (Mikhailov, 2013)

Period	Oligotrophic		Mesotrophic		Mesoevtrophic	
	Min.	Max.	Min.	Max.	Min.	Max.
May	3.3	3.6	3.5	3.6	4	4.4
June	3.9	4.1	4.1	4.3	5.4	5.5
July	4.15	4.5	4.4	4.7	5.02	5.7
August	4.09	4.15	4.4	4.53	5.06	5.36
September	4.13	4.14	4.47	4.53	5.1	5.13

Table 3

Seasonal content dynamics of water-dissolved organic carbon (DOC) in 2011, mg l^{-1} (Mikhailov, 2013)

Date	Mesotrophic community	Oligotrophic community	Mesoeutrophic running swamp
25.05	22.71	28.98	36.13
27.05	27.70	32.08	37.20
Mean in May	25.20	30.53	36.67
02.06	32.49	34.29	53.87
9.06	30.15	40.13	50.28
16.06	32.61	54.49	45.28
Mean in June	31.75	42.97	49.81
01.07	26.32	30.76	37.25
06.07	26.28	28.53	37.84
12.07	28.25	29.02	36.64
29.07	18.92	27.76	36.73
Mean in July	24.94	29.02	37.12
04.08	26.26	30.25	39.17
10.08	23.56	29.22	36.70
19.08	25.20	29.10	38.38
26.08	25.90	27.73	37.75
01.09	29.20	26.65	37.52
Mean in August	26.02	28.59	37.91

green moss-long moss spruce forests of the III quality class with some fir trees, secondary birch forests, and by long moss-sphagnum and sphagnum spruce forests in depressions and on even watershed grounds. Weakly drained watersheds host poorly wet (long-moss blueberry and blackberry) spruce forests with some pine and birch trees. Drained terraces are dominated by (lichen and green-moss cranberry and blackberry) pine forests of the IV quality class and wet terraces – by long-moss pine forests of the V quality class. Above-flood terraces and surfaces of fluvioglacial plains are covered with wet pine forests. Meadows with alluvial soddy and soddy-gley soil types take about 20% of total floodplain area (The Atlas..., 1964; The Soil Atlas..., 2010). Vegetation of peatland Medla-Pev-Nyur will be characterised in Chapters 2 and 3.

References

Miglovets, M.N. 2014. Methane emission in plant communities of mesooligotrophic peatland in meddle taiga. (Unpublished doctoral dissertation). Institute of biology UrD RAS, Syktyvkar.

Mikhailov, O.A. 2013. Seasonal course of vertical CO_2 fluxes in boundary layer of mesooligotrophyc peatland in meddle taiga (Unpublished doctoral dissertation). Institute of biology UrD RAS, Syktyvkar.

Peat Resources of the Komi Republic. 2000. Syktyvkar.

Perevedentsev, Yu.P., and K.M. Shantalinsky. 2014. Assessment of the air temperature and wind direction changes in troposphere of the Northern hemisphere. *Meteorology and Hydrology*. 10: 19-31.

The Atlas of Komi ASSR. 1964. Moscow: Geodesy and cartography department of State geology committee USSR.

The Soil Atlas of the Komi Republic. 2010. Syktyvkar: Institute Biology.

Vegetation of European part of Russia. 1980. Leningrad: Nauka.

Chapter 2
LAND COVER OF THE MESOOLIGOTROPHIC PEATLAND MEDLA-PEV-NYUR

The studies of peatlands in the Komi Republic started in the first half of the 20th century due to industrial and agricultural development of this area. The study results were highlighted in fundamental works as «Peat fund of the Komi ASSR» (1958), «Peat deposits of the Komi ASSR» (1984), «Peat resources of the Komi Republic» (2000) and corresponding maps. They give qualitative and quantitative description of peat deposits but do not have information about flora and vegetation. The first data on peat vegetation cover in the European North-East of Russia were collected by V.V. Tsinzerling, N.Ya. Kats, M.N. Nikonov, M.S. Boch, V.I. Vasilevich, and T.K. Yurkovskaya. But information on peat flora and vegetation of the Komi Republic is still scarce as its area is hardly accessible and spacious (The knowledge..., 1997).

MATERIALS AND METHODS

Land cover of the peatland Medla-Pev-Nyur (Ust-Pojeg) was described using satellite images and aero-photo-images of different scales. They were interpreted by the air-ground method developed by E. Galkina (1953, 1964) with interpretation signs of E. Romanova (1961) and T. Savelyeva (1977). Interpretation signs were used for *in situ* organization of temporal sample plots. Plant communities on sample plots being 10×10 m^2 and 20×20 m^2 in size or within natural boundary were described by the common methods (Field geobotany, 1959; Shennikov, 1964; Oreshkin et al., 2004). Sample plots were organized in typical parts of phytocoenosis. In case of phytocenotic complexes, we described phytocoenosis separately by microrelief elements (Study methods..., 1991), measured height, length, and width of hummocks, ranges and their area of total sample plot in percent. Stagnant ground water level from moss cover surface was fixed. Rare and hardly identifiable plant species were collected and included into herbarium SYKO. Vascular plants were *in vitro* treated and identified according to «Flora of the North-East of the European USSR» (1974-1977). Nomenclature was given according to S. Cherepanov (1995).

RESULTS AND DISCUSSION

The Medla-Pev-Nyur peatland is a complex peatland system of several sites divided by forest ranges, islands, and flowing marshes (Fig. 1). Peat systems of this type are common in the middle taiga subzone, particularly in its north part. Diversity and specific conditions of water chemistry in peatland influence the species composition and diversity of plant communities.

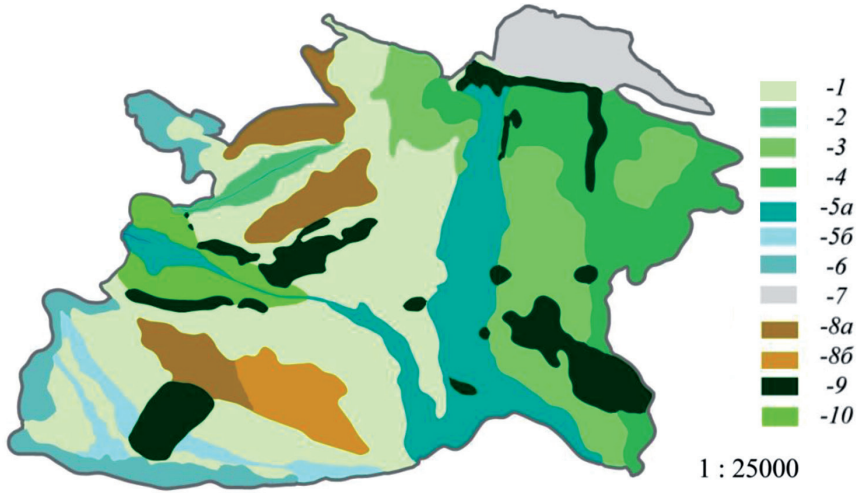

Fig. 1: Sketch-map of vegetation in the Medla-Pev-Nyur peatland. Numbers relate to the following communities as.

1 – mesooligotrophic community with dwarf shrubs and sphagnum mosses on hummocks, with grasses and sphagnum mosses in marshes; 2 – oligotrophic community with dwarf shrubs and sphagnum mosses on hummocks, with *Scheuchzeria palustris* L. and sphagnum mosses in depressions; 3 – mesotrophic community with dwarf shrubs, grasses, and sphagnum mosses; 4 – mesotrophic community with trees, grasses, and mosses; 5a – mesoeutrophic flowing marsh with grasses and hypnum mosses; 5b – mesotrophic marsh with grasses and mosses; 6 – marginal marsh with trees, different grasses, and mosses; 7 – drained peatland with pine trees, dwarf shrubs, and sphagnum mosses; 8a – oligotrophic community with pine trees, dwarf shrubs, cotton grass, and sphagnum mosses; 8b – oligotrophic community with dwarf shrubs, cotton grass, and sphagnum mosses; 9 – mineral forest island with trees, dwarf shrubs, and green mosses; 10 – mesotrophic community with sedge and sphagnum mosses.

The peatland hosts 120 plant species, including mosses. About 95 species of higher vascular plants from 60 genera and 37 families were found (*Annex*). Spore plants, namely ferns and horse-tails, include 4 species. Ferns are represented by one species, *i.e.* oak fern (*Gymnocarpium dryopteris*). Horse-tails are represented by three species, *i.e.* wood horse-tail (*Equisetum sylvaticum*), swamp horse-tail (*E. fluviatile*), and marsh horse-tail (*E. palustre*). Three species are gymnosperms which are conifers (*Picea obovata, Pinus sylvestris,* and *Juniperus communis*). The other species are metasperms, among which 27 are monocotyledons and 61 – dicotyledons.

Among vascular plants, the families of *Cyperaceae* (17), *Rosaceae* (9), *Ericaceae* (8), *Salicaceae* (5), *Orchidaceae* (5), *Asteraceae* (4), *Equisetaceae* (3), *Betulaceae* (3), *Ranunculaceae* (3), *Fabaceae* (3), and *Pyrolaceae* (3) include the majority of species. The other families include 1-2 species.

Among genera, Carex (14) is the most common genus. The second genus by species number is Salix (5). Also important are Equisetum (3), Rubus (4), Eriophorum (3), Vaccinium (3), and Dactylorhiza (3). The others include 1-2 species.

Plants of the Medla-Pev-Nyur peatland represent different geographical latitudes. Seventy five species are boreal. North latitude groups are only hypo-Arctic species (16). South species are as *Lathyrus vernus* and *Crepis paludosa)*.

Polyzonal species which habitats locate in several nature zones are horse-tails (*E. fluviatile* and *E. palustre*).

Longitude groups are dominated by species with broad Holarctic (48) and Eurasian (28) habitats. This situation is typical of the taiga zone of the Holarctic region. There are twelve species distributed in Europe and six species – in Asia.

Grasses are the principal living form. They count 70, *i.e.* more than a three-fourth of biomorphological flora composition. The majority of them are perennial grasses as *Carex aquatilis, Calla palustris, Drosera rotundifolia*, *Viola palustris*, *Cirsium oleraceum,* etc. Only *Melampyrum pratense* which is a semi-parasite of higher plants is an annual plant. Tree living forms include 25 species, among them 5 tree species (*Picea obovata, Pinus sylvestris, Alnus incana*, *Betula pubescens,* and *Sorbus aucuparia).* Shrubs and dwarf shrubs are 10 species each. Shrubs include *Juniperus communis, Salix aurita*, *Salix lapponum*, *Salix myrsinifolia*, *Salix phylicifolia, Salix myrtilloides*, *Betula nana*, *Ribes hispidulum*, *Rosa acicularis*, and *Lonicera pallasii.* Dwarf shrubs include *Empetrum hermaphroditum*, *Chamaedaphne calyculata*, *Ledum palustre*, *Andromeda polifolia, Oxycoccus microcarpus, Oxycoccus palustris, Vaccinium uliginosum*, *Vaccinium vitis-idaea*, *Vaccinium myrtillus*, and *Linnaea borealis.* Some dwarf shrubs are dominants in peatland and forest communities.

There are two plant species which are included into the Red Databook of the Komi Republic (2009), particularly *Dactylorhiza incarnata* and *Hammarbia paludosa* of the *Orchidaceae* family. They were classified as rare species (protection category 3). *Dactylorhiza maculata* of the *Orchidaceae* family needs regular control of population number and is now in the Annexes of the regional Red Book. Some peat plants are used in both common and folk medicine (*Ledum palustre*, *Oxycoccus palustris,* etc.) and some of them are food plants (cloudberry, blueberry, and cranberry).

Vegetation of the peatland includes ecologically different habitats as oligotrophic, mesoeutrophic transitional sites, edge minerotrophic wetlands, forest islands, etc. There are homogenous, mosaic, and complex sites which largely differ by nutrition and moisture conditions and plant communities.

Upland massifs and oligotrophic sites are essential by area. Upland massifs have a low-arched surface, a peak which is not always well expressed and moved to the periphery, and a gentle and more or less wet slope. Vegetation communities change from the centre (peak) of peatland to its edges and are related to the microforms. Peat peak has a hummocky or large-hummocky surface and a homogenous vegetation cover dominated by pine-dwarf shrub-sphagnum and pine-dwarf shrub-cloudberry-sphagnum communities. The centre of peatland counts no or single trees which are normally separate pines on microelevations. They are 0.3-5 m high or 2-3 m on average. Dwarf shrubs are dominated by such typical peat representatives as *Chamaedaphne calyculata, Ledum palustre, Andromeda polifolia*, *Vaccinium uliginosum,* and *Rubus chamaemorus* with total cover of 40-75%. The layer of grasses and dwarf shrubs is also composed of *Drosera rotundifolia, Oxycoccus palustris, O. microcarpus, Carex pauciflora,* and *Eriophorum vaginatum.* Ground cover is dominated by *Sphagnum fuscum* (70-100%) with some representatives of *Sphagnum magellanicum, S. angustifolium, S. russowii, Polytrichum strictum,* and *Pleurozium schreberi* (1-10%). Inter-hummocky depressions take 10-15% of total peat area and host dwarf shrub-cotton grass-sphagnum communities. Their floristic composition is similar to the previously described one but co-dominants are *Chamaedaphne calyculata, Andromeda poli-*

folia, and *Eriophorum vaginatum* (30-50%). *Oxycoccus palustris* and sometimes *Carex pauciflora* increase in number. Moss cover is mosaic and consists of several sphagnum species as *Sphagnum magellanicum, S. angustifolium,* and *S. russowii.*

The slope has hummocks (hillocks) and swampy hollows in microrelief. With distance from peat peak, it becomes less expressed and gradually replaced by hummocks without hollows, hillocks-and-swamps or just swamps. Vegetation cover forms a complex. Microrelief elevations are dominated by the previously mentioned (pine)-dwarf shrub-sphagnum and (pine)-dwarf shrub-cloudberry-sphagnum communities. The polydominant layer of grasses and dwarf shrubs is dominated by peat dwarf shrubs and cloudberry whereas ground cover – by *Sphagnum fuscum*. Microrelief depressions take 20-60% of slope area. They are often wet. Water level is –10...+2 cm from moss cover surface. Swampy hollows host *Scheuchzeria palustris*-sphagnum and swamps – *Scheuchzeria palustris*-sphagnum, sedge-sphagnum, and cotton grass-sphagnum phytocenoses. These communities count few species which form a scarce layer of grasses and dwarf shrubs. Dominating is one of the following species as *Scheuchzeria palustris, Eriophorum vaginatum,* and *Carex limosa.* In depressions there are single *Drosera anglica, D. rotundifolia, Oxycoccus palustris,* and *Andromeda polifolia.* Ground cover is usually continuous and consists of *Sphagnum balticum,* seldom of *S. jensenii* and *S. lindbergii*. In swampy hollows of the central peat part, ground cover is sometimes degraded with sphagnum mosses replaced by liverworts and green mosses (*Warnstorfia*). The slope, especially its periphery, visualizes transitional microrelief elements as small swampy hollows and inter-hillock depressions, low ranges and hillocks, etc. Vegetation cover on such elements is also transitional.

The last area hosts oligotrophic *Scheuchzeria palustris*-sphagnum, sedge-sphagnum, cotton grass-sphagnum and mesotrophic bog bean-sphagnum, sedge-sphagnum phytocenoses. The layer of grasses and dwarf shrubs is dominated by *Scheuchzeria palustris, Carex limosa*, *Eriophorum vaginatum, Menyanthes trifoliata,* and *Carex rostrata*. Species abundance of dominants depends on ecological conditions, first of all on bog water level, and varies within 5-40% for *Scheuchzeria palustris, Eriophorum vaginatum,* and *Carex limosa* and 20-80% for *Menyanthes trifoliate* and *Carex rostrata.* These species often grow together but only one of them attains high abundance values. Swamp additionally includes *Oxycoccus palustris, Andromeda polifolia, Chamaedaphne calyculata, Drosera rotundifolia,* and *Eriophorum polystachion.* Ground cover is continuous and consists of *Sphagnum balticum* or *S. fallax* (90-100%). There are some representatives of *Sphagnum angustifolium, S. magellanicum, S. papillosum*, and the *Warnstorfia* genus.

Transitional swamps and streams which flow out of peatland host mesoeutrophic dwarf-shrub-grassy-moss and grassy-moss communities. They are dominated by plants which prefer mineral-rich water as *Equisetum fluviatile, Menyanthes trifoliata, Comarum palustre, Eriophorum gracile*, *Carex chordorrhiza*, *C. paupercula*, *Pedicularis palustris, Utricularia intermedia, etc.* Mosses are *Sphagnum riparium, S. subsecundum, S. fallax,* species of the *Warnstorfia* and *Calliergon* genera, etc. The majority of them can be dominants or co-dominants in certain conditions (cover of 10-30%).

At peat edges and in narrow necks of land between forest islands, forest layer is formed of *Pinus sylvestris* with some *Picea obovata* and *Betula pubescens.* Crown density makes 0.2-0.3, tree height – up to 10 m. Eutrophic swamps with enough mineral nutrients host equally *Pinus sylvestris, Picea obovata,* and *Betula pubescens.* Trees form a scarce and low (4-6 m) layer. They are often sup-

pressed, especially spruce trees. There are many dead standing trees. Microrelief is hummocky (hillocky), hillocky-swampy, and hillocky with sink holes. Elevations take 5-70% of total area and are covered with polydominant dwarf shrub-sphagnum communities which include not only peat but also some forest species as *Carex globularis, Vaccinium vitis-idaea, V. myrtillus, Maianthemum bifolium,* etc. Microrelief elevations are dominated by *Sphagnum fuscum* (80-100%) or a group of mosses (*Sphagnum magellanicum, S. Angustifolium,* and *S. fuscum* – 20-50%). Inter-hillock depressions and sink holes have a mosaic cover with dwarf shrub-sedge-sphagnum, sedge-sphagnum, and cotton grass-sphagnum phytocenoses. Edges are dominated by *Carex rostrata* and *C. lasiocarpa* in layer of grasses and dwarf shrubs and by *Sphagnum fallax* in ground cover. Co-dominants are ericoid dwarf shrubs (*Chamaedaphne calyculata, Andromeda polifolia*, *Oxycoccus palustris*) and *Betula nana.* Thus, the Medla-Pev-Nyur peatland is a complex and natural system with high species and plant community diversity.

References

Cherepanov, S.K. Vascular plants of Russia and neighboring countries (within the former USSR).1995. St.Petersburg: Mir i semia .

Field Geobotany. V. 1. 1959. Moscow-Leningrad: Nauka.

Flora of the North-East of the European USSR. V. 1-4. 1974-1977. Leningrad: Nauka.

Galkina, E.A. 1953. Usage of aerial photographic survey in telmathology. *Botan. zhurn*. 38(6): 893-901.

Galkina, E.A. 1964. The application methods of aerial photographic images for classification and mapping of peatlands. In *Peatlands and Wetlands of Karelia*. 5-24. Petrozavodsk: Karel'skoe knignoe izdatel'stvo.

Oreshkin, D.G., Mirin D.M., Matveev I.V. 2004. Field practical course on geobotany: For advanced undergraduate students. St.Petersburg: St.Petersburg state university.

Peat Deposits of the Komi ASSR. 1984. Moscow: Torfogeologiya

Peat Resources of the Komi Republic. 2000. Syktyvkar.

Romanova, E.A. 1961. Geobotanical principles for hydrological study of upland peatlands. 244 p. Leningrad: Gidrometeoizdat.

Savelyeva, T.S. 1977. About interpretation signs of peatlands. *Tr. GII. Vopr. Gidrologii bolot*. L., Issue 236: 12-27.

Shennikov A.P. Introduction into Geobotany. 1964. 412 p. Leningrad: Leningrad state university.

The Knowledge Status on Natural Resources of the Komi Republic. 1997. Syktyvkar: Komi scientific centre UrD RAS.

The Peat Fund of the Komi ASSR. 1958. Moscow: Peatgeology.

The Red Databook of the Komi Republic. 2009. Syktyvkar: Institute Biology Komi scientific centre UrD RAS.

The Study Methods of Taiga Peatlands. 1991. Leningrad: Nauka.

Chapter 3
HIGH RESOLUTION LAND COVER AND VEGETATION CARBON STORAGE MAPPING IN FOREST AND PEATLAND ECOSYSTEMS IN MEDLA-PEV-NYUR REGION

When studies on global and regional carbon stocks and circulation are conducted, spatially detailed information about carbon storages is needed. Boreal forests and peatlands form one of the most extensive biomes in the world, and about half of the boreal biome area is located in Russia including a significant carbon stock even in the global scale (FAO, 2001; Houghton et al., 2007; Yu, 2011). Different estimates of Russian forests' carbon stock and its spatial distribution have been published, but the spatial resolution of the studies has been coarse, in most casesthe estimates are produced by forest enterprises or administrative units. Furthermore, the errors in forest inventory data are uncertain (Houghton et al., 2007). In addition to forests, also other ecosystems (treeless peatlands, agricultural areas) include some amount of carbon, but data on their vegetation biomass is sparse. Spatial distribution of the carbon stocks in vegetation varies in landscape due to management, natural disturbances, and micro-environmental factors (Houghton, 2005; Hugelius et al., 2011).

Our work is part of the EU-funded CARBO-North (Quantifying the carbon budget in Northern Russia: past, present and future) research-project, in which our aim was to produce land cover classifications and to estimate the biomass and carbon storage of the vegetation in different spatial resolutions to be used in other studies of the project. In this study we present the living above ground biomass (AGB) in a typical taiga forest and peatland dominated landscape in the Medla-Pev-Nyur region. The estimates are based on field measurements and satellite image classifications.

MATERIALS AND METHODS

Study area

The field data were collected near Sludka (61.57°N, 50.10°E) and Laly (62.16°N, 50.40°E) villages located near Medla-Pev-Nyur-peatland complex. The study area belongs to the middle taiga zone, which is dominated by coniferous forests (Martynenko and Degteva 2004). Some examples of the typical land cover types are presented in Figure 1.

Field plot measurements

The data were collected in July-August 2008 from 186 systematic sample plots aligned on eight transects each 600-1000 m long. By visual interpretation of satellite images, transects were established to cover all main vegetation types present in the study area. Sample plots were located at 100 intervals along the transects (middle plots) and two plots (side plots) were placed orthogonally to the transects (90°) at 15 m from each middle plot.

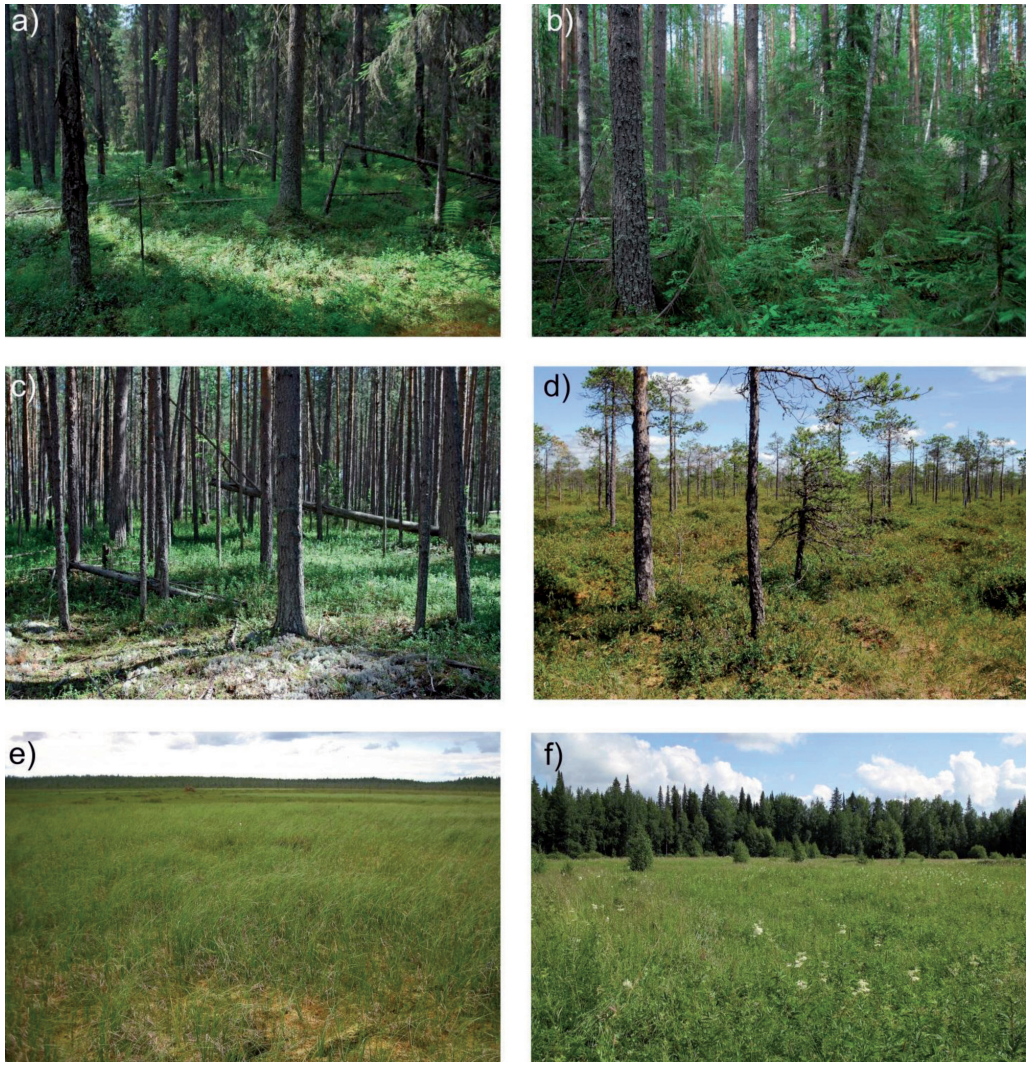

Fig. 1: Some examples of the land cover types in the Medla-Pev-Nyur region. a) spruce forest, b) mixed forest, c) pine forest, d) pine bog, e) fen and f) meadow.

Trees were measured from circular and angle count (relascope) sample plots on the middle plots. On the side plots, only angle count plots were measured. On the circular sample plots dbh (diameter at 1.3 m height) of all the trees that were inside a radius of 5.64 m were measured (tally trees). Only trees with dbh over 1 cm were included. Additionally, one or two sample trees were selected from each tree species. From these, height and diameter at 6 m height (if the tree was taller than 7 meters) were measured. Median diameter tree and dominant tree of each species were selected for sample trees. If there was only one age-class of some species represented, only the median tree was measured. Age was measured by taking a core sample from the dominant tree of the dominant species from every

middle plot. Angle count measurements included basal area estimation of each tree species and height and dbh measurements of the median tree of every tree species. On every sample plot also the total and satellite coverage of trees and the functional groups of understory species were estimated. The total amount of middle plots and side plots was 62 and 124, respectively.

For the estimation of the biomass of field and bottom layer vegetation, the coverage of all vegetation by functional groups (mosses, lichens, grasses, dwarf shrubs, herbs, willows, dwarf birch and other bushes) was estimated using three vegetation sample squares (30×30 cm) on every sample plot. Squares were placed 1 m northwest, northeast and south from the centre of each plot. From the square situated south, all vegetation was collected into paper bags for each functional group. The samples were dried and weighed at the Institute of Biology in Syktyvkar.

In addition to sample plots, the vegetation and land cover types were described from 180 ground truth points, which were selected randomly before field work. The minimum distance between ground truth points was 100 meters. They were used as the reference data to test the accuracy of the satellite image classifications.

Volume of growing stock estimation

Growing stock on the circular sample plots was defined by first calculating the stem volumes of the sample trees with existing functions. For pine (*Pinus sylvestris* L.), spruce (*Picea abies* ssp. *Obovata* (Ledeb.) Domin) and birch (*Betula pendula* Roth. and *B. pubescens* Ehrh.), functions of Laasasenaho (1982) were used, and for other species (aspen, *Populu tremula* L., alder, *Alnus incana* L. Moench, fir, *Abies sibirica* L. and goat willow, *Salix caprea* L.), stem volumes were estimated using different functions presented by Zianis et al. (2005). The volumes of tally trees on the circular sample plots were next estimated employing mixed models (Lappi et al., 2006) developed using the sample trees. Depending on the species, the independent variables in the models predicting the logarithmic volume were: logarithmic dbh, dbh, growth position index and/or site type. After calculation of the volumes per hectare in the circular sample plots, the growing stock of the angle count plots was modeled based on species specific dependencies of volume on basal area and mean height on the circular sample plots. Equations of the used models are available from authors on request.

Tree above ground biomass estimation

Above ground tree biomass (AGB) on the sample plots was calculated from the volumes of growing stock using four different methods. Two of the methods were based on Russian, (Alexeyev and Birdsey, 1998; Shvidenko et al., 1998; Shepashenko et al., 1998), and two on Nordic, (Kauppi et al., 1995; Lehtonen, 2005) studies. The mean values of the four different biomass estimates calculated for each sample plotwere used as the final results.

Satellite image classifications

Thesatellite images used were two consecutive Landsat 7 ETM+ images, acquired on 18.6.2001, path 173, rows 16 and 17. Radiometrically corrected images were derived from Global Land Cover Facility (GLCF) -service and they were georeferenced to the same projection as the sample plots (UTM 38N) and resampled to a spatial resolution of 30 m. In addition, we used one QuickBird

image acquired on 8.7.2007. The image covered 70 km^2 in the Sludka/Medla-Pev-Nyur region and was in 2.4 m spatial resolution (QuickBird © 2007, DigitalGlobe; Distributed by Eurimage/Pöyry).

The classification of the QuickBird satellite images was performed by object-based, multiple-level segmentation usinge Cognition-software. Four channels were used in the classification procedure (blue, green, red and near infrared, 2.4 m pixel sized multispectral image).The procedure is explained in more detail Virtanen and Ek (2014). A supervised classification of the Landsat images was done using a land cover classification of the Quickbird image as reference data. Using Definiens Professional 5.0 software, all the Landsat pixels that were totally covered by just one class according to the Quickbird classification were chosen. These Landsat pixels were classified according to the Quickbird classification and the classes were merged so that all adjacent pixels belonging to the same class were merged together. From each class, 20 of these merged areas were randomly chosen using ArcGIS 9.3 software. Using these areas, spectral signatures for each class were created using Erdas Imagine 9.0 software. Fuzzy convolution was applied to the final classification using a 3×3 window and a 0.12 neighborhood weight factor in order to remove the isolated miss-classified pixels. Classification accuracy was evaluated using field collected ground truth points.

Regional biomass and carbon estimates

Upscaling of the above ground biomass using satellite image classifications was done by assigning each pixel of each vegetated class with the average AGB of the sample plots belonging to the class in question. The AGB values were converted to carbon stock by multiplying by 0.5. Based on literature review, this is the most commonly used conversion method.There were some clouds in the QuickBird image (3.5% of image area). This cloud covered area was masked as no data in both classifications. The area used in the analyses was thus 66.8 km^2.

RESULTS

Volume of growing stock

Average growing stock (m^3/ha) and standard deviation, minimum and maximum of the growing stock on all forested land cover types based on field plot measurements are shown in Table 1. The RMSE of the models used to predict stem volumes of the tally trees varied between 29 and 54 dm^3 depending on the tree species. The RMSE of the models predicting the growing stock on angle count plots varied between 3 and 14 m^3/ha. For consistency, the growing stock estimates produced using the angle count measurements and modeling were used also for the middle plots in the AGB estimation.

Tree above ground biomass on sample plots

Of the four different biomass estimation methods tested, the methods presented by Lehtonen (2005) and Shvidenko et al. (1998) produced the highest AGB estimates (10.7% and 7.2% higher than the mean of all four methods), whereas the method described in Kauppi et al., (1995) and Alexeyev and Birdsey (1998) gave smaller AGB values (6.1% and 11.8% lower than mean of all four methods). The average STD of the AGB calculated with different methods was 0.97 kg/m^2, which accounted for 12.4 % of the average AGB on the sample plots. The mean AGBs in kg/m^{2}on each forested land covertype are presented in Table 1.

Table 1

The average volume of growing stock (m^3/ha) and standard deviation, minimum and maximum of the volume of growing stock on forested land cover types as well as the average tree (AGB) (kg/m^2) and number of plots per land cover type

Land cover type	Growing stock m^3/ha	STD	Min.	Max.	Tree ABG biomass kg/m^2	N
Spruce forest	218.7	79.1	27.7	366.8	12.9	21
Pine forest	265.5	73.0	173.0	429.3	13.8	17
Deciduous forest	227.0	68.1	74.1	307.4	13.5	16
Mixed forest	188.3	70.5	55.1	363.3	10.9	51
Pine lichen forest	117.3	34.9	68.9	184.5	6.0	12
Forested peatland	72.6	34.0	27.3	151.5	4.4	12
Pine bog/fen	11.9	17.4	0.43	58.0	0.65	22

Field and bottom layer above ground biomass

The AGBs of field and bottom layer vegetation were calculated from the dried samples to get the AGB in kg/m^2 for each functional group on each sample plot (Table 2). In the forested sites, field and bottom layers presented approximately 2% of the total above ground biomass, while in the peatlands the field and bottom layer AGB was 2-3 times higher than that of the forested sites.

Table 2

Average AGB kg/m^2 of field and bottom layer functional groups on different land cover types

Land cover type (N)	Above ground biomass kg/m^2							
	Dwarf shrubs	Herbs	Grasses	Mosses	Dwarf birch	Lichens	Other bush	Sum
Spruce forest (21)	0.044	0.013	0.003	0.078	0.000	0.000	0.064	0.201
Pine forest (17)	0.054	0.007	0.003	0.044	0.000	0.000	0.011	0.118
Deciduous forest (16)	0.041	0.022	0.005	0.020	0.000	0.000	0.005	0.092
Mixed forest (51)	0.043	0.010	0.005	0.043	0.000	0.002	0.013	0.116
Pine lichen forest (12)	0.023	0.000	0.000	0.021	0.000	0.258	0.000	0.302
Forested peatland (12)	0.060	0.023	0.030	0.079	0.000	0.000	0.026	0.218
Pine fen (17)	0.068	0.026	0.048	0.148	0.031	0.000	0.002	0.322
Pine bog (5)	0.117	0.021	0.017	0.156	0.001	0.000	0.000	0.312
Fen (14)	0.061	0.006	0.037	0.179	0.006	0.000	0.000	0.288
Bog (15)	0.092	0.000	0.012	0.332	0.003	0.000	0.000	0.439
Meadow (6)	0.000	0.185	0.095	0.006	0.000	0.000	0.030	0.317

Satellite image classifications and their accuracy.

The classification criteria for the Landsat and QuickBird based classifications as well as thecoverage of the land cover typesinthe Medla-Pev-Nyur region (Fig. 2) are presented in Table 3. In the Landsat image classification the kappa value of the classification was 0.53 and 62% of the reference points were correctly classified. Pine forests and forest cuttings had the weakest classification accuracy, while bogs, meadows and pine lichen forests were classified most accurately. The kappa statistics were greatly improved if vegetation was divided into larger groups (forest, forested peatland, meadow, bog, fen and bare land), the kappa value being 0.72 and 86% of the ground reference points correctly classified. However, in the presented biomass calculations the more detailed classification was used. In the Quickbird image classification, the kappa value for the classification was

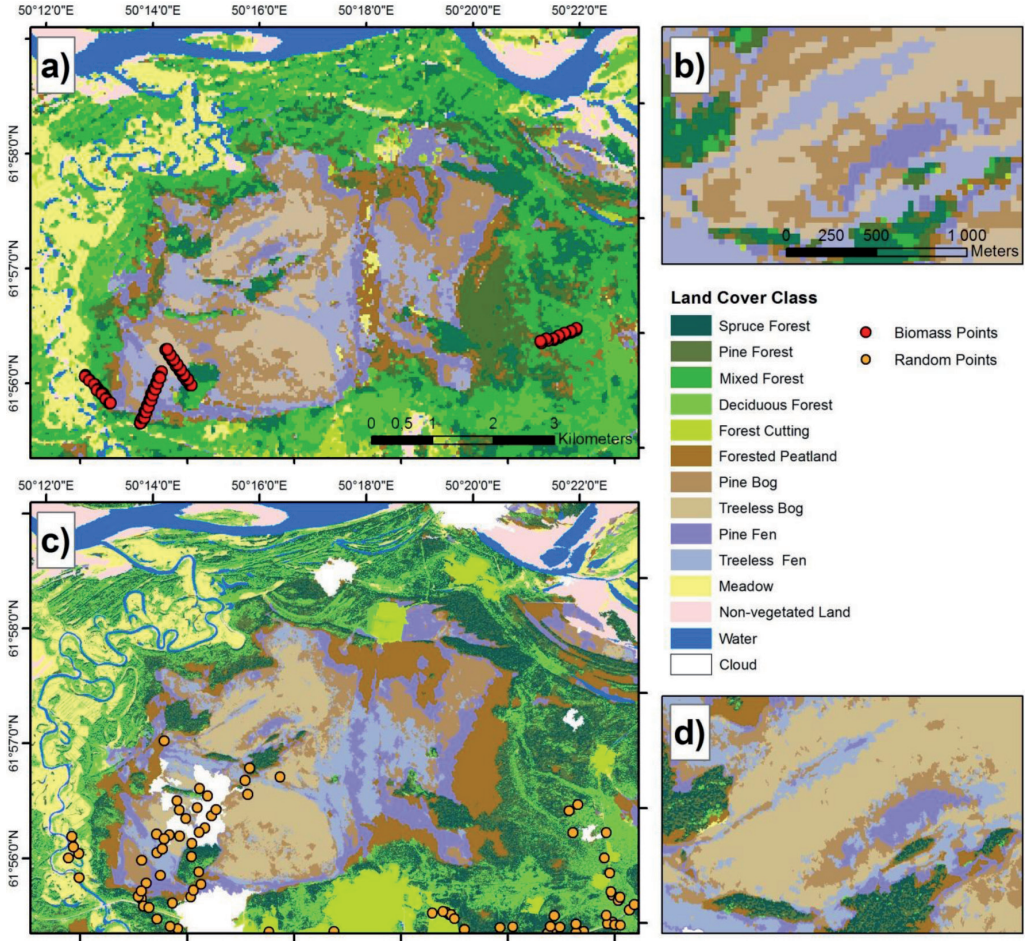

Fig. 2: Land cover classification maps for Medla-Pev-Nyur region. a) Land cover classification of the Landsat image (30 m pixel size), b) Landsat classification zoomed in too see the pixel size, c) Land cover classification of the QuickBird image (2.4 m pixel size), d) QuickBird classification zoomed to same extent as Landsat classification in b).

0.75 and 76% of the reference points were correctly classified. Spruce forests, bogs and meadows were classified by highest accuracy. Overall, the forest cover in the Landsat image classification was 53.5%, and in the Quickbird based image classification 55.3%.

Regional biomass and carbon estimates

Mean carbon stocks for each land cover type in the Medla-Pev-Nyur region are presented in Table 3. Carbon stock in the above ground biomass was highest in closed forests (4.5-6.8 kg/m^2), lower in peatlands where trees are found (0.5-2.3 kg/m^2), and lowest in treeless land cover types (0.1-0.2 kg/m^2). Mean carbon stock in AGB in the Medla-Pev-Nyur region estimated from both Landsat and QuickBird classifications was 2.92 kg/m^2.

Table 3

The coverage of land cover classes in Medla-Pev-Nyur study site based on QuickBird and Landsat image classifications, and estimated mean carbon (C) storage on each land cover type

Land cover type	Class description	Coverage, Landsat/ %	Coverage, QuickBird/ %	Mean C stock/kg/m^2
Spruce forest	>75% of wood volume consist of spruce	6.97	14.09	6.55
Pine forest	>75% of wood volume consist of pine	7.30	13.58	4.53
Pine lichen forest	Pine (>75% of volume), field layer dominated by lichens	1)	1)	1)
Deciduous forest	>75% of wood volume consist of deciduous trees	10.43	15.57	6.80
Mixed forest	Neither spruce, pine or deciduous trees make up >75%	21.41	2)	5.51
Forest cutting	Forest younger than 30 years, includes some fire areas3)	1.94	4.07	0.81
Forested peatland	Peatland with growing stock >50 m^3/ha	5.48	7.99	2.32
Pine fen	Minerotrophic peatland with growing stock < 50 m^3/ha	6.34	7.23	0.49
Pine bog	Ombrotrophic peatland with growing stock < 50 m^3/ha	7.63	5.72	0.48
Fen	Treeless minerotrophic peatland, sedge dominated	6.88	5.89	0.14
Bog	Treeless ombrptrophic peatland, shrub dominated	4.87	6.55	0.22
Meadow	Open area dominated by meadow vegetation	10.55	9.31	0.16
Non-vegetated area	Bare land area, sand, infrastructure	4.05	2.95	0.00
Water	Lake, river	6.24	5.22	0.00

1) Lichen dominated and other pine forests are combined and presented under «Pine forest», as they were not classified separately in land cover classifications. C-stock values area weighted by the proportion they were observed in the field data.

2) In higher resolution QuickBird-classification separate class for mixed forest was not created, and all forested areas were classified to some individual species type.

3) We had no field plots in recently logged or burned forests. These values were estimated based on our knowledge of typical mature stands in the region, and knowledge of forest growth in this kind of environment.

DISCUSSION

Our satellite image classifications were reasonably accurate when tested against field verification plots. Generally, the Landsat and QuickBird based classifications matched relatively well, although the QuickBird based classification included much more information about the heterogeneity of the landscape structure, which can have some important consequences, for example when studying biodiversity and biogeochemical processes in the landscape (Turner, 1989; Hugelius et al., 2011; Virtanen and Ek, 2014). The accuracy values based on agreement statistics in the QuickBird classification correspond to those typically achieved in corresponding land cover classifications (Wilkinson, 2005; Foody, 2008). The accuracy of Landsat classification was not as good when all the classes used in the Quick Bird classification were separated, but when some of these classes were combined together, then accuracy considerably improved.

The classification method was selected for the regional AGB estimation as it was considered robust enough considering the limited number of field plots measured. Another possibility would have been to apply regression models predicting the AGB by band digital numbers and vegetation indices. The non-parametric k-NN method (e.g. Tomppo et al., 2008) would have required a larger number of field plots than was available here. Naturally, erroneous distribution of field plots in e.g. different forest maturity classes within a forest class would cause error to our carbon estimates produced using the classification method.

Alekseyev and Birdsey (1998) reported the average carbon stock in vegetation in Komi Republic to be 3.6 kg/m^2 in the year 1990. Shvidenko et al. (1998) mention the average vegetation biomass in northern European Russia in 1993 to be 8.87 kg/m^2 (4.43 kg/m^2 carbon) of which 18.8 % is in roots. Lakida et al. (1996) report an average vegetation biomass value of 9.32 kg/m^2 (4.66 kg/m^2 carbon) for whole European Russia. However, all studies mentioned above are based on the Russian forest inventory data, although partly from different years, so the main variation in results is derived from different biomass calculation methods.

Bobkova and Galenko (2001) have conducted vegetation biomass studies in Komi Republic independent of the Russian forest inventory. The measurements were done in Komi middle taiga near the Laly research station (62.17°N, 50.40°E). For blueberry type spruce forests, the average tree AGB was reported to be 16.8 kg/m^2 (carbon stock 8.4 kg/m^2) and that for mixed forests 15.4 kg/m^2 (carbon stock 7.7 kg/m^2). For pine forests on different site types the AGB varied from 7.8 to 17.6 kg/m^2 (carbon stock 3.9-8.8 kg/m^2). These values are slightly higher than our results. This might be due to fact that the plots of Bobkova and Galenko (2001) were probably situated in mature forests, whereas our study sites included also younger stands and stands undergone some selective loggings.

CONCLUSION

Understanding and modeling the terrestrial carbon storage requires spatially explicit estimates of carbon in vegetation biomass. We used field plot measurements and satellite image based classifications to estimate the carbon stock in living AGB in the Medla-Pev-Nyur study region. This kind of estimates always include some error, in our case from,at least, field plot selection, stem volume modeling, models converting the volume of growing stock to biomass, and satellite image classification. Despite that, our results were in line with previous studies. Fine spatial resolution studies of carbon stock in Russian forests are rare, and here we could show that they can be produced with decent effort and reasonable accuracy.

ACKNOWLEDGEMENTS

We thank Malin Ek and Sanna Susiluoto for participating in the field work, and their work with biomass and remote sensing data. Thanks for Dr. Vladimir Elsakov arranging phytomass sample analysis in KSC. We also thank other CARBO-North teams for help in logistics and good company in the field. This research was financially supported by the EU 6th Framework Programme Global Change and Ecosystems (CARBO-North, contract number 036993; www.carbonorth.net).

References

Alexeyev, V.A., and R.A. Birdsey. 1998. Carbon storage in forests and peatlands of Russia. USDS Forest Service, Delaware.

Bobkova, K., and E.Galenko. 2001. Process of bioproduction in forest ecosystems of the north. St-Petersburg: Nauka.

FAO 2001. Global forest resources assessment 2000. Main report.FAO Forestry Paper 140. Rome: FAO.

Foody, G. 2008. Harshness in image classification accuracy assessment. *International Journal of Remote Sensing* 29: 3137–3158

Houghton, R.A. 2005. Aboveground forest biomass and the global carbon balance. *Global Change Biology* 11: 945–58

Houghton, R.A., D. Butman, A. Bunn, O.N. Krankina, P. Schlesinger, and T.A. Stone. 2007. Mapping Russian forest biomass with data from satellites and forest inventories. *Environmental Research Letters* 2 (045032): 7.

Hugelius, G., T. Virtanen, D. Kaverin, A. Pastukhov, F. Rivkin, S. Marchenko, V. Romanovsky, and P. Kuhry. 2011. High-resolution mapping of ecosystem carbon storage and potential effects of permafrost thaw in periglacial terrain, European Russian Arctic. *Journal of Geophysical Research Biogeosciences* 116 (3). art. no. G03024, doi:10.1029/2010JG001606.

Kauppi, P.E., E. Tomppo, and A. Ferm. 1995. C and N storage in living trees within Finland since 1950s. *Plant and Soil* 168-169: 633–638.

Laasasenaho, J. 1982. Taper curve and volume functions for pine, spruce and birch. Communicationes. Instituti. Forestalis. Fenniae 108: 1–74.

Lakida, P., S. Nilsson, and A. Shvidenko. 1997. Forest phytomass and carbon in European Russia. *Biomass and Bioenergy* 12(2): 91–99.

Lappi J., L. Mehtätalo, and K. Korhonen. 2006. Generalizing sample tree information. In *Forest Inventory Methodology and Applications*,ed. A. Kangas, and M. Maltamo. 85–106. Netherlands: Springer.

Lehtonen, A. 2005. Carbon stock and flows if forest ecosystems based on forest inventory data. Dissertation, University of Helsinki.

Martynenko, V., and S. Degteva. 2004. Flora and vegetation of the forest and alpine zones. In *The Pechora River Basin*, ed. V. Ponomarev, and M. Munsterman Leummens. Syktyvkar: IB-KSC-RIZA.

Shepashenko, D., A. Shvidenko, and S, Nilsson, 1998. Phytomass (live carbon) and carbon of Siberian forests. *Biomass and Bioenergy* 14(1): 21–31.

Shvidenko, A, S. Nilsson, V. Stolbovoi, and D. Wendt. 1998. Backround information for carbon analysis of the Russian forest sector., Laxembur: International Institute for Applied Systems Analysis.

Tomppo, E, H. Olsson, G. Stehl, M. Nilsson, O. Hagner, and M. Katila. 2008. Combining national forest inventory field plots and remote sensing data for forest databases. *Remote Sensing of Environment* 112: 1982-1999.

Turner, M.G. 1989. Landscape Ecology: The effect of pattern on process. Annual *Review of Ecology and Systematics* 20: 171-197.

Virtanen, T, and M. Ek. 2014. The fragmented nature of tundra landscape. *International Journal of Applied Earth Observation and Geoinformation* 27: 4–12.

Wilkinson, G.G. 2005. Results and implications of a study of fifteen years of satellite image classification experiments. *IEEE Transactions on Geoscience and Remote Sensing* 43 (3): 433–443.

Yu, Z. 2011. Holocene carbon flux histories of the world's peatlands: Global carbon-cycle implications. *The Holocene* 21: 761–774.

Zianis, D., P. Muukkonen, R. Mäkipää, and M. Mencuccini. 2005. Biomass and stem volume equations for tree species in Europe. Silva Fennica.

Chapter 4
SOIL MICROBIOTA OF MESOOLIGOTROPHIC PEATLAND

Peatlands have low pH and temperature values, low oxygen content due to excessive moisture, and inhibiting phenol compounds (Aerts et al., 1999). Ground cover is dominated by sphagnum mosses with strong structural hydrocarbons in cell walls being resistant to destruction by microorganisms (Hajek et al., 2011). Besides, organic matter destruction of sphagnum mosses produces phenol compounds which favor conservation of wetland plants in peat (Thormann et al., 2004). Peat formation depends on living activity of destructive microorganisms and fungi (Thormann et al., 2004; Pankratov et al., 2005; Kachalkin, 2010). Studies on soil fungal communities in upland and lowland peatlands of the East-European Plain and West Siberia using the luminescent microscopy method report that one gram of peat contains hundreds-thousands meters of fungal mycelium and tens-thousands millions spores and yeast-like cells (Golovchenko et al., 2008; Dobrovolskaya et al., 2012). Similar values were obtained for soil litter, sod, and upper humus layers of forest soils (Golovchenko, Dobrovolskaya, 2001).

Soil microorganisms are the main transformation agent of carbon and nitrogen in terrestrial ecosystems. Instead of low content of microbial carbon in the total soil carbon pool, microorganisms are dominant producers of methane and important source of carbon dioxide (Davidson, 1994). In order to predict and model green house gases emission from soil it is necessary to obtain biomass estimations for different groups of microorganisms producing particular gases. Microbiota of forest podzolic, sod-podzol, and alluvial soils of the Komi Republic is described by several authors (Khabibullina, 2001; Vinogradova, 2007). Studies on peatland microorganisms in this region are missing.

The purpose of the present work was to identify the microorganism types and their biomass in below-ground living part of Sphagnum spp. of the mesooligotrophic Medla-Pev-Nyur peatland in the middle taiga subzone.

MATERIALS AND METHODS

Ombrogenous hollow (site 1) and minerogenous hollow (site 3) were studied. The sites differ by plant species composition and abundance. Sphagnum samples were collected at a depth of 10-15 cm from Sphagnum capitula according to the common method (Kurakov, 2001) from May till October 2012. The Sphagnum samples comprised of Sphagnum plants of which the capitulum, a further top 0.5 cm and the lower brown part were removed, leaving stem parts of about 5 cm length and greenish-brown in colour that had been formed during the previous summer. For the microbiological analysis, mixed samples of 10 individual samples were used. The replication rate for Petri dishes was threefold. We utilized standard microbiological media. Ammonificators were extracted with meat-extract agar, mineralizers – with starch-and-ammonium agar, oligonitrophils –

with Ashby medium, and nitrificators – with Vinogradsky medium. Pure agar was applied for oligotrophic microorganisms, acidified Czapek medium – for micromyces, and Getchinson medium – for cellulose-decomposing fungi (Zvyagintsev, 1991).

Identification of microscopic fungi by cultural-morphological signs was carried out using MBI-6 microscope (Russia, Lomo) with a magnification of 12×40, 12×90 and identification books (Litvinov, 1967; Ellis, 1971; Khalabuda, 1973; Kirilenko, 1977; Ainsworth, 1995; Alimova, 2005; Domsch et al., 2007). Taxa were named according to the Internet site http://www.indexfungorum.org. Microscopic fungi were described operating with such parameters as abundance and frequency. By frequency, microorganisms divided into 1) high-frequent typical species – dominants; 2) frequent, 3) rare, and 4) occasional species with frequency index less than 30% (Mirchink, 1988). Relative abundance index of species was calculated as a ratio of colonies number for particular species to total number of colonies (Kurakov, 2001).

Total number of microorganismic cells in soil sample was identified by using the luminescent microscopy Axiovert 200 M (Carl Zeiss, Germany). 12 preparations obtained from one sample. Preparations for bacteria and actinomycetic mycelium were colored with acridine orange solution (1:10000, for 2-3 minutes), for fungal spores and mycelium – with calcofluor white for 15 minutes. Number of (mycelium) cells per 1 soil gram was calculated by the standard formula (Zvyagintsev, 1991):

$$N=S_1an/vS_2c,$$

where N – cell number (mycelium length, μm) per 1 soil g; S_1 – preparation area (μm^2); a – cell number, mycelium length (μm) in sight; n – soil suspension dilution index (ml); v – volume of a drop to be put onto glass (ml); S_2 – microscopic field area (μm^2); c – soil weight sample (g).

Biomass was calculated reasoning from the fact that dry matter biomass for one bacterial cell with a volume of 0.1 μm^3 makes 2×10^{-14} g, one meter of actinomycetic mycelium being 0.5 μm in diameter – 3.9×10^{-8} g, fungal mycelium being 0.5 μm in diameter – 3.9×10^{-8} g, and fungal spore 5 μm in diameter – 1×10^{-11} g (Zvyagintsev, 1991). Biomass data were expressed in mg/dry matter gram. Statistical treatment of data was done using Microsoft Excel 2003 program. Tables and figures contain average means and standard deviations.

RESULTS AND DISCUSSION

Vegetation period 2012 was quite moist and warm (Fig. 1). Air temperature and precipitation gradually increased from May till July. There was warm but dry weather in August followed by already cool but moist weather in September. In terms of quantitative distribution analysis of different groups of microorganisms (bacteria, micromyces, actinomyces), the ombrogenous hollow compared to the minerogenous hollow (Fig. 2).

The differences were possibly related to abundant grassy plants in ground cover and high organic matter content in water at the minerogenous hollow (Miglovets, Mikhaylov, 2012). Any time and at any site, number of mineralizers exceeded that of ammonificators evidencing intensive mineralization process. The same situation was observed for peat (Bubina, 2010) and cryogenic soils in North Siberia (Sorokin et al., 2008). The ombrogenous hollow was characterized by high

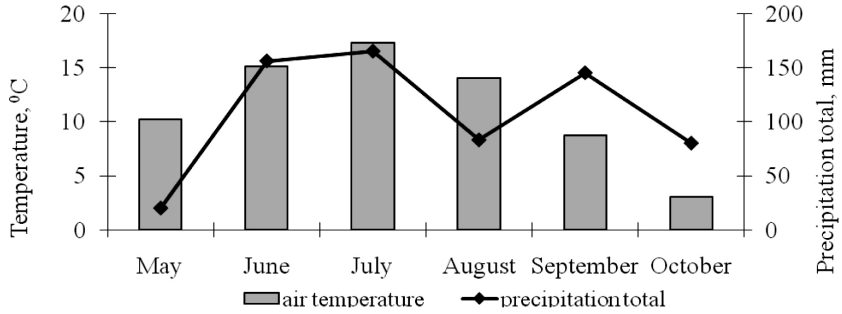

Fig. 1: Mean monthly air temperatures and precipitation (Agro meteorological Bulletin of the Komi Republic for the Ust-Vym Meteorological Station, 2012).

number of oligotrophics, ologonitrophils, and nitrifiers. Some authors found zero nitrifiers in peatlands as peat accumulates nitrogen ammonia (Dyrin, Krasnozhenov, 2007). High number of nitrificators in August could be caused by low precipitation amount at this period and, logically, low ground water level and sufficient aeration of upper peat layers. Number of oligotrophic microorganisms in upper soil sometimes attains 5×10^{11} and 3.8×10^{8} cells per one soil gram (Golovchenko et al., 1993). Number of oligonitrophyllous microorganisms varied insignificantly and increased in the beginning and towards the end of vegetation

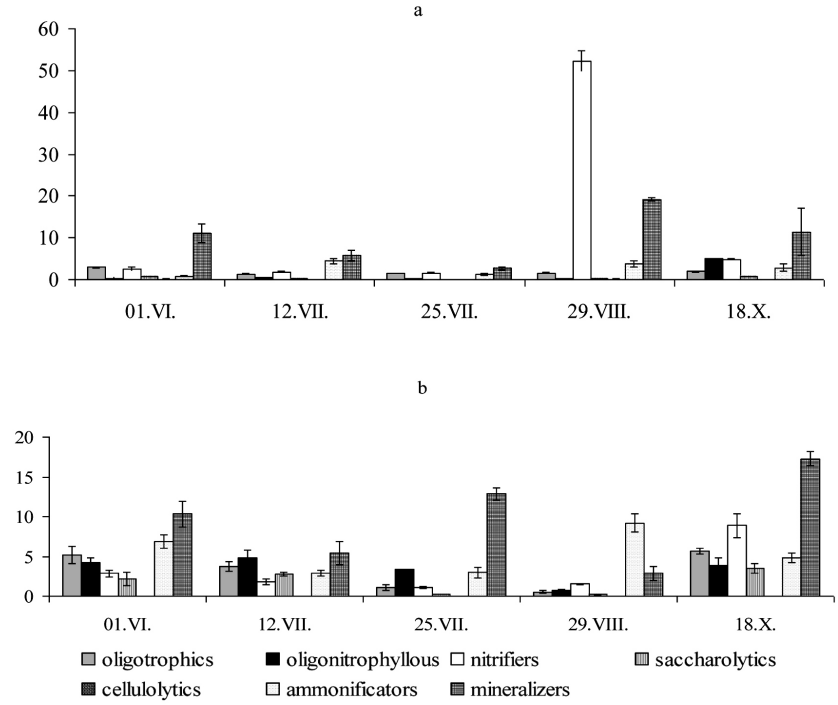

Fig. 2: Seasonal dynamics of the different physiological microorganism groups in the peatland (*a* – site 1, *b* – site 3). Axis Y: mln colony-forming units per absolutely dry soil.

period making 1.5-3 mln CFU (colony-forming units)/g a.d.s. (absolutely dry soil). Number of saccharolytics and cellulolytics was low.

In contrast to forest soils, the study peatland hosted a large number of microorganisms which easily develop in poor soil. Number (representation) of every microorganism group increased in October possibly due to fresh plant litter.

The low pH value of peatland does not hamper fungi but does procaryotes. Fungi dominate in microbe biomass of upper peatlands with pH values of 3.5-5 (Golovchenko et al., 2008). Mycobiota of peatlands has large biomass, is resistant to low temperatures, can decompose organic compounds, tannin acids, cellulose, and pectin, and does not require much nutrients (Golovchenko et al., 2013). Microorganism destruction of sphagnum moss is known to proceed better at +14° C than at +20° C (Thormann et al., 2004) because they are cold-resistant. The main limiting factor for micromyces in upper peat part is a special composition of polysaccharides in sphagnum cell walls which makes moss chemically resistant. When water level is high, peat contains little oxygen which normally decreases diversity of micromyces as aerobic organisms (Golovchenko et al., 2013).

Totally, 73 species of micromyces of the *Zygomycota* and *Anamorphic fungi* orders, including two sterile mycelium types, were extracted from Sphagnum spp. (Table 1). Most numerous were species of the Mortierella, Geomyces, Cephalosporium, Paecilomyces, Penicillium, and Trichoderma genera, as well as *Mycelia sterilia* (Table 2). The majority of extracted anamorphic micromyces belonged to the Penicillium (18 species) and Trichoderma (8 species) genera. The Mortierella genus counted 14 species which are cosmopolites and can survive in various environmental (Khalabuda, 1973).

Seasonally, species number of micromyces increased from June till July and decreased in August and September possibly due to changes in hydrothermal regime. Dominating were *Mortierella cephalosporina, M. verticillata, Geomyces pannorum, Scopulariopsis brevicaulis,* and *Mycelia sterilia* (light-colored) (Table 3). All dominants apart from *Geomyces pannorum* were found at the minerogenous hollow.

Frequent were *Mortierella alpina, M. schmuckeri, Umbelopsis ramanniana, Paecilomyces inflatus, Penicillium griseolum, P. islandicum, P. spinulosum, Trichoderma longibrachiatum, T. polysporum,* and *Mycelia sterilia* (dark-colored). Rare were *Mortierella parvispora, M. cephalosporina, M. polycephala*, *M. oligospora, M. verticillata, Mucor circinelloides, Geomyces pannorum*, *Oidiodendron* sp.1, *Paecilomyces* sp.1, *Penicillium dierckxii*, *P. frequentans*, *P.griseolum, P. funiculosum*, *P. spinulosum*, *Scopulariopsis* sp.1, *Trichoderma lignorum*, *T. piluliferum*. *T. polysporum*, and *Mycelia sterilia* (dark-colored). Occasional were *Acremonium vitis*, *Amblyosporium. echinulatum*, *Gliocladium* sp., *Cephalosporium charticola*, *C. oudemansii*, *Chrysosporium merdarium*, *Cylindrocladium* sp., *Cylindrocarpon* sp., *Fusidium* sp., *Metarhizium anisopliae*, *Monocillium exsolum*, *Rhizopus* sp., *Scopulariopsis brumptii*, *Aureobasidium pullulans, Aureobasidium* sp., *Oidiodendron citrinum*, *O. griseum*, and *O. maius*. Some species of the *Mortierella, Penicillium, Mucor,* and *Trichoderma* were also occasional at certain collection terms.

The species of micromyces were highly diverse at the minerogenous hollow at any collection time. This site was rich in occasional species and species of the Mortierella genus.

The minerogenous hollow covered with dwarf shrubs, grasses, and sphagnum mosses was always dominated or well represented by nonspore-forming (on the used nutrition media) fungi. Sterile mycelium is normally common in peat-

Table 1

Species composition and number of micromycetes in the peatland Medla-Pev-Nyur (average means 10^2 CFU per 1 g absolutely dry soil with standard deviation). 1 – ombrogenous hollow, 3 – minerogenous hollow

Fungal species	Date									
	01.06.		12.07.		25.07.		29.08.		18.10.	
	1	3	1	3	1	3	1	3	1	3
ZYGOMYCOTA										
Mortierella alliacea Linnem.						6±1				
M. alpina Peyronel		188±10		626±35	188±11	189±25				
M. cephalosporina Chalab					125±12	593±52				
M. hygrophila Linnem.						69±10				
M. parvispora Linnem.						132±23				
M. polycephala Coem		63±2	62±5		753±23					
M. spinosa Linnem.				6±1						
M. schmuckeri Linnem.		63±4				147±12		129±11		
M. oligospora Björl.						132±5		129±21		
M. verticillata Linnem.		188±10	62±2		132±12	614±12				
Mortierella sp.1			186±14			63±6				
Mortierella sp.2		188±12		688±42		63±6				
Mortierella sp.3			186±12	563±32						
Mortierella sp.4		125±6								
Mucor hiemalis Wehmer						63±5				
M. circinelloides Tiegh.						126±14				
Mucor sp.						63±4				
Umbelopsis ramanniana (Möller) W. Gams		941±41	63±5			997±45				
ANAMORPHIC FUNGI										
Acremonium charticola (Lindau) Gams						63±3				
A. vitis Catt.						63±6				
Amblyosporium echinulatum Oudem.						630±38				
Aureobasidium pullulans (de Bary) G. Arnaud			63±6	63±5		630±52		61±2		
Aureobasidium sp.					63±5	63±5				
Geomyces pannorum (Link) Hugkes		313±23		62±5	125±26	361±26	1012±88	61±3	124±5	63±4
Gliocladium sp.										62±5
Chrysosporium merdarium (Ehrenb.) J.W. Carmich							62±4			
Cephalosporium charticola Lindau						63±5		61±5		
Cephalosporium sp.								61±4		
C. oudemansii Pidopl.								61±6		

Fungal species	Date									
	01.06.		12.07.		25.07.		29.08.		18.10.	
	1	3	1	3	1	3	1	3	1	3
Cylindrocarpon sp.						630±52				
Cylindrocladium sp.					63±4					
Fusidium sp.						630±42				
Metarhizium anisopliae (Metschn.)						630±52				
Monocillium exsolum Bat. & J.W. Heine						63±9				
Oidiodendron citrinum G.L. Barron	62±7				63±7					
O. griseum Robak					63±7			61±3		
O. maius G.L. Barron					63±6					
Oidiodendron sp.1	62±5	125±25		124±11	188±10	630±59				
Oidiodendron sp.2			63±7							
Paecilomyces. carneus (Duche et Heim) Brown						126±13				
P. inflatus (Burnside) J.W. Carm						473±42			617±54	675±42
P. lilacinus (Thom) Samson		690±52			63±5					
Penicillium brevicompactum Dierckx					188±17	63±5				429±24
P. chrysogenum Thom	62±5	63±8	63±5	124±11	63±5					
P. dierckxii Biourge					63±5	441±32				
P. fellutanum Biorge	62±5	63±8		630±52	125±11					
P. frequentans Westling							185±11		62±4	
P. funiculosum Thom			63±7	124±11		6±1		124±11		
P. glabrum (Wehmer) Westling					63±5	63±5				
P. griseolum G. Sm.					63±4	376±21	123±11			
P. humuli Beyma				63±3						
P. islandicum Sopp									313±52	
P. lividum Westling		63±6								
P. purpurogenum Stoll		63±6		63±5				61±2		
P. restrictum J.C. Gilman & E.V. Abbott					63±5					
P. roquefortii Thom			63±2							
P. spinulosum Thom	124±12		612±41	124±10	187±15	126±11		61±4	370±23	
Penicillium sp.	736±56									
P. thomii Maire					63±5					
P. viridicatum Westling			63±5							
Rhizopus sp.		627±52								
Scopulariopsis sp.				63±3	188±11	126±33				
S. brevicaulis (Sacc.)		188±32				593±23				
S. brumptii Salv.-Duv.										61±2

Fungal species	Date									
	01.06.		12.07.		25.07.		29.08.		18.10.	
	1	3	1	3	1	3	1	3	1	3
Trichoderma flavofuscum (J.H. Mill., Giddens & A.A. Foster) Bissett						63±6				
T. lignorum (Tode) Harz	62±6	63±5		63±5					63±4	
T. longibrachiatum Rifai		125±11	187±11	124±8						
T. piluliferum J. Webster & Rifai	184±9					1323±88			63±4	
T. polysporum Link ex Fries	62±5	63±5	124±2	63±6		1467±78			63±8	
Trichoderma sp.1			63±8			63±8				
Trichoderma sp.2		63±8								
Trichoderma sp.3	62±7									
Mycelia sterilia										
Mycelia sterilia light-colored	409±23	889±42	564±35	310±21	1172±32	1386±102	1426±89	123±11	278±23	613±52
Mycelia sterilia dark-colored		125±10	125±11	372±35		284±25		63±5	86±5	
Species total	11	23	18	20	23	43	5	13	10	6
Total	73 species									

land ecosystems (Thormann, Rice, 2007). It usually includes species which do not bear spores on the used nutrition media and possibly belong to different taxa. Peatland mycobiota can include up to ten morphologically, physiologically, and culturally differing species of *Mycelia sterilia* (Thormann et al., 2001).

Mortierella verticillata cosmopolitan; reported from soil and roots of plants (Domsch et al., 2007), is chitinolytic (Gray and Baxby, 1968). *M. alpina* cosmopolitan; reported from soil (Domsch et al., 2007), is chitinolytic, utilizes other carbohydrates (Mil'ko and Gabryushina, 1968). *Umbelopsis ramanniana* cosmopolitan; reported from soil, decaying vegetation, dung, and animal tissues (Domsch et al., 2007), is pectinolytic and cellulolytic, utilizes starch (Flanagan and Scarborough, 1974).

Penicillium spinulosum was a dominating species at both sites and so confirmed information that the species is typical of humus horizon in north podzols and upland wetlands (Summerbell, 2005; Grum-Grzhimaylo and Bilanenko, 2012). *P. spinulosum* can survive in highly-acid soils and under different temperatures. It can decompose sphagnum mosses (Domsch et al., 2007). Acid soils of the Far North are also inhabited by *P. thomii* and *P. funiculosum* (Domsch et al., 2007). *P. funiculosum* cosmopolitan; reported from soil, cellulolytic (Gochenaur, 1975), utilizes various sugars and starch (Dickinson and Boardman, 1970).

Species of the Oidiodendron genus are usual habitants of peatlands and can decompose sphagnum mosses (Thormann et al., 2004). *O. griseum* inhabits root zone of *Ericaceae* plants and is popular with forest podzolic and peat soils (Sigler, 2005). The ericoid mycorrhizal fungus of *O. maius* cosmopolitan; reported from soil and roots of *Ericaceae* (Rice and Currah, 2006), pectinolytic, cellulolytic, utilizes starch, gelatin, and tannic acid (Thormann et al., 2001). This isolate was used in a study examining the degradation of *S. fuscum* cell walls (Tsuneda et al. 2001).

Table 2

Abundance of fungal genera (%) in the peatland Medla-Pev-Nyur. 1 – ombrogenous hollow, 3 – minerogenous hollow

Micromycete genera	01.06.		12.07.		25.07.		29.08.		18.10.	
	1	3	1	3	1	3	1	3	1	3
Mortierella		45	27	10	28	21		26		
Mucor						2				
Umbelopsis		7		2		11				
Acremonium						1				
Amblyosporium						1				
Aureobasidium				1	1	1		7		
Geomyces		4		1	3	7	27	7	5	8
Gliocladium										8
Chrysosporium							7			
Cephalosporium						1		20		
Cylindrocarpon						1				
Cylindrocladium					1					
Fusidium						4				
Metarhizium						1				
Monocillium						1				
Oidiodendron	6	2		2	8	1		7		
Paecilomyces		2			1	7			24	15
Penicillium	33	6	14	21	19	13	40	26	16	54
Rhizopus		1								
Scopulariopsis		6		1	3	13				8
Trichoderma	27	16	16	5		7			7	
Mycelia sterilia	34	11	43	57	36	7	27	6	48	7

The *Geomyces pannorum* micromycete is a psychrotolerant species and inhabits north tundra soils and permafrost. Its metabolism becomes highly efficient in conditions of low temperatures and zero oxygen **(Shcherbakova et al., 2010). Besides**, it also decomposes sphagnum cell walls (Thormann and Rice, 2007).

Trichoderma polysporum cosmopolitan; reported from soil, plant litter, rhizosphere of plants (Domsch et al., 2007), cellulolytic, weakly chitinolytic, utilizes a variety of sugars (Thormann et al., 2001).

Upland wetlands are known to be dominated by fungal mycelium biomass and lowland wetlands – by bacterial biomass. In lowland peatland, microbial biomass is relatively homogenously distributed throughout peat layer. In upper peatland, it normally accumulates upper peat layers (Golovchenko et al., 2007). In both peatland types, bacteria increase in number during vegetation period. Interseasonal variations in bacterial number largely exceed interannual variations. In contrast with forest soils, peat soils have less fungal mycelium and more procaryotic microorganisms, fungal spores, and yeast cells (Golovchenko et al., 1993).

90% of fungal colonies on agar media develop from fungal spores and so data obtained by the seeding method do not adequately respond for fungal mycelium diversity (Zvyagintsev, 1991). For this reason, we identified biomass of eukaryotic and prokaryotic soil components.

Bacterial biomass at the study peat sites varied from 0.01 to 0.05 mg g^{-1} a.d.s. and fungal biomass – 0.01-0.37 mg g^{-1} a.d.s. Actinomycete mycelium biomass comprised 0.02-0.13 and fungal mycelium biomass – 0.01-3.05 mg g^{-1} a.d.s. (Table 4). The obtained data on microbial biomass in Sphagnum spp. were infe-

Table 3

Taxonomic structure of micromycete communities in the study peatland. 1 – ombrogenous hollow, 3 – minerogenous hollow

Frequency classes	Species	
	1	3
Dominant (>60%)	*Geomyces pannorum* (Link) Hugkes, *Mycelia sterilia* (light-colored)	*Mortierella cephalosporina* Chalab, *M. verticillata* Linnem, *Scopulariopsis brevicaulis* (Sacc.), *Mycelia sterilia* (light-colored)
Frequent (30-60%)	*Mortierella alpina* Peyronel *Mortierella* sp.1, *Mortierella* sp.2, *Penicillium islandicum* Sopp, *P. spinulosum* Thom, *Trichoderma longibrachiatum* Rifai,	*Mortierella alpina* Peyronel., *M. schmuckeri* Linnem., *Umbelopsis ramanniana* (Möller) W. Gams, *Paecilomyces inflatus* (Burnside) J.W. Carm, *P.griseolum* G. Sm., *Trichoderma longibrachiatum* Rifai, *T. polysporum* Link ex Fries, *Mycelia sterilia* (dark-colored)
Rare (10-30%)	*Mortierella polycephala* Coem, *M. cephalosporina* Chalab, *M. verticillata* Linnem., *Oidiodendron* sp.1, *Penicillium frequentans* Westling, *P.griseolum* G. Sm., *Penicillium* sp. 1, *Scopulariopsis* sp.1, *T. piluliferum* J. Webster & Rifai, *Trichoderma polysporum* Link ex Fries, *Trichoderma* sp.3, *Mycelia sterilia* (dark-colored)	*Mortierella parvispora* Linnem., *M. polycephala* Coem, *M. oligospora* Björl., *Mortierella* sp.1, *Mortierella* sp.3, *Mortierella* sp.4, *Mucor circinelloides* Tiegh., *Geomyces pannorum* (Link) Hugkes, *Oidiodendron* sp.1, *Paecilomyces* sp.1, *Penicillium dierckxii* Biourge, *P. funiculosum* Thom, *P. spinulosum* Thom, *Scopulariopsis* sp.1, *Trichoderma lignorum* (Tode) Harz, *T. piluliferum* J. Webster & Rifai.
Occasional (<10%)	*Mortierella* sp.3, *Umbelopsis ramanniana* (Möller) W. Gams, *Aureobasidium* sp., *Chrysosporium merdarium* (Ehrenb.) J.W. Carmich, *Cylindrocladium* sp., *Oidiodendron citrinum* G.L. Barron, *O. griseum* Robak, *O. maius* G.L. Barron, *Paecilomyces inflatus* (Burnside) J.W. Carm, *Paecilomyces* sp.1, *Penicillium dierckxii* Biourge, *P. funiculosum* Thom, *P. glabrum* (Wehmer) Westling, *P. restrictum* J.C. Gilman & E.V. Abbott, *P. thomii* Maire, *Trichoderma lignorum* (Tode) Harz, *Trichoderma* sp.1	*Mortierella alliacea* Linnem., *M. hygrophila* Linnem., *M. spinosa* Linnem., *Mortierella* sp.2, *Mucor hiemalis* Wehmer, *Mucor* sp., *Acremonium vitis* Catt., *Amblyosporium echinulatum* Oudem., *Aureobasidium pullulans* (de Bary) G. Arnaud, *Aureobasidium* sp., *Gliocladium* sp., *Cephalosporium charticola* Lindau, *Cephalosporium* sp., *C. oudemansii* Pidopl., *Cylindrocarpon* sp., *Fusidium* sp., *Metarhizium anisopliae* (Metschn.), *Monocillium exsolum* Bat. & J.W. Heine, *Oidiodendron griseum* Robak, *Penicillium glabrum* (Wehmer) Westling, *P. lividum* Westling, *P. purpurogenum* Stoll, *Rhizopus* sp., *Scopulariopsis brumptii* Salv.-Duv., *Trichoderma flavofuscum* (J.H. Mill., Giddens & A.A. Foster) Bissett, *Trichoderma* sp.1, *Trichoderma* sp.2, *Trichoderma* sp.3

rior to the values obtained by the other authors for upland and lowland Siberian peatlands by several times (Golovchenko et al., 1993, 2007). The situation could be related to plant waste intake towards the end of vegetation period because August saw increase in fungal mycelium length and fungal spores biomass which was comparable with literature data and hold till October. Seasonal changes in bacterial and actinomycete biomass were similar for two study sites: they increased to the end of July and decreased in autumn. At the minerogenous hollow biomass of prokaryotic microorganisms decreased in the mid vegetation period and increased in autumn. Biomass of fungal mycelium and spores was almost

Table 4

Seasonal dynamics of microbial biomass (mg g^{-1} a.d.s.) in Sphagnum litter. 1 – ombrogenous hollow, 3 – minerogenous hollow

Date	Bacteria		Fungal spores		Fungal mycelium		Actynomyces	
	1	3	1	3	1	3	1	3
01.06	0.03±0.03	0.02±0.002	0.01±0.007	0.03±0.01	0.02±0.003	0.02±0.001	0.03±0.002	0
12.07	0.02±0.01	0.01±0.001	0.01±0.007	0.01±0.009	0.03±0.001	0.01±0.003	0.03±0.001	0.04±0.001
25.07	0.04±0.005	0.04±0.002	0.02±0.01	0.05±0.02	0.05±0.002	0.04±0.003	0.13±0.001	0.03±0.001
29.08	0.02±0.004	0.05±0.004	0.15±0.01	0.17±0.09	2.99±0.3	3.05±0.2	0	0.02±0.001
18.10	0.01±0.001	0.03±0.002	0.13±0.01	0.37±0.05	1.30±0.2	2.65±0.2	0	0

the same for June-July and then strongly increased in August-October which corresponds with literature data (Golovchenko et al., 1993). Low biomass values of fungal mycelium in June-July could be related with high precipitation amount which could hamper fungal mycelium development in litter. Spore diameters were 2.9-4.1, hyphae thickness – 2.4-7 μm.

Thus, we identified 73 species of micromycetes from the Medla-Pev-Nyur mesooligotrophic peatland. The Penicillium genus included 18, Mortierella – 14, and Trichoderma – 8 species. The highest diversity of micromyces was observed to the end of July at the minerogenous hollow characterized with high species diversity and number of occasional and Mortierella species. The ombrogenous hollow was always dominated by sterile colorless mycelium. Seasonally, species diversity of micromyces increased to the end of July and decreased towards October. Microbe biomass in Sphagnum spp. of the study peatland was inferior to literature data for lowland and upland peatlands of boreal zone by several times. Seasonally, number and biomass of any microbial group increased in autumn.

References

Aerts R., Verhoeven J. T. A., and D. F. Whigham. 1999. Plant-mediated controls on nutrient cycling in temperate fens and bogs. *Ecology*. 80 (7): 2170-2181.

Ainsworth and Bisby's Dictionary of the fungi. 1995. Ed. D. L. Hawksworth et al. 540 p. CABI Bioscience.

Alimova, F. K. Trichoderma/Hypocrea (Fungi, Ascomycetes, Hypocreales): taxonomy and distribution., 2005. Kazan: Kazan state university.

Bubina A. B. 2010. Characteristic of microflora of eutrophic mires. *Vestnic TGPU*. 3 (93): 142-148.

Dickinson, C. H., and F. Boardman. 1970. Physiological studies of some fungi isolated from peat. Transactions of the British Mycological Society. 55: 293-305.

Davidson, E.A. 1994. Climate change and soil microbial processes: secondary effects are hypothesised from better known interacting primary effects. In *Soil responses to climate change*, ed. M.D.A. Rounsevell and P.J. Loveland). NATO ASI Series. V. I. 23. Springer-Verlag Berlin Heidelberg.. P. 155-168.

Dobrovolskaya, T. G., A. V. Kurakov, A. V. Golovchenko, and N. S. Pavlova. 2012. Antagonistic mutual relations of bacteria and fungi in peatbogs. Vestnik Moskovskogo universiteta. Ser. 17. *Pochvovedenie* 4: 32-35.

Domsch, K.H., W. Gams, and T.H. Anderson. 2007. Compendium of soil fungi. IHW-Verlag Eching.

Dyrin, V. A., and Ye. P. Krasnozhenov. 2007. Microbial activity in the virgin and recultivated peat soils of lowland. *Vestnik Tverskogo gosudarstvennogo universiteta*. Yestestvennye i tochnye nauki. 6 (69): 33-38.

Ellis, M. B. 1971. Dematiaceous Hyphomycetes. Kew: Commonwealth Mycological Institute. 608.

Gochenaur, S. E. 1975. Distributional patterns of mesophilous and thermophilous microfungi in two Bahamian soils. *Mycopathologia* 57: 155-164.

Golovchenko, A. V., L. M. Polyanskaya, T. G. Dobrovolskaya, L. V.Vasilieva, I. Yu. Chernov, and D. G. Zvyagintsev 1993. Peculiarities in space distribution and structure of microbial complexes of boggy-forest ecosystems. *Pochvovedenie* 10: 78-89.

Golovchenko, **A. V., E. Yu. Tikhonova, and D. G. Zvyagintsev. 2007. Abudance, biomass**, structure and activity of the microbial complexe of minerotrophic and ombrotrophic peatlands. *Microbiologiya* 5: 711-719.

Golovchenko, **A. V., and T. G. Dobrovolskaya 2001. Numbers and reserve of micro**organisms in floodplain soil. *Pochvovedenie* 12: 1460-1464.

Golovchenko, **A. V., T. G. Dobrovolskaya, and D. G. Zvyagintsev. 2008. Microbiologi**cal basis for assessing peat as a soil profile body. *Vestnik Tverskogo gosudarstvennogo universiteta. Biologicheskie nauki* 4(78): 46-53.

Golovchenko, A. V., A. V. Kurakov, T. A.Semenova, and D. G. Zvyagintsev. 2013. Abundance, diversity, viability, and factorial ecology of fungi in peatbogs. *Pochvovedenie* 1: 80-97.

Gray, T. R. G., and P. Baxby. 1968. Chitin decomposition in soil. 2. The ecology of chitinoclastic micro-organisms in forest soil. Transactions of the British Mycological Society. 51: 293-309.

Grum-Grzhimaylo, O. A., and E. N. Bilanenko. 2012. The micromycete complexes of bogs at the Kandalaksha bay of the White Sea. Micologiya i fitopatologiya. 46 (5): 297-305.

Flanagan, P. W., and A. M. Scarborough. 1974. Physiological groups of decomposer fungi on tundra plant remains. P. 159-181. In *Soil organisms and decomposition in Tundra*, ed. A. J. Holding. Stockholm.

Hajek T., S. Balance, J. Limpers, M. Zijlsta, and J.Verhoeven. 2011. Cell-wall polysaccharides play an important role in decay resistance of Sphagnum and actively depressed decomposition in vitro. *Biogeochemistry* 103: P. 45-57.

Kachalkin, A. V. 2010. New data on the distribution of certain psychrophilic yeasts in Moscow oblast. *Microbiologiya*. 79 (6): 843-847.

Khabibullina, F. M. 2001. Soil micromycetes in bilberry-green moss spruce forest of the middle. *Lesovedenie*. 1: 43-48.

Khalabuda, T. V. 1973. Fungi of the genus Mortierella Coemans. Moscow: Nauka.

Kirilenko, **T. S. 1977. Atlas of genera of soil fungi (Ascomycetes and Deuteromyce**tes).: 126 p. Kiev: Naukova dumka.

Kurakov, **A. V. 2001. Methods of isolation and characterization of complexes micro**scopic fungi terrestrial ecosystems: Instruction Manual. 92 p. M.: MAKS Press.

Litvinov, **M. A. 1967. Identification guide of microscopic soil fungi. 302 p. Lenin**grad: Nauka.

Miglovets, M. N., and O. A. Mikhaylov. 2012. The reaction of methane emissions on the seasonal changes of hydrothermal and hydrochemical factors on meso-oligotrophic peatland in the middle taiga. In *Aktualnye problemy biologii i ecologii: Materialy dokladov XIX rossiiskoy molodezhnoy nauchnoy konferentsii (Syktyvkar, Komi Republic, Russia, 2-6 April 2012),* 159-161. Syktyvkar.

Mil'ko, A. A., and A. I. Gabryushina. 1968. The behaviour of some *Mortierella* species towards carbohydrates as carbon sources: In *Eksperimentalnaya Mikologiya,* ed. N. M. Pidoplichko, 185-190 p. Kiev: Naukova Dumka.

Mirchink, T. G. 1988. Soil mycology. Moscow: Moscow state university.

Pankratov, **T. A., S. E. Belova, and S. N. Dedysh. 2005. Evaluation of the phyloge**netic diversity of prokaryotic microorganisms in Sphagnum peat bogs by means of fluorescence in situ hybridization (FISH). *Microbiology* 6: 831-837.

Peat Resources of the Komi Republic. 2000. Syktyvkar.

Rice, A. V. and Currah R. S. 2006. Oidiodendron maius: saprobe in sphagnum peat, mutualist in ericaceous roots? *Soil Biology* 9: 227-246.

Shcherbakova, V. A., G. A. Kochkina, N. E. Ivanushkina, K. S. Laurinavichius, S. M. Ozerskaya, and V. K. Akimenko . 2010. Growth of the fungus Geomyces pannorum under anaerobiosis. *Microbiology* 6: 848-85.

Sigler, L., C. Gibas, and C. Fe. 2005. Utility of a cultural method for identification of the ericoid mycobiont Oidodendron maius confirmed by IST sequence analysis. *Studies in Mycology* 53: 63-74.

Sorokin, N. D., S. Yu. Evgrafova, I. D. Grodnitskaya, and A. V. Bogorodskaya. 2008. Ecological characteristics of microflora incryogenic forest soils of the north of Central Siberia. *Sibirskiy ekologicheskiy zhurnal*. 6: 859-865.

Summerbell, R. C. 2005. Root endophyte and mycorrhizosphere fungi of black spruce, Picea mariana, in a boreal forest habitat: influence of site factors on fungal distributions. *Studies in Mycology*. 53: 121-145.

Thormann, M. N., S. E. Bayley, and R. S. Currah. 2004. Microcosm test of the effects of temperature and microbial species number on the decomposition of Carex aquatilis and Sphagnum fuscum litter from southern boreal peatlands . *Can. J. Microbiol*. 50: 793-802.

Thormann, M. N., R. S. Currah, and S. E. Bayley. 2001. Microfungi isolated from Sphagnum fuscum from a southern boreal bog in Alberta, Canada . *The Bryologist*. 104(4): 548-559.

Thormann, M. N. and A. V. Rice. 2007. Fungi from peatlands. *Fungal Diversity* 24: 241-299.

Tsuneda, A., M. N. Thormann, and R. S. Currah. 2001. Modes of cell-wall degradation of *Sphagnum fuscum* by *Acremonium cf. curvulum* and *Oidiodendron maius*. *Canadian Journal of Botany* 79: 93-100.

Vinogradova, Yu. A. 2007. The influence of environmental conditions on the formation of microbial communities of alluvial soils of the middle taiga. Avtoref. diss. ... kand. biol. nauk. Syktyvkar: Institute Biology.

Zvyagintsev, D. G. 1991. Methods of soil microbiology and biochemistry. Moscow: Moscow state university.

Chapter 5
PALUDIFICATION RATE AND TOTAL ECOSYSTEM CARBON STORAGE

Peatlands occupy about 24% of the boreal region and represent a very significant soil carbon pool. Current estimates of the northern peatland carbon pool range between 400-600 PgC (Gorham, 1991; Yu et al., 2010; Loisel et al., 2014). This large C pool is due to the long-term accumulation of organic matter, referred as peat, because net primary productivity at the surface exceeds the very slow rates of decomposition due to cool and anaerobic conditions prevailing in the peat profile. The C stored in the peatland varies with externally driven environmental conditions and the time since peatland inception and usually represents a greater C storage per surface area as compared with adjacent forest soils. While carbon storage in deep peat deposits and boreal forest soils have been extensively documented, the transition phase during paludification when forest upland becomes a peatland habitat has been largely overlooked. In this chapter, we present the evolution of C storage over time partitioned in all ecosystem layers along forest-peatland transitions in the Medla-Pev-Nyur peatland.

PALUDIFICATION RATE

The processes by which a peatland is initiated can be either through terrestrialization, where organic deposit fills up water ponds, or through paludification. The latter is the most widespread process for peatland initiation and consists of the lateral expansion of a peatland over an upland forest (Charman, 2002). In the Medla-Pev-Nyur peatland, the presence of buried wood and forest humus at the peat-mineral subsoil transition and the absence of confirm that the investigated parts of the peatland were formed through paludification. To study the expansion rate of the peatland, 3 transects perpendicular to the peatland edge were established, from forest upland to inner peatland (Fig. 1). Sampling points were cored along the transects every 50 m near the peatland-forest transition zone and every 100 m in the peatland proper. This approach allows for a more accurate assessment of the recent paludification rates by increasing the resolution in the transition areas. At each sampling point, basal peat at the peat-mineral contact was sampled using a fixed volume Russian peat corer. Paludification rates (or expansion rates) were assessed using basal peat radiocarbon ages and distances from the edge of the peatland (considered 0 years). The initiation of peat accumulation was determined by radiocarbon dating of 10 bulk peat samples, of which 6 were from sampling points within 100 m from the edge of the peatland. For a more detailed description of the methodology, please refer to Pluchon et al. (2014).

The peat core stratigraphy showed that a large part of the central area of the peatland has peat depths between 160 and 200 cm. The margins of the three transects have steep slopes with a rapid increase of peat depth to a maximum

observed depth of 205 cm within a few hundred meters from the peatland edge. The oldest basal peat date found was dated around 9600 calyr BP (calibrated years before present), but it cannot be assumed that this corresponds to the earliest peatland development in the area. Basal dates between 8000 and 1500 calyr BP were found along the transects with youngest dates of ca. 50 calyr BP found in the peatland-forest transition zones. A linear regression model including the recent eight data points from the three transects show a consistent slow replacement of forest by peatland at ca. 2.6 m per century (p-value: <0.001; n=8; not shown), while basal dates for the older part of the peatland overlying flatter terrain give a higher mean lateral expansion rate of ca. 7.6 m per century (p-value: 0.033; n=6; not shown).Furthermore, the correlation between slope and expansion rate is strong and significant for the eight points of the Medla-Pev-Nyur peatland (Pearson correlation coefficient: r^2: −0.886; p-value: 0.004; n=8; not shown). These values of lateral expansion rates are within the intervals reported by Peregon et al., (2009) and Loisel et al., (2013) of 2.3-792 m per century and 1-47 m per century, respectively. As such, the topography appears to be a main driving factor behind changes in lateral expansion rates, as also reported by Korhola (1994) in Finnish raised bogs and Loisel et al., (2013) in Alaskan peatlands.

Altogether, these data indicated that initial peat formation in Medla-Pev-Nyur began more than 9600 years ago through paludification. Initially, the peatland expanded at a rate of ca. 8 m per century in flat terrain until it reached steeper slopes associated with a river terrace paleo-landscape, after which the lateral expansion rate slowed down to ca. 3 m/century.

TOTAL ECOSYSTEM CARBON STORAGE

To investigate the change in total ecosystem carbon storage induced by paludification, we measured the C storage in phytomass and soil/peat along the 3 transects from forest to inner peatland presented above (Fig. 1, 2). Using a space for time replacement we assumed that the initial total forest ecosystem C storage at the recently paludified sites was similar to that of the currently adjacent forest sites. The ecosystem C storage was measured as the sum of the phytomass C storage, the C from the full depth of the soil organic layer (which corresponds to the peat layer in the peatland) and 30 cm of mineral subsoil. The tree phytomass (trees > 1 cm diameter at breast height (dbh)) was determined based on the measurements of species-specific basal area (Bitterlich, 1984), dbh, tree height, and diameter at 6m height from median diameter tree in 5.64 m radius circular plots. Then, the tree phytomass values were computed from stem volume and growing stocks using different models (for more detailed methodology, see Pluchon et al., (2014); and Chapter, 2). The understory phytomass was measured by sampling all living vegetation from one 30×30 cm square. The phytomass C of the harvested samples was estimated as 50% of the vegetation dry weight. Forest soils were sampled to 1 m depth, with a vertical resolution of 5-10 cm, using a fixed volume sampler inserted in the vertical wall of an open pit. In some cases deeper soil layers were sampled by coring into the bottom of the pit. A fixed volume Russian peat corer was used to sample four complete peat cores with a vertical resolution of 5-10 cm. Two cores were collected in the ombrothrophic part of the peatland and two from the minerothrophic part (see Chapter, 1). In addition to the four fully samples cores, the peat depth was recorded at each

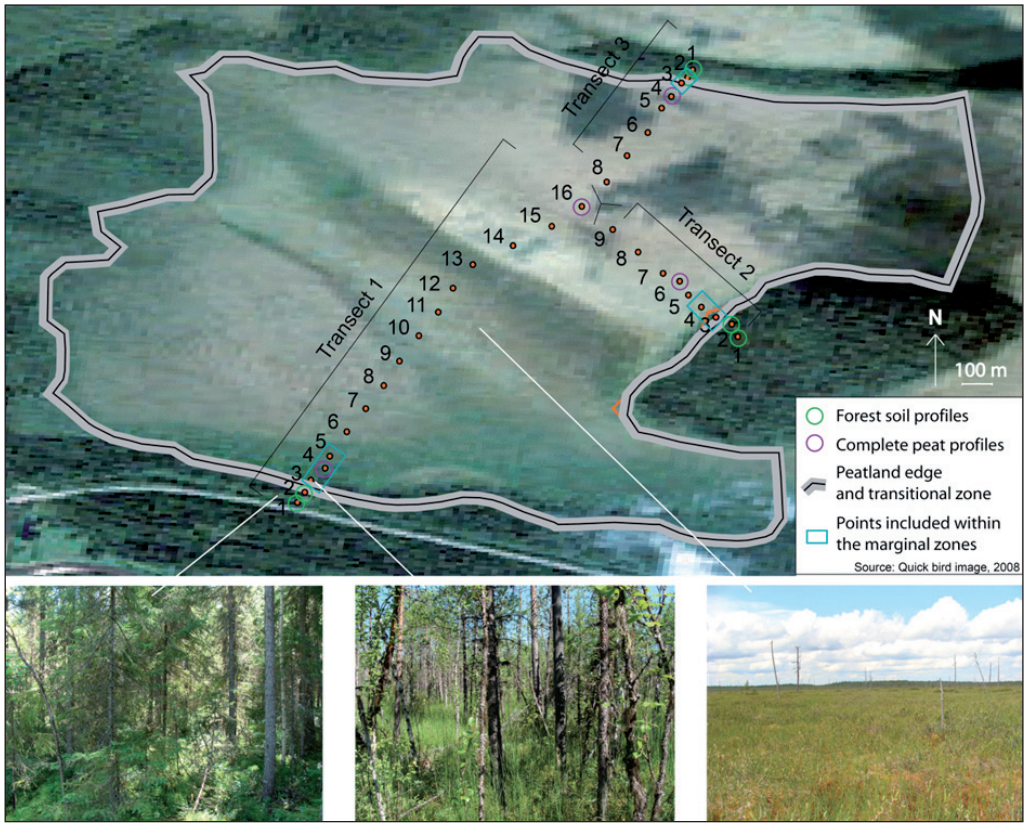

Fig. 1: Total ecosystem carbon storage distribution along the three investigated transects of the Medla-Pev-Nyur peatland. The '0' distance represents the edge of the peatland.

sampling point along all three transects and mineral soil from below the peat-mineral contact was collected at some points along the transects. The C storage of soil/peat samples was derived from the dry bulk density and loss-on-ignition (LOI) analysis (550 ˚C for 2 h) to determine organic content (Dean, 1974), and elemental organic C and N content for a subset of samples. Then, regression models were used to predict the percentage of organic C for the peat/soil samples for which only LOI and peat depth measurements were available(see Pluchon et al., 2014).

The carbon partitioning (storage in phytomass and in different soil layers) in the forest sites showed that aboveground phytomass representes about 25% of the total ecosystem C with a mean value of 4.0kg C/m^2 (Table 1 and Fig. 2). These phytomass C storage values from Medla-Pev-Nyurare comparable with the reported values of 3.6 kgC/m^2 for the whole boreal forest region (Alexeyev, Birdsey, 1998), between 4 to 8 kg C/m^2 for the middle taiga (Bobkova, Galenko, 2001) and 4.4 kgC/m^2 in the forested lands of European northern Russia (Shvidenko et al., 1998). The forest soil C storage for the reference 1 m depth ranges from 14.4 kg C/m^2 to 40.3 kg C/m^2, with a mean value of 21.5 kg C/m^2 (Table 1). This estimated forest soil C storage (down to 1 m depth) is higher

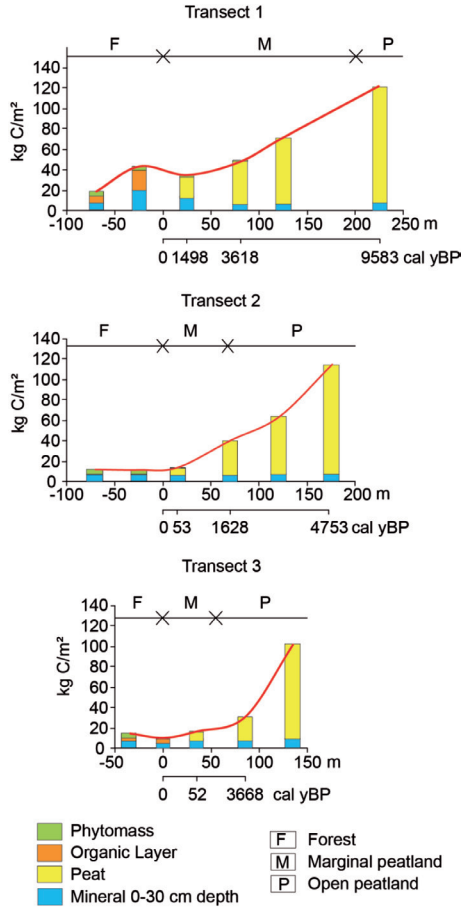

Fig. 2: Positions of the transects and sampling points within Medla-Pev-Nyur peatland area.

in comparison with other reported values such as 10.2 to 13.2 kg C/m² in Canadian boreal forests (Bhatti et al., 2002), 11.4 kg C/m² on average in Russian forest soils (Stolbovoi, 2006) and between 11.1 and 19.0 kg C/m² in the global boreal forest biome (Post et al., 1982), but in a similar order of magnitude of values reported for moist (herbaceous) spruce forests in northern Komi (on average 20.3 kg C/m²) by Hugelius, Kuhry (2009). These higher values could result from the proximity to the peatlands indicating early stages of paludification.

The total C storage in peatland sites varies from 13.5 kg C/m² in the marginal parts to >100 kg C/m² in the central parts of the peatland with the peat layer being the major reservoir of C (Table 1 and Fig. 2). The phytomass C storage is on average 0.9 kg C/m² in the marginal parts of the peatland area, with sparse and stunted trees, and 0.2 kg C/m² in the central, more open parts (Table 1). Phytomass C storage in these different parts of the peatland represents 10% and 0.1% of the total ecosystem C storage, respectively. Some previously reported phytomass values include 1.6 kg C/m² for Russian peatlands (Shvidenko et al., 2000) and 0.2 kg C/m² in a peatland site of the southern boreal forest in North America (Weishampel et al., 2009). The C storage in the 30 cm of mineral subsoil below the peat-mineral contact is estimated at 7.2 kg C/m² in the marginal parts and 7.6 kg C/m² in the central parts of the peatlands (up to 11.2 kg C/m² where buried top soil organic horizons

Table 1

Summary table of the partitioning of the carbon storage (± SE) in the 3 ecosystem types encountered during paludification

Ecosystem type (number of sites)	Phytomass C storage (kg C/m²)	OL/peat C storage (kg C/m²)	Mineral (30cm) C storage (kg C/m²)*	Total ecosystem C storage (kg C/m²)*	Forest soil 1 m C storage (kg C/m²)
Forest (n=6)	4.0 ± 0.6	5.9 ± 2.9	8.3 ± 2.2	18.2 ± 5.2	21.5 ± 4.1
Margin of the peatland (n=6)	0.9 ± 0.3	28.3 ± 8.5	7.2 ± 0.8	32.5 ± 20.8	
Open peatland (n=21)	0.2 ± 0.01	97.4 ± 5.5	7.6 ± 0.2	105.3 ± 5.4	

* Including the 30 cm of mineral subsoil below the top soil organic or peat layer.

from the previous forest soil stage are present beneath the peat column) (Table 1). Turunen, Moore (2003) and Moore, Turunen (2004) reported 7.8 kg C/m^2 for 70 cm depth in sandy soils beneath peat deposits. The difference with the higher values obtained for the Medla-Pev-Nyur peatland is likely related to the different soil textures as the latter is developed on finer textured soils(silty and clayey loam) which typically have higher C contents than sandy soils (Jenny 1980). The peatland C storage values in the Medla-Pev-Nyur peatland range between 23.4 and 130.4 kg C/m^2, and are lower than previously reported peat C storage values in the northern taiga of East European Russia (from 63.6 to 241.6 kg C/m^2; Hugelius, Kuhry, 2009) and in Canadian boreal peatlands (from 74.1 to 178.2 kg C/m^2; Bhatti et al., 2002). These lower values can partly be explained by the sampling methodology which focused on the marginal, shallower areas of the peatland. The net peat accumulation rates were compiled based on peat C storage and peat initiation dates and show two contrasting rates: 15 g C/m^2/y for the 8 sites which were initiated more than 1000 years ago and 145 g C/m^2/y for the two younger sites initiated less than 100 years ago. Higher values for recent sites have also been reported by Van Bellen et al. (2011) and can be explained by the fact that surface peat accumulation is only to a limited extent reduced by peat decomposition. In deeper and older peat deposits, the cumulative aerobic (in the acrotelm) and anaerobic (in the catotelm) decay significantly reduces net C accumulation rates on longer time scales (Clymo et al., 1998). The accumulation rate from the older sites is within the lower range reported by Loisel et al., (2014) from a synthesis of 215 northern peatlands and comparable with values reported by Yu et al., (2014) from a synthesis of Canadian peatlands.

Overall, the peatland ecosystem stores more C than the forest ecosystem (Table 1 and Fig. 2). The decrease of phytomass C storage is more than compensated by peat C accumulation. However, the increase of the total ecosystem C storage from forest to peatland is not linear (Fig. 2). All three transects show a decrease of total ecosystem C storage in the transition zone from forest to peatland, from −10.1 to −0.4 kg C/m^2 (average value −5.0±2.8kg C/m^2, n=3) (Fig. 2). The losses are caused both by reductions in the aboveground phytomass and belowground carbon pools in the mineral layer but not in the organic layer. It is likely that the higher water table in the marginal peatland zone causes the drowning of the forest, in addition to the presence of flowing water in this area which provides nutrients which may prime microbial communities to accelerate decomposition rates and transport organic material away as dissolved organic C (Blodau, 2002). The estimated recovery times required to compensate for initial ecosystem C losses following paludification are 35 and 335 years based on measured C loss and peat accumulation rates in recent and older sites, respectively. From the empirical observations along each transect, initial losses had been compensated by peat accumulation in less than 50 years in two transects whereas one transect showed a similar C storage as that of the forest after more than 1500 years of peat accumulation. Very few studies have focused on the transitional stage between boreal forest and peatland ecosystem. Previous studies have postulated a continuous increase in total ecosystem C storage from forest to peatland, but these studies differed in their classification and considered our corresponding marginal peatland area as forest (Bauer et al., 2009; Bhatti, Errington, 2006). The scarcity of such studies with dense sampling resolution highlights the need for more research in the marginal parts of peatlands in order to obtain a wider perspective on the effects of initial paludification on total ecosystem C storage.

CONCLUSION

The Medla-Pev-Nyur peatland shows a development history initiated during the early Holocene period (i.e. ca 9600 years ago) and expansion rates were driven by topography with a current average lateral expansion rate of ca 3 m/century. The C storage in the different ecosystem components is in the same magnitude of those previously reported in the boreal ecosystems with 25 kg C/m^2 in averaged for forest sites and up to more than 100 kg C/m^2 in the peatland. Furthermore, the investigation of the C storage along the transects have focused on total ecosystem C storage in the forest-peatland transition area and has revealed a loss of C during the initial paludification process, of on average ca −5 kg C/m^2. Periods of decades to centuries of peat accumulation were necessary to compensate for the losses induced by shifting from forest to peatland habitat. These observations might have large implications for C storage in the boreal region if paludification rates change over time.

References

Alexeyev, V.A., and R.C. Birdsey. 1998. Carbon storage in forests and peatlands of Russia. Delaware.

Bauer, I.E., J.S. Bhatti, C. Swatson, R.K. Wieder, and C.M. Preston. 2009. Organic Matter Accumulation and Community Change at the Peatland–Upland Interface: Inferences from 14C and 210Pb Dated Profiles. *Ecosystems*, 12(4): 636–653.

Van Bellen, S., P.-L. Dallaire, M. Garneau, and Y. Bergeron. 2011. Quantifying spatial and temporal Holocene carbon accumulation in ombrotrophic peatlands of the Eastmain region, Quebec, Canada. *Global Biogeochemical Cycles*, 25(2): 1–15.

Bhatti, J.S., M.J. Apps, and C. Tarnocai. 2002. Estimates of soil organic carbon stocks in central Canada using three different approaches. *Canadian Journal of Forest Research*, 32(5): 805–812.

Bhatti, J.S., and R. Errington. 2006. Carbon stock trends along forested peatland margins in central Saskatchewan. *Canadian journal of soil Science* 86: 321-333.

Bitterlich, W. 1984. The relascope idea: relative measurements in forestry.Farnham Royal, UK.

Blodau, C. 2002. Carbon cycling in peatlands - A review of processes and controls. *Environmental Reviews*. 10:111–134.

Bobkova, K. , and E.Galenko. 2001. Process of bioproduction in forest ecosystems of the north, St Petersburg.

Charman, D.J. 2002. Peatlands and Environmental Change, Chichester: John Wiley and Sons Ltd.

Clymo, R.S., J. Turunen, and K. Tolonen. 1998. Carbon Accumulation in Peatland. *Oikos*, 81(2): 368–388.

Dean, W.E. 1974. Determination of carbonate and organic matter in calcareous sediments and sedimentary rocks by loss on ignition: Comparison with other methods. *Journal of Sedimentary Petrology*. 44: 242–248.

Gorham, E. 1991. Northern Peatlands: Role in the Carbon Cycle and Probable Responses to Climatic Warming. *Ecological Applications*, 1(2): 182–195.

Hugelius, G., and P. Kuhry. 2009. Landscape partitioning and environmental gradient analyses of soil organic carbon in a permafrost environment. *Global Biogeochemical Cycles*. 23(3): 1–13.

Jenny, H. 1980. The soil resource: origin and behaviour (Ecological Studies). Springer-V., New-York.

Korhola, A.A.. 1994. Radiocarbon Evidence for Rates of Lateral Expansion in Raised Mires in Southern Finland. *Quaternary Research*. 42(3): 299–307.

Loisel, J., Z. Yu, D.W. Beilman, P. Camill, J. Alm, M.J. Amesbury, D. Anderson, S. Andersson, C. Bochicchio, K. Barber, L.R.elyea, J. Bunbury, F.M. Chambers, D.J. Charman, F. De Vleeschouwer, B. Fialkiewicz-Kozel, S.A. Finkelstein, M. Galka, M. Garneau, Hammarland, D., Hinchcliffe, W., Homquist, J., Hughes, P., **Jones, M.C.**, Klen, E.S., U. Kokfelt, A. Korhola, P. Kuhry, A. Lamarre, M. Lamentowicz, D. Lage, M. Lavoie, G. MacDonald, G Magnan, M. Mäkilä, G. Mallon, P. Mathijssen, D. Mauquoy, J. McCarroll, T.R. Moore, J. Nichols, B. O'Reilly, P. Oksanen, M. Packalen, D. Peteet, P.J.H. Richard, S. Robinson, T. Ronkainen, M. Rundgren, A.B.K. Sannel, C. Tarnocai, T. Thom, E.S. Tuittila, M. Turetsky, M. Vдliranta, M. van der Linden, B. van Geel, S. van Bellen, D. Vitt, Y. Zhao, and W. **Zhou. A database and synthesis of northern peat**land soil properties and Holocene carbon and nitrogen accumulation. 2014. *The Holocen*. 24(9): doi/10.1177/0959683614538073.

Loisel, J., Z. Yu, A. Parsekian, J. Nolan, and L. Slater. 2013. Quantifying landscape morphology influence on peatland lateral expansion using ground-penetrating radar (GPR) and peat core analysis. *Journal of Geophysical Research: Biogeosciences*. 118(2): 373-384.

Moore, T.R., and J. Turunen. 2004. Carbon Accumulation and Storage in Mineral Subsoil beneath Peat. *Soil Science Society of America Journal*. 68(2). 690.

Peregon, A., M. Uchida, and Y. Yamagata. 2009. Lateral extension in Sphagnum mires along the southern margin of the boreal region, Western Siberia. *Environmental Research Letters. 4.*

Pluchon, N. , H. Hugelius, N. Kuuzinen, and P. Kuhry. 2014. Recent paludification rates and effects on total ecosystem carbon storage in two boreal peatlands of Northeast European Russia. *The Holocene*. 24(9): 1126-1136. doi/10.1177/0959683614523803.

Post, W.M., W.R. Emanuel, P.J. Zinke, and A.G. Stangenberger. 1982. Soil carbon pools and world life zones. *Nature*. 208: 156-159.

Shvidenko, A.Z., S. Nilsson, V.S. Stolbovoi, M. Gluck, D.G: Shchepashchenko, and V.A. Rozhkov. 2000. Aggregated estimation of the basic parameters of biological production and the carbon budget of Russian terrestrial ecosytems: 2. Net primary production. *Russian Journal of Ecology*. 31(6): 371-378.

Shvidenko, A.Z., S. Nilsson, V. Stolbovoi, and D. Wendt. 1998. Background information for carbon analysis of the Russian forest sector. Laxenburg.

Stolbovoi, V. 2006. Soil carbon in the forests of Russia. *Mitigation and Adaptation Strategies for Global Change*. 11(1): 203-222.

Turunen, J., and T.R. Moore. 2003. Controls on carbon accumulation and storage in the mineral subsoil beneath peat in Lakkasuo mire, central Finland. *European Journal of Soil Science*. 54(2): 279-286.

Weishampel, P., R. Kolka, and J.Y. King. 2009. Carbon pools and productivity in a 1-km2 heterogeneous forest and peatland mosaic in Minnesota, USA. *Forest Ecology and Management*. 257(2): 747-754.

Yu, Z., D.H. Vitt, and R.K. Wieder. 2014. Continental fens in western Canada as effective carbon sinks during the Holocene. *The Holocene*. 24(9): 1090-1104. doi/10.1177/0959683614538075.

Chapter 6
GROWTH CHARACTERISTICS OF CONIFEROUS TREES GROWING ON A BOREAL PEATLAND AND THEIR APPLICATION AS MARKERS FOR DATING RECENT PEAT DEPOSITS

Although wet mires provide harsh conditions for tree growth, wooded and forested mires are common in continental boreal regions (Rydin and Jeglum, 2006). In Komi Republic, the zonal taiga vegetation consists of *Picea obovata* forests in different formations (Walter and Breckle, 1994) and *Picea* swamp forests can be found on water saturated soils or shallow peat deposits (Økland et al., 2001; Vitt, 2006; Bauer et al., 2009). They sometimes form a zone between upland forest and mire (Rydin and Jeglum, 2006), but their cover is limited (Walter and Breckle, 1994). *Pinus sylvestris* is the second dominant tree species and its occurrence is restricted to early successional stages or to less favourable habitat conditions like on poor sand or peat soils (Walter and Breckle, 1994; Wieder, 2006).

Species composition, stand density and growth performance of trees are generally affected by abiotic site conditions, such as light, soil oxygen and nutrient supply (Schweingruber, 1988; 1996; Fritts, 2001). For example, along transects from the mineral upland to the centre of a mire, different site conditions are usually reflected in a sequence from boreal upland forest into swamp forest, then into sparsely wooded mire, and finally into open mire areas (Rydin and Jeglum, 2006). Tree growth on the mire Medla-Pev-Nyur exhibits this general pattern and since growth conditions of trees are recorded in their tree ring record, dendroecological methods can be used to study environmental conditions of the sites, where the trees grow (Kaennel et al., 1995; Schweingruber, 1996; Fritts, 2001).

Natural mires are usually characterised by an upward growth of the mire surface by peat accumulation. The rate at which peat accumulates is strongly dependent on the short-term processes in the acrotelm, i. e. the upper aerobic layer of the peat column. Especially in ombrotrophic bogs, Sphagnum forms successive sedentary peat layers on the surface. This upward growth presents a challenge to tree establishment and survival and thus tree survival in mires is expected to depend amongst others on the interaction between trees and Sphagnum mosses. This substantially influences trees growing on mires, since their lower stem sections are buried in a fresh peat layer (Ohlson et al., 2001). Tree seedlings have to compete with Sphagnum and in order not to become overgrown, their height growth has to exceed those of the mosses (Gunnarsson and Rydin, 1998; Ohlson, 1995; Ohlson et al., 2001; Rydin et al., 2006). However, the buried stem sections of mire trees can provide information on recent mire development and has been used by several authors for dating recent peat deposits (Borggreve, 1889; Koff et al., 1998; Ohlson and Dahlberg, 1991; Ohlson and Økland, 1998; Ohlson et al., 2001; Økland and Ohlson, 1998; Schulze et al., 2002; Turetsky et al., 2004).

Dendroecological research on mire trees in Medla-Pev-Nyur was done along a transect from the marginal swamp forest to the last stunted individuals towards the peatland centre in order to assess how trees in a forest-mire ecotone can cope with the growing peat surface and to estimate recent peat growth in the acrotelm of a growing mire.

MATERIALS AND METHODS

Transect and tree stand characteristics

The two coniferous tree species *Picea obovata* and *Pinus sylvestris* (in the following referred to as Picea and Pinus) were investigated along theforest-mire ecotone at the southern margin of Medla-Pev-Nyur. Four study plots covered a range of wooded mire area from the marginal swamp forest to the last stunted individuals near the mire centre. Following Scandinavian mire ecologists, the two sample plots closer to the edge were classified as "peatland margin", while those closer to the centre were denoted as "peatland expanse" (see Økland et al., 2001). The peatland margin was characterized by a distinct micro relief with hummocks of up to 60 cm above the water table and depressions with open water. The peatland expanse showed a closed cover of *Sphagnum* mosses with surface differences ranging from 10 to 45 cm above the water table.

Both studied tree species occurred in the peatland margin, while the tree cover in the peatland expanse was exclusively built up by Pinus. Beside the coniferous tree species, the tree cover in the peatland margin was complemented by *Betula pubescens* and *Alnus incana*. Ground cover vegetation was dominated by Sphagnum mosses. In direction to the peatland centre, the cover of dwarf shrubs increased and those of herbaceous vegetation decreased. Calculated weighted mean Ellenberg nitrogen values for the occurring plant species (Ellenberg, 1992) showed a slightly better nutrient supply for the peatland margin (with a mean N-value of 2.4) than for the peatland expanse (with a mean N-value of 1.8).

Tree sampling in Medla-Pev-Nyur was done during July 2008. Tree species, height of tree above surface and tree diameter at surface level were recorded in the field for a general description of stand structure. Since stunted trees that do not reach breast height occur numerous in mires (Schweingruber, 2007), diameter at surface level was used for stand density estimation rather than diameter at breast height, which is commonly used in forests (Kramer and Akça, 2008). To account for differences in micro-sites, the distance from surface to water table was measured for each tree. The measured distances were corrected for a water table drop from

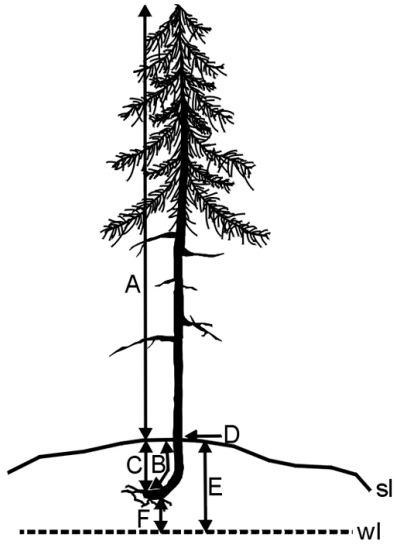

A... Height of tree above surface
B... Length of stem below surface
C... Hypocotyl position below surface
D... Diameter of tree at surface level (sl)
E... Distance from surface to water level (wl)
F... Distance from hypocotyl to water level

Fig. 1: Measured field parameters of each sampled tree.

July (time of tree sampling) to August (time of lowest water table) of about 10 cm. In this way, the minimum water table and thus the thickness of the aerobic zone in summer was estimated. Figure 1 gives an overview on the measured variables at each tree.

Sampling of tree stems and the hypocotyl method

In the mire, measured tree height was underestimated because accumulated peat has buried the lower stem section of trees. The burial of stem wood of living trees is often associated with reduction of radial growth, anatomical changes and the formation of adventitious roots in the buried part of the stem (Shroder, 1978; Kaennel et al., 1995). This burial of the original germination point can be used to investigate the relationship between age and depth of a surface peat layer (Ohlson and Dahlberg, 1991; Koff et al., 1998; Økland and Ohlson, 1998; Ohlson and Økland, 1998; Ohlson et al., 2001; Schulze et al., 2002). The so-called "pine method" originally described by Borggreve (1889) combines the depth of an accumulated peat column around a pine stem with the time interval it needed to develop (Ohlson and Dahlberg, 1991). By developing a root system, tree seedlings become anchored in the peat (Rydin and Jeglum, 2006). Although new accumulating peat raises the mire surface, the position of the original germination point, i. e. the hypocotyl, remains constant in relation to deeper peat layers (Schulze et al., 2002; Walter and Breckle, 1994). Consequently, the tree's age corresponds to the age of the peat increment above its hypocotyl. Table 1 gives an overview on possible uses of the method. In Medla-Pev-Nyur it was used to estimate surface peat growth and peat accumulation and to assess how trees in the forest-mire ecotone did cope with the decreasing growing conditions from the margin to the centre of the mire. Since the number of pine trees decreased near the peatland edge, Picea trees, which occurred in the peatland margin, were included as well. Due to the use of both species, the "pine method" is denoted in the following as "hypocotyl method".

For the application of the hypocotyl method, whole living tree specimens were pulled up by the root and the distance from the hypocotyl position to the present-day surface was measured. As several trees showed a bending in their lower stem section, distance was also measured along the stem (see Fig. 1). A bending factor was calculated as the ratio of hypocotyl depth and stem length below the surface. A value equal or close to 1 means that no bending occurred, while a higher degree of bending is indicated by a bending factor lower than 1.

Table 1

Applications of the hypocotyl method compiled from literature (and complemented with this study)

Application of the hypocotyl method	Author
Measurement of bog growth	Borggreve, 1898
Comparison of peat increment rates in hummock and lawn communities	Ohlson and Dahlberg, 1991
Study of age-depth relationship and compaction in surface peat	Økland and Ohlson, 1998
Estimation of spatial variation in C- and N-accumulation in a bog	Ohlson and Økland, 1998
Dating of the peat column for a paleoecological study	Koff et al. ,1998
Study interaction between *Sphagnum*-mosses and *Pinus sylvestris*	Ohlson et al., 2001
Estimation of net ecosystem productivity and peat accumulation	Schulze et al., 2002
Using peatland pines as proxy for water table fluctuations	Smiljanic et al., 2014
Study peat accumulation and interaction between trees and Sphagnum in a forest-mire ecotone	This study

Additionally, the below-ground proportion of each extracted tree stem was determined. The sampling of complete individuals was biased towards smaller trees, since pulling up of larger trees was not possible.

Dendroecological analyses

Dendroecological analyses were done for 7 Picea and 36 Pinus trees growing on the peatland and11 individuals (all *Picea* trees) growing in the adjacent boreal forest with an organic soil layer less than 30 cm. Main objectives were to determine tree age, detect missing outer rings and other anatomical features influenced by the growing peat surface, and to determine height growth of trees.

For tree age determination, tree rings were counted at hypocotyl level, where most rings are supposed to be built (Fritts, 2001; Niklasso, 2002). However, under unfavourable conditions, growth can decrease substantially and trees sometimes do not form annual rings in the lower stem section (Kolishchuk, 1990; Norton and Ogden, 1990; Schweingruber, 1996; Kozlowski et al.,1997; Fritts, 2001; Wilmking et al., 2012). Due to possible missing rings, a careful investigation of the tree stems at different heights from the hypocotyl to the upper stem section is necessary to prevent underestimation of tree ages (Kolishchuk, 1990; Norton and Ogden, 1990; DesRochers and Gagnon, 1997; Niklasson, 2002). Therefore, serial sectioning (Kolishchuk, 1990) was applied on all extracted tree stems. Two to eleven stem discs from different heights between the hypocotyl and surface level were cut and prepared for tree ring measurements. On each stem disc two to four radii were measured on a treering measuring system (Lintab 6) using the software TSAP-Win (Rinn, 2003). As the compass direction was marked on the tree stems, corresponding radii could be measured on different heights. Wedging rings, which can occur due to failure of cambial activity in some part of the cross section (Kaennel et al., 1995; Kozlowski et al., 1997), were inserted as zero values in radii where rings were absent. A tree ring series for each stem disc was built by averaging the radii.

Tree age was determined using within-tree crossdating (Niklasson, 2002) which is based on the interannual agreement between ring width series of different stem discs (Kaennel et al., 1995; Rinn, 2003). Since the tree's ring width pattern is observable along the whole stem (Kolishchuk, 1990; Schweingruber, 1996), cross sections from different positions along a tree stem can be subsequently fit into a tree ring series for the whole tree. The synchronous run of overlapping ring width series was compared from the uppermost stem disc down to the hypocotyl. Missing outer rings were detected and the tree ring series was shifted to the appropriate position compared to the overlapping series from higher stem sections. Statistical quality control of crossdating results was done using the program COFECHA (Holmes, 1999; Grissino-Mayer, 2001).The possible influence of the growing peat surface on outer ring formation was tested by linear regression or ANCOVA using the occurrence of missing outer rings as binary response variable (classified as either absent of present). Tested possible explanatory variables were: depth of hypocotyl below the surface, length of tree below surface, position of hypocotyl relative to the lowest water table, tree age, peatland zone and species. Dependent variables were tested by successive model simplification and only the best explaining variable was included in the model.

Height growth of trees is associated with the formation of new stem area. Along a tree stem the current year's radial growth builds the first tree ring in the newly formed upper stem section and the last ring at lower stem sections

(Fritts, 2001). Consequently, the difference between cambial ages of two cross sections from different stem positions corresponds to the time the tree needed to overcome the distance between these crosssections. This age-distance relationship can be used to estimate height growth. Cumulative height growth above the hypocotyl of extracted and dated trees was used to assess the height growth abilities of young trees. Since the first years of growth are crucial in the struggle of trees with growing mosses (Ohlson, 1995; Ohlson et al., 2001), height growth models were based on the first ten years of tree growth after germination.

A comparison was done by calculating the difference in slope of the linear regression models for two height growth subsets at a time (Jurasinski, 2007). This was applied for the subsets $Picea_{forest}$ versus $Picea_{margin}$, $Picea_{margin}$ vs. $Pinus_{margin}$ and $Pinus_{margin}$ vs. $Pinus_{expanse}$.

Additionally, height growth rates (HGRs) of individual trees were calculated as:

$$HGR = l_{buried} / (age_{total} - age_{surface}), \quad (1)$$

with l_{buried} = length of the buried stem from hypocotyl to surface, age_{total} = tree age at hypocotyl (corrected for missing rings) and $age_{surface}$ = age of the stem disc at surface level. Ohlson (1995) reported that young pines have an up to two times higher HGR when compared to pines older than 20 years. Since a calculation of HGRs based on age and total tree height may underestimate growth abilities of young trees, HGRs were calculated on the basis of the buried part of the tree stems.

Estimation of growth and decomposition of surface peat

The hypocotyl method was used to date surface peat and to express relationships between age and depth in 43 peat columns in which the respective dated trees were embedded. Mean vertical peat growth rates (PGRs) were calculated as depth-age ratios:

$$PGR = h/t, \quad (2)$$

where h is hypocotyl depth and t the age of a peat column (i.e. time since germination of the tree). Subsequent consolidation and decomposition (in the following subsumed as compaction) of the peat layers lead to an underestimation of the growth rate of surface peat with increasing age (Økland and Ohlson, 1998; Ohlson et al., 2001). To estimate the recent addition of fresh material to the peat column, PGRs were corrected for compaction. The underlying assumptions for an adequate description of recent vertical peat growth along a tree trunk are: (1) a constant growth rate of the peat forming vegetation for the time period since tree germination, and (2) a constant rate of peat compaction (α) in the same period (Økland and Ohlson, 1998). The relationship between PGR and age can be regarded as a decay process and described by an exponential model (Clymo, 1984). This model assumes that the rate of compaction remains constant over time, when calculated as a proportion of the remaining organic material. Therefore, PGRs were ln-transformed prior to further analysis. Most of the compaction of the surface peat layer occurs during the first 40 to 50 years after formation. This compaction process is expected to be more or less linear during this time, afterwards showing no distinct relationship between PGR and age (Ohlson and Dahlberg, 1991; Ohlson et al., 2001; Økland and Ohlson, 1998). Following assumptions (1) and (2) for the description of recent vertical peat growth, a linear regression model was fit to the data set for corresponding values of age and ln-transformed PGR. In order to confirm the time period in which the relationship

between ln-transformed PGR and age is linear and to identify influential points in the dataset, the model was checked visually and with inspection of diagnostic plots in R (R Development Core Team, 2009). All trees in the resulting time period were used for an adequate description of the height growth of surface peat.

Compaction corrected peat growth rates (CPGRs) for these trees were calculated following Ilkland and Ohlson (1998) as:

$$CPGR = PGR_0 = h \cdot \alpha \cdot (1 - e^{-\alpha(t-1)})^{-1}, \quad (3)$$

This follows Clymo's model for peat growth in the acrotelm (Clymo, 1984). Due to the assumed constant growth rate, CPGRs correspond to the peat growth at $t = 0$ when compaction is absent. The values for h and t in formula (3) were obtained with the hypocotyl method.

The site specific compaction rate α was estimated in an iterative procedure: formula (3) was applied on all corresponding age and depth measurements for young trees and α was identified as the value where the correlation coefficient r between tree ages and ln-transformed PGRs equals zero and thus the estimated vertical peat growth rates became unrelated to the ages of the trees or peat columns (Økland and Ohlson, 1998). Both, the specific compaction rate α and the CPGRs were estimated and calculated for the whole dataset, as well as for the two mire zones (i.e. mire margin and mire expanse). Means for the obtained vertical peat growth rates were compared using two-tailed independent t-tests.

RESULTS

Stand characteristics in the peatland zones and specifics of sampled trees

Peatland zones revealed significant differences in the stand characteristics of the two studied tree species. Picea occurred only in the peatland margin. In a distance from the peatland edge of approx. 35 m, the stand density expressed as surface area was 2.5 m^2/ha with 0.17 individuals per m^2, while 75 m closer to the peatland centre, the last individuals of Picea (0.01 individuals/m^2) covered a surface area of 0.1 m^2/ha. Pinus occurred with a similar number of individuals

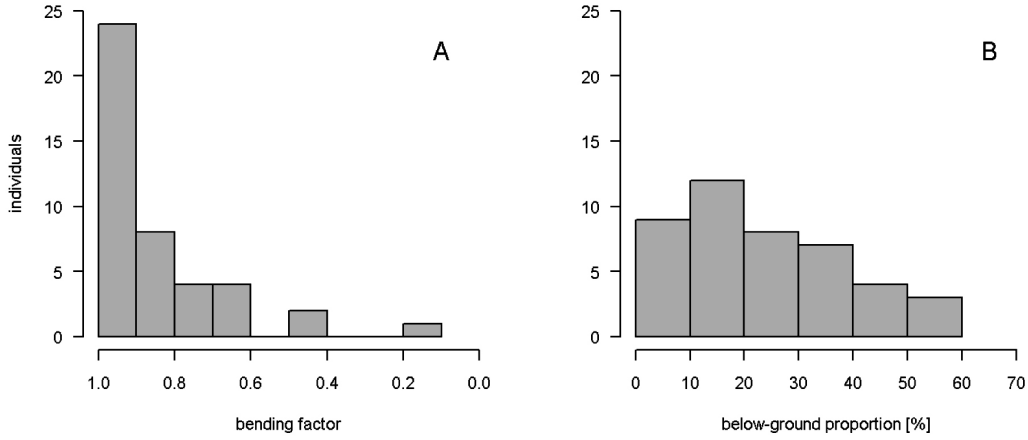

Fig. 2: Frequency of bending factors (A) and of the below-ground proportion of stems (B) for extracted peatland trees. The bending factor is calculated as quotient of hypocotyl depth and stem length and is thus an inverse expression of the visual bending. A high bending factor (i.e. factor 1) means that there is no bending, while bending is higher for lower bending factors. The below-ground proportion expresses how much of the total stem length of a tree is situated below the peat surface.

per m^2 in both, peatland margin and expanse (0.23 and 0.25 individuals/m^2), but differed in the occupied surface area (13.11 m^2/ha in the peatland margin and 4.23 m^2/ha in the peatland expanse). Tree height showed no differences between species, but was significantly higher in the peatland margin (mean ± standard deviation (SD): 3.53 ± 2.52 m) than in the expanse (1.88 ± 1.01 m; Welch Two Sample t-test, $t = 6.08$, $p < 0.001$ (two-tailed)).

Extracted and successfully dated peatland trees ($n = 43$) had a median age of 27 years. Only few individuals ($n = 3$) were older than 60 years (the oldest individual was 122 years) and no tree was younger than 11 years. The sampled trees had a mean height ± SD above the surface of 139 ± 82 cm and the mean position ± SD of their hypocotyl was 30.7 ± 14.6 cm below the surface. Bending of the lower stem section was a common phenomenon and occurred in different intensities. Approximately 50% ($n = 23$) of the extracted trees showed no or only a slight bending. Bending was higher in the remaining trees with the highest bending factor in an 18-year old individual that had a length of 70 cm below surface while rooting depth was only 12 cm. Figure 2A summarizes the bending factors of all dated trees. Correlated with this bending was the below-ground proportion of trees (Fig. 2B). Mean values of the below-ground proportion of trees showed that about one quarter (24.3 ± 24.75% SD) of the tree stem was buried in the peat.

Both, bending factor and below-ground proportion of tree stems showed no correlation with tree age. The mean difference in age when sampling the same trees at hypocotyl and at surface level was 8.9 ± 5.7 years. In some individuals, up to the first 20 years of growth were buried in the peat. Other visually detected characteristics of the buried tree stems included eccentric tree rings (connected with the bending of the stem) and unclear, root-like ring boundaries in many stems. These ring-boundaries (i.e. the change of previous year's latewood to the next year's early wood) were often only marked by one layer of narrow latewood cells. This phenomenon started at about 40 cm stem length below surface which was situated approx. 30-40 cm deep in the peat. Due to the occurrence of very eccentric rings and unclear ring-boundaries near the hypocotyl of the extracted trees, several individuals ($n = 7$) could not be successfully dated. Adventitious roots were built by Picea trees already close below the peat surface, while no adventitious roots were detected for individuals of Pinus.

Occurrence of missing outer rings

Within-tree cross-dating showed that counting of tree rings at hypocotyl level led to an underestimation of the true ages in 21 of 43 dated peatland trees (Fig. 3). However, there were only seven individuals that showed missing outer rings in successive years. The remaining 14 trees did not start to build up the current year's growth ring until July.

The occurrence of missing outer rings was significantly correlated to

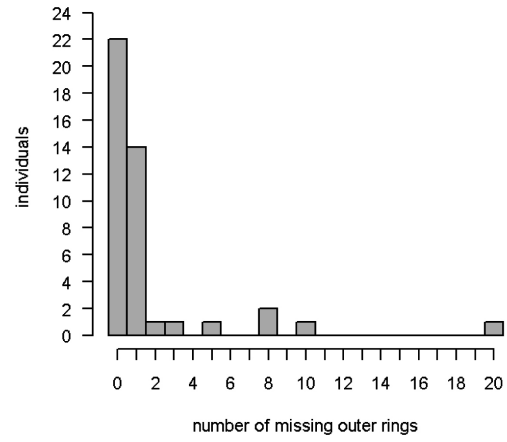

Fig. 3: Frequency of the number of missing outer rings in the dataset.

the position of the hypocotyl in relation to the estimated depth of the permanently water-logged zone ($p < 0.01$), to the hypocotyl depth below surface ($p < 0.01$) and to the length of the tree stem below the peat surface ($p < 0.05$). Since the difference between hypocotyl and estimated depth of the permanently water-logged zone revealed the highest significance within this group of related variables, the other two variables were not further considered. Missing outer rings were also significantly related to peatland zone ($p < 0.05$). They occurred more often in the peatland expanse. No correlation was detected between the occurrence of missing rings and tree age or tree species. Analysis of covariance showed no significant interaction between the different variables. Model simplification revealed that the occurrence of missing rings in the dataset can be explained most effective by the relative position of the hypocotyl to the lowest water table. Missing outer rings occurred in several depths relative to the water table, in the oxic as well as in the anoxic zone of the peat column, while trees without missing rings occurred exclusively in the oxic zone.

Height growth abilities of young peatland trees

The comparison of juvenile growth (i.e. growth in the first ten years after germination) of trees showed no significant difference between the cumulative height growth (CHG) models for Picea from the forest and from the peatland margin (Fig. 4A). In the peatland margin, where Picea and Pinus occurred together, the height growth of Pinus was significantly higher than the one for Picea (CHG $Picea_{\text{margin}} <$ CHG $Pinus_{margin}$, $p < 0.01$; see Figure 4B). Furthermore, the comparison of height growth of *Pinus* in the peatland margin and in the expanse showed a significant difference in slope (CHG $Pinus_{\text{margin}} >$ CHG $Pinus_{expanse}$, $p < 0.01$; see Fig. 4C).

Mean height growth rates were very variable between species. The mean HGR ± SD of Picea trees was 29.4 ± 10.5 mm/a, while those of Pinus was 63.4 ± 50.6 mm/a. The range of growth rates for Picea was smaller than for *Pinus*. The height growth rate of young trees was significantly correlated ($p < 0.001$) with the calculated bending factor. Trees with a high bending showed a higher height growth rate than trees without bending.

Age-depth relationship in surface peat

The depth of a peat column surrounding a tree trunk was positively correlated with the tree's age ($r = 0.47$; $p < 0.01$). In general, older trees rooted in deeper peat layers. Since no data exists for trees younger than 10 years, and only few data points for trees older than 60 years ($n = 3$), the examination of the age-depth relationship was mainly restricted on dated trees covering the age interval from 11 to 60 years. Age and depth of peat columns for trees in this interval confirmed the expected positive correlation between age and depth ($r = 0.73$; $p < 0.001$). However, on shorter time scales, e.g. for dated trees from 11-30 years or from 31-60 years, respectively, the data showed no significant correlation between age and depth. Peat columns of the same depth varied considerably in ages, mostly by a factor of two to three.

Vertical peat growth in the acrotelm of peatland zones

Calculated vertical peat growth rates (PGRs) showed an inverse trend concerning the age. Ln-transformed PGRs and age of the accumulated columns showed a negative correlation ($r = -0.65$; $p < 0.001$), which can be described

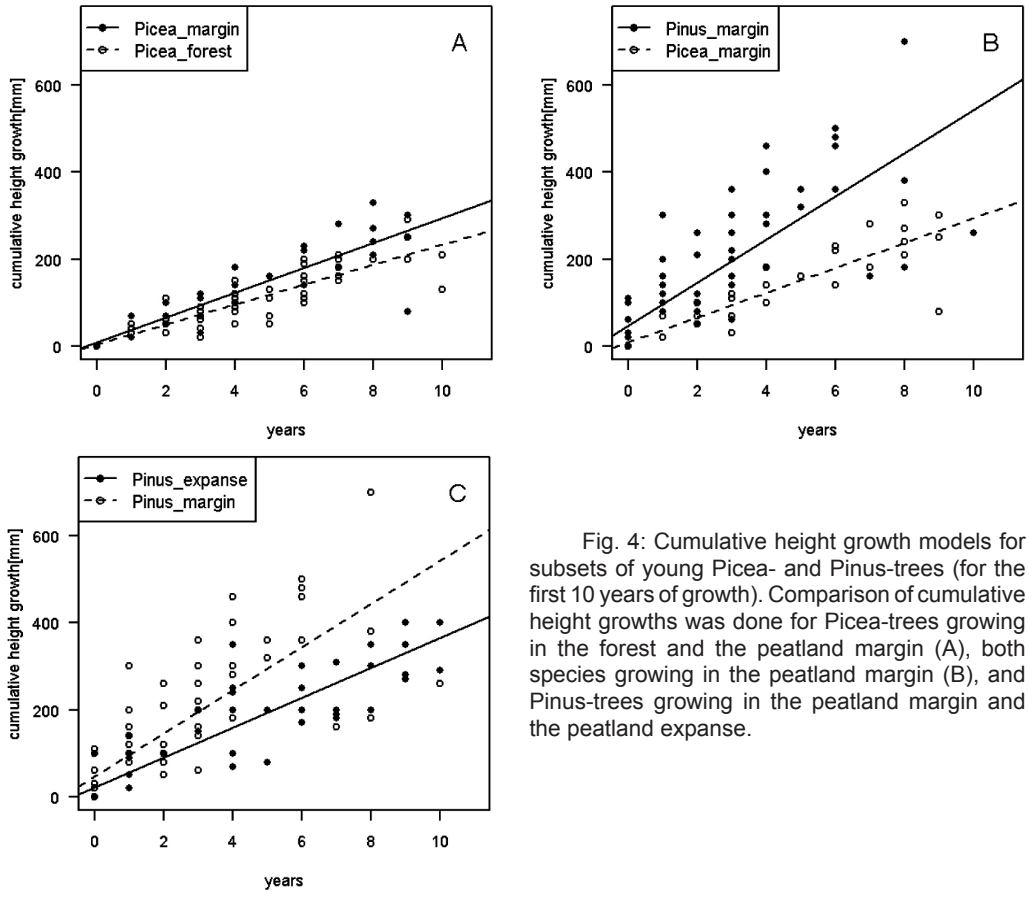

Fig. 4: Cumulative height growth models for subsets of young Picea- and Pinus-trees (for the first 10 years of growth). Comparison of cumulative height growths was done for Picea-trees growing in the forest and the peatland margin (A), both species growing in the peatland margin (B), and Pinus-trees growing in the peatland margin and the peatland expanse.

by a linear regression model ($y = 2.80–0.02x$; adjusted RI = 0.41; $p < 0.001$; $n = 43$). Mean yearly PGR decreases with age and thus, younger trees generally indicate a higher PGR than older individuals. The relationship between PGR and age showed for young trees in the age class 11-30 years a linear negative correlation ($r = -0.69$; $p < 0.001$; $y = 3.43–0.05x$; $n = 25$), while PGR and age did not significantly correlate for trees between 31 and 60 years. However, since the two individuals between 31 and 40 in the dataset did neither significantly lower the correlation in the PGR – age relationship for young trees ($r = -0.62$; $p < 0.001$) nor significantly change the linear regression model ($y = 3.17–0.04$ x; adjusted $R^2 = 0.36$; $p < 0.001$; $n = 27$), they were included in the calculation of compaction corrected vertical peat growth rates.

The estimated site specific compaction rate α for the whole dataset was 0.144 $year^{-1}$, which corresponds to an annual compaction of 14.4%. The associated compaction corrected vertical peat growth rates (CPGRs) had an overall mean value (± standard deviation) of 35.8 ± 12.3 mm/year ($n = 27$). Mean CPGRs ± SD for the peatland margin ($n = 20$) were 33.4 ± 11.8 mm/year with 12.5% annual compaction, and those for the peatland expanse ($n = 7$) were 32.4 ± 9.8 mm/year with 14.4% compaction per year. There was no significant difference in variance or mean of the CPGRs from both peatland zones. Calculated CPGRs were de-

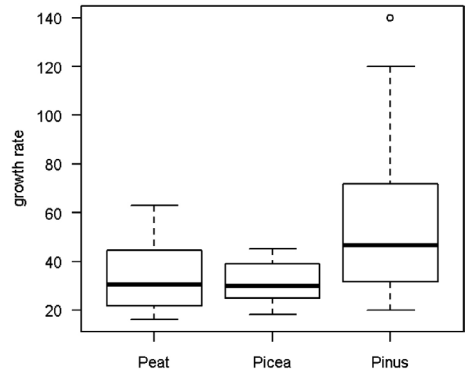

Fig. 5: Comparison of the growth rates for peat (corrected for compaction), Picea and Pinus in the peatland expanse.

tected to influence growth of young trees. The height growth rate of trees was positively correlated with CPGRs ($p < 0.01$).

In the peatland expanse, where data on the height growth rate of both studies species was recorded, CPGR was slightly higher than HGR of young Picea trees, while it was lower than HGR of young Pinus trees (Fig. 5).

DISCUSSION

The struggle of Picea and Pinus trees with the growing Sphagnum mosses

Sphagnum – species are the main peat forming plants in boreal peatlands and provide a moist and light substrate suitable for the germination of tree seedlings (Gunnarsson and Rydin, 1998; Rydin et al., 2006). However, after germination, the trees have to grow faster than the surrounding Sphagnum. If not, they become overgrown and die off. The interaction between specimens of *Pinus sylvestris* and Sphagnum mosses can be fatal (Ohlson et al., 2001). The height growth abilities of young trees in this study showed, however, that pine trees seem to cope well with the growing Sphagnum. At least for the sampled trees, which survived the seedling stage, it has been shown that growing mosses may even enhance the height growth of the young pine trees. Pinus is a pioneer tree species showing fast initial height growth under light canopy conditions. These are given in the peatland expanse, but closer to the peatland margin shading of other tree species inhibit pine growth. For individuals of Picea, which showed a much slower height growth than Pinus, the interaction with the growing mosses might be more important. The height growth rates of Picea found in the peatland did not differ from the rates found on the adjacent mineral soils and were consistent with rates reported for suppressed individuals of *Picea abies* in Norwegian forests (Niklasson, 2002). Thus, the ability to enhanced height growth in Picea – trees is low and *Sphagnum* is likely to overgrow rather young spruce than pine seedlings. This might be a cause for the species turn-over from the peatland margin to the peatland expanse and might contribute to the explanation why *Pinus sylvestris* is the main tree species colonizing boreal peatlands in this region (Walter and Breckle, 1994).

Dating of trees growing in a peatland environment and missing outer rings

The depth of the original germination point of trees growing in a peatland has been shown to be highly variable. The bending in the lower stem sections as well as the large scatter of individual height growth rates of trees detected in the dataset reveal the necessity to sample whole individuals up to their roots in order to obtain the true ages of peatland trees. However, pulling up of peatland trees is only the starting point for a correct age determination which is crucial when trees are used as a proxy to date surface peat and to estimate peat height growth rates. Peatlands represent a distributional margin for most trees (Wilm-

king et al., 2012) and with the growing peat surface and the subsequent burial of the tree stem, peatland trees are subjected to permanently changing environmental conditions (Smiljanic et al., 2014). The trees' reactions to these extreme site conditions include changes in wood anatomy and growth patterns which can influence a successful age determination. During dating of peatland trees for this study several of these modifications were detected and considered.

The bending of the below-ground proportion of tree stems is a common phenomenon in peatland trees. It leads to the formation of eccentric and wedging rings and is considered to be a reaction of the tree to compensate imbalance (Schweingruber et al., 2006). This imbalance can be caused by the unstable rooting ground in peat, the weight of snow cover on young trees, as well as by growth and subsequent compaction of surface peat (Schulze et al., 2002; Schweingruber et al., 2006). Dating of trees was further complicated by the fact that many of the extracted trees did not show distinct ring-boundaries in the lower stem section. The ring-boundaries became more root-like, which means that latewood cells were smaller and cell walls thinner (Schweingruber, 2007). This phenomenon might be caused by at least two factors. Firstly, the deeply embedded stems are protected in the peat and thus subject to less mechanical stress (Schweingruber, 2007). And secondly, due to heat insulation from the overlaying moss layer in combination with the high heat capacity of the water-logged peat, annual temperature changes are buffered. Dyukarev et al., (2009), for example, reported an annual air temperature fluctuation of 64.4 °C for a bog in Western Siberia. In a peat depth of 10 cm and 40 cm below the surface, these differences were only 19.1 °C and 8.6 °C, respectively. The more stable temperature regime in deeper peat layers may lead to a less pronounced influence of seasons on tree-ring formation.

In addition, the occurrence of missing outer rings in the lower stem section complicated the correct dating of peatland trees. Missing outer rings may lead to a substantial underestimation of the true tree ages when counting tree rings only at hypocotyl level. Missing rings at lower stem sections have been shown for a variety of woody plants in stressful environments, mainly for shrubs at high elevations (Kolishchuk, 1990; Hallinger et al., 2010;), suppressed trees under a dense canopy (Niklasson, 2002), or trees in peatlands (for an overview see Wilmking et al., 2012). There are several possible reasons for the occurrence of missing outer rings (such as drought or insect infestation), but for trees growing in peatlands, nutrient limitation, oxygen deficiency due to a rising catotelm and a short growing season caused by lagged temperature responses in deeper peat layers seem to be contributing factors. In peatlands that are mainly fed by precipitation, nutrient limitation for trees might be enhanced by *Sphagnum* mosses which form a close ground cover with their capitulum and thus effectively trap nutrients from rainwater before they can reach the root zone of trees (Rydin and Jeglum, 2006). The influence of the autogenic rising water table and thus the subsequent incorporation of tree roots in the anoxic zone is a factor which has been demonstrated partly within this study. Although missing outer rings occurred in both, the oxic and the anoxic zone of the peat columns, no tree was found that rooted in the anoxic zone and managed to build the complete tree-ring pattern. Furthermore it has been shown that many trees of the dataset did not build the current year's growth ring until the tree sampling in July. This seems to reflect a shortening of the growing season in deeper peat layers. The thermal regime of the peat layers lead to a time lag between temperature changes at the surface and

responses in the peat. In a peatland in Western Siberia, for example, the temperature peak at surface and in a depth of 40 cm occurred with a lag of about one month (Dyukarev et al., 2009). Although low peat temperatures are expected to slow down the initiation of cambial activity from the apical growing point down to the stem base, it is unlikely that this factor alone may account for missing outer rings in successive years (Wilmking et al., 2012).

During the analysis of tree samples it turned out that serial sectioning and within-tree cross-dating (Kolishchuk, 1990; Niklasson, 2002) are not only a useful tool to detect wedging rings and measurement errors, but in fact an essential method to obtain reliable age determinations for peatland trees.

Dating of peat columns and estimation of vertical peat growth in the acrotelm with the 'hypocotyl method'

The 'hypocotyl method' is a useful tool to estimate recent peat height growth rates in peatland environments when trees are present. It has been applied e.g. to estimate recent carbon uptake rates in boreal peatlands (Ohlson and Økland, 1998; Schulze et al., 2002). Limitations of this approach are given by absolute tree ages and the spatial resolution of sampling a vertical peat column, which is increasingly compacted with depth. Furthermore, the oxygen demand of tree roots restrains the use of the 'hypocotyl method' to peat growth processes in the upper aerobic peat layer. With the autogenic rising water table in the peatland, the growing conditions for peatland trees deteriorate as a result of anoxic conditions and trees die off (Ohlson and Dahlberg, 1991; Schulze et al., 2002).

The time interval of 40 years obtained in this study, where the linear relationship between ln-transformed vertical peat growth rates and age is significant, is in line with other studies (Ohlson and Dahlberg, 1991; Ohlson and Økland, 1998; Ohlson et al., 2001; Økland and Ohlson, 1998). In this study the sampled trees were generally relatively young (oldest individual 122 years) and the sample size above 60 years was too limited to further test the relationship between peat height above the hypocotyl and tree age for trees exceeding this age.

In general, as shown above, correct dating of tree growth initiation in relation to peat stratigraphy is a prerequisite for the successful application of this technique. While endogenic factors such as missing outer rings can cause problems in dating, exogenic disturbances of the hypocotyl position may occur as well (such as trampling by animals, bioturbation and windfall) and cause substantial dating errors. While exogenic factors are difficult to assess, it might be worthwhile to briefly discuss possible dating errors and their consequences on calculated peat growth rates due to endogenic factors. One third of the trees that were younger than 40 years and thus used to estimate vertical peat growth rates, showed missing outer rings. Continuously missing outer rings (Wilmking et al., 2012), however, were only found in older individuals, while in the younger trees often only the current year's growth ring was missing. When serial sectioning would not have been applied, the underestimation of absolute tree ages would have led to an overestimation of peat height growth (same amount of peat growth divided by a smaller number of years) of around 11% in the peatland expanse, while it would have had no influence on the mean vertical peat growth rate at the margin. This pattern is, however, caused by the fact that trees in the peatland expanse showed more often missing rings than trees growing in the margin. In single peat columns missing outer rings would have led to an overestimation of vertical peat growth rates of approx. 10% for young trees in both, the

peatland margin and the expanse. Continuously missing outer rings in older individuals can lead to an overestimation of vertical peat growth rates up to 25%.

In summary, a larger sample size would have allowed for a better assessment of the spatial variability of peat height growth rates along the studied transect, and possibly an extension of the window of tree ages usable for peat growth determination beyond the 40 years shown in the literature and this study. In theory, this should be possible, especially when applying the serial sectioning technique to larger and presumably older trees, but it may also yield false information since larger trees are expected to slow down peat growth in their understorey (Ohlson et al., 2001).

Spatial variation of peat-forming processes in the acrotelm

The application of the 'hypocotyl method' on Clymo's model for peat growth in the acrotelm (Clymo, 1984; Økland and Ohlson, 1998) provided values for the two key processes that are expected to control the rate of peat formation: namely the growth of the peat forming vegetation and the successive compaction of dead organic matter (Malmer and Wallen, 2004). The corresponding age and depth measurements for peat columns in the studied peatland showed that deeper peat layers are in general older than peat layers closer to the surface. This general pattern is an inherent feature of peat columns since each new layer of the peat forming vegetation grows up directly on top of the dead organic matter from previous growing seasons (Joosten and Succow, 2001). However, on shorter time-scales this pattern was less pronounced and peat layers of the same age were found to be situated in different depths relative to the peat surface. Assuming that no external factor has forced the hypocotyls of trees to change their position relative to deeper peat layers (i.e. to penetrate down into the peat), the internal processes in peat formation must be taken into consideration to explain the deviation from the general pattern. The imbalance between productivity and decomposition defines the rate of peat formation (Joosten and Succow, 2001; Malmer and Wallen, 2004; Moore and Basiliko, 2006; Wieder 2006). Thus the spatial variation of productivity and decomposition in a peatland may lead to differences in peat growth and consequently to a within-site variation in the age-depth relationship of peat layers (as shown as well by Ohlson and Dahlberg, 1991; Ohlson and IIIkland, 1998; Økland and Ohlson, 1998). The low correlation between age and depth measurements for certain time windows in the dataset may thus be explained by the variable growth and productivity (Ohlson and Dahlberg, 1991; Wieder, 2006) or by differences in decay resistance (Moore and Basiliko, 2006) of the peat forming vegetation. An additional factor that leads to variation in surface peat compaction is the occurrence of dwarf shrubs that can strengthen the peat matrix with their high below-ground compound (Ohlson and Dahlberg, 1991).

The two designated peatland zones, i.e. peatland margin and peatland expanse, were expected to express variation in recent peat growth on a microtope scale, while micro-site differences operate on a smaller nanotope scale (for an overview of scale levels of mire surfaces see Couwenberg and Joosten, 1999). However, the trees in Medla-Pev-Nyur were primarily found on hummocks which were elevated 30 cm or more above the estimated minimum water table in summer and thus did not allow for comparison of distinct micro-site levels as applied in similar studies (Ohlson and Dahlberg, 1991; Økland and Ohlson, 1998). Since the mean height of micro-sites supporting tree growth was nearly the same

in both peatland zones (44 cm above the water table in the peatland margin and 41 cm in the peatland expanse), compaction corrected peat growth and site-specific compaction rates could be calculated to account for differences on a microtope scale. The analysis revealed that differences between peatland zones were marginal. This is in line with the findings of other authors (Ohlson and Dahlberg, 1991; Økland and Ohlson, 1998) who stated that the peatland-specific hydrology is the most decisive factor for peat accumulation. The site specific compaction rate and the compaction corrected peat growth rates for 'Ust Pojeg' were analogue to rates reported by other studies (Ohlson and Økland, 1998; Økland and Ohlson, 1998). However, the 'hypocotyl method' may overestimate peat growth in the acrotelm since trees grew mainly on hummocks, while micro-sites that do not support tree growth were neglected (Schulze et al., 2002). The extension of the 'hypocotyl method' on dwarf shrubs growing on lower elevated micro-sites might be a promising tool to investigate differences in peat growth on a nanotope scale. This would also need a better understanding of the spatial resolution and the relative importance of different micro-sites within peatland zones.

References

Bauer, I. E., J. S. Bhatti, C. Swanston, R. K. Wieder, and C. M. Preston. 2009. Organic Matter Accumulation and Community Change at the Peatland-Upland Interface: Inferences from C-14 and Pb-210 Dated Profiles. *Ecosystems* 12: 636-653.

Borggreve, B. 1889. Über die Messung des Wachstums von Hochmooren. *Mitteilungen des Vereins zur Fųrderung der Moorkultur im Deutschen Reiche* 7: 20-23.

Clymo, R. S. 1984. The limits to peat bog growth. *Philosophical Transactions of the Royal Society of London Series B-Biological Sciences* 303: 605-654.

Couwenberg, J. and H. Joosten. 1999. Pools as missing links: The role of nothing in the being of mires. In *Patterned mires and mire pools - Origin and development; flora and fauna.* Ed. V. Standen, J. Tallis, and R. Meade, 87-102. British Ecological Society.

DesRochers, A. and R. Gagnon, 1997. Is ring count at ground level a good estimation of black spruce age? *Canadian Journal of Forest Research-Revue Canadienne De Recherche Forestiere* 27: 1703-1703.

Dyukarev, E. A., E. A. Golovatskaya, A. D. Duchkov, and S. A. Kazantsev. 2009. Temperature monitoring in Bakchar bog (West Siberia). *Russian Geology and Geophysics* 50: 579-586.

Ellenberg, H. 1992. Zeigerwerte von Pflanzen in Mitteleuropa. Goltze.

Fritts, H. C. 2001. Tree rings and climate. Blackburn Press.

Grissino-Mayer, H. 2001. Evaluating Crossdating Accuracy: A Manual and Tutorial For The Computer Programm COFECHA. *Tree-Ring Research* 57: 205-221.

Gunnarsson, U. and H. Rydin, 1998. Demography and recruitment of Scots pine on raised bogs in eastern Sweden and relationships to microhabitat differentiation. *Wetlands* 18: 133-141.

Hallinger, M., M. Manthey, and M.Wilmking. 2010. Establishing a missing link: warm summers and winter snow cover promote shrub expansion into alpine tundra in Scandinavia. New Phytologist.

Holmes, R. L. 1999. Users Manual for Program COFECHA. Laboratory of Tree-Ring Research, University of Arizona, Tucson, Arizona USA.

Joosten, H. and Succow, M. (eds.) 2001. Landschaftsökologische Moorkunde. E. Schweitzerbart'sche Verlagsbuchhandlung.

Jurasinski, G. 2007. simba: A collection of functions for similarity calculation of binary data. R package version 0.2-5. http://www.r-project.org.

Kaennel, M., and F. H. Schweingruber. 1995. Eidgenössische Forschungsanstalt für Wald Schnee und Landschaft. Multilingual glossary of dendrochronology: terms and definitions in English, German, French, Spanish, Italian, Portuguese and Russian. – Haupt.

Koff, T., J. M. Punning, and M. Yli-Halla, 1998. Human impact on a paludified landscape in northern Estonia. Landscape and Urban Planning 41: 263-272.

Kolishchuk, V. G. 1990. Dendroclimatological Study of Prostrate Woody Plants. In: *Methods of Dendrochronology: Applications in the Environmental Sciences*, ed. E. R. Cook, and L. A. Kairiukstis. Kluwer Academic Publishers & International Institute for Applied Systems Analysis.

Kozlowski, T. T., S. G.Pallardy, T. K. Theodore, and G. P. Stephen. 1997. Vegetative Growth. In: *Physiology of Woody Plants (Second Edition)*, 34-67. Academic Press.

Kramer, H., and A. Akça. 2008. Leitfaden zur Waldmesslehre. Sauerlдnder.

Malmer, N., and B. Wallen, 2004. Input rates, decay losses and accumulation rates of carbon in bogs during the last millennium: internal processes and environmental changes. *Holocene* 14: 111-117.

Moore, T. and Basiliko, N. 2006. Decomposition in Boreal Peatlands. In *Boreal Peatland Ecosystems*, ed. R. K. Wieder, and D. H. Vitt, 124-143. Springer.

Niklasson, M. 2002. A comparison of three age determination methods for suppressed Norway spruce: implications for age structure analysis. *Forest Ecology and Management* 161: 279-288.

Norton, D. A. and J. Ogden. 1990. Problems with the Use of Tree Rings in the Study of Forest Population Dynamics. In *Methods of Dendrochronology: Applications in the Environmental Sciences*, ed. E. Cook, and L. A. Kairiukstis. Kluwer Academic Publishers and International Institute for Applied Systems Analysis.

Ohlson, M. 1995. Growth and nutrient characteristics in bog and fen populations of Scots Pine (Pinus-sylvestris). *Plant and Soil* 172: 235-245.

Ohlson, M. and B.Dahlberg. 1991. Rate of peat increment in hummock and lawn communities on Swedish mires during the last 150 years. *Oikos* 61: 369-378.

Ohlson, M., and R. H. Økland. 1998. Spatial variation in rates of carbon and nitrogen accumulation in a boreal bog. *Ecology* 79: 2745-2758.

Ohlson, M., R. H. Økland, J. F. Nordbakken, and B. Dahlberg, 2001. Fatal interactions between Scots pine and Sphagnum mosses in bog ecosystems. *Oikos* 94: 425-432.

Økland, R. H., and Ohlson, M. 1998. Age-depth relationships in Scandinavian surface peat: a quantitative analysis. *Oikos* 82: 29-36.

Økland, R. H., T. Økland, and K. Rydgren. 2001. A Scandinavian perspective on ecological gradients in north-west European mires: reply to Wheeler and Proctor. *Journal of Ecology* 89: 481-486.

R Development Core Team. 2009. R: A language and environment for statistical computing. R Foundation for Statistical Computing.Vienna, Austria. ISBN 3-900051-07-0, URL http://www.R-project.org.

Rinn, F. 2003. TSAP-Win, Time Series Analysis and Presentation for Dendrochronology and Related Applications. Version 0.53, User Reference.

Rydin, H., Gunnarsson, U. and Sundberg, S. 2006. The Role of Sphagnum in Peatland Development and Persistence. In: *Boreal Peatland Ecosystems,* ed. R. K. Wieder, and D. H. Vitt. 47-65. Springer

Rydin, H. and Jeglum, J. K. 2006. The biology of peatlands. – Oxford University Press.

Schulze, E. D., A. Prokuschkin, , A. Arneth, N. Knorre, and E. A. Vaganov. 2002. Net ecosystem productivity and peat accumulation in a Siberian Aapa mire. *Tellus Series B-Chemical and Physical Meteorology* 54: 531-536.

Schweingruber, F. H. 1988. Tree rings: basics and applications of dendrochronology. D. Reidel Pub. Co., Sold and distributed in the U.S.A. and Canada by Kluwer Academic Publishers.

Schweingruber, F. H. 1996. Tree Rings and Environment. Dendroecology. Haupt.

Schweingruber, F. H. 2007. Wood structure and environment. Springer.

Schweingruber, F. H., A. Börner, and E. D. Schulze. 2006. Atlas of woody plant stems: evolution, structure, and environmental modifications. Springer.

Shroder, J. F. 1978. Dendrogeomorphological analysis of mass movement on Table Cliffs Plateau, Utah. *Quaternary Research* 9: 168-185.

Smiljanić, M., Seo, J.-W., Läänelaid, A., van der Maaten-Theunissen, M., Satjić, B. and M. Wilmking. 2014. Peatland pines as a proxy for water table fluctuations: Disentangling tree growth, hydrology, and possible human influence. *Science of the Total Environment* 500-501: 52-63.

Turetsky, M. R., S. W. Manning, and R. K. Wieder. 2004. Dating recent peat deposits. *Wetlands* 24: 324-356.

Vitt, D. H. 2006. Functional Characteristics and Indicators of Boreal Peatlands. In *Boreal Peatland Ecosystems*, ed. R. K. Wieder, and D. H. Vitt, 9-24. Springer.

Walter, H., and S.-W. Breckle. 1994. Spezielle Ökologie der Gemäßigten und Arktischen Zonen Euro-Nordasiens. Gustav Fischer.

Wieder, R. K. 2006. Primary Production in Boreal Peatlands. In *Boreal Peatland Ecosystems*, ed. R. K. Wieder, and D. H. Vitt . Springer.

Wilmking, M., Hallinger, M., Van Bogaert, R., Kyncl, T., Babst, F., Hahne, W., Juday, G., de Luis, M., Novak, K. and C. Völlm, 2012. Continuously missing outer rings in woody plants at their distributional margins. *Dendrochronologia* 30: 213-222.

Chapter 7
PHOTOSYNTHETIC PRODUCTIVITY OF PEATLAND PLANT COMMUNITIES AT MESOOLIGOTROPHIC

Northern peatlands are known as relatively stable sink of atmospheric carbon dioxide (Vompersky, 1994). Microlandscape, hydrological and nutrition regimes are responsible for plant cover mosaic structure and CO_2 gas exchange in different plant communities of the peatland. Depressions where ground waters locate close to soil surface are normally a stable sink of carbon dioxide from atmosphere whereby micro-elevations are a usual source (Heikkinen et al., 2002; Maanavilja et al., 2011; Mikhailov et al., 2011). Primary photosynthetic productivity at ombotrophic peatland calculated by the chlorophyll index equals 200 g m^{-2} whereas the annual photosynthetic carbon sink (net ecosystem productivity – NEP) from atmosphere into peatland was 83 g m^{-2} (Voronin et al., 1995). The purpose of the present work was to estimate the photosynthetic productivity in plant communities of the mesooligotrophic peatland in the middle taiga subzone.

MATERIALS AND METHODS

Three plant communities on two different sites in the centre of peatland Medla-Pev-Nyur were investigated. The elevated oligotrophic site had mosaic microrelief and plant cover. The first plot was on hummocks and was dominated by communities **1)** ***Chamaedaphne calyculata + Vaccinium uliginosum + Rubus chamaemorus – Sphagnum fuscum***. The hollow was dominated by **2)** ***Eriophorum vaginatum – Sphagnum fallax+ Sphagnum angustifolium***. The third plot was on mesotrophic site and was dominated by sedge-sphagnum communities **(3)** ***Carex rostrata + Scheuchzeria palustris + Oxycoccus palustris – Sphagnum fallax***. Plant samples were collected in late July-early August when aboveground shoots finished their growing. Aboveground biomass of plants was measured by clipping five sample plots 20×20 cm in every community and sorting the material by species and into leaves and shoots according to the standard methods (Khramov, Valutsky, 1977). Sphagnum biomass was measured by clipping at the base of the capitululum. Plant tissues were oven-dried at 80 °C.

Leaves of dominating plant species were collected additionally for pigment content determination. Mixed leaf sample from all communities was fixed in boiling acetone in threefold replication according to the standard methods (Shlik, 1971). Chlorophyll and carotenoid concentration was measured by the UV-1700 spectrophotometer (Shimadzu, Japan). The obtained values were recalculated for absolutely dry weight.

The visual photosynthesis of dominating plant species was registered by the gas analyzer Li 6400 (LiCor, USA) and light Conifera camera. For dwarf shrubs and grasses, measurements were attributed to safe (non-cut) leaves and shoots from 10 a.m. to 3 p.m. hours in threefold replication. For Sphagnum mosses, we

used aboveground green parts. The photosynthesis rate was started to be registered 3-5 min after material had been put into camera with a 1-min interval. Measurement continued 10-15 min for each sample. The obtained values were recalculated for absolutely dry weight. PAR (physiologically active radiation), air temperature, and moisture content were registered by internal camera sensors.

RESULTS AND DISCUSSION

About 120 species of dwarf shrubs and grasses were observed at mesooligotrophic peatland, but only ten plant species was dominating in aboveground biomass experimental plots. The mass of leaves ranged across three sites from 620 to 934 g m^{-2} (Table 1), it is dominated by Sphagnum.

Table 1

Mass of leaves (g m^{-2}) in different communities at mesooligotrophic peatland (Mean ± SE)

Plant species	Community number*		
	1 (n=5)	2 (n=5)	3(n=5)
Polytrichum strictum	10.7±5.4	0	0
Sphagnum sp.	542.5±33.7	847.5±304.8	376.0±38.3
Carex paupercule	0	2.0±1.0	27.0±3.5
Carex rostrata	0	0	159.5±76.0
Carex limoza	0	0	25.1±3.5
Eriophorum vaginatum	9.5±7.1	0	0
Scheuchzeria palustris	0	56.0±25.5	0
Ledum palustre	0	15.48±7.2	0
Chamedaphne calyculata	66.7±38.3	2.60±0.5	0
Andromeda polyfolia	19.0±4.1	0	0
Oxycoccus palustris	19.9±8.3	10.0±6.6	19.9±5.5
*Vaccinium uliginos*um	0	0	5.1±2.5
Total	668.3	933.6	612.6

Note: * communities are described in text.

Dwarf shrubs become abundant on oligotrophic hummocks and grasses – in mesotrophic sedge-sphagnum communities (Fig. 1). The "green" biomass at peatlands of Western Siberia varies from 180 to 555 g m^{-2} (Efremova et al., 1994). Chloroplast pigment content in Sphagnum mosses was by two times less than in vascular plants, and photosynthesis was very low (Table 2).

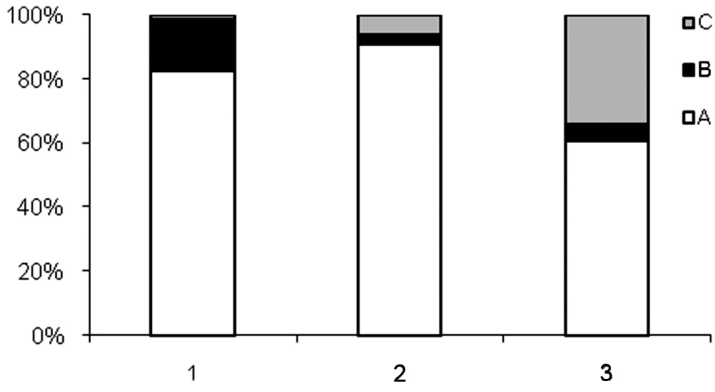

Fig. 1: Distribution of leaf mass between sphagnum mosses (A), dwarf shrubs (B), and grasses (C) in communities of mesooligotrophic peatland. *1-3* – community numbers correspond to those in text.

Table 2

Photosynthesis and pigment content in leaves of some peatland plants in August (T_{air} = 18-25 °C, PAR > 1000 μmol CO_2 $g^{-1}s^{-1}$, RH > 60%)

Plant species	Photosynthesis rate, μmol CO_2 $g^{-1}s^{-1}$	Content of *a+b* chlorophylls, mg g^{-1}	Content of carotenoids, mg g^{-1}
Grasses:			
Menyanthes trifoliata	0.063±0.006	3.723±0.752	1.184±0.199
Rubus chamaemorus	0.059±0.012	3.036±0.217	0.681±0.065
Scheuchzeria palustris	–	2.310±0.158	0.847±0.078
Carex rostrata	0.018±0.005	2.068±0.183	0.983±0.052
Average	0.047	2.783	0.923
Dwarf shrubs:			
Betula nana	0.048±0.006	2.926±0.148	0.602±0.008
Chamaedaphne calyculata	0.080±0.020	2.092±0.140	0.686±0.041
Andromeda polyfolia	0.075±0.015	3.752±0.209	0.949±0.030
Ledum palustre	0.046±0.009	–	–
Oxycoccus palustris	0.031±0.004	2.506±0.593	0.593±0.103
Vaccinium uliginosum	0.079±0.019	–	–
Average	0.060	2.819	0.708
Sphagnum sp.	0.005±0.002	1.447±0.220	0.475±0.039

Note: "–" means no data.

In the same time, the potential photosynthesis of Sphagnum mosses comprises 0.0086 μmol CO_2 $g^{-1}s^{-1}$ (Voronin et al., 1997) which exceeds our data by almost twice. Sedge and cranberry also have low rate of photosynthesis. In contrast to deciduous species, winter-green dwarf shrubs hold leaves on shoots for two years. In two-year-old leaves of *Chamedaphne calyculata* and *Ledum palustre* photosynthesis was lower by 1.5-2 times in April compared to July. Some authors associate low photosynthesis of winter-green dwarf shrubs in spring with a negative impact of frequent soil frosts on root system and transpiration water flow rate through stomatos (Maanavilja et al., 2011). According to other authors, temperature rise in root zone from April to June increases nitrogen and chlorophyll *a* content in plant leaves and so advances gross-photosynthesis in peatland phytocoenoses (Moore et al., 2006).

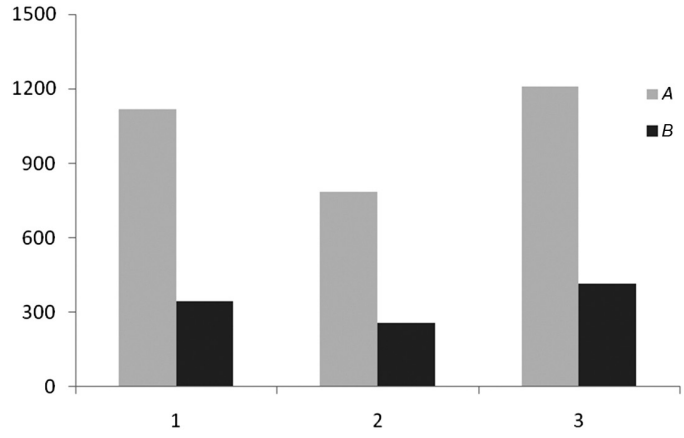

Fig. 2: Content of chlorophylls (A) and carotenoids (B) in peat plant communities in August, g m^{-2}. 1-3 – community numbers correspond to those in Table 1.

Chlorophyll index or projective content of chlorophyll is one of the common assessment methods of photosynthetic carbon sequestration in plants. The annual photosynthetic carbon sink value for continuous sphagnum cover at top peat makes 83 g C m^{-2} (Voronin et al., 1995).

The chlorophyll index for three communities in Medla-Pev-Nyur varied from 1.1 to 1.4 g C m^{-2} (Fig. 2). It is a fact that 1 kg chlorophyll per 1 ha sequestrated of 145 kg C from atmosphere during vegetation (Voronin et al., 1995). In this case the annual photosynthetic sink in oligotrophic plant community on hummock will be 162, in hollows – 212, and in mesotrophic community – 175 g C m^{-2}.

CONCLUSION

The carbon sink increasing in plant communities dominated by grasses in biomass of peatland Medla-Pev-Nyur. Sphagnum mosses had a low photosynthesis rate but as they have low temperature optimum of photosynthesis they can assimilate carbon from atmosphere for a longer period of time in spring and autumn compared with grasses and dwarf shrubs (Kurets et al., 1993). According to the earlier gas exchange measurements by the method of static cameras at mesooligotrophic petland, carbon dioxide sequestration exceeds its flux into atmosphere in hollows with grasses and sphagnum mosses (Mikhailov et al., 2011). In our study, the same plant communities have high chlorophyll content in leaves and active photosynthetic carbon stock.

References

Efremova. T.T., S.P. Efremov, N.P. Kosykh, N.P. Mironycheva-Tokareva, and A.A. Titljanova. 1994. Biological productivity and peat soils of south Vasyuganya. *Sibirskiy ekoogicheskiy zhurnal* 3: 253-267.

Heikkinen. J.E.P., V. Elsakov, and P.J. Martikainen. 2002. Carbon dioxide and methane dynamics and annual carbon balance in tundra wetland in NE Europe, Russia. *Global Biogeochemical Cycles* 16(4): 62-77.

Khramov, A.A., and V.I. Valutsky. 1977. Forest phytocenoses of West Vasyuganya. Novosibirsk: Nauka.

Kurets, V.K., E.N.Ikkonen, Yu.Alm, A. Talanov, S.N Drozdov, E. Silvova, and E.G. Popov. 1998. Influence of temperature-and-light regime and ground water level on CO_2-gas exchange at open plot of oligotrophic peatland. *Ekologia* 1: 14-18.

Maanavilja, L., T. Riutta, M. Aurela, M. Pulkkinen, T. Laurila, and E-S. Tuittila. 2011. Spatial variation in CO_2 exchange at a northern aapa mire. *Biogeochemistry* 104: 325-345.

Mikhailov, O.A., S.V. Zagirova, M.N. Miglovets, Y. Shnaider, M. Gagovich, and L. Kutzbach. 2011. Assessment of carbon dioxide fluxes in plant communities of mesooligotrophic middle-taiga peatland. *Teoreticheskaya i prikladnaya ekologia* 2: 44-51.

Moore, T., P. Lafleur, D. Poon, B. Heumann, J. Seaquist, and N. Roulet. 2006. Spring photosynthesis in a cool temperate bog. *Global Change Biology* 12: 2323-2335.

Moore, T., J. Bubier, S. Frolking, P. Lafleur, and N. Roulet. 2002. Plant biomass and production and CO_2 exchange in an ombrotrophic bog. *Journal of Ecology* 90: 25-36.

Shlyk, A.A. 1971. Chlorophyll and carotenoids determination in extract of green leaves. In Biochemical methods in plant physiology, ed. **O.A. Pavlinskaia. 154-170. Moscow: Mir.**

Voronin, P.Yu., E.I. Efimtsev, A.A. Vasilyev, O. Vatkovskiy, and A.T. Mokronosov. 1995. Projective chlorophyll content and vegetation biodiversity of main botanic-geographical zones in Russia. *Russ. J. Plant Physiol.* 42(2): 295-302.

Voronin, Yu. P., A.V. Makeev, I.A. Gukas'an, A.A. Vasil'ev, E.V. Terent'ev, and A. T. Mokronosov 1997. Chlorophyll index and annual photosynthetic sink of carbon into sphagnum assosiations. *Russ. J. Plant Physiol.* 44 (1): 31-38.

Chapter 8
INTERANNUAL VARIABILITY OF CARBON DIOXIDE FLUXES IN MESOOLIGOTROPHIC PEATLAND

Research on CO_2 fluxes between the atmosphere and peatland ecosystem are important as are related with global climate warming. The models described in literature highlight a clear positive correlation between carbon cycle in terrestrial ecosystems and climate warming (Heimann and Reichstein, 2008). The studies conducted in different peatlands of the Northern hemisphere revealed highly variable carbon dioxide fluxes. The study aims to examine interannual variability of carbon dioxide fluxes at the mesoologotrophic peatland of the middle taiga subzone in summer.

METHODS

The studies were conducted at the mesoologotrophic peatland Medla-Pev-Nyur in 2012-2013. Vegetation cover is described in Chapter 1. The measurements based on micrometeorological eddy covariance method (EC). The equipments were placed at a height of 3.93 m from upper moss cover border. Microclimate parameters (air temperature and moisture, photosynthetic active radiation (PAR), incoming and outgoing solar radiation intensity, radiation balance) were registered using the automatic meteorological station with CR3000 logger (Campbell Scientific Inc., USA). This method means immediate identification of air turbulent flow direction and CO_2 concentration in this air flow at the measuring time (Baldocchi, 2003). The measuring system included three axis anemometer (Gill Instruments Ltd., USA) combined with open-path CO_2/H_2O gas analyzer (Li-7500A, Li-Cor Inc., USA). Data were registered at a 10-Hz-frequency rate. The obtained data were acquired by the EddyPro software (Li-Cor Inc., USA) and averaged by half-hourly period.

Subsequent data treatment included several stages. At the first stage, we identified best-quality measuring data flagged as '0' or '1' and deleted data flagged as '2' or marked with '−9999'. CO_2 gas exchange measurement errors could be caused by a row of factors (Foken, Wichura, 1996) as 1) instable work of the system, calibration, replacement of filters and parts; 2) insufficient air mixing at low turbulence; and 3) instable environmental factors. The next stage included qualitative assessment of the obtained data using the ratio of stability index in the atmospheric boundary layer (z/L) and footprint area ($d_{fetch70}$) to friction velocity (u^*) at the measuring time as it was described by the authors for greenhouse gas flux measurements in terrestrial ecosystems (Kutzbach et al., 2007; Lund et al., 2015). Finally, all flux data with $u^* < 0.1$ m s^{-1} were discarded. They were usually measured at night with low turbulence in the atmospheric boundary layer.

The CO_2 fluxes were gapfilled using the method proposed by Falge et al. (2001). Simultaneously we regarded co-variations of fluxes with meteorological variables and temporal auto-correlation of fluxes (Reichstein et al., 2005). For that, we used the online instrument of the Max Plank Institute (http://www.bgc-jena.mpg.de/~MDIwork/eddyproc/) which also allowed for partitioning CO_2 vertical fluxes into gross-photosynthesis (P_{gross}) and ecosystem respiration (R_{eco}). The volume of used data for statistic analysis is given in Table 1.

Table 1

Volume of used data from June, 10 till September, 10 2012-2013

Data volume	2012		2013	
	Number of points	%*	Number of points	%*
Before gap-filing	2920	65.4	3356	75.2
After gap-filing	4352	97.5	4051	90.7

* From total number of measuring points.

The obtained values on CO_2 vertical flux (F_{CO2}) corresponded with the net ecosystem carbon dioxide exchange (NEE) of peatland-atmosphere interaction. Total balance of carbon dioxide fluxes was calculated using of daily average values of CO_2 gas exchange ($Q > 20$ μmol m^{-2} s^{-1}). To reveal the interannual fluctuation of carbon dioxide fluxes we used data of June-September 2012 and 2013 where the system worked very stable.

RESULTS AND DISCUSSION

Weather conditions

The weather was different remarkably in June-September 2012 and 2013 (Table 2). June and July 2012 was warm with abundant rain cases. In August, mean monthly air temperature comprised +14.0 °C and rose towards +22.0 °C on August, 23-24. Precipitation exceeded the norm by 24%. The beginning of September saw frosts at night but mean monthly air temperature exceeded the norm by 2 °C. Precipitation in September was by 116% above the norm.

Table 2

Air temperature and precipitation in June-September 2012-2013*

Year	Month	Parameters			
		Mean monthly air temperature, °C	Deviation from the norm, °C	Precipitation, mm	% of the norm
2012	June	15.1	1.0	156	233
	July	17.3	1.0	165	239
	August	14.0	0.0	83	124
	September	9.0	2.0	145	216
2013	June	16.6	2.9	35	52
	July	19.0	3.0	32	46
	August	15.9	2.2	48	72
	September	8.5	1.0	36	54

* By the Centre on Meteorology and Environmental Monitoring of the Komi Republic for the Ust-Vyum station: Agrometeorological…, 2012; Agrometeorological…, 2013.

Summer 2013 was warm and dry. The weather in June was instable with strong air temperature fluctuations. In the first decade, there was no rain. The majority of rain fell in the second decade of June. The weather in July was hot and relatively dry, mean daily air temperature varied within +14...+21 °C with precipitation amount being half of the norm. August was warm with mean air temperature of +15 °C, rains were often. In September, weather was cool with abundant rains towards its end.

Carbon dioxide fluxes

For two observation years, we revealed similar features in the seasonal dynamics of carbon dioxide fluxes between peatland and atmosphere (Fig. 1).

CO_2 uptake from atmosphere to peatland gradually increased in May-June and reached peak values (−0.43...−0.44 mg $m^{-2}s^{-1}$) in mid July. Gradual decrease of CO_2 gas exchange was observed in the second half of vegetation period. In spite of different weather conditions, we did not recognize any statistically true interannual differences in mean monthly CO_2 gas exchange in 2012 and 2013 at the Medla-Pev-Nyur peatland (Table 3).

Our *NEE* values obtained by EC in July (Table 4) compared with published CO_2 gas exchange data from Northern Swedish mesotrophic peatland (Christensen et al., 2012) and Russian tundra (Marushchak et al., 2013) but exceeded data at the mesotrophic peatland in Northern Finland (Aurela et al., 2002) and grassy tundra in north Alaska (Kwon et al., 2006).

In mid vegetation period, P_{gross} value agreed well with previously reported range from Northern Finnish mesotrophic peatland (Aurela et al., 2002), European Russian south tundra (Marushchak et al., 2013), and Greenland mesotrophic peatland (Westergaard-Nielsen et al., 2013). Quite similar were R_{eco} values obtained by different authors for north peatlands.

Total carbon dioxide flux (*NEE*) between peatland Medla-Pev-Nyur and atmosphere from June, 10 till September, 10 2012 and 2013 was similar and corresponded −471.37 g m^{-2} and −432.50 g m^{-2}. For two years, it averaged −451.93±27.49 g

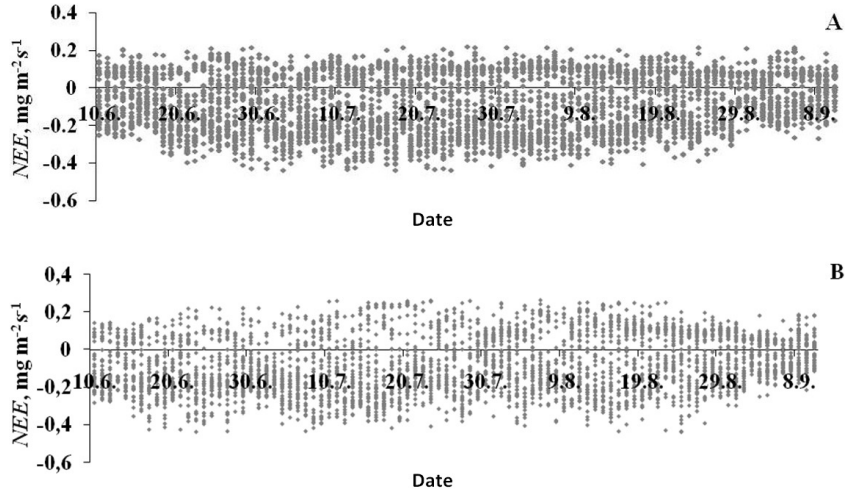

Fig. 1: The seasonal dynamics of carbon dioxide vertical fluxes for the period of June, 10 – September, 10 2012-2013 (*A* – 2012, *B* – 2013).

Table 3

Mean monthly carbon dioxide gas exchange values between peatland and atmosphere for June-September 2012-2013 (mg $m^{-2}s^{-1}$)

	June, 10-30		July, 1-31	
	2012	2013	2012	2013
NEE	–0.08±0.15	–0.11±0.14	–0.10±0.17	–0.10±0.16
R_{eco}	+0.10±0.02	+0.07±0.04	+0.11±0.02	+0.16±0.10
P_{gross}	–0.23±0.14	–0.26±0.21	–0.26±0.16	–0.32±0.24
	August, 1-31		September, 1-10	
	2012	2013	2012	2013
NEE	–0.06±0.16	–0.04±0.16	–0.01±0.11	–0.02±0.09
R_{eco}	+0.11±0.03	+0.12±0.04	+0.07±0.02	+0.04±0.02
P_{gross}	–0.21±0.16	–0.24±0.16	–0.14±0.10	–0.11±0.08

Table 4

Mean CO_2 gas exchange values obtained by EC in terrestrial ecosystems of the Northern hemisphere (mg $m^{-2}s^{-1}$)

Study area	Coordinates	Vegetation	*NEE* (mg $m^{-2}s^{-1}$)	R_{eco} (mg $m^{-2}s^{-1}$)	P_{gross} (mg $m^{-2}s^{-1}$)	Author
North Sweden	N 68°20′ E 19°03′	Mesotrophic peatland	–0.086±0.01	No data	No data	Christensen et al., 2012
North-East of European Russia	N 67°03′ E 62°56′	South tundra	–0.078	0.15	–0.23	Marushchak et al., 2013
Northern Finland	N 69°08′ E 27°17′	Mesotrophic peatland	–0.052±0.03	0.09±0.01	–0.14±0.03	Aurela et al., 2002
South-west Greenland	N 64°07′ E 51°21′	Mesotrophic peatland	–0.07	0.11	–0.18	Westergaard-Nielsen et al., 2013
North Alaska	N 71°19′ E 156°36′	Grassy tundra	–0.044±0.02	0.03±0.02	–0.07±0.04	Kwon et al., 2006
North-East of European Russia	N 61°56’ E 50°13’	Meso-oligotrophic peatland	–0.10±0.00	0.13±0.03	–0.29±0.04	Present paper

CO_2 m^{-2} (−123.25±7.50 g C m^{-2}) which agreed well with published data for northern peatlands. For instance, NEE value comprised −111.8±10.3 g C m^{-2} at mesotrophic peatland of Northern Norway from May till September (Lund et al., 2015) and −79±35 g C m^{-2} in south tundra of the northwestern Russia (Marushchak et al., 2013). Nevertheless NEE values at peatland Medla-Pev-Nyur almost twice exceeded balance of carbon fluxes at mesotrophic peatland of Northern Finland for the period of end June-mid September (Aurela et al., 2002). By perennial measuring results of CO_2 gas exchange at mesooligotrophic peatland of Northern Sweden, balance of vertical carbon dioxide fluxes within vegetation period possibly varies from −48 to −142 g C m^{-2} depending on ground water level (Peichl et al., 2014). Besides, meteorological factors play the leading role for vertical carbon fluxes at snow melting and early vegetation periods. We are seeing relative consistency in the carbon sink function at mesooligotrophic peatland Medla-Pev-Nyur in June-August 2012-2013. Despite interannual differences in weather conditions, gas exchange in 2012 and 2013 was similar. Peatland ecosystem was a sink of atmospheric carbon dioxide and accumulated 0.9 kg CO_2 m^{-2} in 2012-2013. Carbon flux values were comparable with that for mesotrophic and mesooligotrophic peatlands of the Northern hemisphere.

References

Agrometeorological Bulletin of the Agricultural Year 2012 of the Komi Republic. 2012. The Komi Republician Centre on Hydrometeorology and Environmental Monitoring. Syktyvkar.

Agrometeorological Bulletin of the Agricultural Year 2013 of the Komi Republic. 2013. The Komi Republician Centre on Hydrometeorology and Environmental Monitoring. Syktyvkar.

Aurela, M., T. Laurila, and J.-P. Tuovinen. 2002. Annual CO_2 balance of a subarctic fen in northern Europe: importance of the wintertime efflux. *Journal of Geophysical Research*: 107. doi:10.1029/2002JD002055

Baldocchi, D.D. 2003. Assessing the eddy covariance technique for evaluating carbon dioxide exchange rates of ecosystems: past, present and future. *Global change biology* 9: 479-492.

Christensen, T.R., M. Jackowicz-Korczynski, M. Aurela, P. Crill, M. Heliasz, M. Mastepanov and T. Friborg. 2012. Monitoring the multi-year carbon balance of a subarctic palsa mire with micrometeorological techniques. *Ambio* 41: 207-217.

Falge, E., D. Baldocchi, R. Olson, P. Anthoni, M. Aubinet, C. Bernhofer, G. Burba, R. Ceulemans, R. Clement, H. Dolman, A. Granier, P. Gross, T. Grünwald, D. Hollinger, N.-O. Jensen, G. Katul, P. Keronen, A. Kowalski, C. T. Lai, B. E. Law, T. Meyers, J. Moncrieff, E. Moors, J.W. Munger, K. Pilegaard, Ь. Rannik, C. Rebmann, A. Suyker, J. Tenhunen, K. Tu, S. Verma, and T. Vesala. 2001. Gap filling strategies for defensible annual sums of net ecosystem exchange. *Agricultural and Forest Meteorology* 107 (1): 43-69.

Foken, Th., and B. Wichura. 1996. Tools for quality assessment of surface-based flux measurements. *Agricultural and forest meteorology* 78: 83-105.

Heimann, M., and M. Reichstein. 2008. Terrestrial ecosystem carbon dynamics and climate feedbacks. *Nature* 451: 289-292.

Kutzbach, L., C. Wille, and E.-M. Pfeiffer. 2007. The exchange of carbon dioxide between wet arctic tundra and the atmosphere at the Lena River Delta, Northern Siberia. *Biogeosciences*. 4: 869-890.

Kwon, H-J., W.C. Oechel, R.C. Zulueta, and S.J. Hastings. 2006. Effects of climate variability on carbon sequestration among adjacent wet sedge tundra and moist tussock tundra ecosystems. Journal of Geophysical Research: 111. doi:10.1029/2005JG000036.

Lund, M., J.W. Bjerke, B.G. Drake, O. Engelsen, G.H. Hansen, F.J.W. Parmentier, T.L. Powell, H. Silvennoinen, M. Sottocornola, H. Tømmervik, S. Weldon, and D.P. Rasse. 2015. Low impact of dry conditions on the CO_2 exchange of a Northern-Norwegian blanket bog. *Environment research letters*. 10: doi:10.1088/1748-9326/10/2/025004.

Marushchak, M. E., I. Kiepe, C. Biasi, V. Elsakov, T. Friborg, T. Johansson, H. Soegaard, T. Virtanen, and P. J. Martikainen. 2013. Carbon dioxide balance of subarctic tundra from plot to regional scales. *Biogeosciences* 10: 437-452.

Peichl, M., M. Öquist, M. Ottosson Löfvenius, U. Ilsted, J. Sagerfors, A. Grelle, A. Lindroth, and M.B. Nilsson. 2014. A 12-year record reveals pre-growing season temperature and water table level threshold effects on the net carbon dioxide exchange in a boreal fen. *Environment research letters* 9 (5). doi:10.1088/1748-9326/9/5/055006.

Reichstein, M., E. Falgez, D. Baldocchi, D. Papale, M. Aubinet, P. Berbigier, C. Bernhofer, N. Buchmann, T. Gilmanov, A. Granier, T. Grünwald, K. Havrankova, H. Ilvesniemi, D. Janous, l A. Knoh, T. Laurila, A. Lohila, D. Loustau, G. Matteucci, T. Meyers, F. Miglietta, J.-M. Ourcival, J. Pumpanen, S. Rambal, E. Rotenberg, M. Sanz, J. Tenhunen, G. Seufert, F. Vaccari, T. Vesala, D. Yakir, and R. Valentini. 2005. On the separation of net ecosystem exchange into assimilation and ecosystem respiration: review and improved algorithm. *Global change biology* 11: 1424-1439.

Westergaard-Nielsen, A., M. Lund, B.U. Hansen, and M.P. Tamstorf. 2013. Camera derived vegetation greenness index as proxy for gross primary production in a low Arctic wetland area. ISPRS *Journal of Photogrammetry and Remote Sensing* 5: P 89-99.

Chapter 9
BOREAL PEATLAND NET ECOSYSTEM CO_2 EXCHANGE – AN INTEGRATIVE COMPARISON BETWEEN FLUXES MEASURED BY CLOSED CHAMBER AND EDDY COVARIANCE TECHNIQUE

Many studies have been conducted to quantify the exchange of CO_2 between the atmosphere and the biosphere and to analyze the underlying processes (e.g. Alm et al., 1997; Valentini et al., 2000; Bubier et al., 2003; Dore et al, 2003; Goulden et al., 2004; Coulter et al., 2006; Grant et al., 2009; Sierra et al., 2009; Gilmanov et al., 2010). The closed chamber method and the eddy covariance (EC) technique are the two measurement techniques that are mainly used to determine the CO_2 fluxes. The two techniques are used at different spatial and temporal scales. The chamber measurements provide discontinuous data on the plot scale (10^{-2}-10^{0} m^2) while, under ideal conditions, the EC measurements provide continuous flux data on the ecosystem scale (10^{4}-10^{6} m^2). The comparability of the plot- and ecosystem-scale measurements of CO_2 flux has been mainly tested on areas with homogenous surfaces, e.g. Dore et al. (2003) in forests, Kabwe et al. (2005) on bare soils in a uranium mine. Some studies were conducted at more heterogeneous sites with one dominant surface type, e.g. Griffis et al. (2000) at a subarctic fen which was covered by *Carex* spp. hummocks up to 70% or Heikkinen et al. (2002) at a patterned boreal mire with a 60%-predominance of wet flarks and Laine et al. (2006) at an oceanic mire with a predominance of lawns. Comparisons at heterogeneous study sites are rare, e.g. Fox et al. (2008) at a tundra site covered by six different mosaic elements which occupied relatively even proportions. At the homogenous study sites and the subarctic fen studied by Griffis et al. (2000), the CO_2 flux measured by EC and the estimates obtained by areally weighted chamber measurements were within the maximum probable error of each methodological approach. On the other hand, Heikkinen et al. (2002) and Fox et al. (2008) found a discrepancy between the fluxes obtained by the two different approaches. It is thus not easy to upscale chamber or downscale eddy covariance measurements (Forbrich et al., 2011) – the chamber method does not capture the full temporal variability and the EC technique can capture the small-scale spatial variability of the carbon fluxes only if the detailed information on the distribution of microforms or leaf area index (LAI) is available.

The objective of this study is to investigate the comparability of in situ CO_2 flux measurements conducted at different temporal and spatial scales by the chamber method and the EC technique at a patterned boreal peatland.

METHODS

Experimental setup and flux calculations

Chamber measurements – plot scale

CO_2 exchange was measured in peatland Medla-Pev-Nyur four times per week from 23 April to 20 October 2008 applying a closed chamber approach.

Peatland and the study region were described intensively in Schneider et al. (2012). To capture the variance of the CO_2 fluxes over the day, we conducted a series of measurements once per week during the morning (5 am to 11 am local time) and once per week during the evening (6 pm to 12 pm local time); two additional measurement series per week were conducted around midday from 11 am to 4 pm. The total number of measurements was 5517. A total of 18 measurement plots were established within the intensive study site in different microform types: 2 replicates each in ombrogenous hollows (OHO), lawns (OL) and hummocks (OH), and 3 replicates each in minerogenous hollows (MHO), lawns (ML) and hummocks (MH), and *Carex rostrata* lawns (CL). The NEE was measured using a transparent chamber (60 cm x 60 cm x 32 cm) made of polycarbonate sheets with a thickness of 1.5 mm. The chamber was equipped with a fan, and the headspace air temperature was controlled to within approximately ±1 °C of the ambient temperature by an automatic cooling system. A sensor of photosynthetically active radiation (SKP212, Skye Instruments Ltd., UK) was installed inside the chamber. During the flux measurements, the chamber was put on the preinstalled collars, which were equipped with a water-filled groove around the top to avoid air exchange between the headspace and the ambient air. The CO_2 concentrations were measured using a CO_2/H_2O infrared gas analyzer (LI-840, Licor, USA). CO_2 readings were taken at 1 second intervals over 180 seconds. The data was recorded using a data logger (CR850, Campbell Scientific, USA). The CO_2 flux was calculated from the change in CO_2 concentration in the chamber headspace over time by fitting an exponential model and determining the rate of the initial concentration change at the start of the closure period. More detailed information about the fitting method can be found in Kutzbach et al. (2007). If the curvature of the nonlinear curves was not explainable by the theoretical model presented in Kutzbach et al. (2007), a linear function was fitted to the data, the slope of which was used for the flux calculation.

Eddy covariance flux measurements – ecosystem scale

The fluctuations of wind speed components were measured from April until December 2008 using a three-dimensional sonic anemometer (Solent R3, Gill Instruments Ltd., UK) installed 3 m above the ground level. From the sample intake 15 cm below the anemometer, a vacuum pump drew the sample air through a CO_2/H_2O infrared gas analyzer (LI-7000, LI-COR Inc., USA). All analogue signals were digitized at 20 Hz and stored on a PC running EcoFlux software (InsituFlux, AB, Sweden). The analyzer and the PC were housed in temperature regulated boxes (InsituFlux, AB, Sweden).

Raw data of the eddy covariance flux measurements were processed and turbulent fluxes calculated over 30 min intervals using the EdiRe software (R. Clement, University of Edinburgh, UK). Two coordinate rotations were applied to the wind components so that the mean transverse and the mean vertical wind components were reduced to zero. The time lag between wind and gas concentrations measurements was determined and removed. Flux losses due to the limited frequency response of the eddy covariance system were corrected in the flux calculation process. The fluxes were corrected for the frequency attenuation due to tube attenuation, sensor path separation and spectral response of the instruments (Moore, 1986; Moncrieff et al., 1997). Webb correction adapted for closed-path eddy covariance systems was applied (Ibrom et al., 2007). Integral turbulence characteristics (ITC) were calculated and data were

screened accordingly. Data were removed if the deviation of the measured ITC parameter from the modeled ITC parameter was greater than 30 %. Stationarity characteristics were calculated and used to discard the data obtained during non-stationary conditions (Foken and Wichura, 1996). In total, the filtering methods removed 40% of CO_2 data, and 8013 half-hour CO_2 flux values remained for further analysis. The data post-processing procedures are presented in more detail in Sachs et al. (2008) and Runkle et al. (2014).

Ancillary measurements

Additional instruments installed near the eddy tower include sensors for air temperature and relative humidity (CS215, Campbell Scientific Ltd., UK), wind speed (M15103, R.M. Young, MI, USA), and photosynthetically active radiation (QS2 Delta-T Devices Ltd., UK). All signals from the ancillary sensors were automatically logged (CR-1000, Campbell Scientific Ltd., UK). At each measurement plot, soil temperature was measured at depths of 5 cm, 10 cm, 20 cm and 40 cm with a sampling frequency of 30 minutes (HOBO U12, HOBO, USA). The depth of ground water near the collars was measured manually each sampling date.

The green leaf area index (GAI) was determined to describe the vegetation development over the growing season and calculated as a sum of the green leaf area of vascular plants and of the green leaf area of mosses. The method was described thoroughly by Wilson et al. (2007). The green leaf area index of vascular plants was calculated as a product of the leaf size and number of green leaves in 2-week intervals. The green leaf area of mosses was estimated as the projection coverage of living moss capitula. More detailed description on the green leaf area index determination can be found in Schneider et al. (2010). The effective temperature sum index (ETI) was used to describe the thermal characteristics of the investigated area over the measurement period. ETI was calculated by dividing the effective air temperature sum by day number, starting from 1st of April=day 1 (Alm et al., 1997; 1999).

Empirical time series modeling

Chamber measurements – plot scale

As the chamber measurements are discontinuous, we modeled the time series of net ecosystem CO_2 exchange fluxes (NEE, in µg CO_2 $m^{-2}s^{-1}$) over the investigation period. Models based on photosynthetically active radiation (PAR, in µmol $m^{-2}s^{-1}$), air temperature (T_{air}, in °C), and GAI (in m^2 m^{-2}) or ETI were used. Each measurement plot was modeled separately using the following nonlinear functions:

$$NEE = \frac{a_1 \times T_{air} \times GAI \times PAR}{PAR + k_1} + p_1 \times \exp(p_2 \times T_{air}) \quad (1)$$

or

$$NEE = \frac{a_1 \times T_{air} \times ETI \times PAR}{PAR + k_1} + p_1 \times \exp(p_2 \times T_{air}) \quad (2)$$

where a_1, k_1, p_1 and p_2 are fitting parameters. The first part of the equation including the parameters a_1, k_1 represents the control of the microform photosynthesis, the second part with the parameters p_1 and p_2 represents the control of the microform respiration.

In this study, NEE is defined positive when carbon dioxide is released to the atmosphere and negative when it is taken up from the atmosphere.

Chamber walls reduce the radiation inside the chamber and result in lower photosynthetic rates inside the chamber as compared to outside. Thus, for the seasonal modeling of NEE not disturbed by a chamber, the NEE flux model derived from chamber PAR measurements was driven using the half-hourly mean PAR value measured at the weather station Schneider et al. (2012).

Empirical modeling was conducted by nonlinear least-squares fitting using the function *nlinfit* of the MATLAB® software package (version 7.1, The MathWorks Inc., Natick, USA).

Eddy covariance flux measurements – ecosystem scale

The NEE time series obtained by the EC approach was modeled in two periods: 4 May to 3 August using equation (3) and 4 August to 4 November using equation (4). Models were based on photosynthetically active radiation (PAR, in µmol $m^{-2}s^{-1}$), air temperature (T_{air}, in °C), and soil temperature in 10 cm and 20 cm depth (T_{10} and T_{20}, respectively, in °C). The modeled data was used for gapfilling.

$$NEE = \frac{a_1 \times T_{20} \times PAR}{PAR + k_1} + p_1 \times \exp(p_2 \times T_{air}) \quad (3)$$

$$NEE = \frac{a_1 \times T_{20} \times PAR}{PAR + k_1} + p_1 \times \exp(p_2 \times T_{10}) \quad (4)$$

where a_1, k_1, p_1 and p_2 are fitting parameters.

Determination of the microform coverage and remote sensing

The relative coverage of the different microform types was determined at the beginning of August 2008 along eight 300 m long transects at the intensive study site. The transects started at the eddy covariance tower and headed towards the cardinal and intercardinal directions. The distribution of the microform types along transects were recorded, and the percentage contribution was assumed to be representative for the spatial coverage of the microform types in the 45° sectors around the transects (Fig. 1). The main wind direction was SSE (Fig. 2),

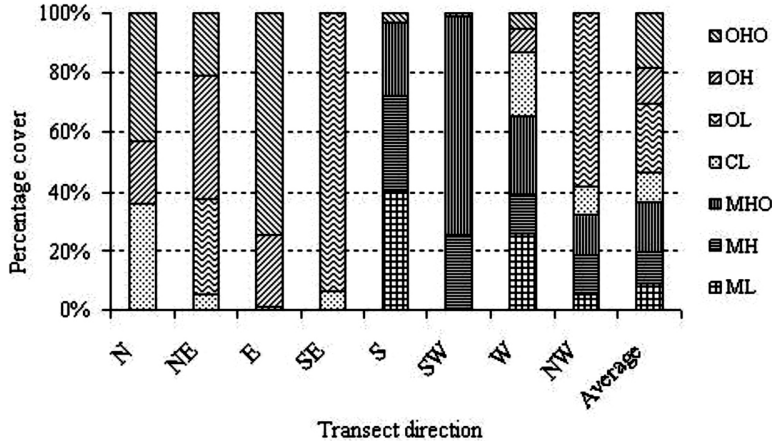

Fig. 1: Percentage cover of microforms along the 8 transects at the intensive study site. The microforms are ombrogenous hollows (OHO), lawns (OL) and hummocks (OH), and minerogenous hollows (MHO), lawns (ML) and hummocks (MH), and *Carex rostrata* lawns (CL).

as there were no direct measurements along the SSE transect, we decided to use the microform distribution of the S transect for upscaling (Fig. 1).

For land cover classification, a QuickBird satellite image acquired on 8 July 2008 and covering 70 km^2 was used in this study (QuickBird © 2007, DigitalGlobe; distributed by Eurimage/Pöyry). QuickBird image has five channels; four of them are multichromatic channels, with 2.4 m×2.4 m pixel resolution, and one is a panchromatic channel with a 0.6 m×0.6 m resolution. The four multichromatic channels were resampled to resolution of 0.6 m×0.6 m pixel size using the panchromatic channel. The resampling was done using Erdas Imagine 8.6 software (Leica Geosystems, Germany) and a cubic convolution method. It was orthorectified and mapped to a cartographic projection, and radiometric, sensor and geometric corrections were applied. The image was georeferenced using field measured GPS points. The accuracy assessment was based on 79 points randomly defined along transects (see above). Definiens Professional 5.0 program (Definiens AG, Germany) was applied for the land cover classification using the multiresolution segmentation method. The Kappa coefficient, which is a statistical measure of agreement – where a value of 1 means perfect agreement, was 0.94 for the classification in this study. The aim of the land cover classification by using the very high spatial resolution of the QuickBird image was to recognize the different microform types of the peatland. Regardless of this high spatial resolution, the size of some microforms e.g. minerogenous hollows was often smaller (0.25-0.5 m^2) than the spatial resolution of the image. Technically pixel area of classified QuickBird image was 0.36 mI, but as it was based on resampling technique described above, real precision for object separation was to some extent lower. Thus, we decided to group the microforms to classes based on the vegetation and water table depth characteristics. The following classes were therefore used for the footprint analysis: ombrogenous part (OC), minerogenous part (MC) and transition zone (TC) (Fig. 3). For the use of the land cover classification in the footprint modeling, we created one image for each class covering the area of interest. These images were resampled to 1 m pixel resolution by nearest neighborhood method. The pixels incorporated the information about the presence of the respective land cover class (value 1 = land cover class present, value 0 = land cover class not present).

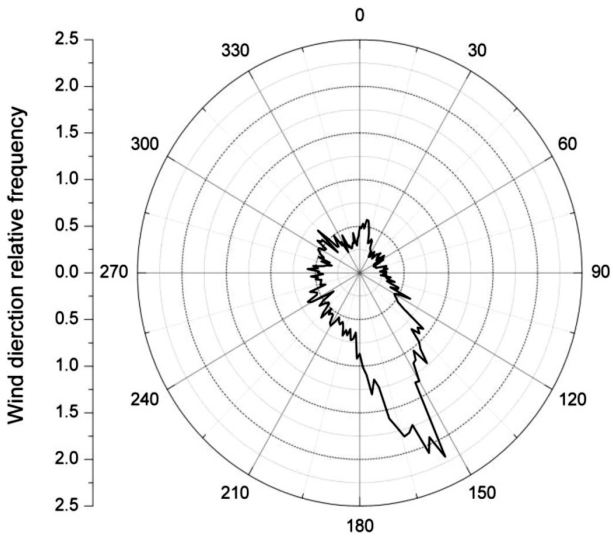

Fig. 2: Frequency distribution of wind directions measured at the eddy covariance tower.

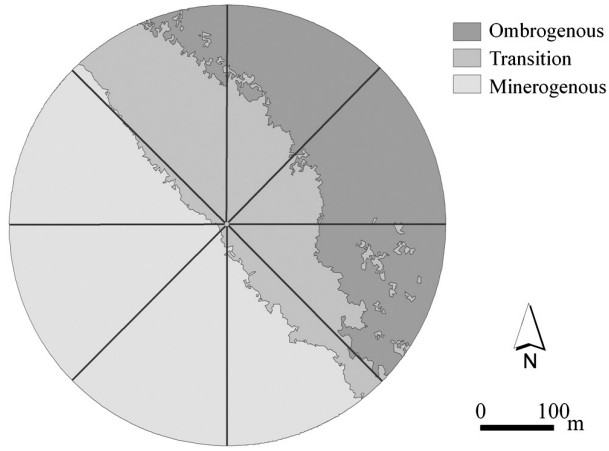

Fig. 3: Land cover classification of the intensive study site. The lines indicate the transects.

Footprint modeling

Footprint modeling was conducted to analyze how the source areas of the observed EC fluxes were characterized with respect to the coverage of land cover classes. The footprint model used in this study was the analytical model according to Kormann and Meixner (2001) which was developed for boundary layer conditions with non-neutral stratification. The two-dimensional footprint density function was determined based on the micrometeorological data from the EC measurements. To calculate the weighted fraction of each land cover class within each 30 min source area, the output of the footprint model was combined with the images of the land cover distribution. Therefore, a coordinate system with the tower in the origin was constructed, and the images were rotated into the main wind direction. Finally, the footprint density function was summed up for all pixels representing one land cover class. The contribution of each land cover class (j) is given as a weighted fraction (Ω_j) of the total source area of the 30 min EC flux.

As the footprint extension commonly exceeded the bounds of the area of interest, the sum of the source fractions of all land cover classes was usually less than 100%. We assumed that the distribution of the land cover classes in the footprint area which lay outside of the area of interest was similar to the land cover class distribution in the footprint area which lay inside the area of interest. Thus, we scaled the source fraction of each land cover class so that the sum of them was 100%. A check of the input parameters was then conducted and data characterized by low turbulence (friction velocity $u^* < 0.1$ m s^{-1}), high crosswind fluctuations (standard deviation of the lateral wind $\sigma_v > 1$), and zero sensible heat flux were excluded from further calculations. The missing values were replaced by means of source area fractions calculated for one degree intervals of wind direction for both stable and unstable atmospheric conditions.

Fox et al. (2008) described a critical assumption for using this source area function modeling over a nonuniform surface: the CO_2 fluxes are influenced by spatial variation of the surface properties whereas the influence on the momentum flux is insignificant, and the mechanical setting of the exchange processes is thus approximately uniform throughout the entire potential source area for the instrument. For our study, this assumption seems to be reasonable, given that the vegetation of each land cover class was uniformly relative short and the topography of the site was relatively flat.

Upscaling of CO_2 fluxes from plot scale to ecosystem scale

Three different approaches were used to integrate the plot-scale chamber measurements of NEE with the larger-scale EC measurements of NEE: 1. upscaling based on the average microform distribution in the area of interest and the mean NEE flux for each microform type, 2. upscaling based on areal weighting which accounts for main wind direction and the mean NEE flux for each microform type, and 3. upscaling based on the weighted fractions of the land cover classes within the source area of the 30 min EC source areas estimated by footprint modeling and the mean NEE flux for each microform type. To estimate the contributions of the different microforms to the EC source areas, the weighed fractions of land cover classes within the EC source areas were multiplied by the average relative microform coverage of the microforms within the respective land cover classes (Fig. 4). The following equations were used for different upscaling methods:

$$F_{AV} = \sum_{i=1}^{N} A_{AV\,i} \times F_i, \text{ for the upscaling method 1} \quad (5)$$

$$F_{WD} = \sum_{i=1}^{N} A_{WD\,i} \times F_i, \text{ for the upscaling method 2} \quad (6)$$

$$F_{FP} = \sum_{j=1}^{N} \Omega_j \sum_{i=1}^{N} A_{ji} \times F_i, \text{ for the upscaling method 3,} \quad (7)$$

where F_i is the mean NEE flux of the different microform types which was calculated as the mean of the replicates for each half-hour. A_i is the mean relative coverage of the different microform types within the area of interest, which is different depending on the upscaling method and Ω_j the source area fraction for the different land cover classes.

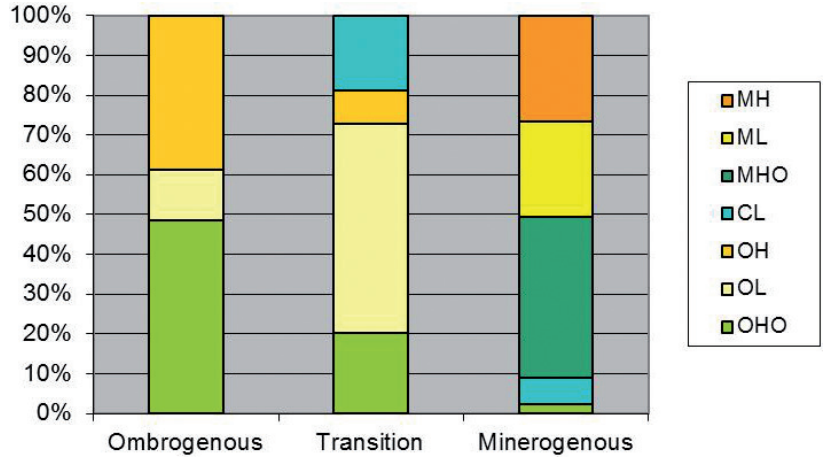

Fig. 4: Percentage cover of microforms for the different land cover classes. The microforms are ombrogenous hollows (OHO), lawns (OL) and hummocks (OH), and minerogenous hollows (MHO), lawns (ML) and hummocks (MH), and *Carex rostrata* lawns (CL).

Uncertainty analysis

The error of the area estimates for the different microforms cannot be considered as random error. Thus, the error propagation routine for random errors is not suitable for the uncertainty analysis of the upscaled CO_2 fluxes, and we used the method of maximum error estimation.

In order to estimate the uncertainty of the upscaled fluxes (δ_F), we used the formula:

$$\delta_{F_{AV}} = \sum_{i=1}^{N} A_{AVi} \times \delta F_i + \left|F_i\right| \times \delta A_{AV\,i}, \text{ for the upscaling method 1} \quad (8)$$

$$\delta_{F_{WD}} = \sum_{i=1}^{N} A_{WDi} \times \delta F_i + \left|F_i\right| \times \delta A_{WD\,i}, \text{ for the upscaling method 2} \quad (9)$$

and for the upscaling method 3:

$$\delta_{F_{FP}} = \sum_{j=1}^{N} (\Omega_j \times (\sum_{i=1}^{N} A_{ji} \times \delta F_i + \left|F_i\right| \times \delta A_{ji}) + (\sum_{i=1}^{N} A_{ji} \times F_i) \times \delta\Omega_j), \quad (10)$$

where F_i is the mean NEE flux of the different microform types and δF_i is the uncertainty of the mean NEE flux. A_i is the mean relative coverage of the different microform types within the area of interest and δA_i is the uncertainty of the coverage estimation, both are different depending on the upscaling method. Ω_j is the source area fraction for the different land cover classes (j) and $\delta\Omega_j$ is the uncertainty of the source area fraction estimation.

For CO_2 estimates by EC technique, we calculated the random error from the difference between the observed and modeled half-hourly fluxes following Aurela et al. (2002). Systematic errors in EC measurements have their origin in the limited frequency response of the EC system. An uncertainty of 30 % was assumed for the frequency and Webb correction procedures itself (Aurela et al., 2002).

Evaluation of the model performance

To compare the results of modeled and upscaled chamber measurements to measurements observed by the EC technique, the Willmott index of agreement, *d* (Willmott, 1982; Yurova et al., 2007) was calculated using daily sums values.

$$d = 1 - \left[\sum_{i=1}^{N} (M_i - O_i)^2 / \sum_{i=1}^{N} (\left|M_i'\right| + \left|O_i'\right|)^2 \right], \quad (11)$$

where $M_i' = M_i - \bar{O}$, $O_i' = O_i - \bar{O}$, M – modeled values (modeled and upscaled chamber measurements or results of LPJ-GUESSS model) and O – observed values (EC technique). $\bar{O}$ is the mean of observed values. The Wilmott index varies between 0 and 1, with $d = 1$ indicating a perfect match.

RESULTS

Variability of NEE fluxes at plot and ecosystem scales

The NEE fluxes measured by the closed chamber technique varied strongly on spatial and temporal scales (Fig. 5). The main difference between the microforms

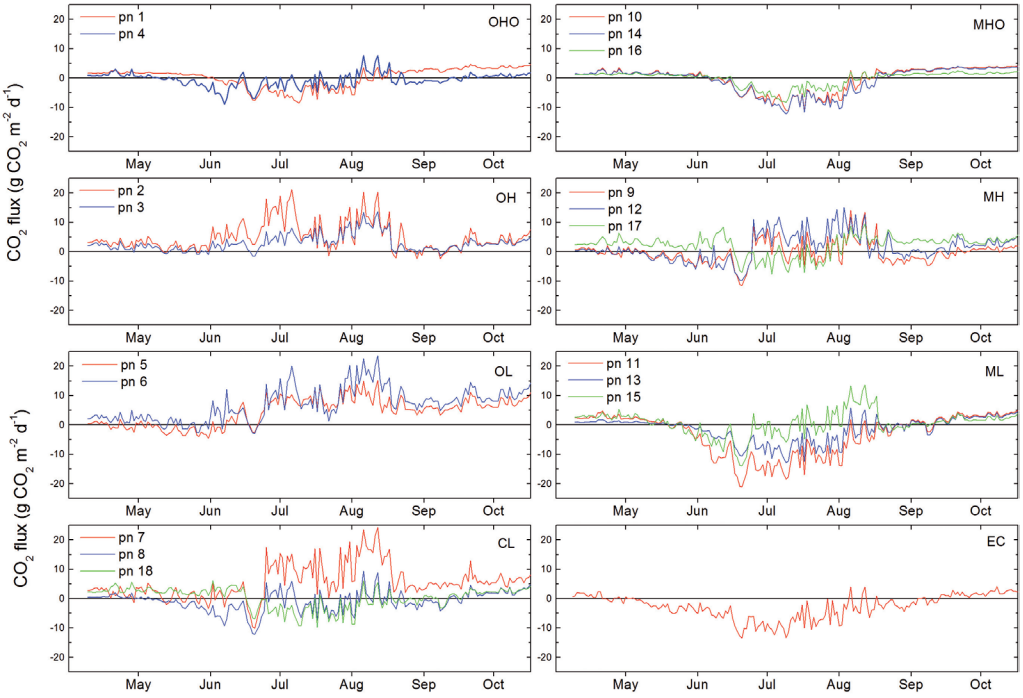

Fig. 5: Daily sums of NEE measured by chamber measurements and the eddy covariance technique. The chamber measurements are grouped by microform type. The microforms are ombrogenous hollows (OHO), lawns (OL) and hummocks (OH), and minerogenous hollows (MHO), lawns (ML) and hummocks (MH), and *Carex rostrata* lawns (CL).

regarding the seasonal variations of the CO_2 fluxes was the date when the daily sum of NEE fluxes became negative (CO_2 sink) in spring or again positive (CO_2 source) in autumn. The MHO sites, for example, changed from being a daily CO_2 source to a daily CO_2 sink at the end of June while this change from source to sink occurred at the ML sites about three weeks earlier. Also, the ML sites became CO_2 sources in autumn about three weeks later than MHO sites, resulting in a much longer net CO_2 uptake period. The OH sites were CO_2 sources over the complete investigation period and OL as well as one of the CL sites became a CO_2 source already in July after a very short period being CO_2 sink. The seasonal cycle of NEE at two of the MH sites was exceptional. They were CO_2 sources in spring, during summer and in autumn and changed in between to CO_2 sinks in early summer and in early autumn.

On the spatial scale, the NEE fluxes varied not only between the minerogenous and ombrogenous parts of the peatland but also between different microforms and between replicate plots of the same microform. The net CO_2 uptake as a result of photosynthesis and respiration was usually higher in the minerogenous part of the peatland compared to ombrogenous part. NEE fluxes ranged from strong CO_2 sinks (ML) to strong CO_2 sources (OL, OH) over the investigated period. The biggest differences between the replicates of one microform type were determined at ML, OL and CL sites. At *Carex* lawn sites, for example, one plot was a strong CO_2 source; one plot a weak CO_2 source and one plot a CO_2 sink over the investigated period apparently related to their leaf area.

Daily NEE fluxes detected by EC showed a similar seasonal pattern as fluxes detected by chamber measurements: NEE fluxes were highest during the summer and on a shorter time scale similar day-to-day variability could be observed (Fig. 5). The daily net ecosystem uptake varied from 0 to −12 g CO_2 m^{-2} d^{-1} during the period from the end of May to the end of September. During the other months, the CO_2 flux was characterized by a relatively steady CO_2 loss of 0 to 2 g CO_2 m^{-2} d^{-1}. More detailed information on the results of the EC flux measurements can be found in Chapter 10.

The empirical regression models of microform NEE which were used to integrate the chamber fluxes over the investigated period explained 24-94% of the variation in NEE. 70% of the regression models had an R^2_{adj} (coefficient of determination adjusted for the number of independent variables and the number of measurements) between 0.64 and 0.94. There were differences in model performance between different seasons. A general trend could not be observed, but the trends within the microform type were consistent; for example at minerogenous hollows, the model performance during the summer was weakest. We found contrary results for the minerogenous lawns; here the model performance was best in summer. The empirical model output for the data measured by the EC system agreed reasonably well with measured data (R^2_{adj} of 0.88 and 0.92, for the 4 May to 3 August and 4 August to 4 November model periods, respectively).

Microform distribution at the intensive study site

The average microform distribution in the area of interest were estimated as 18.4%, 11.8%, 23.0%, 10.1%, 17.3%, 10.5% and 8.9% for OHO, OH, OL, CL, MHO, MH and ML, respectively (Fig. 1). OL was the most common and ML the least common of all microform types. The microform distribution along the transects reflected the clear boundary between the bog in the northern part and the fen in the southern part of the intensive study site. Along the E, SE, SW and NW transects a dominance of one microform type could be observed. If we consider the average microform distribution, no such dominance could be detected. The transect of the main wind direction (S) was composed of the microform types ML (40.4%), MH (31.7%), MHO (25%) and OHO (2.9%) (Fig. 1). In the ombrogenous as well as in the minerogenous parts of the peatland, a frequent change of microforms could be observed along the transects. The extension of the microforms varied from 0.5 m to 30 m. The transitional zone was characterized by CL and OL, which occurred in stripes of 50 m to 150 m. The microform distribution varies strongly between the land cover classes (Fig. 4). The ombrogenous class is characterized by OHO (48.4%), OH (38.9%) and OL (12.7%), the minerogenous class by OHO (2.3%), MHO (40.5%), MH (26.6%), ML (24%) and CL (6.5%) and the transition class by OHO (20.3%), OH (8.3%), OL (52.6%) and CL (18.3%).

Footprint analysis

The footprint analysis indicated that for 3998 half-hour flux values 80% of the EC flux source area lay within 300 m of the measurement tower, and the most sensitive distance was at 18 m. The relative frequency of the source area fraction for each of the land cover class is illustrated in Fig. 6. The source area fractions of the minerogenous and the transition class were very high, and they were sampled evenly, whereas the ombrogenous class never exceeded

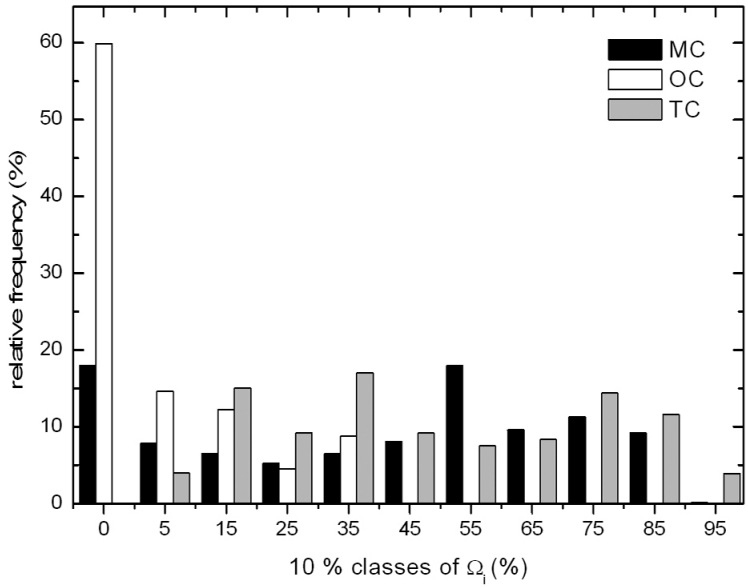

Fig. 6: Relative frequency of the weighed source area fractions for each land cover class (ombrogenous (OC), minerogenous (MC) and transition (TC)) during the study period. The contribution of each land cover class (j) is given as a weighted fraction (Ω_j) of the total source area of the 30 min EC flux. On the X-axis the class mean is shown.

30% of the source area and for much of the study period (60%) was zero. The footprint analysis showed that the ombrogenous class was under-sampled by the EC measurement set-up and the EC measurements were representative only for the minerogenous and transition part of the investigated peatland.

Comparison of CO_2 fluxes observed from chamber and eddy covariance measurements

The chamber method and the eddy covariance technique were compared using three different upscaling approaches (Fig. 7). Independently of the upscaling or measurement method, the CO_2 fluxes showed similar seasonal trends - they were highest during the summer and lowest during spring - but the date when the daily sum of NEE fluxes measured by the EC technique became negative was earlier than for the upscaled fluxes and became again positive later in autumn. In addition, shorter scale variations such as the first strong uptake peak in the middle of June were also captured by both methods. However, the magnitude of the modeled fluxes varied between the methods used.

The NEE estimates from chamber measurements upscaled based on the average microform distribution in the area of interest (NEE_{AV}) were positive most time of the investigated period and showed higher net CO_2 release then estimates by EC. The NEE estimates from chamber measurements based on areal weighting which accounts for the microsite distribution in the sector of the main wind direction (NEE_{WD}) were lower than NEE_{AV} estimates but still higher then EC estimates. Best agreement could be observed during some periods in summer. The comparison of the NEE estimates from chamber measurements upscaled using the simulated source area fraction (NEE_{FP}) and the EC CO_2 flux estimates showed high dis-

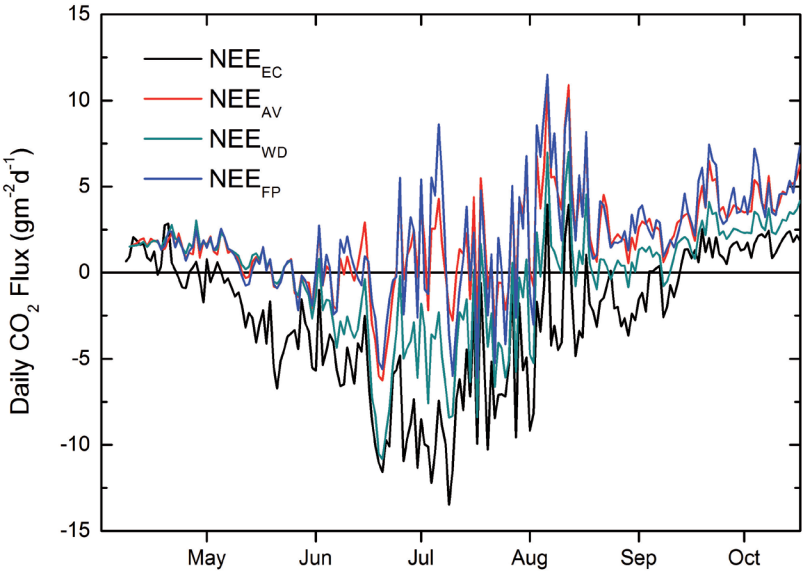

Fig. 7: Daily sums of NEE calculated from eddy covariance measurements (NEE_{EC}) and upscaled chamber measurements based on average microform distribution (NEE_{AV}), on areal weighting which accounts for the main wind direction (NEE_{WD}), and on simulated source area fraction (NEE_{FP}).

crepancies between the two methods: the EC measurements showed a much higher uptake of the CO_2 fluxes. The Willmott index for the comparison of modeled and upscaled chamber measurements to measurements observed by EC technique is 0.59 (NEE_{AV} to NEE_{EC}), 0.85 (NEE_{WD} to NEE_{EC}) and 0.57 (NEE_{FP} to NEE_{EC}).

The results of continuous eddy covariance observations were also compared with modeling results based on chamber measurements at different plots. The best agreement was observed for plot number 13 which was a ML site and represented the intermediate minerogenous lawns with respect to the water level and CO_2 fluxes. Even higher uptake of CO_2 was observed at plot number 15 which was a ML site with higher water table level than plot number 13. MH microsites (plot 9 and 12) showed the early change (around 21 May) of daily NEE budget from source to sink of CO_2 in spring as it was measured by EC (Fig. 5). These were the same microforms that showed CO_2 uptake in early autumn (September).

The comparison of the half-hourly NEE fluxes measured by the EC method (NEE_{EC}) and NEE_{FP} showed that the two methods agreed better during nighttime (PAR<10µmol m^{-2} s^{-1}) than during the daytime (PAR > 10 µmol m^{-2} s^{-1}). The EC method showed much higher daytime uptake of CO_2 than the upscaled chamber fluxes.

The cumulative sum of the CO_2 fluxes over the investigation period showed the differences in CO_2 fluxes measured by the EC technique and upscaled using the chamber measurements even more clearly (Fig. 8). The cumulative flux of −533 ± 6 g CO_2 m^{-2}, 344 ± 533 g CO_2 m^{-2}, −68 ± 591 g CO_2 m^{-2}, and 367 ± 593 g CO_2 m^{-2} were estimated for the NEE_{EC}, NEE_{AV}, NEE_{WD} and NEE_{FP}, respectively. Although the error of the upscaling methods is high, the estimates of the NEE by the EC method are not within the range of the uncertainty of the NEE_{AV}

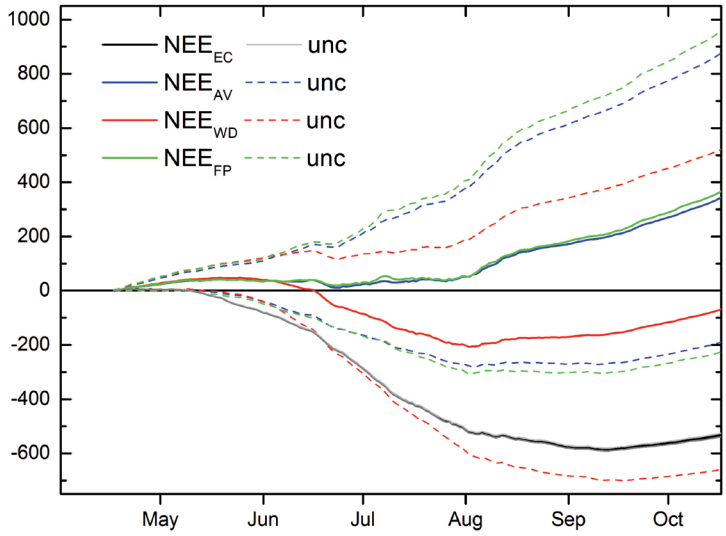

Fig. 8: Cumulative sum of the CO_2 fluxes over the investigation period measured by the EC technique (NEE_{EC}) and upscaled chamber measurements based on average microform distribution (NEE_{AV}), on areal weighting which accounts for the main wind direction (NEE_{WD}), and on the simulated source area fraction (NEE_{FP}) and uncertainty estimates (unc) for all methods.

and NEE_{FP} fluxes. Interestingly, the CO_2 flux estimates based on the upscaling method using the average microform distribution and CO_2 flux estimates using the simulated source fraction do not differ by much. They show similar seasonal pattern and budgets over the investigated period. The estimates based on the simulated source fraction are characterized by higher uncertainty as this upscaling method included more calculation steps, all of which contained errors.

DISCUSSION

Mismatch between NEE fluxes upscaled from chamber and observed from eddy covariance measurements

The observed strong difference between the CO_2 budgets derived from the closed chamber method and the eddy covariance approach calls for intensified search for biases in both measurement approaches. Estimates based on chamber measurements are subject to systematic and sampling errors. Many of the systematic errors are known and can be prevented or corrected for, for example (1) the increase in temperature and humidity beneath the chamber (Wagner and Reicosky, 1992; Welles et al., 2001), (2) length of the sampling interval (Griffis et al., 2000), (3) inaccurate determination of chamber headspace volume (Livingston and Hutchinson, 1995), (4) leakage at chamber components or via the underlying soil pore space (Hutchinson and Livingston, 2001), (5) elimination of turbulence within the chamber (Reicosky, 2003), (6) gradient problems – build-up or reduction of CO_2 concentration within the chamber which alters the underlying concentration gradients and results in modified CO_2 fluxes (Hutchinson et al., 2000; Livingston et al., 2006; Kutzbach et al., 2007), (7) lack of temporal representation with limited number of sampling points during

early morning and late afternoon hours (Griffis et al., 2000). In this study all of the errors described above were considered and minimized by careful experiment planning, chamber design and data analysis, as described in sections 2.2 and 2.3. But some errors, such as limited area and measurement intervals, are inherent to the method and can not be prevented, only be reduced by, for example, using bigger measurement plots (in this study 0.36 m^2) and increasing the number of measurements (in this study 5517).

A substantial error occurs if the sampling routine does not account for the spatial heterogeneity in NEE fluxes (Janssens et al., 2001; Drewitt et al., 2002). In a peatland ecosystem, the pronounced heterogeneity can be caused by differences in vegetation type and coverage, water table depth and nutrient supply. In this study the sampling design was adjusted to the heterogeneity of the investigated site by increasing the number of measurement plots. However, an increased number of replicates would have enhanced the accuracy of the mean of the replicate measurements.

The choice of the modeling and reconstruction method influences the CO_2 flux estimates for a peatland investigation site (Laine et al., 2009). The models can be parameterized by individual sample plots, plant communities or the entire investigation site. According to the findings of Laine et al. (2009), the spatial variation is best captured by the plot method, and the reliability of estimates is also improved. Fluxes were modeled on plot level in this study.

The EC technique has well-known limitations, for example, stable atmospheric conditions lead to a systematic underestimation of CO_2 fluxes if not properly accounted for (Goulden et al., 1996). Therefore, the obtained data was carefully checked and gap- filled. A prerequisite is that the method should be applied over flat terrain. This is fulfilled at the Medla-Pev-Nyur study site.

Both closed chamber and eddy covariance methods were carried out simultaneously to allow for comparison by empirical modeling of the flux time series and a footprint model to integrate the point based chamber measurements with the larger scale eddy covariance measurements.

Strikingly, the measurements by the EC approach showed much higher uptake of CO_2 during the daytime compared to the upscaled chamber measurements, whereas during the nighttime the difference in CO_2 flux estimates of the two approaches was minor. The photosynthetic action spectrum of plants is not restricted to the wavelength of photosynthetically active radiation (PAR). Leaves are also effective in ultraviolet (UV) absorption. Mantha et al. (2001) described in their study that the photosynthetic rates at UV-A radiation were up to 10 % higher than at PAR. For the construction of transparent chambers two materials are mainly used: polycarbonate and polyacrylics (mainly Plexiglas®). Polycarbonate, which was also used in this study, has very low or no UV-A-transmission whereas polyacrylics are usually more transparent for these wavelengths. The low UV-A-transmission of the polycarbonate chambers might suppress the photosynthetic activity of plants within the chamber and might be a source of error (underestimation of CO_2 uptake during photosynthesis) in NEE chamber measurements. As this potential error only influences the CO_2 uptake, there is a high potential for a serious bias in the carbon balance which might explain some of the differences in our (higher) NEE flux estimates by the EC approach compared to the upscaled fluxes based on the polycarbonate chambers. Griffis et al. [2000] observed a difference in net photosynthesis between measurements by a gradient technique and upscaled chamber measurements of about 21%.

Biases in land cover classification and upscaling

The NEE measurements were conducted at different spatial scales. The environmental variables which influence the CO_2 exchange, e.g. peat physical and chemical properties, vegetation or water flow, showed also variability on the different spatial scales. The exchange of CO_2 between the peatland and atmosphere is characterized by a nonlinear response to spatial variations in the driving variables (Baird et al., 2009). The upscaling methods used in this study do not account for this nonlinear response which might lead to the observed discrepancies between the NEE fluxes upscaled chamber measurements and those measured by eddy covariance measurements.

Due to the small size of some microforms, it was not possible to classify the land cover on the microform level of detail even with our extreme high resolution QuickBird image (0.6 m pixel in panchromatic channel, 2.4 m in multispectral channels). In autumn 2008, GeoEye-1 images (0.41 m pixel in panchromatic channel, 1.65 m in multispectral channels) became available. This increased resolution might already allow a detailed microform classification. An alternative strategy still would be the use of aerial images. Due to failure in microform classification, we used the microform distribution within the land cover class for upscaling. We had to assume that the microforms were evenly distributed within the class. This assumption might be an important source of error in upscaling of the CO_2 fluxes. Due to high spatial heterogeneity of the vegetation and water table levels in a peatland and thus of the CO_2 fluxes, the upscaling of the fluxes from plot to ecosystem level is characterized by higher potential errors than upscaling at homogenous study sites as presented in studies by Dore et al. (2003), Kabwe et al. (2005), Laine et al. (2006) and Yurova et al. (2007). Fox et al. (2008) described pronounced discrepancies in CO_2 flux estimates between the closed chamber and EC approaches when used at heterogeneous tundra study sites.

Due to the similar mean microform distribution of the upscaling methods based on the average microform distribution and based on footprint modeling, there was no significant difference in seasonal trends and in budgets over the investigation period between NEE_{AV} and NEE_{FP}. The explanation for the substantial difference in the results NEE_{AV} and NEE_{FP} compared to NEE_{WD} might be the large difference in the percentage cover of the different microforms along the south transect compared to the mean percentage cover in the area of interest.

The microform OL had the strongest control on the upscaled fluxes. This is due to their relatively large surface coverage and, more importantly, the large flux values observed for respiration. Although there were microforms which show the early uptake of CO_2 in spring, the upscaling methods integrated all microforms in an ecosystem flux, and this showed the change in daily CO_2 flux from release to uptake much later compared to the flux measurements by the EC technique.

A study by Soegaard et al. (2000) using a footprint model in an arctic valley showed that for the interpretation of the CO_2 fluxes measured by EC the LAI was more important than the vegetation type. It might be more suitable to base the upscaling methods not on the microform distribution but on the leaf area index classes or on a combination of both.

Comparison to other peatland studies and forest flux estimates

Although peatlands cover vast areas of boreal Russia, there are not many boreal peatland carbon flux study sites established. Arneth et al. (2002) and Friborg et al. (2003) published NEE values measured by the EC technique for peatlands in European Russia, Central Siberia and West Siberia, respectively. The CO_2 uptake measured by the EC technique at the Medla-Pev-Nyur site was representative for the minerogenous part of the peatland and was much higher than reported by Arneth et al. (2002), possibly because the study sites of Arneth et al. (2002) were bogs. In contrast, the range and the seasonal dynamics of the CO_2 fluxes at the Medla-Pev-Nyur site and the fen studied by Friborg et al. (2003) were in good agreement.

There are more studies on CO_2 exchange between peatlands and atmosphere in Russia and at other boreal peatlands measured by the closed chamber technique (e.g. Golovatskaya and Dyukarev, 2009; Alm et al., 1997, 1999; Griffis et al., 2000; Riutta et al, 2007a, 2007b). A detailed comparison of the CO_2 fluxes at the Medla-Pev-Nyur site and other boreal peatland study sites was given in Schneider et al. (2012).

CONCLUSION

In this study, we compared NEE of a boreal peatland site measured by closed chambers, EC and modeled by LPJ-GUESS. While the general trend and even shorter scale variations of NEE were similar between chambers and EC, the summed seasonal NEE showed strong disagreement between the methods. Based on the EC technique measurements, the peatland was a sink of -533 ± 6 g CO_2 m^{-2} over the investigation period May-October 2008 whereas the upscaled chamber measurements showed a release of 344 ± 533 g CO_2 m^{-2}, 367 ± 593 g CO_2 m^{-2} or a small uptake of -68 ± 591 g CO_2 m^{-2} for the upscaling methods based on the average microform distribution, the results of the footprint modeling or the microform distribution of the main wind direction, respectively. The upscaled cumulative NEE fluxes are characterized by high uncertainty and can vary from CO_2 sink to source.

To simulate the vegetation and carbon dynamics of the peatland, different runs and soil organic matter decomposition scenarios were used in the LPJ-GUESS model, altogether 6 combinations. The cumulative NEE varied from 15 to -800 g CO_2 m^{-2} for the investigation period between the different model runs. The wet runs showed highest uptake of CO_2 by the peatland, followed by dry and standard runs.

The main error sources in the upscaling of the fluxes probably were the calculation of the area occupied by the different microform types and the high variability of the CO_2 fluxes within one microform type. As the individual microforms were smaller than the resolution of the QuickBird image, we used the vegetation description along eight transects within the investigated site for the upscaling of the CO_2 fluxes. This method is characterized by higher uncertainty than using the land cover classification provided that the classification resolves the land forms of interest. The variability in CO_2 fluxes within one microform type could be mainly explained by differences in LAI. We recommend basing future upscaling methods not only on microform distribution but also on the spatial distribution of LAI or biomass. These values can be evaluated from high resolution satellite images.

It might happen that even the next generation ecosystem models will not be able to reproduce the heterogeneity in vegetation, hydrology and nutrient supply of a peatland, but it will be possible to model the properties and hence the carbon fluxes of different microform types. So if we would like to model the recent and future carbon budgets of a peatland it might be an alternative to couple these microform models with the microform distribution of the peatland of interest to obtain more realistic results.

ACKNOWLEDGEMENTS

We gratefully acknowledge the contribution of J. Ibendorf, O. Michajlov, M. Miglovec, P. Schreiber, C. Wille and U. Wolf for assisting us in carrying out the CO_2 flux chamber measurements and of N. Kuusinen and M. Ek (University of Helsinki) for the help in the field and in processing the land cover data. The main funding for the project was provided by the EU Project "CarboNorth" (036993), the German Science Foundation (WI −2680 1/1 and 2/1) and a Sofja Kovalevskaja Research Award to M. Wilmking. During the period of data analysis and manuscript preparation, L. Kutzbach was supported through the Cluster of Excellence\CliSAP" (EXC177), University of Hamburg, funded through the German Research Foundation (DFG).

References

Alm, J., A. Talanov, S. Saarnio, J. Silvola, E. Ikkonen, H. Aaltonen, H. Nykänen, and P. J. Martikainen. 1997. Reconstruction of the carbon balance for microsites in a boreal oligotrophic pine fen. Finland. *Oecologia 110*: 423-431.

Alm, J., L. Schulman, J. Walden, H. Nykänen, P. J. Martikainen, and J. Silvola. 1999. Carbon balance of a boreal bog during a year with an exceptionally dry summer. *Ecology 80* (1): 161-174.

Arneth A., J. Kurbatova, O. Kolle, O. B. Shibistova, J. Lloyd, N. N. Vygodskaya, and E.-D. Schulze. 2002, Comparative ecosystem-atmosphere exchange of energy and mass in a European Russian and central Siberian bog II. Interseasonal and interannual variability of CO_2 fluxes. *Tellus, Ser. B, 54*: 514-530.

Aurela, M., T. Laurila, and J. P. Tuovinen. 2002. Annual CO_2 balance of a subarctic fen in northern Europe: Importance of the wintertime efflux. *J. Geophys. Res. 107*(D21): 4607. doi:10.1029/2002JD002055.

Baird, A. J., L. R. Belyea, and P. J. Morris. 2009. Upscaling of peatland-atmosphere fluxes of methane: small-scale heterogeneity in process rates and the pitfalls of "bucket-and-slab" models. In *Carbon Cycling in Northern Peatlands*, ed. A. J. Baird, L. R. Belyea, X. Comas, A. S. Reeve, and L. D. Slater. American Geophysical Union. Washington D. C. USA: 37-54.

Bubier, J. L., P. M. Crill, A. Mosedale, S. Frolking, and E. Linder. 2003. Peatland responses to varying interannual moisture conditions as measured by automatic CO_2 chambers, *Global Biogeochem. Cycles. 17* (2). doi: 10.1029/2002GB001946.

Ciais, P., A. S. Denning, P. P. Tans, J. A. Berry, D. A. Randall, G. J. Collatz, P. J. Sellers, J. W. C. White, M. Trolier, H. A. J. Meijer, R. J. Francey, P. Monfray, and M. Heimann. 1997. A three-dimensional synthesis study of $\delta^{18}O$ in atmospheric CO_2 1. Surface fluxes. *J. Geophys. Res. 102*(D5): 5857−5872.

Coulter, R. L., M. S. Pekour, D. R. Cook, G. E. Klazura, T. J. Martin, and J. D. Lucas 2006. Surface energy and carbon dioxide fluxes above different vegetation types within ABLE. *Agric. For. Meteorol. 136*: 147-158.

Dore, S., G. J. Hymus, D. P. Johnson, C. R. Hinkle, R. Valentini, and B. G. Drake. 2003. Cross validation of open-top chamber and eddy covariance measurements of ecosystem CO_2 exchange in a Florida scrub-oak ecosystem. *Global Change Biol. 9*: 84-95.

Drewitt, G. B., T. A. Black, Z. Nesic, E. R. Humphreys, E. M. Jork, R. Swanson, G. J. Ethier, T. Griffis, and K. Morgenstern. 2002. Measuring forest floor CO_2 fluxes in a Douglas-fir forest. *Agric. For. Meteorol. 101*: 299–317.

Foken, T., and B. Wichura. 1996. Tools for quality assessment of surface-based flux measurements. *Agric. For.* Meteorol. *78*: 83-105.

Forbrich, I., L. Kutzbach, C. Wille, T. Becker, J. Wu, and M. Wilmking. 2011. Cross-evaluation of measurements of peatland methane emissions on microform and ecosystem scales using high-resolution landcover classification and source weight modeling. *Agric. For. Meteorol. 115(7)*: 864-874.

Fox, A. M., B. Huntley, C. R. Lloyd, M. Williams, and R. Baxter. 2008. Net ecosystem exchange over heterogeneous Arctic tundra: Scaling between chamber and eddy covariance measurements. *Global Biogeochem. Cycles 22*, (GB2027). doi:10.1029/2007GB003027.

Friborg, T., H. Søgaard, T. R. Christensen, C. R. Lloyd, and N. S. Panikov. 2003. Siberian wetlands: Where a sink is a source. *Geophys. Res. Lett. 30*. doi:10.1029/2003GL017797.

Gilmanov T.G., L. Aires, Z. Barcza, V. S. Baron, L. Belelli, J. Beringer, D. Billesbach, D. Bonal, J. Bradford, E. Ceschia, D. Cook, C. Corradi, A. Frank, D. Gianelle, C. Gimeno, T. Gruenwald, H. Guo, N. Hanan, L. Haszpra, J. Heilman, A. Jacobs, M. B. Jones, D. A. Johnson, G. Kiely, S. Li, V. Magliulo, E. Moors, Z. Nagy, M. Nasyrov, C. Owensby, K. Pinter, C. Pio, M. Reichstein, M. J. Sanz, R. Scott, J. F. Soussana, P. C. Stoy, T. Svejcar, Z. Tuba, and G. Zhou. 2010. Productivity, respiration, and light-response parameters of world grassland and agroecosystems derived from flux-tower measurements, *Rangeland Ecol. Manage. 63*: 16-39.

Golovatskaya, E. A., and E. A. Dyukarev. 2009. Carbon budget of oligotrophic mire sites in the Southern Taiga of West Siberia. *Plant Soil. 315*: 19-34.

Goulden, M. L., J. W. Munger, S.-M. Fan, B. C. Daube, and S. C. Wolfsy. 1996. Measurements of carbon sequestration by long-term eddy covariance: Methods and critical evaluation of accuracy. *Global Change Biol. 2*: 169-182.

Goulden, M. L., S. D. Miller, H. R. da Rocha, M. C. Menton, H. C. de Freitas, A. M. e Silva Figueira and C. A. D. de Sousa. 2004. Diel and seasonal patterns of tropical forest CO_2 exchange. *Ecol. Appl. 14*: 42-54.

Grant R.F., A. G. Barr, T. A. Black, H. A. Margolis, A. L. Dunn, J. Metsaranta, S. Wang, J. H. McCaughey, and C.A. Bourque. 2009. Interannual variation in net ecosystem productivity of Canadian forests as affected by regional weather patterns – A Fluxnet-Canada synthesis. *Agric. For. Meteorol. 149*: 2022-2039.

Griffis, T.J., W. R. Rouse, and J.M. Waddington. 2000. Scaling net ecosystem CO_2 exchange from the community to landscape-level at a subarctic fen. *Global Change Biol. 6*: 459-473.

Heikkinen, J. E. P., M. Maljanen, M. Aurela, K. J. Hargreaves, and P. J. Martikainen. 2002. Carbon dioxide and methane dynamics in a sub-Arctic peatland in northern Finland. *Polar Res.*, *21*(1): 49–62.

Hutchinson, G. L., and G. P. Livingston. 2001. Vents and seals in non-steady state chambers used for measuring gas exchange between soil and the atmosphere. *Eur. J. Soil Sci.*, *52*: 675-682.

Hutchinson, G. L., G. P. Livingston, R. W. Healy, and R. G. Striegl. 2000. Chamber measurement of surface-atmosphere trace gas exchange: numerical evaluation of dependence on soil, interfacial layer, and source/sink properties, *J. Geophys. Res. 105* (D7): 8865-8875.

Ibrom, A., E. Dellwik, H. Flyvbjerg, N. O. Jensen, and K. Pilegaard 2007. Strong low-pass filtering effects on water vapour flux measurements with closed-path eddy correlation systems. *Agric. For. Meteorol. 147*: 140-156.

Janssens, I. A., A. S. Kowalski, and R. Ceulemans. 2001. Forest floor CO_2 fluxes estimated by eddy covariance and chamber-based model. *Agric. For. Meteorol. 102*: 61–69.

Kabwe, L. K., R. E. Farrell, S. K. Carey, M. J. Hendry, and G.W. Wilson. 2005. Characterizing spatial and temporal variations in CO_2 fluxes from ground surface using three complementary measurement techniques. *J. Hydrol. 311*: 80-90.

Kormann, R., and F. Meixner. 2001. An analytical footprint model for non-neutral stratification. *Boundary Layer Meteorol. 99* (2): 207-224.

Kutzbach, L., J. Schneider, T. Sachs, M. Giebels, H. Nykänen, N. Shurpali, P. Martikainen, J. Alm, and M. Wilmking. 2007. CO_2 flux determination by closed-chamber methods can be seriously biased by inappropriate application of linear regression. *Biogeosciences*, *4*: 1005–1025.

Laine, A., M. Sottocornola, G. Kiely, K. A. Byrne, D. Wilson, and E.-S. Tuittila. 2006. Estimating net ecosystem exchange in a patterned ecosystem: Example from blanket bog. *Agric. For. Meteorol. 138*: 231-243. doi: 10.1016/j.agrformet.2006.05.005.

Laine, A., T. Riutta, S. Juutunen, M. Väliranta, and E.-S. Tuittila. 2009. Acknowledging the spatial heterogenity in modeling/reconstructing carbon dioxide exchange in a northern aapa mire. *Ecol. Modell. 220*: 2646-2655. doi:10.1016/j.ecolmodel.2009.06.047

Livingston G. P., and G. L. Hutchinson. 1995. Enclosure-based measurement of trace gas exchange: Applications and sources of error. In *Biogenic Trace Gases: Measuring Emissions from Soil and Water*, ed. P. A. Matson, and R. C. Harriss. 15-51. Blackwell Science Ltd, Oxford, UK:

Livingston, G. P., G. L Hutchinson, and K. Spartalian. 2006. Trace gas emission in chambers a non-steady-state diffusion model. *Soil Sci. Soc. Am. J. 70*: 1459-1469.

Mantha, S. V., G. A. Johnson, and T. A. Day. 2001. **Evidence from action and fluo**rescence spectra that UV-induced violet-blue-green fluorescence enhances leaf photosynthesis. *Photochem. Photobiol.*: *73*, 249-256.

Moore, C. J. 1986. Frequency-response corrections for eddy-correlation systems. *Boundary Layer Meteorol. 37* (1-2): 17-35.

Moncrieff, J., R. Valentini, S. Greco, S. Guenther, and P. Ciccioli. 1997. Trace gas exchange over terrestrial ecosystems: Methods and perspectives in micrometeorology. *J. Exp. Bot. 48* (310): 1133-1142.

Reicosky, D. C. 2003. Tillage-induced soil properties and chamber mixing effects on gas exchange. In Proceedings of the 16th Triennial Conference of International Soil Tillage Research Organizations, 13-18 July 2003, Brisbane, Australia.

Riutta, T., J. Laine, M. Aurela, J. Rinne, T. Vesala, T. Laurila, S. Haapanala, M. Pihlatie, and E.-S. Tuittila. 2007a. Spatial variation in plant community functions regulates carbon gas dynamics in a boreal fen ecosystem. *Tellus. SerB. 59*: 838-852.

Riutta, T., J. Laine, and E.-S. Tuittila. 2007b. Sensitivity of CO_2 exchange of fen ecosystem components to water level variation. *Ecosystems, 10*: 718-733.

Runkle, B.R.K, C. Wille, M. Gažovič, M. Wilmking, and L. Kutzbach. 2014. The surface energy balance and its drivers in a boreal peatland fen of northwestern Russia. *J. Hydrol.* 511: 359-373

Sachs, T., C. Wille, J. Boike, and L. Kutzbach. 2008. **Environmental controls on eco**system-scale CH_4 emission from polygonal tundra in the Lena River Delta. Siberia, *J. Geophys. Res. 113*: G00A03 doi:10.1029/2007JG000505.

Schneider, J., L. Kutzbach, and M. Wilmking. 2012. Carbon dioxide dynamics of a boreal peatland over a complete growing season. Komi Republic, NW Russia. *Biogeochemistry*, *111*: 485-513.

Sierra C. A., H. W. Loescher, M.E. Harmon, A. D. Richardson, D. Y. Hollinger, and S. S. Perakis. 2009. Interannual variation of carbon fluxes from three contrasting evergreen forests: the role of forest dynamics and climate. *Ecology. 90*: 2711-2723.

Soegaard, H., K. Nordstroem, T. Friborg, B. U. Hansen, T. Christensen, and C. Bay. 2000. Trace gas exchange in a high-arctic valley 3. Integrating and scaling CO_2 fluxes from canopy to landscape using flux data, footprint modelling, and remote sensing. *Global Biogeochem. Cycles. 14* (3): 725-744.

Valentini, R., S. Dore, G. Marchi, D. Mollicone, M. Panfyorov, C. Rebmann, O. Kolle, and E.-D. Schulze. 2000. Carbon and water exchanges of two contrasting Central Siberia landscape types: regenerating forest and bog. *Funct. Ecol. 14*: 87-96.

Wagner, S. W., and D. C. Reicosky. 1992. Closed-chamber effects on leaf temperature, canopy photosynthesis, and evapotranspiration. *Agron. J. 84* (4): 731-738.

Willmott, C. J. 1982. Some comments on the evaluation of model performance. *Bull. Am. Meteorol. Soc. 63*: 1309-1913.

Wilson, D., Alm, J., Riutta, T., Laine, J., Byrne, K. A., Farrell, E.P., and E.-S. Tuittila. 2007. A high resolution green area index for modelling the seasonal dynamics of CO_2 exchange in peatland vascular plant communities. *Plant Ecol. 190*: 37-51.

Welles, J. M., T. H. Demetriades-Shah, and D. K. McDermitt. 2001. Considerations for measuring ground CO_2 effluxes with chambers. *Chem. Geol. 177*: 3-13.

Yurova, A., A. Wolf, J. Sagerfors, and M. Nilsson. 2007. Variations in net ecosystem exchange of carbon dioxide in a boreal mire: Modeling mechanisms linked to water table position. *J. Geophys. Res.*: *112*. G02025 doi:10.1029/2006JG000342.

Chapter 10
ANNUAL VARIABILITY OF CO_2 AND CH_4 FLUXES FROM BOREAL PEATLAND

Considering the vast area of Russian arctic and boreal peatlands and the studies conducted (Panikov and Dedysh, 2002; Arneth et al., 2002; Friborg et al., 2003; Kutzbach et al., 2007; Golovatskaya and Dyukarev, 2009; Schneider et al., 2011), still little is known about their C cycling compared to e.g. Fennoscandia and North America. Especially continuous C-flux data from peatlands in the Russian boreal region are very limited (but see Arneth et al., 2002; Friborg et al., 2003).

Although continuous C-flux measurements are of high interest, static chamber measurements can help to resolve high spatial and temporal variations of both CO_2 and CH_4 fluxes. In this paper we therefore combine continuous eddy covariance measurements of CO_2 and CH_4 fluxes from a boreal peatland in the Komi Republic, Russian Federation, with the results of CO_2 and CH_4 chamber field campaigns from the same site during the same year.

When studying relationships between measured fluxes and environmental variables, linear or nonlinear response functions determined by regression are typically used to describe these relationships. Often, these regression functions are computed for annual or seasonal time scales and do thus not allow the identification of time-dependent changes in these relationships (Biondi, 1997). To capture the dynamical variability of signals, moving response function analysis (moving windows) can be applied. This technique employs a fixed time interval progressively slid across the time series of the fluxes (predictand) and the respective environmental control variables (predictors) to compute the response coefficients (Biondi, 1997; Mahecha et al., 2010). In the context of C-flux measrements, "moving windows" were e.g. previously used for the estimation of short-term temperature sensitivity of ecosystem respiration (Reichstein et al., 2005). A similar concept of temporally variable parameters is incorporated in the Kalman filter method (Visser, 1986; Rastetter et al., 2010).

Since the objective of this study was to quantify annual emissions of CO_2 and CH_4, and to explore the time dependency of environmental mechanisms controlling carbon (C) turnover and the measured fluxes on landscape and micro scales, we employed moving windows in our CO_2 flux analyses.

METHODS

Experimental setup

Eddy covariance

Detailed description peatland Medla-Pev-Nyur can be found in Chapter 9 and elsewhere (Gazovic et al., 2010; Schneider et al., 2011; Runkle et al., 2012). The fluctuations of the wind speed components were measured using a three-dimensional sonic anemometer (Solent R3, Gill Instruments Ltd., UK) installed 3 m

above ground level. From the sample intake 15 cm below the central point of the sensor array of the anemometer, a vacuum pump drew the sample air through a CO_2/H_2O infrared gas analyser (LI-7000, LI-COR Inc., USA) and through a CH_4 fast methane analyser (RMT-200, Los Gatos Research Inc., Mountain View, CA, USA). Both analyzers and the PC were housed in temperature-regulated boxes (InsituFlux, AB, Sweden). In October 2008, heating cables were installed at the intake tubes. Additional instruments installed near the EC tower include sensors for air temperature and relative humidity (CS215, Campbell Scientific Ltd., UK), wind speed and direction (M15103, R.M. Young, MI, USA), incoming and outgoing shortwave and long-wave radiation (CNR 1, Kipp and Zonen B.V, The Netherlands), incoming photosynthetic photon flux density (PPFD; QS2 Delta-T Devices Ltd., UK) and barometric pressure (RPT 410, Druck Messtechnik, GmbH, Germany). Liquid precipitation was monitored with a tipping bucket rain gauge. All signals from additional sensors were logged on a data logger (CR-1000, Campbell Scientific Ltd., UK). Soil temperature was measured at depths of 5 cm, 10 cm, 20 cm and 40 cm with automatically logged soil temperature sensors (HOBO U12 Outdoor/Industrial, Onset Computer Corp., Bourne, USA) under the surfaces of various representative microforms. At these microforms, additional chamber measurements of CO_2 and CH_4 fluxes were conducted, as well as measurements of **the green leaf area index (LAI). The eddy covariance measurements** were previously described also in Gazovic et al. (2010) and Runkle et al. (2012).

Raw data processing and flux calculation

Data were logged at 20 Hz, and eddy covariance fluxes were calculated over 30 min intervals. The time lag between wind and scalar concentration measurements was determined and removed for every averaging period. Turbulent fluxes were calculated using the EdiRe software (Robert Clement, University of Edinburgh, UK). Two coordinate rotations were applied to the wind components so that the mean transverse and the mean vertical wind components were reduced to zero. Flux losses due to the limited frequency response of the eddy covariance system were corrected in the flux calculation process. The fluxes were corrected for the frequency attenuation due to tube attenuation, sensor path separation and spectral response of the instruments (Moore, 1986; Moncrieff et al., 1997). The frequency correction in our study was on average 12.8±1.1% and 10.4±0.4% for CO_2 and CH_4 fluxes, respectively. The Webb correction adapted for closed-path eddy covariance systems was applied to the CO_2 flux (Ibrom et al., 2007). The Webb correction for open-path eddy covariance system was applied for CH_4 fluxes as no water concentration measurements were available in the CH_4 analyser measurement cell. Integral turbulence characteristics (ITC) were calculated, and data were screened accordingly (Foken and Wichura, 1996). Data were removed, if the deviation from the ITC parameter was greater than 30%. Instationarity characteristics were calculated and used to discard the data obtained during non-stationary conditions (Foken and Wichura, 1996).

Due to technical problems, instrument calibration and maintenance, gaps in the data series were introduced lasting from a few hours to days. The largest gap occurred from 29 June–10 August in the CH_4 measurements due to malfunctioning of the analyzer and shipment problems of the spare parts. In total, fraction of gaps after quality control screening was 40% for CO_2 and CH_4 data, respectively. For this study, positive flux values indicate upward fluxes, e.g. emission

from the peatland ecosystem; negative flux values indicate the contrary, e.g. uptake by the peatland ecosystem.

Chamber measurements

Microsites for CO_2 exchange, as well as chamber methods used, were previously described by Schneider et al. (2011) and won't be repeated here in full. As the CH_4 chamber measurements took place on the same micro sites, we briefly remark the general conditions. A total of 18 measurement plots were established within the area of interest on different microform types: 2 replicates each in ombrogenous hollows (OHO), lawns (OL) and hummocks (OH), and 3 replicates each in minerogenous hollows (MHO), lawns (ML) and hummocks (MH), and *Carex rostrata* lawns (CL). The sample plots were chosen subjectively, after a visual inspection of the site.

CO_2 exchange measured by the chamber methods was measured four times per week from 23 April to 20 October 2008 applying a closed chamber approach. A transparent chamber was placed on the permanent collars and change of CO_2 concentration was measured for 120 seconds using LICOR 700 portable infra red gas analyzer.

CH_4 emissions were measured using the closed chamber technique as well. From 18 June until 30 September, measurements were performed once a week. For CH_4 exchange measurements, 25 cm high opaque aluminum chambers were put on the groove of the collars. Six air samples per CH_4 flux measurements were taken from the chamber headspace with 60 ml plastic syringes. The chamber closure period for a single flux measurement was 20 minutes or, from 9 July on, 15 minutes, which was selected by the amount of CH_4 concentration measured. Five air samples were taken in an interval of either 3 or 4 minutes, additionally one sample was always taken after 30 seconds after closing of the chamber. The air sample analysis was usually done within the day following field-sampling with a gas chromatograph (GC, Hewlett Packard) equipped with a GFT PORAPAK a 80/100 (MESH-COND1900GC-015-9239, Hewlett Packard, USA) column and a flame-ionization detector (FID). Chromatogram peak integration was made by using the software GC Chem Station, Rev. A0903 [1417] (Agilent Technologies). Before entering the GC, the samples were passed through an attached molecular filter including a moisture indicator (0.3 nm, Merck). Thus, carrying moisture off the plastic syringe into the column of the GC was avoided.

From each air sample (40 ml), two 20 ml volumes were analyzed to detect possible measurement errors, and the mean value was used for further calculations. The required sample volume of the GC sample loop was 1 ml. But by using each time 20 ml it was assured that the whole sample loop was only filled with the current sample and possible leftovers from previous samples were eliminated. Flux rates of the chamber measurements were calculated from the linear rate of change in CH_4 concentration vs. time inside each chamber headspace according to the ideal gas law.

LAI of vascular plants was calculated as a product of the leaf size and number of green leaves. The green leaf area of mosses was estimated as the projection coverage of living moss capitula (about 0.75 m^2 m^{-2}). The estimated moss cover was set constant over the growing season. Total LAI was calculated as a sum of both vascular plants and mosses (for further details see Schneider et al., 2011). Water table (WT) fluctuations were monitored using water level loggers (type MDS, Seba Hydrometrie GmbH, Kaufbeuren, Germany) installed at four differ-

ent locations in the peatland, representing ombrogenic bog, minerogenic fen, the transition zone mostly consisting of *Carex* and *Sphagnum* lawns and the minerogenic depression. Manual WT readings were performed at each microsite collar during CO_2 and CH_4 chamber measurements campaigns.

Gap-filling model for fluxes measured by eddy covariance

To estimate the annual carbon balance, the gaps in the eddy covariance CO_2 and CH_4 flux time series were filled by empirical models of net ecosystem exchange of CO_2 and CH_4 (details see below).

CO_2 flux model

In this study, we used a moving window analysis to determine the model parameters at smaller than seasonal scale. Data were divided into night (PPFD< 20 μmol m^{-2} s^{-1}) and day (PPFD > 20 μmol m^{-2} s^{-1}) measurements. The term net ecosystem exchange (NEE), which is the sum of gross photosynthesis (P_g) and ecosystem respiration (R_{eco}), is equivalent to the calculated CO_2 fluxes. In our study we adapted a multiplicative nonlinear model based on Michaelis-Menten kinetics for gross photosynthesis P_g (Kettunen, 2000):

$$P_g = a1 \cdot PPFD / (PPFD + k1) \quad (1)$$

where *a1* indicates maximum photosynthesis (P_{max}), PPFD is photosynthetic photon flux density, and *k1* is the PPFD value for which the P_g reaches half of P_{max}. For ecosystem respiration, relationships with air and soil temperatures were studied, using data representing fluxes during dark periods (PPFD < 20 μmol m^{-2} s^{-1}). After the initial inspection, respiration rates R_{eco} were modelled using the following exponential function

$$R_{eco} = p1 \cdot e\,[p2 \cdot T] \quad (2)$$

where T is air temperature (T_{air}) or soil temperature (T_{soil}), parameter *p1* represents y-axis offset (magnitude of R_{eco} during the specific period/temperature regime) and parameter *p2* represents the curvature of the exponential function. The NEE time series was modelled by combining equations 1 and 2, resulting in the following equation

$$NEE = a1 \cdot PPFD / (PPFD + k1) + p1 \cdot \exp(p2 \cdot T) \quad (3)$$

with parameters and predictor variables as described above. We expected P_g to be zero during the night-time, and thus the CO_2 flux should represent R_{eco}. For this reason we fitted equation (2) to the night-time data with soil temperature in 20 cm as a predictor, giving the best fit. Equation (3) was fitted to the day-time data as we expected non-zero respiration during the day with air temperature as a predictor. This was done on raw data prior to gap filling.

The empirical models were then fitted to the flux data with a 10-day long window. The window was then slid one day forward to produce a second set of fit coefficients and so on. As a result we obtained time series of model parameters, coefficients of determination (R^2_{adj}) and root mean square errors (RMSE) indicating the performance of the fit function between measured fluxes and environmental predictor variables within the window.

The results of the moving response analysis in this manuscript were always plotted in a way that each single plotted parameter or coefficient value belonged to the centre of the 10-day long window (±5 days) and thus was representative for the whole window period.

During periods when we could not successfully model the time series with the described empirical models (for CO_2 before 4 May and after 5 November), the existing flux data sets were linearly interpolated. In order to estimate reasonable winter emissions during the period 19 February to 6 April when no data were available, the average flux values of the last three measurement days during the winter campaign in February 2009 were used as estimates.

CH_4 flux model

CH_4 fluxes were exponentially related to temperature and were modelled as

$$FCH_4 = a \cdot \exp [b \cdot T_{soil}] \quad (4)$$

where T_{soil} is soil temperature in 20 cm, a represents y-axis offset (magnitude of CH_4 flux during the specific period/temperature regime) and parameter b represents the curvature of the exponential function.

This model was used from 3 May until the end of the measurements on 12 February. From 6 to 21 April and from 5 November to 12 February, the existing data sets were linearly interpolated, and from 21 April until 3 May an empirical model with surface temperature as regulating variable describing diurnal variations during the snow melt period was applied (Gažovič et al., 2010). To estimate the winter emissions during the period 12 February to 6 April when no data were available, the average flux values of the last three measurement days during the winter campaign in February 2009 were used as estimates.

Footprint modelling

To estimate the EC source area fractions (Ω_i) of the land cover classes (i) in the area of interest, an analytical footprint model (Kormann and Meixner, 2001) was combined with landcover raster maps with 1 m resolution based on Quickbird imagery. These maps contain the information about the absence or presence of a class coded as 0 or 1, respectively. For each 30 min flux calculation interval and each class, each pixel was weighted with the footprint model function and multiplied with the code value (0 or 1) and the pixel area (1 m^2). Ω_i was then calculated as the sum of the pixels belonging to each class (Forbrich et al., 2011). The time series was filtered for low turbulence (friction velocity $u^* < 0.1$m/s), high cross-wind fluctuations ($\sigma_v > 1$ m/s) and periods when sensible heat flux was zero, leading to the removal of 43% of the data points of the 11-month time series. The gaps were filled with means of Ω_i which were calculated for one- degree intervals of wind direction for stable and unstable atmospheric conditions, respectively.

Estimating the annual C balance

The estimates of annual CO_2 and CH_4 emissions were calculated by integrating the gap-filled half-hour EC flux time series over time. When quantifying the annual budget based on EC measurements, various types of errors have to be considered (Moncrieff et al., 1996) as they are introducing uncertainty to the final estimate. For CO_2 estimates, we calculated the random error from the difference between the observed and modelled half-hourly fluxes (Aurela et al., 2002). The random error was calculated for three periods with different gap filling methods: a) linear interpolation before 4 May, b) empirical model (equation 3) from

4 May until 4 November and c) linear interpolation after 5 November. To estimate the random error for the periods when linear interpolation was used, we linearly interpolated between beginning and end points of the groups of measured data, and the random error was calculated as a difference between measured and linearly interpolated values (Rinne et al., 2007). Systematic errors in EC measurements have their origin in the limited frequency response of the EC system. An uncertainty of 30% was assumed for the frequency and Webb correction procedures itself (Aurela et al., 2002). For winter measurements with no data coverage where average values were used, 20% uncertainty of the balance of this season was assumed (Aurela et al., 2002). Additionally, the systematic error associated with selection of the gap filling method with moving and fixed parameters was estimated.

For CH_4, the random errors were estimated for the two periods when linear interpolation and the empirical models were used for gap filling. Systematic errors were considered, due to frequency and Webb corrections, and for winter estimations. The biggest source of possible systematic error in the annual CH_4 estimate was a 5-week gap in the summer period. Although the gap- filling procedure was shown not to have a strong effect on annual methane emission estimation (Rinne et al., 2007), we have used different gap-filling methods in our case in order to fill the gap during the summer, namely 1) linear interpolation, 2) gauss function and 3) an exponential function. The difference between the methods giving the smallest and the highest annual emission was considered as a systematic error for this period.

RESULTS

Weather characteristics

When instruments were set up at the end of March, the peatland was snow-covered (ca. 40 cm, P. Schreiber, personal communication) with a few snow-free hummocks. Mean daily temperatures were below 0 °C rising rapidly, reaching 3.5 °C on 1 April. High daily mean temperatures and rainfall accelerated snowmelt. From 12 to 16 April, mean daily temperatures decreased again below zero (Fig. 1a). All snow had disappeared by 17 April. No snow cover was established before the end of October (field observations). After this time, direct observations of snow accumulation are not available, but values of incoming and outgoing solar radiation indicate, that snow cover started to establish only at the end of November and probably even later. The first week in December was characterized by high- for this time of the year- temperatures, and thus we expect that the permanent snow cover was present only from the second third of December onwards.

After snowmelt, the WT stayed close to the surface in the ombrogenic, the minerogenic and the transition zone, at times rising slightly above the surface. The WT in the minerogenic depression stayed above the peat surface until 18 June, and hence only hummocks were protruding out of the water surface. The WT was at its lowest reaching around 22 cm below the peat surface on 19 August in the ombrogenic part, while in the minerogenic depression it only fell to around 5 cm below the peat surface. Frequent rainfall in the second half of August amounting to 115 mm (29% of all liquid precipitation measured from April to October) caused a considerable rise in the WT (Fig. 2).

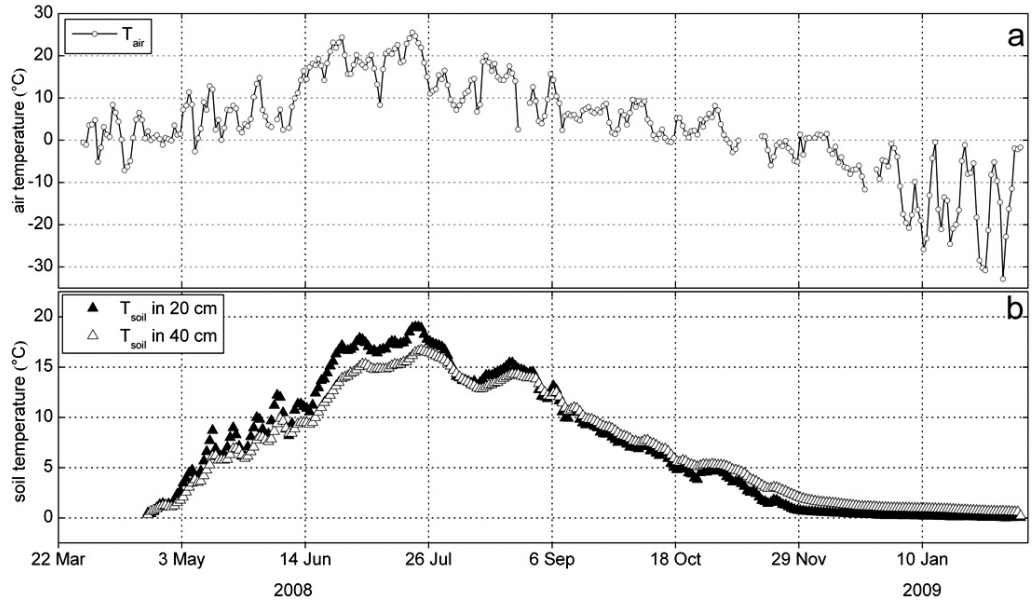

Fig. 1: Development of a) average daily air temperatures (○) and b) average daily soil temperatures in 20 cm (▲) and 40 cm (Δ) depth from April 2008 until February 2009.

The average July and January temperatures were 18.3 ˚C and −15.6 ˚C, respectively, which was 0.1 ˚C above and 2.9 ˚C below long term mean, respectively. Liquid precipitation measured from April to October was 388 mm. Mean daily temperatures during the study period reached a peak of 25 ˚C (diurnal maxima 31.1 ˚C) on 20 July. Lowest mean daily temperature of −32.8 ˚C (diurnal minima −40.1 ˚C) was measured on 6 February 2009. Interestingly, the air temperatures during winter showed high variability, and differences between night and day temperatures of up to 40 ˚C were observed at the site (similar amplitudes were measured at the meteorological station in Syktyvkar at the same time). Soil temperatures measured in different depths reached mean seasonal peak values of 19.7 ˚C in 10 cm and 16.5 ˚C in 40 cm, respectively, on 20 July and were

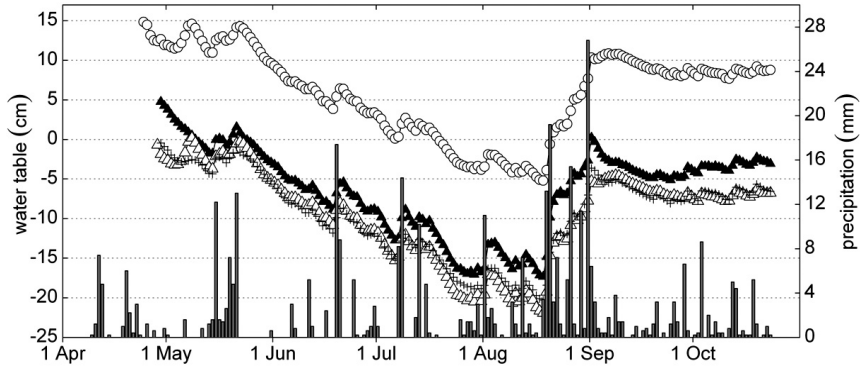

Fig. 2: Average daily values of water table (cm) and precipitation (mm, bar plot). Water table was measured in the minerogenic depression (○), the ombrogenic (▲), minerogenic (Δ) and transition (+) mire parts, showing very similar behaviour and strong coupling to precipitation events.

decreasing thereafter. Soil temperatures in 20 cm and 40 cm depth did not reach the freezing point until the end of measurements in February. Soil temperatures in 5 cm and 10 cm depth occasionally dropped below zero in January and February 2009, with the lowest temperature −0.5 °C in 5 cm depth measured on 7 February, when the lowest night air temperature −40.1 °C was measured.

Winds from south-east were predominant, but south, south-west and north-west winds also frequently occurred. The mean wind speed during the study period was 2.3±1.4 m s^{-1}.

EC CO_2 flux

Seasonal development of photosynthesis and ecosystem respiration

The late winter from 6 April to 16 April 2008 was characterised by moderate but variable CO_2 fluxes, on average 26±23 mg m^{-2} h^{-1}. After the snowmelt, without the presence of vascular plants and mosses being the only active green plants, R_{eco} – though at low levels – dominated the CO_2 flux. After 16 April, when all snow disappeared, the fluxes were increasing and reached 187 mg m^{-2} h^{-1} on 19 April, followed by a decline due to increasing photosynthesis. Diurnal oscillations were observed from 16 April right after the snowmelt, and several half-hourly fluxes during midday showed small CO_2 uptake. The daily NEE was oscillating between a small sink and a small source from the beginning of May. As the growing season progressed, the influence of T and PPFD on daytime NEE steadily increased, the photosynthesis was increasing, and on 20 May the peatland turned into a net daily CO_2 sink. Rapidly rising temperatures from 8 June onwards were followed by a rapid increase of vascular plants LAI from 14 June onwards when the first LAI measurements were conducted (Fig. 2). In this period a steeper increase in day and night NEE was observed (Fig. 5). CO_2 uptake during day-time culminated in the second half of July with NEE values of up to −1900 mg m^{-2} h^{-1}, while the night-time CO_2 releases reached 1000 mg m^{-2} h^{-1}. With the culmination of plant growth in July and the beginning of August and starting senescence, photosynthesis and plant-mediated respiration during the night slowly declined. In the beginning of August, a decrease in both day- and night- time fluxes due to cold temperatures was observed, although the CO_2 flux increased again in the middle of August prior to autumnal decline (Fig. 3).

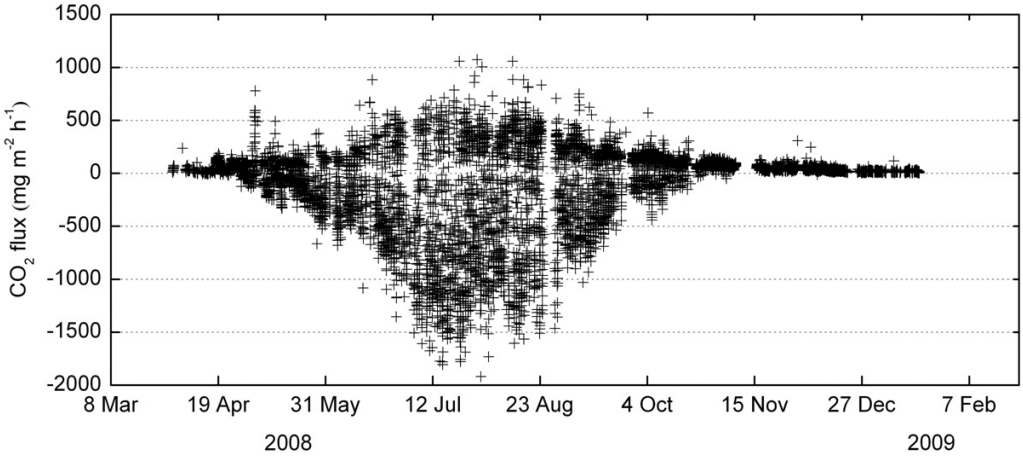

Fig. 3: Annual pattern of half-hourly measured CO_2 fluxes. Negative values indicate uptake of CO_2, positive values indicate CO_2 release.

From the end of September on, respiration dominated the CO_2 flux and the peatland turned into a net daily CO_2 source with increasing positive fluxes, reaching up to 150 mg m^{-2} h^{-1} at the end of October. This value is similar to the magnitude of ecosystem respiration after the snowmelt. The night- and day- time NEE at the end of the vegetation season was due to soil respiration controlled by soil temperature. The positive CO_2 release was decreasing towards winter minima. Diurnal oscillations, however small, could be observed until beginning of November. The winter measurements in January 2009 showed positive CO_2 fluxes with an average of 16.7±9.3 mg m^{-2} h^{-1}.

Moving window analysis of CO_2 fluxes

For day-time NEE, the maximum photosynthesis (P_{max}) was steadily increasing from the beginning of May (Fig. 4a). The increase in P_{max} calculated to the middle of a 10 day long window was not as rapid and was slightly delayed behind the steep increase in soil temperature in the beginning of June (Fig. 4a and 4b), although it seemed to follow the development of the green LAI (Fig. 4c), with the peak of P_{max} coinciding with the peak in LAI. After the peak LAI and P_{max} was reached and LAI was decreasing in August, changes in P_{max} were influenced more by the temperature (Fig. 4). For night-time NEE- R_{eco}, the parameter *p1* indicating the level of R_{eco} during a specific phenological period was increasing from the spring time, reached peak values at the end of July, and was decreasing thereafter (Fig. 5a). The parameter *p2* representing the curvature of the exponential function and so the temperature sensitivity of R_{eco} during a specific phenological period was increasing from the end of May. The rapid increase in the temperatures after 8 June (Fig. 1 and Fig. 4b) seemed to be responsible for

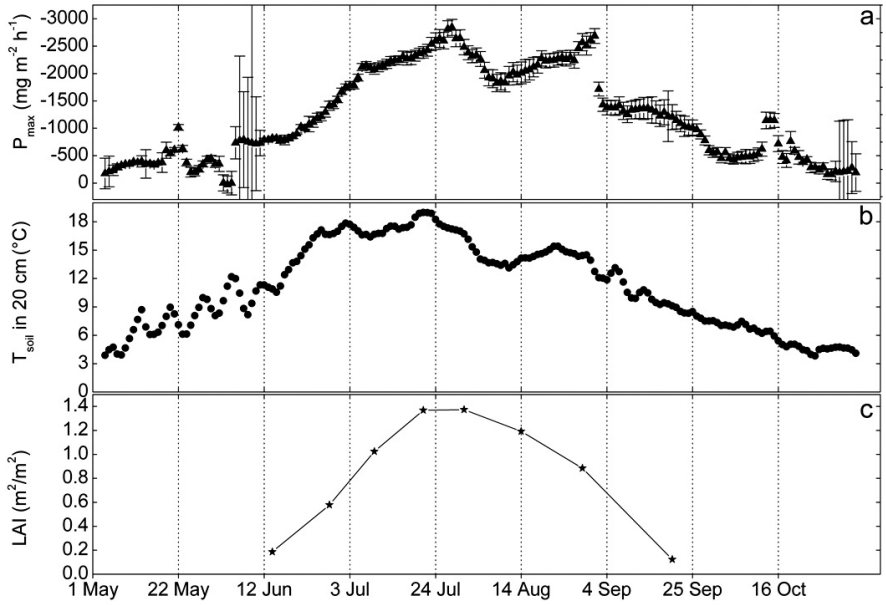

Fig. 4: Time series of a) maximum photosynthesis P_{max} (▲) obtained by moving window analysis with 10- day long window, b) soil temperature in 20 cm depth (•), and c) green leaf area index (*) at the Medla-Pev-Nyur mire from May to November. Note that the y-axis for P_{max} is reversed.

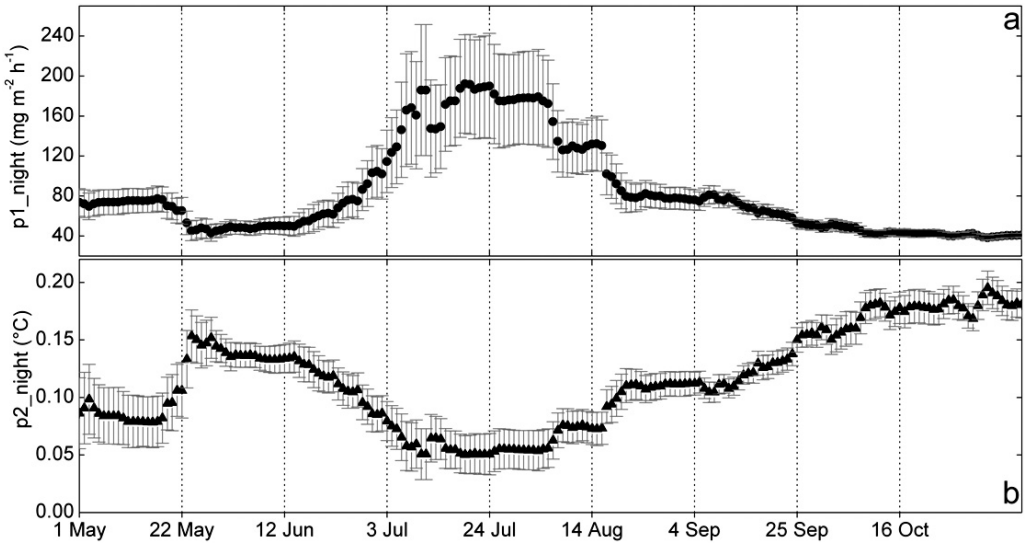

Fig. 5: Results of moving window analysis on CO_2 night fluxes as exponential functions of soil temperature in 20 cm (Eq. 2): a) estimated parameter *p1* (•) and b) parameter *p2* (▲) of the exponential model for 10-day window with 95% confidence intervals.

changing the exponential relationship between R_{eco} and temperature (parameter *p2*). A strong decrease of the values of the parameter *p2* was observed from the middle of June indicating a lower sensitivity of R_{eco} to T_{soil} during this period (Fig. 5b). An increase of the parameter *p2* was observed again from the beginning of August indicating a more pronounced temperature sensitivity of R_{eco}.

CH_4 flux

The Medla-Pev-Nyur peatland acted as a CH_4 source throughout the investigation period (Fig. 6). The lowest, but positive fluxes with on average 0.53±0.13 mg m^{-2} h^{-1} were measured from the snow-covered surface at the

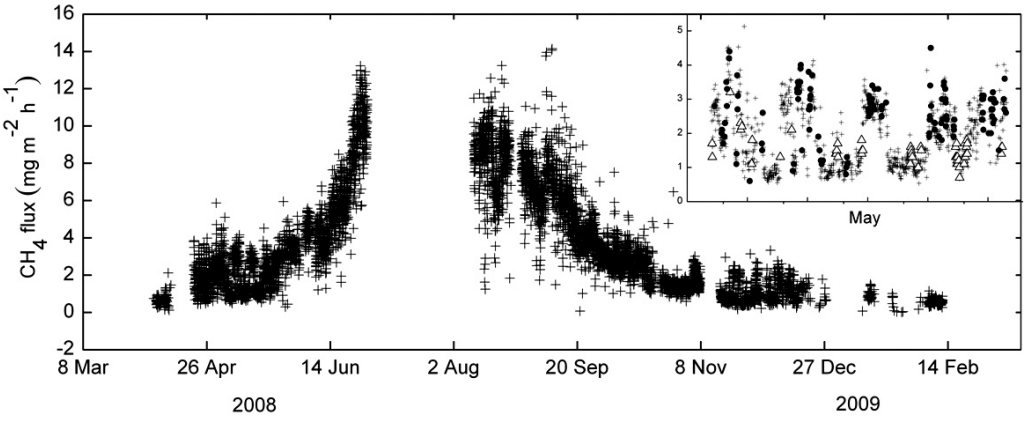

Fig. 6: Annual course of methane fluxes measured half-hourly. The inset illustrates spatially weighted CH_4 flux from minerogenic (Δ) and transition part (•) during May. The y-axis of the inlet is in the same units as the main plot. Gap in mid-season was due to technical failure.

beginning of April 2008. In the beginning of May, the highest emissions were 5 mg m^{-2} h^{-1}, followed by a slight decline. The fluxes were increasing from the end of May; however, a steep increase in CH_4 fluxes was observed from 12 June until 29 June. The highest emissions before and after the gap from 29 June to 10 August in the measurements were about 13 mg m^{-2} h^{-1}. From the beginning of September, CH_4 emissions were decreasing until reaching the winter minima. Beside diurnal variations observed in the period from 21 April to 3 May (Gažovič et al., 2010), no systematic diurnal variation was found based on the normalized medians method (Rinne et al., 2007). The empirical model driven by soil temperature showed a good performance (R^2_{adj}=0.82; RMSE=1.18 mg m^{-2} h^{-1}) and was used to fill missing data gaps.

Footprint analysis

Because the source area of the measured flux regularly extended over the area of interest, the sum of source area fraction Ω_i for each 30-min period ranged between 53-100%. We restricted the analysis on the 92% of all the flux data points which originated at least by 70% in the area of interest, after this restriction the sum of Ω for the minerogenic area (Ω_{min}) ranged from 0 to 87% (mean: 37 %), for the ombrogenic area (Ω_{omb}) from 0 to 29% (mean: 5%) and for the transition zone (Ω_{trans}) from 4 to 100% (mean: 46%). As the main wind direction was South (Fig. 2 in Chapter 9), the ombrogenic part situated in the north was under-sampled and in 60 % of the cases its area contribution was approximately 0%. On the other hand, the minerogenic and transition parts of the peatland were sampled evenly. Thus, further analysis was restricted to the minerogenic and transition parts by filtering the time series of measured fluxes for Ω_{min} or $\Omega_{trans} \geq 80\%$.

Filtering the time series of measured fluxes did not result in significantly different model parameters ($\rho<0.05$) for CO_2 or CH_4, respectively. Hence, we applied the gap-filling models for CO_2 (eq. 3) and CH_4 (eq. 4) on all fluxes which remained after the flux evaluation with no footprint function weighing.

Insight into small scale variations based on chamber measurements

The microforms in the minerogenous part of Medla-Pev-Nyur had higher CO_2 uptake compared to the ombrogenous part. The highest uptake with decreasing strength was measured on minerogenous lawns – *Carex* lawns – minerogenic hummocks - and minerogenic hollows. On the other hand, highest CO_2 release with decreasing strength was measured from *Carex* lawns- minerogenic and ombrogenic hummocks – and minerogenic hollows. Maximum CO_2 uptake was observed between 23 July and 10 August, following the seasonal LAI development. From 5 September, daytime respiration at the hollow sites exceeded photosynthesis, while *Carex* lawns and hummocks continued to have stronger photosynthesis than daytime respiration until end of the measurements. Unlike ombrogenous hollows, ombrogenous hummocks had higher respiration than photosynthesis during summer. Minerogenous hollows and hummocks showed the same pattern as the ombrogenous part, but at ombrogenous hummocks CO_2 release was higher than the uptake. The highest maximum day time respiration was measured from minerogenous hummocks and ombrogenous lawns, followed by Carex lawns and ombrogenous hummocks. The highest maximum photosynthesis was observed at minerogenous lawns, followed by Carex lawns and minerogenous hummocks. More details on small scale CO_2 flux dynamics can be found elsewhere (Schneider

et al., 2011). CH_4 measured in chambers showed positive fluxes during the chamber measurement period indicating net CH_4 release from our study site. The fluxes varied greatly within and between microforms. As can be seen from the median values for the whole measurement period for each microform, in general microforms raised above the peat surface like hummocks and microforms situated in the ombrogenous part released the least CH_4, while microsites situated in the minerogenous and transition part released the most. Ombrogenous hummocks released 1.2-2.2 mg m^{-2} h^{-1}, minerogenous hummocks 1.3-10.3 mg m^{-2} h^{-1}. Similar CH_4 fluxes were measured from different lawn types-minerogenous lawns 11.3-21.6 mg m^{-2} h^{-1}, Carex lawns 11.3-16.6 mg m^{-2} h^{-1} and slightly lower fluxes from ombrogenous lawns 7.7-9.8 mg m^{-2} h^{-1}. The highest CH_4 emissions were generally observed from minerogenous hollows (14.5-17.6 mg m^{-2} h^{-1}), but the difference to minerogenous lawns was small (Fig. 7). Not all microform plots revealed clear seasonal trend, but minerogenous and ombrogenous lawns did. Evident correlation of CH_4 fluxes measured in chambers with T and WT existed (data not shown), as well as correlation with LAI (Fig. 10). Minerogenous hollows, microforms with the lowest CO_2 uptake and release showed the highest CH_4 emission and had the highest maximal LAI during the season, while e.g. ombrogenous hummocks with the smallest LAI also had the smallest CH_4 fluxes. Carex lawns in the transition zone with one of the highest LAI values showed also high CH_4 fluxes (Fig. 8).

For comparison, the annual methane output measured by eddy covariance was 30±3 g CH_4 m^{-2} yr^{-1}, while the mean cumulative methane output from 18 June until 30 September calculated from chamber measurements ranged from 3.6 g CH_4 m^{-2} to 38.6 g CH_4 m^{-2}.

Annual carbon balance and uncertainty estimates based on EC data

The cumulative gap-filled NEE flux in our study was −458 g CO_2 m^{-2} y^{-1}. The random errors associated with the annual CO_2 estimate were ±3.8%, ±4.1% and ±1.3% and correspond to 1.2 g, 24 g and 0.9 g CO_2 m^{-2} for the time periods of different gap-filling procedures: a) linear interpolation before 4 May, b) empirical model (equation 3) from 4 May until 4 November and c) linear interpolation after 5 November, respectively. The wintertime (February to April) uncer-

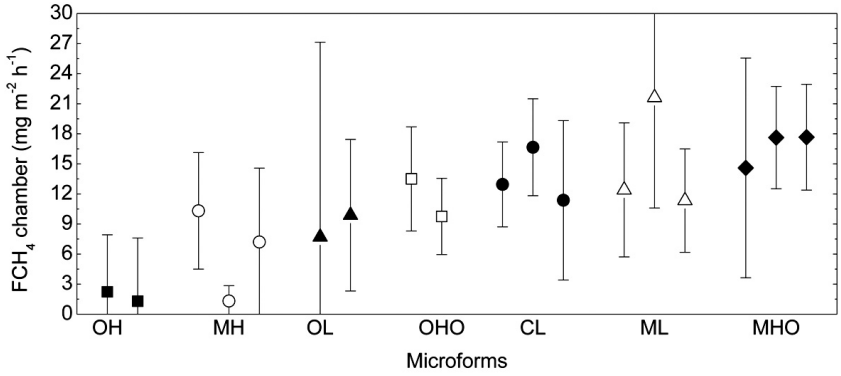

Fig. 7: Median values of methane flux measured in chambers from the various microforms during the measurement period (with standard deviations). OH – ombrogenous hummocks, MH – minerogenous hummocks, OL – ombrogenous lawns , OHO – ombrogenous hollows, CL – carex lawns, ML – minerogenous lawns, MHO – minerogenous hollows.

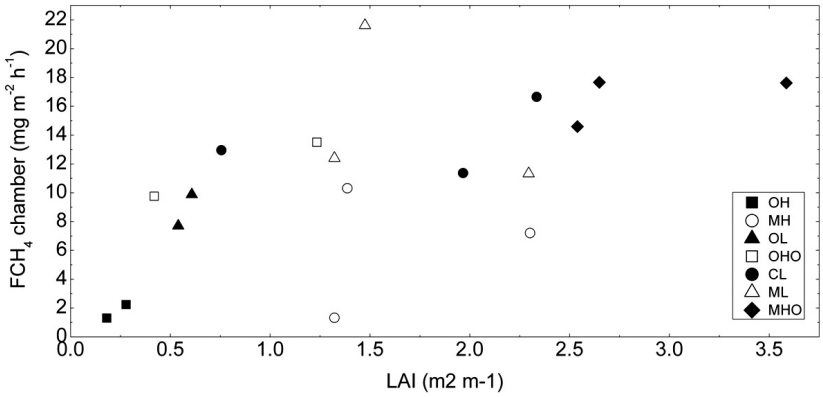

Fig. 8: Median values of methane flux measured in chambers versus maximal leaf area index during the measurement period in each microform (r=0.59, RMSE=4.71, p=0.009). Microforms abbreviations as in figure 9.

tainty was 5.6 g CO_2 m^{-2} yr^{-1} which corresponds to ±1.2% of the annual balance. The uncertainty associated with the CO_2 flux frequency correction was 3.8% or ±17.4 g CO_2 m^{-2} yr^{-1}. The uncertainty introduced by applying the Webb correction to the CO_2 flux of 5%, corresponded to ±22.9 g CO_2 m^{-2} yr^{-1}. Systematic error associated with selection of the gap-filling method by comparing the models with fixes and moving parameters in our case accounted for an error of 13%. Combining these errors following the standard error propagation, a relative uncertainty of 15.6% was obtained, which corresponds to ±71 g CO_2 m^{-2} yr^{-1}.

In terms of CH_4, the peatland was a source of methane to the atmosphere of 30 g CH_4 m^{-2} yr^{-1}. For CH_4, the random errors of gap filling were 3 % and 0.4% and correspond to 0.01 and 0.11 g CH_4 m^{-2} yr^{-1} for linear interpolation and empirical model data gap-filing. During the winter period, when average fluxes were used, an uncertainty of 0.47% corresponds to 0.14 g CH_4 m^{-2} of the annual balance. The uncertainty of the frequency correction procedure was 3.1%, corresponding to 0.93 g CH_4 m^{-2} in the annual balance. The systematic error associated with the long gap in summer was 7.2% or 2.12 g CH_4 m^{-2} yr^{-1}. Standard error propagation resulted in a combined error of 8.5% or ±2.5 g CH_4 m^{-2} yr^{-1}.

Taking the uncertainty in the measurements into account, the studied peatland acted as a CO_2 sink with an accumulation of ~458±71 g CO_2 m^{-2} yr^{-1}. In terms of CH_4, the peatland was a source of methane to the atmosphere of ~30±2.5 g CH_4 m^{-2} yr^{-1}. Considering the balances of both gases measured in our study, the peatland represented a net carbon sink of ~−102±21 g C m^{-2} yr^{-1}.

DISCUSSION

Annual carbon balance

The CO_2 and CH_4 estimates from our study of −458 ± 71g CO_2 m^{-2} yr^{-1} and 30±3 g CH_4 m^{-2} yr^{-1}, respectively are consistent with a range of other studies from the Russian boreal region. Friborg et al. (2003) reported an annual CO_2 flux estimate of −396 g CO_2 m^{-2} yr^{-1} based on eddy covariance measurements from the boreal peatland Bagchar Bog in western Siberia. The annual CO_2 balance from a sedge-Sphagnum fen in the same peatland complex estimated by combining bi-

omass sampling and CO_2 emissions was −443 g CO_2 m^{-2} yr^{-1} (Golovatskaya and Dyukarev, 2009). However, a very low annual NEE of −34±49 g CO_2 m^{-2} was also reported during a dry summer at an ombrotrophic boreal bog in Canada (Lafleur et al., 2003). Gažovič et al. (2013) estimated annual CO_2 flux, for one dry and one wet year, in a boreal *Sphagnum* fen in Finland of −339±47 and 566±69 g CO_2 m^{-2} yr^{-1}, respectively. Annual methane output from Medla-Pev-Nyur peatland was 30±3 g CH_4 m^{-2} yr^{-1}. For Finnish boreal mire sites, relatively low annual CH_4 estimates determined by eddy covariance measurements of 12.6±1 g CH_4 m^{-2} were reported (Rinne et al., 2007). Forbrich et al. (2011) estimated growing season (May-December) CH_4 emissions measured by eddy covariance of 11.7±0.2 g CH_4 m^{-2}, which (considering low emissions in missing winter months) is similar to estimates by Rinne et al. (2007). Annual CH_4 budgets in Russian boreal sites show higher values. Friborg et al. (2003) reported an annual CH_4 estimate for boreal site Bagchar Bog of 26 g CH_4 m^{-2} yr^{-1}.

To explain the relatively high CO_2 uptake and CH_4 emission in our study, we have to consider the conditions at the site during the measurements. The bias in the wind directions during the study, causing uneven sampling of different parts of the peatland, caused an under sampling of the ombrogenic part by the EC method. The results of CO_2 chamber measurements indicated higher CO_2 uptake in the minerogenous microforms, and Schneider et al. (2011) reported much higher variability in seasonal balance based on chamber data for various microforms. Thus, the measured EC fluxes seem to be representative for the nutrient-richer and more productive minerogenous and transition mire parts only. The high NEE from our study could be a result of the combination of high primary production and lower soil respiration in the minerogenous and the transition zones due to high WT (Gažovič et al., 2013). As was shown, differences in CO_2 fluxes between microforms could be explained by differences in LAI and WT, and even microforms with higher LAI, but lower WT, did show smaller CO_2 uptake (Schneider et al., 2011). Microforms with lower WT could experience higher C loss through soil respiration which was responsible for lower CO_2 uptake on these microforms. On the other hand, due to the waterlogged conditions, soil respiration is most likely limited by insufficient oxygen supply which is a substrate for respiration of soil microbes and roots (Davidson et al., 2006b), and the reduction of organic matter to CH_4 might be a more important mechanism for mineralization of organic matter than CO_2 soil respiration. This could be expected on microforms with higher WT.

Based on our data, CO_2 flux from Medla-Pev-Nyur peatland seemed to be controlled by abiotic factors such as temperature mainly during the transition periods winter-spring and summer-autumn. Temperature as an abiotic factor was responsible for vascular plant development after which biotic control seem to be a strong regulator. After senescence, when the active role of vascular plants decreased, CO_2 fluxes again seemed to be controlled mainly by temperature. Generally, it is difficult to answer the question of biotic vs. abiotic control of the CO_2 flux. However, a strong decrease of temperatures in the beginning of August was also visible in the decrease of CO_2 day- and night-time fluxes, which seem to indicate that the temperature is a strong controlling factor also when vascular plants are fully developed and reaching peak LAI values (Fig. 5 and 6c). The "recovery" of the CO_2 fluxes after this "cold" period supports this hypothesis, although the decrease of temperatures in this case was rather strong with night temperatures reaching −0.5 °C which could also affect some of the physiological functions.

Effects of biotic and abiotic factors on CH_4 fluxes

The seasonal trend of CH_4 fluxes was well explained by the influence of temperature in combination with changes in plant phenology induced by changes in temperature. Methane emissions are typically increasing with rising temperatures (Williams and Crawford, 1984; Christensen et al., 2003). But vascular plants can have a twofold influence on CH_4 fluxes: first as substrate suppliers for anaerobic microbial CH_4 production (Whitting and Chanton, 1993; Christensen et al., 2003) and second as CH_4 transport mediators (Morrissey and Livingstone, 1992; Lai, 2009). At our study site, a rapid increase of temperatures after 8 June was closely followed by LAI development and the senescence phase was also closely related to the temperature development. We can assume a substantial influence on CH_4 fluxes by the rapid development of vascular plants as substrate suppliers and CH_4 transport mediators in conditions with high and relatively stable WT level as in our study.

Beside a clear seasonal trend, the CH_4 fluxes normally showed short-term fluctuations ranging from diurnal to several days. While diurnal cycles were mostly attributed to plant activity (e.g. Kim 1998, Hendriks et al. 2010, Long et al. 2009) or freeze-thaw cycles (Gažovič et al., 2010), an additional explanation for the variability of the eddy covariance CH_4 flux measurements is the variation of the strength of the CH_4 source within the EC source area (Fan et al., 1992; Edwards et al., 1994; Forbrich et al., 2011). These variations are not restricted to diurnal cycles of temperature and/or radiation, so that they could explain the lack of a clear diurnal trend in the CH_4 flux data. Furthermore, they would explain the large scattering in fluxes from both the minerogenic and transition parts. Both parts consist of a mosaic of hollows, lawns and hummocks, with CH_4 flux strength decreasing strongly from hollows and lawns towards hummocks. During May, CH_4 fluxes from the transition part are higher than from the minerogenic part (Fig. 8, inset). One explanation of this difference could be the WT level. The WT was above the peat surface in the minerogenic depression, whereas it was below the surface in all other parts of the area of interest (Fig. 3). In turn, water standing above the surface represents a high diffusion resistance; therefore the fluxes from the waterlogged part could be smaller. However, we did not detect similar clear differences between the two parts in autumn, when the difference in water table position was similar as during May.

However, a detailed analysis on this scale requires high-resolution (<1 m^2) landcover maps (Becker et al., 2008; Forbrich et al., 2011) which are lacking for this site. To detect differences in CH_4 flux from the minerogenic and transition parts with the applied techniques, the CH_4 source strength of the two parts have to be similarly distinct as e.g. between hollows and hummocks on the microform scale. This seems not to be the case for the entire vegetation period because we could not identify significantly different model parameters for the minerogenic and transition peatland parts.

Winter Fluxes of CO_2 and CH_4

Winter (snow-covered surface) CO_2 and CH_4 fluxes amounted to 16.7-26 mg m^{-2} h^{-1} and 0.53±0.13 mg m^{-2} h^{-1}, respectively from the peatland Medla-Pev-Nyur and show very little variation. They represented 10.3% and 6.8% of annual carbon balance, respectively.

In a subarctic fen, Aurela et al., (2002) measured winter CO_2 fluxes of 20 mg m^{-2} h^{-1} in Finland, while a study from a boreal peatland in Siberia reported pre-

snowmelt CO_2 flux of 36 mg m^{-2} h^{-1} (Arneth et al., 2007). Average winter CO_2 emissions from Finish bog and fen sites measured by the chamber method of 20 mg m^{-2} h^{-1} and 37 mg m^{-2} h^{-1}, respectively, were reported by Alm et al., (1999).

Winter CH_4 fluxes from Minnesota peatlands ranged from 0.125-0.66 mg m^{-2} h^{-1} (Dise, 1992), whereas Panikov and Dedysh (2000) measured winter emissions from a West Siberian peatland of 0.054-0.36 mg m^{-2} h^{-1}. We did not find a relationship which could explain the emission controls of either of the gases measured during the winter in our study, while Aurela et al., (2002) explained part of their CO_2 flux variation by the correlation with the friction velocity. However, we could not identify a similar relationship in our study. During winter, several occasions with positive winter air temperatures were observed. Considering the strong influence of snow and ice on winter fluxes (Melloh and Crill, 1995), positive temperatures can cause melting of snow, and flux barriers in the form of thin ice layers within the snow-pack can occur during refreezing. This would effectively decrease the wind-induced emission. Winter methane emission can correlate with CO_2 flux (Panikov and Dedysh, 2000) which could be an indication of a common emission control. We did not find such a relationship in our study either; however, no final conclusion on winter emission controls can be drawn at this stage, as only few CH_4 flux data are available, and parallel measurements of both gas species from snow covered surface are rare.

CONCLUSION

The results of our study brought additional and new estimates of carbon flux dynamics in the boreal peatlands of the Russian Federation, a largely undersampled region of the Earth. Net annual carbon accumulation in the Medla-Pev-Nyur peatland was -102 ± 14 g C m^{-2} y^{-1}. The results show that the CH_4 emissions play an important role in annual estimates and in our study amount to 19% (22.5 g C m^{-2} yr^{-1}) of the annual carbon balance. No differences in trace gas exchange among the minerogenic and the transition mire peatland areas could be identified during the entire vegetation period, possibly due to undersampling of the ombrogenic areas. Using moving-window analysis, we could demonstrate a changing strength of the parameters of the CO_2 flux model at sub-seasonal scale. Over the course of a season, the CO_2 exchange was predominately influenced by temperature, in combination with changes in PPFD and in plant phenology. The seasonal trend of CH_4 exchange was strongly influenced by changes in soil temperature and plant phenology, and no clear relationship with WT was detected on a landscape scale, but only on the microform scale.

ACKNOWLEDGEMENTS

The study was conducted within the framework of the research project EURAPECC – "Eurasian peatlands in a changing climate", and funds were provided by a Sofja Kovalevskaja Research Award and a DFG grant # Wi 2680/2-1 to M. Wilmking. Michal Gažovič was supported by a KAAD scholarship and a Slovak Gas Industry travel grant. During the phase of data analysis and manuscript writing, L. Kutzbach and C. Wille were supported through the Cluster of Excellence "CliSAP" (EXC177), University of Hamburg, funded through the German Research Foundation (DFG). Infrastructure was partially supported by the Carbo North Project (6th FP of the EU, Contract # 036993). Special thanks goes to I. Beil for preparing figures in GIS.

References

Arneth, A., J. Kurbatova, O. Kolle, O.B. Shibistova, J. Lloyd, N.N. Vygodskaya, and E.D. Schulze. 2002. Comparative ecosystem-atmosphere exchange of energy and mass in a European Russian and a central Siberian bog. II. Interseasonal and interannual variability of CO_2 fluxes. *Tellus* B 54: 514-530. doi: 10.1034/j.1600-0889.2002.01349.x

Aurela, M., T. Laurila, and J.P. Tuovinen. 2002. Annual CO_2 balance of a subarctic fen in northern Europe: Importance of the wintertime efflux. *J. Geophys. Res.- Atmos.* 107 (D21): 4607. doi: 10.1029/2002JD002055

Becker, T., L. Kutzbach, I. Forbrich, J. Schneider, D. Jager, B. Thees, and M.Wilmking. 2008. Do we miss the hot spots? – The use of very high resolution aerial photographs to quantify carbon fluxes in peatlands. *Biogeosciences*. 5: 1387–1393. doi:10.5194/bg-5-1387-2008

Biondi, F. 1997. Evolutionary and moving response functions in dendroclimatology. *Dendrochronologia*. 15: 139-150.

Christensen, T.R., A. Ekberg, L. Strцm, M. Mastepanov, N. Panikov, M. Öquist,. B. H. Svensson, H. Nykänen, P.J. Martikainen, and H. Oskarsson. *2003.* Factors controlling large scale variations in methane emissions from wetlands. *Geophys. Res. Lett*. 30*: 1414, doi:*10.1029/2002GL016848.

Davidson, E.A., I.A. Janssens, and Y.Q. Luo. 2006b. On the variability of respiration in terrestrial ecosystems: moving beyond Q_{10}. *Glob. Change Biol*. 12: 154-164. doi: 10.1111/j.1365-2486.2005.01065.x

Dise ,N.B.1992. Winter fluxes of methane from Minnesota peatlands. *Biogeochemistry*. 17(2): 71-83.

Edwards, G, H. Neumann, G. den Hartog, G. Thurtell, and G. Kidd 1994. Eddy correlation measurements of methane fluxes using a tunable diode laser at the Kinosheo Lake Tower Site during the Northern Wetlands Study (NOWES). *J. Geophys. Res.-Atmos.* 99: 1511–1517. doi: 10.1029/93JD02368

Fan, S., S. Wofsy, P. Bakwin, D. Jacob, S. Anderson, J. Kebabian, J. McManus, and C. Kolb. 1992. Micrometeorological measurements of CH4 and CO2 exchange between the atmosphere and subarctic tundra. *J. Geophys. Res.-Atmos*. 97: 16627–16643. doi: 10.1029/91JD02531

Foken, T, and B. Wichura. 1996. Tools for quality assessment of surface-based flux measurements. *Agric. For. Meteorol*. 78: 83-105. doi: 10.1016/0168-1923(95)02248-1

Forbrich, I., L. Kutzbach, C. Wille, T. Becker, J. Wu, and M. Wilmking. 2011. Cross-evaluation of measurements of peatland methane emissions on microform and ecosystem scales using high-resolution landcover classification and source weight modeling. *Agric. For. Meteorol.* 151(7): 864–874 DOI: 10.1016/j.agrformet.2011.02.006

Friborg, T., H. Soegaard, T.R. Christensen, C.R. Lloyd, and N.S. Panikov. 2003. Siberian wetlands: Where a sink is a source. *Geophys. Res. Lett*. 30(21): 4. DOI: 10.1029/2003GL017797.

Gažovič, M., I. Forbrich, D.F. Jager, L. Kutzbach, C. Wille, and M. Wilmking. 2013. Hydrology-driven ecosystem respiration determines the carbon balance of a boreal peatland. *Sci. Total Environ*.: 675–682. Doi: 10.1016/j.scitotenv.2013.06.077

Gažovič, M., L. Kutzbach, P. Schreiber, C. Wille, and M. Wilmking. 2010. Diurnal dynamics of CH_4 from a boreal peatland during snowmelt. *Tellus* B 62: 133–139. doi: 10.1111/j.1600-0889.2010.00455.x

Golovatskaya E. A., and E.A.Dyukarev. 2009. Carbon budget of oligotrophic mire sites in the Southern Taiga of Western Siberia. *Plant Soil*: 315(1-2): 19-34.

Hendriks, D., J. van Huissteden, and A. Dolman. 2010. Multi-technique assessment of spatial and temporal variability of methane fluxes in a peat meadow. *Agricultural and Forest Meteorology* 150 (6): 757–774.

Ibrom, A., E. Dellwik, S.E. Larsen, and K.Pilegaard. 2007. On the use of the Webb-Pearman-Leuning theory for closed-path eddy correlation measurements. *Tellus* B 59: 937-946. doi: 10.1111/j1600-0889-2007-00311-x

Kettunen, A. 2000. Short-term carbon dioxide exchange and environmental factors in a boreal fen. *Verh. Internat. Verein. Limnol.* 27: 1446-1450.

Kim J., S. Verma, D. Billesbach, and R. Clement. 1998. **Diel variation in methane emissions from a midlatitude prairie wetland: Significance of convective throughflow in Phragmites australis.** *Journal of Geophysical Research* 103 (D21): 28029–28039. DOI: 10.1029/98JD02441.

Kormann, R., and F.X. Meixner. 2001. An analytical footprint model for non–neutral stratification, *Boundary–Layer Meteorology* 99(2): 207.

Kutzbach, L., C. Wille, and E.M. Pfeiffer. **2007. The exchange of carbon dioxide between wet arctic tundra and the atmosphere at the Lena River Delta, Northern Siberia.** *Biogeosciences.* 4(5): 869-890. doi:10.5194/bg-4-869-2007.

Lafleur, P. M., N.T. Roulet, J.L. Bubier, S. Frolking, *and* T.R. Moore. 2003. Interannual variability in the peatland-atmosphere carbon dioxide exchange at an ombrotrophic bog. *Global Biogeochem. Cycles*. 17*: 1036. doi:*10.1029/2002GB001983,

Lai, DYF. 2009. Methane Dynamics in Northern Peatlands: A Review. *Pedosphere* 19(4): 409-421.

Long, K., L.B. Flanagan, and T. Cai. 2009. Diurnal and seasonal variation in methane emissions in a northern Canadian peatland measured by eddy covariance. *Global Change Biology*. 16 (9): 2420–2435. doi: 10.1111/j.1365-2486.2009.02083.x

Mahecha, M.D., L.M. Fürst, N. Gobron, and H. Lange. 2010. Identifying multiple spatiotemporal patterns: A refined view on terrestrial photosynthetic activity. *Pattern Recogn. Lett*. 31(14): 2309-2317. doi: 10.1016/j.patrec.2010.06.021

Melloh, R. A., and P.M. Crill. 1995. Winter methane dynamics beneath ice and in snow in a temperate poor fen. *Hydrol. Proc.* 9: 947-956.

Moncrieff, J.B., Y. Malhi, and R. Leuning. 1996. The propagation of errors in long-term measurements of land-atmosphere fluxes of carbon and water. *Glob. Change Biol.* 2(3): 231-240.

Moncrieff, J., R. Valentini, S. Greco, G. Seufert, and P. Ciccioli. 1997. Trace gas exchange over terrestrial ecosystems: Methods and perspectives in micrometeorology. *J. Exp. Bot*. 48: 1133-1142. doi: 10.1093/jxb/48.5.1133

Moore, C.J. 1986. Frequency response corrections for eddy correlation systems. *Bound. Layer Meteor.* 37: 17–35.

Morrissey, L.A., and G.P. Livingston. 1992. Methane emissions from Alaska Arctic tundra: An assessment of local spatial variability. *J. Geophys. Res*. 97*:* 16661–16670*, doi:*10.1029/92JD00063.

Panikov, N.S., and S.N. Dedysh. 2000. Cold season CH_4 and CO_2 emission from boreal peat bogs (West Siberia): Winter fluxes and thaw activation dynamics. *Global Biogeochem. Cycles* 14: 1071-1080. doi: 10.1029/1999GB900097

Rastetter, E.B., M. Williams, K.L. Griffin, B.L. Kwiatkowski, G. Tomasky, M.J. Potosnak, P.C. Stoy, G.R. Shaver, M. Stieglitz, J.E. Hobbie, and **G.W. Kling. 2010. Processing** arctic eddy-flux data using a simple carbon-exchange model embedded in the ensemble Kalman filter. *Ecol. Appl*. 20 (5): 1285-1301. doi.org/10.1890/09-0876.1

Reichstein, M., E. Falge, D. Baldocchi, D. Papale, M. Aubinet, P. Berbigier, C. Bernhofer, N. Buchmann, T. Gilmanov, A. Granier, T. Grunwald, K. Havrankova, H. Ilvesniemi, D. Janous, A. Knohl, T. Laurila, A. Lohila, D. Loustau, G. Matteucci, T. Meyers, F. Miglietta, J.M. Ourcival, J. Pumpanen, **S. Rambal, E. Rotenberg, M. Sanz, J. Tenhunen**, G. Seufert, F. Vaccari, T. Vesala, D. Yakir, and R. Valentini. 2005. On the separation of net ecosystem exchange into assimilation and ecosystem respiration: review and improved algorithm. *Glob. Change Biol.* 11: 1424-1439. doi: 10.1111/j.1365-2486.2005.001002.x

Rinne, J., T. Riutta, M. Pihlatie, M. Aurela, S. Haapanala, J.P. Tuovinen, E.S. Tuittila, and T. Vesala. 2007. **Annual cycle of methane emission from a boreal fen measured by the eddy covariance technique.** *Tellus* B. 59 (3): 449-457. doi: 10.1111/j.1600-0889.2007.00261.x

Runkle, B.R.K., C. Wille, M. Gažovič, and L. Kutzbach. Attenuation Correction Procedures for Water Vapour Fluxes from Closed-Path Eddy-Covariance Systems. *Boundary-Layer Meteorology* 2012; 142(3): 401-423, doi:10.1007/s10546-011-9689-y.

Schneider, J., L. Kutzbach, and M. Wilmking. 2011. Carbon dioxide exchange fluxes of a boreal peatland over a complete growing season, Komi Republic, NW Russia. *Biogeochemistry*. 111: 485-513, doi 10.1007/s10533-011-9684-x.

Whiting, G.J., and J.P. Chanton. 1993. Primary Production Control of Methane Emission from Wetlands. *Nature* 364(6440): 794-795. doi:10.1038/364794a0.

Williams, R.T., and R.L. Crawford. 1984. Methane production in Minnesota peatlands. *Applied Environmental Microbiology* 47: 1266-1271.

Visser, H. 1986. Analysis of tree-ring data using the kalman filter technique. *Iawa Bulletin* 7(4): 289-297.

Chapter 11
LONG-TERM DYNAMICS OF METHANE EMISSION IN MESOOLIGOTROPHIC PEATLAND

Peatlands being typical for the Komi Republic are oligotrophic domed range-hollow sphagnum, mesotrophic sphagnum, and eutrophic flood peatlands in the north and middle taiga subzones; aapa mires in the far north and north taiga subzones; peat plateaus in the forest-tundra zone (Forestry..., 2000). The studies on methane fluxes in peatland in the northwestern Russia are rare (Slobodkin et al., 1992; Heikkinen et al., 2002). There are data on methanotrophic microbe communities for peat and coarse-humus cryozems of the High Arctic tundra area (Berestovskaya et al., 2002).

MATERIALS AND METHODS

This paper presents the results of methane emission investigation in Medla-Pev-Nyur mesooligotrophic peatland in 2008, 2011, 2013, and 2014. Vegetation cover of studied plots is given in Table 1.The warmest weather in the study region in June-July was observed in 2011 and 2013 and the coolest one – in 2014 (Table 2). In August 2011 the deviation of mean monthly temperature from perennial norm was −1.3 °C.

Table 1

Microform and vegetation characteristics on the study plots

Plot, №	Site	Microform	Dominant plants
1	Bog	Ombrogenous hollow	*Sphagnum* (100%). *Scheuchzeria palustre* (10%), *Oxycoccus palustris* (5%).
2	Transition zone	*Carex rostrata* lawn	*Sphagnum* (100%). *Carex rostrata* (20%), *Oxycoccus palustris* (10%), *Carex limoza* (10%), *Andromeda polifolia* (4%)
3	Fen	Minerogenous hollow	*Sphagnum* (80%). *Scheuchzeria palustre* (<50%), *Utricularia intermedia* (15%), *Menyanthes trifoliata* (15%), *Oxycoccus palustris* (4%), *Carex limoza* (4%)
4	Bog	Ombrogenous hummock	*Chamaedaphne calyculata* (5%), *Oxycoccus palustris* (7%), *Andromeda polifolia* (10%), *Rubus chamaemorus* (5%)

To measure methane emission rate from peatland surface we applied the method of static dark chambers. In 2008, air sampling utilized aluminum chambers with volume of 0.108 m^3. Frames which limited peat plots were 0.36 m^2 in area. In 2011-2014, we used chamber of 0.075 m^3 and frames of 0.25 m^2.

The chamber had a thermometer, a fan which mixed air inside chamber, and a tube which provided for a stable atmospheric pressure inside tube. Air sampling was done with 60-ml plastic syringes in 4-min intervals during total chamber exposition of 20 min.

Table 2

Weather conditions for four observation years (by Centre on Hydrometeorology and Environmental Monitoring of the Komi Republic, Ust–Vym station)

Year	Month	Parameters					
		Average air temperature, °C	Deviation, °C	Min	Max	Precipitation, mm	% at norm
2008	May	5.5	–1.3	–6	23	51	106
	June	14.3	0.6	–1	30	48	72
	July	18.6	2.3	8	31	42	61
	August	13.3	–0.4	2	24	144	215
	September	6.5	–1	–1	19	72	107
2011	May	10.6	3.8	–4	27	39	81
	June	15.9	2.2	3	31	26	39
	July	19.4	3.1	3	34	35	51
	August	12.4	–1.3	–1	26	54	81
	September	8.9	1.4	2	19	83	124
2013	May	8.4	1.6	–3	25	37	77
	June	16.6	2.9	2	33	35	52
	July	19	2.7	6	32	32	46
	August	15.9	2.2	7	27	48	72
	September	8.5	1	–2	20	36	54
2014	May	9.7	2.9	–6	30	39	81
	June	12.8	–0.9	1	26	67	100
	July	14.3	–2	2	27	37	54
	August	15.9	2.2	4	30	84	125
	September	8.9	1.4	–2	21	40	60

Methane volume ratio in air samples was determined by the method of gas chromatography using Kristall 5000.2 gas chromatographer (CSC SKB "Khromatek", Russia) with a flame-ionizing detector. Packed column (M 2*3) was filled with HayesepN 80/100 adsorbent; carrier-gas was nitrogen. Gas mixture of hydrogen and air was used to maintain detector's flame. Column's temperature equaled 60°C and detector's temperature - 160°C. Air samples were analyzed in two replications. In 2014, methane volume ratio was measured with GGA 28p mobile gas analyzer (LosGatosResearch, USA) which worked by the principle of off-axis laser spectroscopy.

Emission rate was calculated by the equation:

$$F(CH_4) = \frac{M \cdot \rho \cdot V \cdot dC/dt}{R \cdot A \cdot T}, \quad (1)$$

where $F(CH_4)$ – methane emission rate value (μg m^{-2} s^{-1}); M – methane molar weight (16.043 g mol^{-1}); ρ – atmospheric pressure at measuring time (Pa); V – chamber volume (m^3); dC/dt – gas concentration change in time t (ppm s^{-1}); R – universal gas constant (8.314472 Pa m^3 mol^{-1} K^{-1}); A – area of limiting frame (m^2); T – temperature inside chamber at measuring time (K).

Total efflux value was calculated by the function:

$$Total = Me \cdot P \quad (2)$$

where Me – median of seasonal methane emission (g m^{-2} h^{-1}), P – active methane emission period (h) which exceeds summer-autumn period duration by 12% (Suvorov, Glagolev, 2007).

Area of study sites (elementary associations) where we conducted our measurements was identified using high-resolution satellite images via graticule layout in Adobe Photoshop CS5.

Stagnant water table level from moss capitulum was fixed using plastic tubes put into peat layer. The values were negative when water level was under moss capitulum and positive when it was above.

Microclimatic parameters during season were automatically registered with sensors (Hobo USA) which were mounted at 1.5-m height from plant cover surface. Temperature sensors measured temperature in peat layer at 5- and 30-cm depths. In 2013, soil temperature sensors measured at 5- and 20-cm depths because of other recorder's modification.

Statistic data analysis was fulfilled using STATISTICA v.10 program package. Distribution normality was checked by Shapiro-Wilk test. Correlation analysis applied Spearman's nonparametric criterion for small sample groups (correlation of methane emission diurnal dynamics and microclimatic parameters) and Pearson's parametric criterion (correlation of seasonal methane emission and ecological factors). Comparison of emission intensity at different plots applied Student's t-criterion. The method of principle components identified relation between microclimatic factors and seasonal methane emission changes. All statistic calculations were done at $p=0.05$. Emissions were assessed by the box-and-whiskers method.

RESULTS AND DISCUSSION

Summer months 2011 and 2013 were also poor in precipitation amount. The year of 2008 was characterized by cool weather in spring and autumn with abundant rains in August. Vegetation periods 2008 and 2011 included 149 and 159 days with summer-autumn period of 147 and 164 days, respectively. In 2013 and 2014, summer-autumn period lasted for 144 and 178 days, respectively, with vegetation period of 143 days.

Diurnal dynamics

In 2013 methane emission rate from the Medla-Pev-Nyur mesooligotrophic peatland at different plots varied largely. In May, methane emission increased in night when air temperature dropped and soil temperature at 10-20-cm depth remained stable (Fig. 1). But methane emission rate at fen site exceeded that at ombrogenous hollow by 60-70%. Towards the third decade of June remarkable through active grass growth, the above situation resisted (t-test, $\alpha=0.00002$) with emission rate being higher than that in May in both cases. Some authors relate this increase with high mean daily temperatures (Macdonald et al., 1998) or gradual aboveground phytomass increment (Whiting, Chanton, 1992). Methane emission rate in June attained its highest values in evening and night hours. Towards the third decade of July and in August, rain showers increased daily variation of methane flux from surface of ombrotrophic hollow.

In 2013, early start of the vegetation period led to mean diurnal emission values of 1.28-2.02 μg $m^{-2}s^{-1}$ for minerogenous and 0.75-1.55 μg $m^{-2}s^{-1}$ for ombrogenous plot which attained in middle summer 4.8 μg $m^{-2}s^{-1}$ and 7.94 μg $m^{-2}s^{-1}$ correspondingly. Some authors relate intensive methane emission in evening and night hours with soil temperature increase (Mikkelä et al., 1995; Glagolev, Smagin, 2006). By our data, the highest daily emission rate values corresponded with the highest soil temperature at a 20-cm depth.

According to the correlation data analysis, methane emission from ombrogenous hollow in May had a negative dependence on air temperature which can

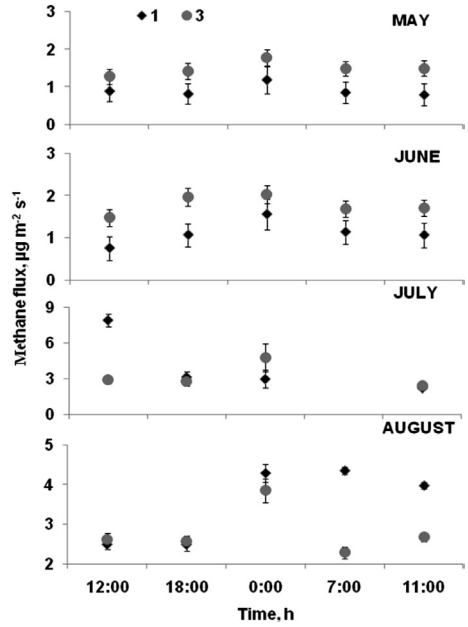

Fig. 1: Diurnal course of methane emission in 2013.1, 3 – numbers of plots (see Table 1). Bars correspond to standard measurement error.

be demonstrated by a logarithmic function (Table 3). Methane flux intensity decreased when air temperature rose from 0 to +10°C. Water-covered plots of fen site demonstrated similar but less significant dependence.

By results of nonparametric Spearman's test, methane emission rate did not correlate with microclimatic parameters at $p<0.05\%$. However, minerogenous hollow showed a close correlation of emission with soil temperature at 20-cm depth (Table 3). Both study plots tended to increase methane emission rate together with soil temperature at that depth which agrees with the other authors' results (Macdonald et al., 1998).

In July, 23 and August, 21 methane emission at ombrotrophic site closely correlate with atmospheric pressure. Inverse correlation of CH_4 emission and atmospheric pressure was caused by physical impact of pressure on methane ebullition. Low atmospheric or hydrostatic pressure in wetland ecosystems is known to increase the proportion of CH_4 ebullition in total methane emission. Interestingly, combined action of atmospheric and hydrostatic pressure responds for 40% of bubble methane flux (Deshmukh et al., 2014).

Table 3

Diurnal correlation of methane emission at peatland with temperature and atmospheric pressure in 2013 (Spearman's correlation coefficient)

Date	Plot, №	Number of measurements, n	Air temperature, °C	Soil temperature, °C		Atmospheric pressure, Pa
				5 cm	20 cm	
22.05-23.05	1	5	–1*	–0.6	–0.3	–0.1
	3	5	–0.1	0.3	0.3	0.5
25.06-26.06	1	5	–0.7	–0.3	0.7	–0.3
	3	5	–0.3	0.2	1*	–0.5
23.07-24.07	1	5	0.8	0.8	–0.4	–1*
	3	5	–0.2	0.2	–0.6	–0.4
21.08-22.08	1	5	–0.6	–0.3	0.1	–0.6
	3	5	–0.6	0.2	0.5	–0.1

* Significant at $p<0.05$.

Seasonal dynamics

Methane emission ranged across four study plots from 0.005 to 15.5 μg $m^{-2} s^{-1}$ from June until September 2008, median corresponded to 1.35/3.76/5.47 μg $m^{-2} s^{-1}$ (here and then we indicated 1st quartile/median/3rdquartile). In May-September 2011 methane emission comprised 0.017-14.76 μg $m^{-2} s^{-1}$ with median of 02/2.26/4.93 μg $m^{-2} s^{-1}$.

From May to September 2013, emission rate varied within 0.75-12.2 μg $m^{-2} s^{-1}$ with median of 1.25/2/2.9 μg $m^{-2} s^{-1}$. In 2014 methane emission was not as variable as previously observed ones (0.001-4.3 μg $m^{-2} s^{-1}$), median was 0.13/1.8/2.7 μg $m^{-2} s^{-1}$.

Generally, methane emission gradually increased from May to June and reached its highest values in July independently of observation year (Fig. 2). Methane emission gradually decreased in August and was close to zero in September. Despite summer months 2014 were cool, methane emission did not have any significant differences from the data obtained for the other years (t-criterion, α=0.94).

Some authors relate intensive methane emission in July with active vegetation period of grasses which means intensive exudation of fresh organic matter, i.e. nutrition for methanogenic archaea (Alfordetal., 1997). But other connect intensive methane emission in mid vegetation period to high biomass of grassy plants which can conduct methane from soil to atmosphere through aerenchyma tissues (Whiting and Chanton, 1992).

Statistic analysis did not identify true differences between emission rates in 2008 and 2011. Among four observation years, only 2014 significantly differed from the others by mean emission values as it was characterized by cool weather in early and mid vegetation period (Table 4).

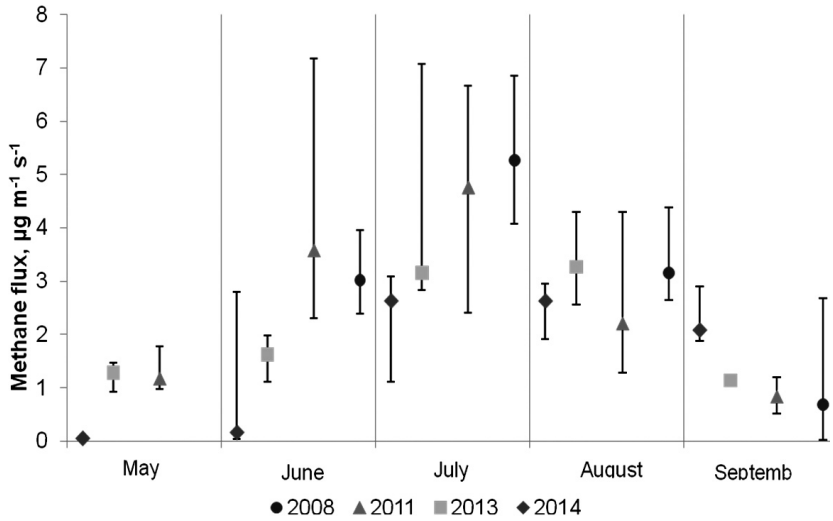

Fig. 2: Seasonal course of methane emission in four years. Markers correspond to monthly flux median. Negative values of error margin correspond to 1st quartile and positive values – to 3rdquartile.

Table 4

Matrix of mean methane emission values for four observation years (t-test). Figures in table cells indicate confidence level of differences (α)*

Year	2008	2011	2013	2014
2008	1	0.4	0.007	0
2011	0.4	1	0.03	0.001
2013	0.007	0.03	1	0.01
2014	0	0.001	0.01	1

* Data significantly differ at α<0.05.

The highest methane flux values for four observation years were recorded for the *Carex rostrata* lawn (plot 2). In 2008, emission median at minerogenous (plot 3) and transition site (plot 2) was similar but in the former case its variation diapason was higher (Fig. 3). Many authors describe intensive methane flux from surface of excessively moist areas and relate it to grassy plants. They can strengthen methane production due to root exudation of sugars which are available for microorganisms (Rovira, 1969; Russell, 1977) and even emission itself as they passively transport methane through aerenchyma tissues (Schimel, 1995; Nykänen et al., 2002).

Ombrogenous hummock (plot 4) emitted visually less methane. Wide variation range of methane flux at plot 4 in 2011 was possibly produced by a short-time methane ebullition from peat layer.

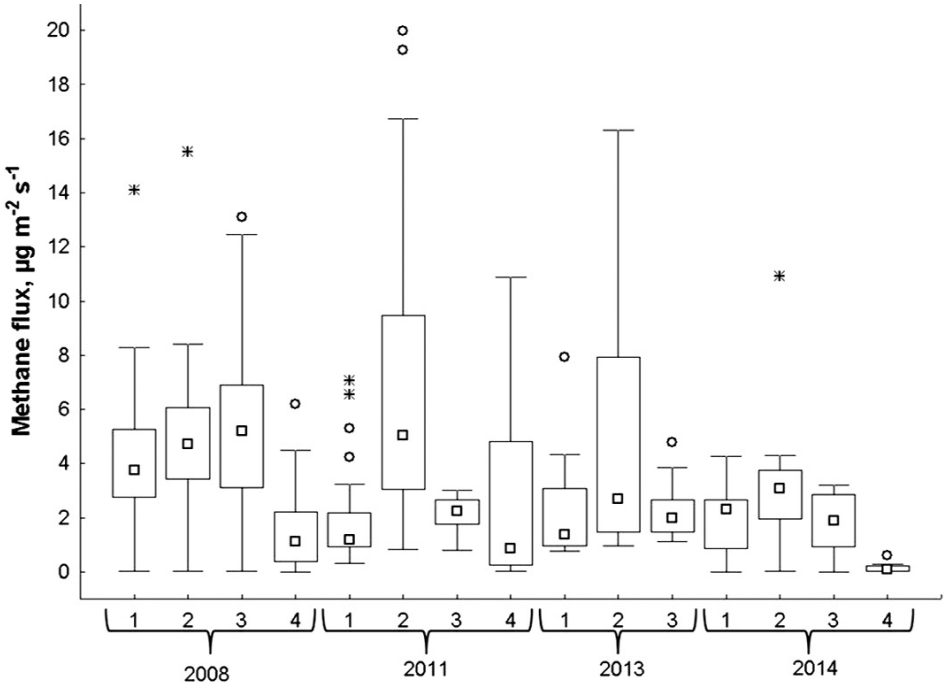

Fig. 3: Methane flux medians from surface of the study plots in different observation years. Numbers of plots correspond to those in Table 1.

According to the statistic analysis method of principle components, the main factors responsible for seasonal methane flux intensity in 2008 and 2013 were soil temperature at 20-cm depth and water table level which together regulated more than 50% of methane flux (Table 5). In 2011, water table level was the first-important factor for methane emission whereby air temperature was less important. For 2014, the analysis was not conducted due to insufficient data amount.

Table 5

Principle analysis components of main environmental factors for 3 observation years

Variable	2008		2011		2013	
	F1	F2	F1	F2	F1	F2
Flux	***0.87***	–0.43	***0.94***	0.01	0.64	–0.05
T_{soil}	***0.81***	0.50	0.57	–0.53	***0.93***	–0.02
WTL	***0.73***	–0.61	***–0.91***	–0.04	***–0.86***	–0.42
T_{air}	0.53	***0.79***	–0.28	***0.87***	–0.47	***0.88***
Variance, %	57.6	22.8	53	26	55.5	35.6

During vegetation period of 2008, high ground water level increased methane emission. The years of 2011 and 2013 showed an inverse trend (Fig. 4). High methane emission values in 2011 and 2013 were possibly caused by intense methane ebullition in dry summer (Table 2). The results obtained by Rinneet et al. (2007) were similar. They measured methane emission by the Eddy covariance method and related high methane flux to methane ebullition to low hydrostatic pressure.

In 2008, 2011,and 2013, methane emission closely correlated with soil temperature at 20-cm depth and weakly correlated with surface temperature (0-5 cm). For three observation years, methane flux intensity to 20-cm soil temperature connection can be presented as an exponential function (r=0.7, p>0.05) (Fig. 5) which agrees with data of earthy studies (Bubieretal., 1993; MacDonald, 1998; Hargreaves et al., 2001; Glagolev et al., 2010).

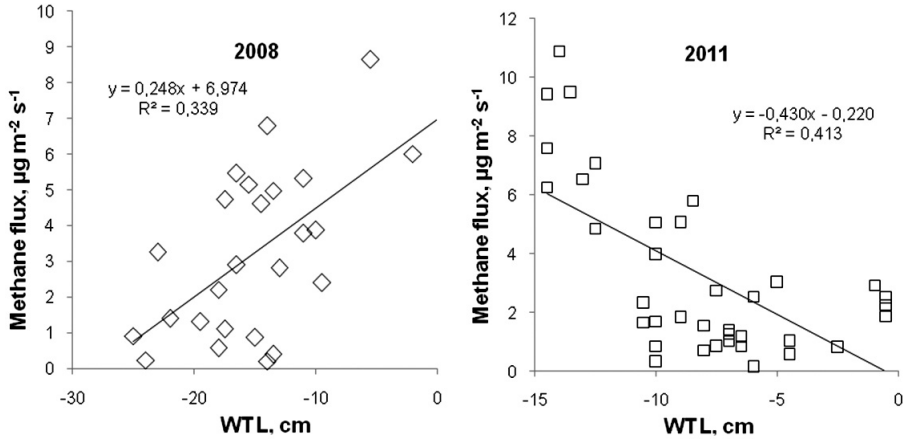

Fig. 4: Correlation of methane emission and water table level in 2008 and 2011.

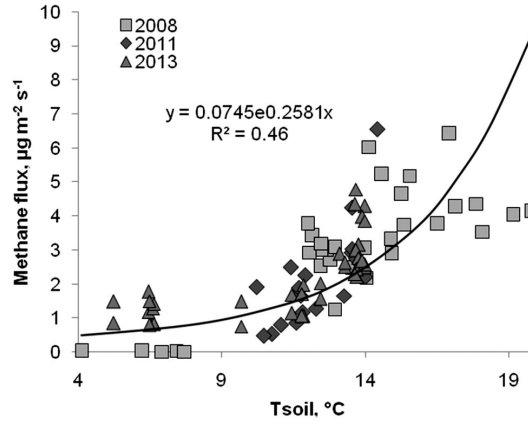

Fig. 5: Correlation of methane emission and soil temperature at 20-cm depth in 2008, 2011 and 2013.

Based on high-resolution satellite images and geo-botanic description data, we determined contribution of every plant community type into total methane efflux into atmosphere. Besides, ombrotrophic pine bog was provisionally divided into small plots with reference to projective cover of hummocks and hollows. Finally, total methane flux from the Medla-Pev-Nyur peatland (1 598 581 m^2 or 1.6 km^2) was assessed for different years accounting for area every community type occupied and emission median from its surface (Table 6). The highest methane efflux into atmosphere was found for 2008 and the lowest one – for 2014 (cool summer).

Table 6

Total methane emission from peatland in three observation years*

Wetlands class	Area, m^2	2008	2011	2014	2008	2011	2014
		Median, g m^{-2} h^{-1}			Total emission*, Mg $year^{-1}$		
Bog (hummocks 70-80%)	475 181	0.004	0.00397	0.00040	7.50	8.30	0.001
Bog (hummocks 30%)	294 971	0.008	0.00421	0.00097	9.35	5.47	1.40
Bog (hollows 80%)	82 484	0.0136	0.00423	0.00828	4.42	1.50	3.27
Transition zone	317 385	0.017	0.01751	0.01105	21.33	24.50	16.78
Fen (swamp)	428 560	0.0187	0.00805	0.00684	31.70	15.20	14.00
Total	1 598 581	–	–	–	74.30	54.97	35.45

* Total emission for the active methane emission period: 2008 (3951 hours), 2011 (4408 hours), 2014 (4784 hours).

Our results on total methane flux for three observation years resembled those obtained for minerotrophic peatlands in the USA (Wilson et al., 1989; Dise et al., 1993; Shannon and White, 1994) but greatly differed from data on sub-Arctic tundra areas (Heyer et al., 2002; Heikkinen et al., 2004) and oligotrophic bog of the south taiga subzone (Vompersky et al., 2000). But our results confirmed the idea of the other authors that different weather conditions during vegetation period responded for interannual variability of total methane emission from one and the same peatland (Shannon and White, 1994; Huttunen et al, 2003).

CONCLUSION

Favorable weather conditions increased methane flux from peat into atmosphere in evening and night because of soil temperature rise at 20-cm depth. In case of shower rains, daily methane emission dynamics were not expressed. Seasonally, methane flux increased in July. The highest methane flux values ranged across four observation years were registered for transition plots dominated by sedges in plant cover. The main factor influencing on methane emission was wa-

ter table level. Total methane efflux varied from 35.5 to 74.3 Mg CH_4 depending on weather conditions during vegetation period.

References

Alford, D.P., R.D. Delaune, and C.W. Lindau. 1997. Methane flux from Mississippi river deltaic plain wetlands. *Biogeochemistry* 37: 227–236.

Berestovskaya Yu.Yu, L.V. Vasilyeva, O.V. Chestnykh, and G.A. Zavarzin. 2002. Methanotrophic organisms of psychrophilous microbe community from High Arctic tundra area of Russia. *Mikrobiologia* 71(4): 538-544.

Bubier, J.L., T.R. Moore and N.T. Roulet. 1993. Methane emissions from wetlands in the midboreal region of northern Ontario, Canada. Ecology 74(8): 2240–2254.

Deshmukh, C., D. Serɜa, C. Delon, R. Tardif, M. Demarty, C. Jarnot, Y. Meyerfeld, V. Chanudet, P. Guŭdant, W. Rode, S. Descloux, and F. Guŭrin. 2014. Physical controls on CH_4 emissions from a newly flooded subtropical freshwater hydroelectric reservoir: Nam Theun 2. *Biogeosciences* 11: 4251–4269.

Dise, N.B. 1993. Methane emission from Minnesota peatlands: spatial and seasonal variability. *Global Biogeochemical Cycles* 7: 123–142.

Forestry and Forest Resources of the Komi Republic, ed. by G.M. Kozubov, and A.I. Taskaev, 2000. Moscow: DiK

Glagolev, M.V., A.A. Sirin, E.D. Lapshina, and I.V. Filippov. 2010. The study on fluxes of carbon-containing greenhouse gases in wet ecosystems of West Siberia. *Vestnik TGPU* 3(93): 120-127.

Glagolev, **M.V., and A.V. Smagin. 2006. Quantitative assessment of methane emis**sion by peatlands: from soil profile to region (devoted to the 15th anniversary of studies in the Tomsk Region). *Reports on Ecological Soil Science* 3(3): 75-114.

Hargreaves, K.J., D. Fowler, C.E.R. Pitcairn, and M. Aurela. 2001. Annual methane emission from Finnish mires estimated from eddy covariance campaign measurements. *Theoretical and Applied Climatology* 70: 203–213.

Heikkinen, J.E.P, V. Elsakov and P.J. Martikainen. 2002. Carbon dioxide and methane dynamics and annual carbon balance in tundra wetland in NE Europe, Russia. Global Biogeochemical Cycles 16(4): 62–77.

Heyer, J., U. Berger, I. L. Kuzin, and O.N. Yakovlev. 2002. Methane emissions from different ecosystem structures of the subarctic tundra in Western Siberia during midsummer and during the thawing period. *Tellus* 54B: 231–249.

Huttunen, J.T., H. Nykanen, J. Turunen, and P.J. Martikainen. 2003. Methane emissions from natural peatlands in the northern boreal zone in Finland, Fennoscandia. *Atmospheric Environment* 37: 147–151.

McDonald, J.A., D. Fowler, K.J. Hargreaves, U. Skiba, I.D. Leith, and M.B. Murray. 1998. Methane emission rates from a northern wetland: response to temperature, water table and transport. *Atmospheric Environment* 32(19): 3219–3227.

Mikkelä, C., Sundh, B.H. Svensson, and M. Nilsson. 1995. Diurnal variation in methane emission in relation to the water table, soil temperature, climate and vegetation cover in a Swedish acid mire. *Biogeochemistry* 28: 93–114.

Nykänen, H., H. Vasander, J.T. Huttunen, and P.J. Martikainen. 2002. Effect of experimental nitrogen load on methane and nitrous oxide fluxes on ombrotrophic boreal peatland. *Plant and Soil* 242: 147–155.

Peat Resources of the Komi Republic. 2000. Syktyvkar.

Rinne, J., T. Riutta, M. Pihlatie, M. Aurela, S. Haapanala, J-P. Tuovinen, E-S. Tuittila, and T. Vesala. 2007. Annual cycle of methane emission from a boreal fen measured by the eddy covariance technique. *Tellus* 59B (3): 449–457.

Rovira, A.D. 1969. Plant root exudates. *Botanical Review*. 35: 35–57.

Russell, R.S. 1977. Plant root systems: their function and interaction with the soil. R.S. Russell. McGraw-Hill, London.

Schimel, J.P. 1995. Plant transport and methane production as controls on methane flux from arctic wet meadow tundra. *Biogeochemistry* 28: 183–200.

Shannon, R.D., and J.R. White. 1994. A three-year study of controls on methane emissions from two Michigan peatlands. *Biogeochemistry* 27: 35–60.

Slobodkin A.I., N.S. Panikov and G.**A. Zavarzin. 1992. Methane formation and utilization** by microorganisms in tundra and middle-taiga wetlands. *Mikrobiologia* 61(4): 683-691.

Vompersky, S.E., A.G. Kovalev, **T.V. Glukhova, and M.V. Smagina. 2000. Carbon dioxide** and methane emission from soil surface of differently-moistured forest and peatland ecosystems in the south taiga subzone of European Russia. In *Emission and Sink of Greenhouse Gases on the Territory of North Eurasia*. Abstracts of the National Conference with International Participation. 83. Pushchino.

Whiting, G.J., and J.P. Chanton. 1992. Plant-dependent CH_4 emission in a subarctic Canadian fen. *Global biogeochemical cycles* 6: 225–231.

Wilson, J.O., P. M. Crill, K. B. Bartlett, D.I. Sebacher, R.C. Harriss, and R.L. Sass. 1989. Seasonal variation of methane emissions from a temperate swamp. *Biogeochemistry* 8: 55-71

Chapter 12
MICROFORM-RELATED BELOWGROUND CH_4 CONCENTRATIONS AND STABLE CARBON ISOTOPE SIGNATURES AS PROXIES FOR DETERMINATION OF CH_4 TURNOVER PROCESSES IN A BOREAL PEATLAND

Application of stable isotopes is an approach to identify the patterns of CH_4 turnover (Whiticar, 1999; Conrad, 2005). For instance, based on the ratio of "light" and "heavy" C ($^{12}C/^{13}C$, typically presented as standardized "delta" ^{13}C, i.e. $\delta^{13}C$) the sources of CH_4 production – the so called methanogenic pathways – can be identified. Thus, CH_4 produced by acetate cleavage (acetoclastic pathway) is not as depleted in ^{13}C as CH_4 produced from CO_2 reduction with H_2 (hydrogenotrophic pathway). The latter process results in simultaneous ^{13}C enrichment of bulk CO_2 as the enzymatic system of methanogens is strongly discriminates against ^{13}C preferentially utilizing ^{12}C (Whiticar et al., 1986). Knowledge about the contribution of different methanogenic pathways to the total CH_4 production within peat profile helps to identify the pattern of decompositionof recent (acetates rich) vs. older (acetates depleted) organic matter pools (Beer and Blodau, 2007). Based on vertical profiles of $\delta^{13}C$-$CH_4$and $\delta^{13}C$-CO_2 it was shown that the upper peat profile of wetlands was dominated by acetoclastic and the lower profile by hydrogenotrophic methanogenesis (Hornibrook et al., 1997; Popp et al., 1999).

Furthermore, other processes are also affecting $\delta^{13}C$ characteristics of both CH_4 and CO_2. Thus, the methanotrophic activity brings to the enrichment of ^{13}C in CH_4 as there is a discrimination of methanotrophic organismsagainst ^{13}C. As a result, the end-product of CH_4oxidation – CO_2 – becomes more depleted in ^{13}C (Whiticar, 1999; De Visscher et al., 2004). Additionally, transport of CH_4 either mediated by plants or due to gas diffusion through the peat profile also preferentially removes ^{12}C-$CH_4$and ^{12}C-$CO_2$from the system. This fractionation depends on transport mechanism, water table level, time of day, and season (Popp et al., 1999; De Visscher et al., 2004; Chanton et al., 2005).

In the current study we aimed to assess the dominating processes of the CH_4 turnover, e.g. production, transport and oxidation in peat profiles below distinct microrelief forms – hummocks, lawns and hollows – of minerotrophic, transition and ombrotrophic areas within a minerogenic tall-sedge pine peatland in Komi Republic, North-West Russia. We measured concentrations of porewater CH_4 at increasing depths and used stable C isotope characteristics of CH_4 and CO_2 to differentiate between production, transport and oxidation of CH_4 throughout the peat profile as related to microrelief. We hypothesized methanogenesis (production) and CH_4 transport are the dominating processes affecting $\delta^{13}C$ of $CH_4$and CO_2 at the bottom-middle peat horizons, whereas CH_4 oxidation affects isotopic signatures in the topsoil. The CH_4 oxidation should depend on a microform type and increase from wet hollows to dry hummocks through intermediate lawns.

MATERIALS AND METHODS

Porewater gas sampling

The study was conducted on a natural minerogenic, oligotrophic-minerotrophictall-sedge pine fen Medla-Pev-Nyur. The porewater gas sampling was carried out at the end of the vegetation season in September 2010. To collect water with dissolved gases, PVC tubes (inner diameter 45 mm) were installed at each of microform types within ombrogenic, minerogenic and transition zones of the experimental site to five depths: 0.25, 0.5, 1.0, 1.5 and 2.0 m. A single tube was used for each depth level. To avoid water mixing with other depths and prevent the peat material to block a tube, the bottom of tubes was closed with a cap. The adjusted 10-12 cm of a tube bottom was drilled to let the horizontal water circulation through the holes in the tube at a certain depth level. The total number of tubes installed was estimated to comprise minimal statistical representativeness, e.g. in triplicate for each microform type and depth horizon at each of the peatland zones. The installation of tubes was conducted two months prior the sampling (June-July 2010).

The collection of water with dissolved gases was done from all the installed tubes using Teflon tubings (inner diameter 2 mm) of necessary length connected to gas-tight 50 ml plastic syringes equipped with 3-way stopcocks. To omit the blockage of tubings with peat material, a nylon mesh was tightly fixed on tips of each sampler. 20-30 ml of water were collected into syringes from all of the studied depths. Samples were transferred first to 100 ml N_2 flushed glass vials closed with septa, shacked well to remove dissolved gases into the headspace, and then a subsample of gas was taken for measurements on a gas chromatograph (see below). Another subsample of headspace gas (10-15 ml) was inserted to 30 ml N_2-flushed glass vials closed with butyl septa for isotope analyses. To preserve gas samples and their isotopic composition, 30 ml bottles were filled with N_2-bubbled, saturated NaCl solution thus no air space was left inside. Concentration of NaCl prevented any microbial activity. Gas samples were accurately inserted to bottles by removing the respective volume of the solution through a “water lock” in a way that no atmospheric air could contaminate gas samples.

CH_4 concentration measurements and stable C isotope analysis of CH_4 and CO_2

The concentration of headspace CH_4 (1 ml) was measured on a gas chromatograph “Tsvet” 800 equipped with a 2 m steel column (sorbent Porapak N) and FID detector in the Institute of Biology, Komi Science Centre of the Ural Division RAS, Syktyvkar. Two concentrations of standard gases (5.1 and 17.5 ppm CH_4, LindaGasRus, Moscow) were used for calibration.

The $^{13}C/^{12}C$ ratios in CH_4 and CO_2were determined in duplicate by gas chromatography isotope ratio mass spectroscopy (GC-IRMS, Delta Plus, ThermoScientific, Dreieich, Germany) in the Institute of Soil Science, University of Hamburg, Germany. The GC-IRMS was equipped with a 25 m capillary column (Poraplot, 0.32 mm ID). Analytical replicate precision was generally $<0.2‰$. For samples with nearatmospheric CH_4 concentrations, a preconcentration system (PreCon, ThermoScientific, Dreieich, Germany) was used with standard error of replicate measurements generally less than 0.5‰. Value sare expressed relative to VPDB (Vienna Pee Dee Belemnite Standard) using the reference standard NGS3 8561($\delta^{13}C = -73.27‰$ VPDB; NIST, Gaithersburg, USA) (Preuss et al., 2013).

Calculations and statistics

Porewater CH_4 concentrations were recalculated from instrument data (in ppm) into μmol l^{-1}using Ideal Gas Law:

$$n = P \cdot V / R \cdot T, \quad (1)$$

wheren is the amount of gas (in moles), P is the atmospheric pressure (101.325 kPa), V is the volume of gas in the headspace (L), R is the Ideal Gas Constant (8.31 $JK^{-1}mol^{-1}$) and T is the temperature as absolute temperature in Kelvin (K).

The $^{13}C/^{12}C$ ratio in $CH_4$and $CO_2$was denoted as $\delta^{13}C$ in per mil PDB [‰]:

$$\delta^{13}C\ (‰) = [(R_{sample} / R_{PDB}) - 1] \cdot 1000, \quad (2)$$

where R_{sample} is the isotopic ratio $^{13}C/^{12}C$ of CH_4 in the sample, and R_{PDB} is the isotopic ratio of Pee Dee Belemnite as the standard for C (described above).

The determination of statistically significant differences in porewater CH_4, $\delta^{13}C$-$CH_4$and $\delta^{13}C$-CO_2values between microforms, depths and zones of peatland were performed withtwo-way-ANOVA and Fischer LSD test ($p \leq 0.05$) using STATISTICA 7.0 software (StatSoft, USA). Prior the testing of significances of differences all the data were processed for normal distribution (Kholmogorov-Smirnov test) and homogeneity (Levene's test). The variables were treated as independent for all depths of a microform type and a certain depth between microforms.

RESULTS

Porewater methane concentrations [CH_4]

Porewater [CH_4] showed large variation between microforms and depths within three studied zones of the peatland (Fig. 1). Thus, in hummocks of minerogenic zone [CH_4] increased ca. 4 times (from 97 to 431 μmol l^{-1}) from the top to bottom of the peat profile. In ombrogenic zone, however, the highest [CH_4] was measured in 1.0 m horizon (517 μmol l^{-1}) without clear depth pattern (Fig. 1 A). Similar to hummocks, the increasing [CH_4] with depth was detected in hollows of minerogenic zone but no clear pattern characterized the [CH_4] in ombrogenic zone (Fig. 1 C). There was no significant difference found between depths below lawns of minerogenic, ombrogenic and transition zones of the peatland (Fig. 1 B).

The mean porewater [CH_4] (Fig. 2, average between two zones (for hummocks and hollows) and three zones (for lawns)of the peatland) showed increasing trend from the topsoil up to 1.0-1.5 m depths below all microforms. Remarkably, in lawns and hollows, [CH_4] decreased by ca. 30% at 2.0 m as compared with 1.5 m. However, due to high spatial variation, all the differences in [CH_4] between microforms and depths were insignificant (Fig. 2).

$\delta^{13}C$ of porewater CH_4 and CO_2

In contrast to [CH_4], $\delta^{13}C$ of CH_4 and CO_2 revealed pronounced and significant differences between microforms and depths of hydrologically distinct zones of the peatland. Thus, the most enriched $\delta^{13}C$-CH_4 values (−47.8 to −49.0‰) were measured in 0.5 m depth of hummocks, lawns and hollows of minerogenic zone (Fig. 3, left side, black color). Significantly more depleted $\delta^{13}C$-CH_4 (−50.3 to −68.7‰) was found in the upper most and deeper peat horizons within same microforms of the minerogenic zone. The most depleted $\delta^{13}C$-CH_4 values (−53.8 to −70.3‰) were measured in microforms of the ombrogenic zone (Fig. 3, left side, red color). Except of the top 0.25 m horizon in the minerogenic zone, there was an overall depletion in $\delta^{13}C$-CH_4 with depth below all microforms. This pat-

tern was especially pronounced in lawns of the transition zone (Fig. 3 B, left side, blue color).

In general, patterns of $\delta^{13}C\text{-}CO_2$ with depth were counteracting the respective $\delta^{13}C\text{-}CH_4$ in studied microforms (Fig. 3, right side). The most depleted $\delta^{13}C\text{-}CO_2$ values (−37 to −42.4‰) were measured in the topsoil of hummocks, lawns and hollows of minerogenic and transition zones. The most enriched $\delta^{13}C\text{-}CO_2$ (up to −9.3‰) were measured in the 0.5-1.5 m depths of lawns in the transition zone (Fig. 3 B).

The overall enrichment of mean $\delta^{13}C\text{-}CO_2$ with depth corresponded to the depletion of mean $\delta^{13}C\text{-}CH_4$ in all microforms (Fig. 4). The exceptions of the general pattern were the significantly depleted $\delta^{13}C\text{-}CH_4$ in the 0.25 m of hummocks (−62.5‰) as compared to lawns (−53.8‰) and hollows (−50.3‰) as well as $\delta^{13}C\text{-}CO_2$ in lawns at 2.0 m (−32.2‰) as compared to hollows at the same depth (−14.8‰) (Fig. 4).

Relationship between $\delta^{13}C\text{-}CH_4$ and $\delta^{13}C\text{-}CO_2$

The cross-plot of $\delta^{13}C\text{-}CH_4$ and $\delta^{13}C\text{-}CO_2$ revealed clear grouping of data between microforms and depths of two contrasting peatland's zones – oligotrophic and minerotrophic (Fig. 5). Thus, in all microforms of both zones, three depth intervals were identified, where isotope characteristics of CH_4 and CO_2 were distinct: upper (0.25-0.5 m), intermediate (1.0 m) and bottom (1.5-2.0 m) horizons. Generally, in the upper horizon cross-plot data comprised of relatively enriched $\delta^{13}C\text{-}CH_4$ and broad range of $\delta^{13}C\text{-}CO_2$ (Fig. 5, green solid circle). Intermediate horizon was characterized by more depleted $\delta^{13}C\text{-}CH_4$ as compared with the upper one, though $\delta^{13}C\text{-}CO_2$ values were similarly broad (Fig. 5, blue dotted circle).

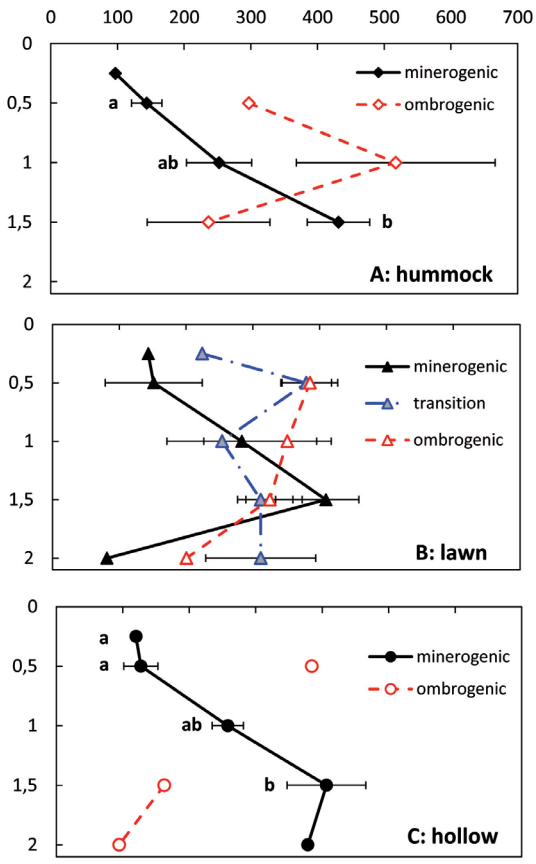

Fig. 1: Porewater concentrations of CH_4 in (A) hummocks, (B) lawns and (C) hollows at four (hummocks) and five (lawns, hollows) depth horizons (0.25, 0.5, 1.0, 1.5, 2.0 m) of ombrogenic, minerogenic and transition zones of Medla-Pev-Nyur peatland. Values followed by the same letters are not significantly different (at $p \leq 0.05$) between depth horizons of the same zone and microform. There were no differences between ombrogenic, minerogenic (for hummocks and hollows) and transition (for lawns) zones of the same depth horizon. Lack of letters corresponds either to measurements with one replication available or the insignificance of differences. Absissa – porewater CH_4 concentration, μmol l^{-1}; ordinate axis – depth, m.

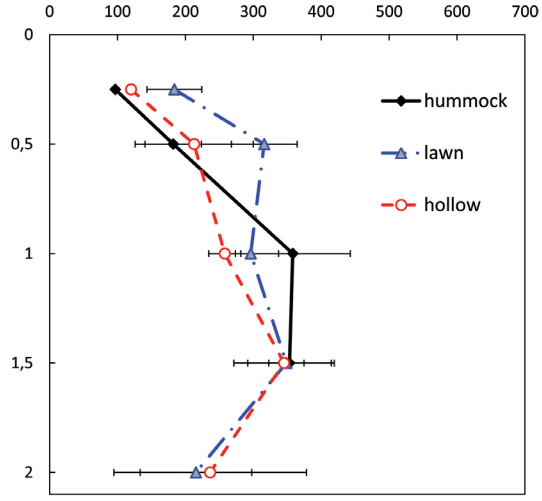

Fig. 2: Mean porewater concentrations of CH_4 in hummocks, lawns and hollows at four (hummocks) and five (lawns, hollows) depth horizons (0.25, 0.5, 1.0, 1.5, 2.0 m) of Medla-Pev-Nyur peatland. There were no differences between hummocks, lawns and hollows of the same depth horizon as well as between depth horizons of each microform type (at $p \leq 0.05$). Absissa – porewater CH4 concentration, μmol l^{-1}; ordinate axis – depth, m.

The highest variation in cross-plot data was observed in the bottom horizon: two groups of data – with enriched and depleted $\delta^{13}C\text{-}CO_2$ – were recognized (Fig. 5, dashed orange circle). Range of $\delta^{13}C\text{-}CH_4$ included the most depleted values and values similar for the intermediate horizon, though not overlapping with $\delta^{13}C\text{-}CH_4$ of the upper horizon. The grouping of cross-plot data in the bottom horizon was especially pronounced for the minerotrophic zone of the peatland. In the same zone, the cross-plot data for the 0.25 m hummock could not be grouped to any of the data sets (Fig. 5, bottom).

DISCUSSION

Porewater [CH_4]: effects of microtopography and peat depth

The observed increase of porewater CH_4 with depth on the studied boreal peatland is in agreement with the results of many other studies (Hornibrook et al., 1997; Chasar et al., 2000; Steinmann et al., 2008; Dorodnikov et al., 2013). In a similar study on comparable boreal peatland in Eastern Finland (Dorodnikov et al., 2013) the pronounced increase in [CH_4] occurred down to 1.0 m depth below hummocks, lawns and hollows without any further significant differentiation to bottom of profiles (2.0 m). Here, we distinguished between hydrologically distinct zones of the peatland, but no significant difference was detected between microforms of ombrotrophic, minerotrophic and transition zones (Fig. 1). Still, the most pronounced increase in porewater CH_4 was measured down to 1.5 m in all microforms of the minerogenic zone. Interestingly, the overall lower [CH_4] was observed at 2.0 m depth of peatlands in Finland and Russia as compared with upper peat horizons (Fig. 2 and Dorodnikov et al., 2013). The *in situ* ascending concentrations of porewater CH_4 with depth are contradicting to the *in vitro* lowest methanogenic potential of deep peat (deeper as 1.0 m) as compared to the topsoil (Krohn et al., **submitted). The imbalance between lab and field observations** is apparently related to the natural conditions and physical properties of the peat. Thus, the deeper vs. upper peat horizons have higher soil density and lower hydraulic conductivity (Hornibrook et al., 1997), therefore the produced CH_4 (though rather slowly) is accumulating in the former. Remarkably, the observed decrease in [CH_4] at the very bottom of the peat profile could be related to the proximity of the groundwater. The latter typically contains higher concentrations of the dissolved inorganic compounds, such as sulphates, nitrates, am-

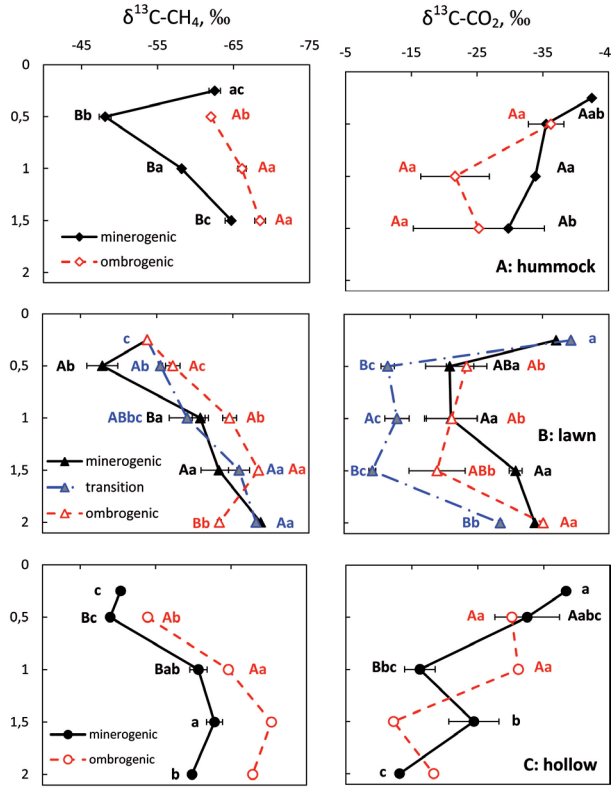

Fig. 3: Stable C isotope composition ($\delta^{13}C$) of CH_4 and CO_2 in (A) hummocks, (B) lawns and (C) hollows at four (hummocks) and five (lawns, hollows) depth horizons (0.25, 0.5, 1.0, 1.5, 2.0 m) of ombrogenic, minerogenic and transition zones of Medla-Pev-Nyur peatland. Values followed by the same letters are not significantly different (at $p \leq 0.05$) between (i) depth horizons of the same zone and microform (lowercase letters) and between (ii) ombrogenic, minerogenic (for hummocks and hollows) and transition (for lawns) zones of the same depth horizon (uppercase letters). Lack of letters corresponds to measurements with one replication available. Ordinate axis – depth, m.

monium, iron etc., which may serve as inhibitors of methanogenesis (Clarens et al., 1998; Eriksson et al., 2010). As the measured depth-related [CH_4] pattern below all microforms was insignificant (Fig. 2) due to large spatial variation, the additional measurements of porewater gas concentrations and dissolved inorganic compounds are necessary to better explain the dynamics of CH_4 in relation to peatland microforms and peat depth.

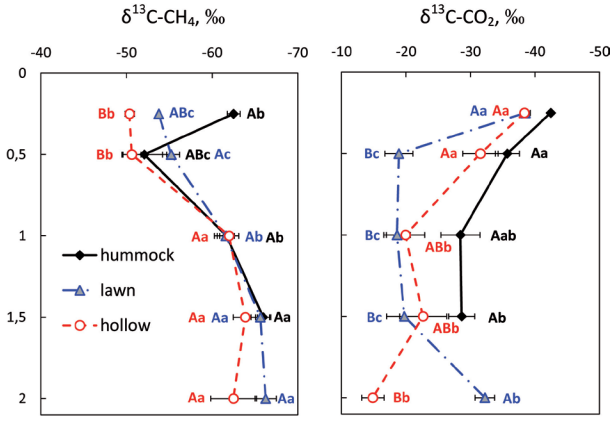

Fig. 4: Mean stable C isotope composition ($\delta^{13}C$) of CH_4 and CO_2 in hummocks, lawns and hollows at four (hummocks) and five (lawns, hollows) depth horizons (0.25, 0.5, 1.0, 1.5, 2.0 m) of Medla-Pev-Nyur peatland.alues followed by the same letters are not significantly different (at $p \leq 0.05$) between depth horizons of the same microform (lowercase letters) and between microforms of the same depth horizon (uppercase letters). Lack of letters corresponds to measurements with one replication available. Ordinate axis – depth, m.

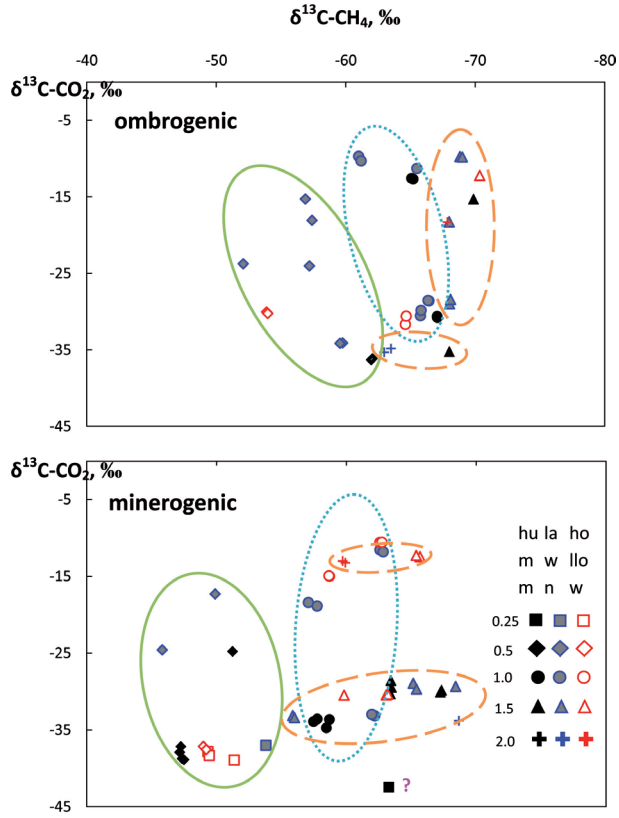

Fig. 5: Cross-plot of stable C isotope values ($\delta^{13}C$) of CH_4 and CO_2 in hummocks, lawns and hollows at depth horizons (0.25, 0.5, 1.0, 1.5, 2.0 m) of ombrogenic (top) and minerogenic (bottom) areas of Medla-Pev-Nyur peatland.Circles of different color and patterns demonstrate the grouping of data in the upper (0.25-0.5 m, green solid circle), intermediate (1.0 m, blue dotted circle) and bottom (1.5-2.0 m, dashed orange circle) peat horizons below all microforms. Pink question mark indicates whether data point should be considered as an outlier.

$\delta^{13}C$-CH_4 and $\delta^{13}C$-CO_2 as proxies for CH_4 production, transport and oxidation

Porewater CH_4 in Medla-Pev-Nyur mire showed strong depletion in ^{13}C with depth. This pattern was more pronounced in ombrogenic vs. minerogenic and transition zones of the peatland (Fig. 3, left side). In contrast, there was an overall enrichment in ^{13}C of porewater CO_2 with depth, especially in hummocks and hollows of ombrogenic and minerogenic zones (Fig. 3, right side). The obtained data are in a good agreement with most of the reported results from *Typha*-dominated fen in Canada (Hornibrook et al., 1997), littoral wetlands in the United States (Chasar et al., 2000), acidic *Sphagnum* bog in Switzerland (Steinmann et al., 2008) and low-sedge pine fen in Finland (Dorodnikov et al., 2013). Between the microforms, the significantly higher $\delta^{13}C$-CH_4 (more enriched in ^{13}C) was observed in hollows at 0.25 and 0.5 m depths as compared to lawns and hollows, whereas significantly more enriched $\delta^{13}C$-CO_2 was measured in lawns at 0.5, 1.0 and 1.5 m as compared to other two microforms (Fig. 4). Measured differences in isotope values of gases between microforms are firstly observed in the current study. Thus, lack of the significant differences in $\delta^{13}C$-CH_4 between microforms was reported for a Finnish boreal mire of the similar origin and type (Dorodnikov et al., 2013).

Overall depletion of ^{13}C in CH_4 along with the respective enrichment of ^{13}C-CO_2 with depth suggests the increasing contribution of hydrogenotrophic or CO_2 reduction pathway to the total methanogenesis (Whiticar **et al., 1986; Horni-**

brook et al., 1997; Conrad, 2005).This mechanism is based on the discrimination by methanogens of archaea domain against heavier ^{13}C, when enzymatic system of microorganisms preferentially consumes "lighter" ^{12}C (Whiticar et al., 1986). Therefore, there is typically "heavier" CO_2 accumulating in the environment, whereas "lighter" CO_2 serves as a substrate for strongly ^{13}C-depleted CH_4 (Popp *et al*. 1999). In contrast to the hydrogenotrophic pathway, microorganisms discriminate less against ^{13}C during methanogenesis through the acetoclastic pathway (splitting of fermentation-derived acetic acid/acetates) resulting in relatively more ^{13}C-enriched CH_4 (Whiticar et al., 1986). The $\delta^{13}C$-CO_2 values are also reflecting other microbial processes, such as respiration and decomposition of soil organic matter.

It is important to note, that $\delta^{13}C$-CH_4 and $\delta^{13}C$-CO_2values in different peat horizon (but especially in the upper peat profile above 1.0 m) of the studied peatland could have been affected by the processes of CH_4 transport and oxidation (Popp et al., 1999; Whiticar, 1999; Chanton et al., 2005; Dorodnikov et al., 2013). Indeed, molecular diffusion affects isotopic composition of CH_4 as $^{12}CH_4$ diffuses faster than $^{13}CH_4$ (Chanton et al., 2005; Liptay et al., 1998; De Visscher et al., 2004). The same is true for the CO_2 gas diffusion. Oxidation or consumption of CH_4 by methanotrophs also influences the $\delta^{13}C$-CH_4 and $\delta^{13}C$-CO_2. Both microbial culture studies (Coleman et al., 1981; Liptay et al., 1998) and field studies (Tyler et al., 1994; Chanton et al., 2005) have shown that methanotrophic organisms preferentially consume "lighter" $^{12}CH_4$, leaving residual CH_4 enriched in ^{13}C. Simultaneously, the product of CH_4 oxidation – the released CO_2 – becomes strongly ^{13}C-depleted. Therefore, the cross-plot of $\delta^{13}C$-CH_4 and $\delta^{13}C$-CO_2 represents the relationship between two values and allows to differentiate the gas turnover processes (production, transport, consumption) contributing to measured isotope characteristics (Knorr et al., 2008).

Our cross-plot data revealed clear differentiation between depths below microforms of the Medla-Pev-Nyur peatland (Fig. 5). Overall three main depth intervals – the upper (0.25-0.5 m), intermediate (1.0 m) and bottom (1.5-2.0 m) – were identified for the microforms of hydrologically distinct zones of the peatland. According to the prerequisites in changes of stable C isotopes due to main gas turnover processes (described above) these depth intervals could be characterized as following (Fig. 6).

At the bottom of peat profile the methanogenesis (predominantly over the hydrogenotrophic pathway) contributed the most to the cross-plot characteristics of CH_4 (strongly depleted $\delta^{13}C$-CH_4) and CO_2 (strongly enriched $\delta^{13}C$-CO_2) (Whiticar et al., 1986; Hornibrook et al., 1997; Conrad, 2005). Simultaneously, there was further enrichment of $\delta^{13}C$-CH_4 and $\delta^{13}C$-CO_2 towards the direction of intermediate depth horizon (Fig. 6, green area, dashed arrow). This indicates the removal of porewater gas through the diffusion over the concentration gradient, when "heavier" molecules are accumulating in the system (Liptay et al., 1998; De Visscher et al., 2004, Knorr et al., 2008).

Change in isotopic characteristics within intermediate depth interval (between 0.5 and 1.5 m) was presumably stipulated by the CH_4 oxidation (Fig. 6, blue area, dotted arrow). The process discriminates against "heavier" ^{13}C-CH_4 (Liptay et al., 1998, Chanton et al., 2005), therefore along with the enrichment of $\delta^{13}C$-CH_4 there was an overall depletion of $\delta^{13}C$-CO_2 as an end-product of oxidation. It is important to note, the intermediate depth interval was a water-saturated peat horizon, where the conventional oxygen diffusion was limited. Instead,

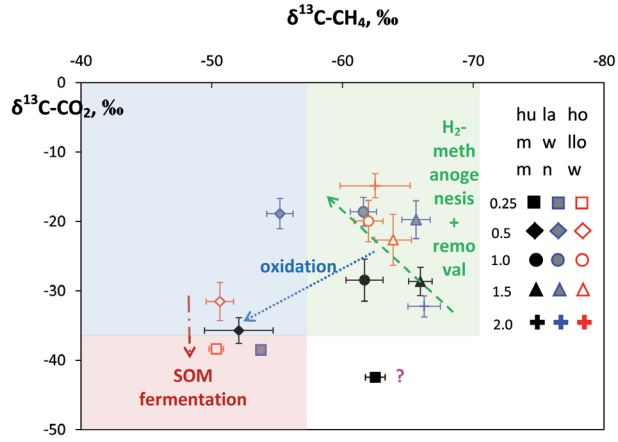

Fig. 6: Cross plot of mean stable C isotope values ($\delta^{13}C$) of CH_4 and CO_2 in hummocks, lawns and hollows at depth horizons (0.25, 0.5, 1.0, 1.5, 2.0 m) across oligotrophic and minerotrophic zones of Medla-Pev-Nyur peatland.Areas of different color demonstrate a dominating process of hydrogenotrophic (H_2) methanogenesis and removal of gases (green), methane oxidation (blue) and SOM fermentation (red) contributing to the measured $\delta^{13}C$-CH_4 and $-CO_2$ values at peat horizons below all microforms. Arrows showing the direction of $\delta^{13}C$-CH_4 and $-CO_2$ change along the peat profile from bottom to top horizons. Data with the pink question mark were not considered as a potential outlier.

the oxidation of CH_4 could occur via two main ways: (a) in the rhizosphere of vascular plants, which deliver oxygen through their aerenchyma (Joabsson and Christensen, 2001; Lai, 2009). Indeed, the developed root system of dominant vascular plant communities was observed onsite down to depths of 1.0-1.2 m. (b) The second way is so called anaerobic oxidation of methane – AOM (Smemo and Yavitt, 2011). AOM is driven by microorganisms, which oxidize CH_4 with various terminal electron acceptors (other than oxygen), e.g. sulphate, nitrate, nitrite, some metals (Fe, Mn) or organic compounds. The process is common in marine ecosystems, where it is linked to microbial sulphate reduction (SR) and consumes 20-300 Tg CH_4 yr^{-1} (up to 60-80% of the global annual flux into the atmosphere) produced in marine sediments (Valentine, 2002; Smemo and Yavitt, 2011). Though some evidence on AOM in peatlands has been provided (reviewed by Smemo and Yavitt, 2011), it is still unclear which mechanisms control the AOM in terrestrial ecosystems, *i.e.* which alternative-to-oxygen electron acceptors are involved and what is the contribution of different microbial groups (bacteria vs. archaea) to the process. Therefore, detailed studies are necessary to assess the role of AOM for the CH_4 turnover in terrestrial ecosystems.

At the top most depth interval (0.25-0.5 m) the assumed CH_4 oxidation (as depicted by decreasing concentrations (Fig. 2) and further depletion in ^{13}C-CO_2 (Fig. 6, red area) was apparently compensated by the decomposition of relatively fresh plant-derived deposits. Under anaerobic and semi-anaerobic conditions, the products of SOM fermentation – among other compounds – acetic acid and acetates are the precursors of the acetoclastic methanogenesis. **The process cor-**responds to $\delta^{13}C$-CH_4 values of −65 to −50‰ (Whiticar et al., 1986), which is in agreement with our results (Fig. 6). Between the microforms, the cross-plot data for 0.25 m hummocks revealed both strongly negative (low ^{13}C) $\delta^{13}C$-CH_4 and $\delta^{13}C$-CO_2 values (Fig. 6, white area). This contradicts to the general concept, and could be connected either to limits in sampling and analytical procedures, or to the situation out of the proposed concept. Thus, $\delta^{13}C$-CH_4 suggests the hydrogenotrophic methanogenesis not very typical for the topsoil rich in recent

and poorly processed SOM (Popp et al.,1999). Simultaneously, the most depleted $\delta^{13}C\text{-}CO_2$ should reflect the decomposition of a respective ^{13}C-poor substrate and/or CH_4 oxidation. Because of the high uncertainty, we did not consider isotope characteristics of gases in 0.25 m hummocks (labelled with a question mark on the Fig. 6). Additional measurements are necessary to clarify the observed pattern.

CONCLUSION

Stable C isotopic composition of porewater CH_4 and CO_2 proved to be an effective tool to differentiate between processes of CH_4 turnover within peat profile below microforms of a boreal peatland. Based on $[CH_4]$ in porewater and measured $\delta^{13}C\text{-}CH_4$ and $\delta^{13}C\text{-}CO_2$ values we conclude:

The change of cross plot values from bottom to the top of peat profiles was predominately attributed to hydrogenotrophic methanogenesis and gas removal (1.5-2.0 m depths), CH_4 oxidation (0.5-1.0 m) and fresh organic matter decomposition (0.25-0.5 m).

The water saturated peat layer between 0.5 and 1.0 m was found to contribute the most to the process of CH_4 oxidation, presumably through the occurrence of oxygen in the rhizosphere of aerenchimatous plants and/or anaerobic methane oxidation.

There were no significant differences in porewater $[CH_4]$ in depths of peat between microforms of hydrologically distinct zones of the peatland suggesting other factors than microrelief, *i.e.* peat quality, availability of alternative-to-oxygen electron acceptors, distribution of methanogenic and methanotrophic microorganisms, are controlling the CH_4 turnover in the ecosystem

ACKNOWLEDGEMENTS

Authors would like to greatly acknowledge the staff of the Forest Department of the Institute of Biology, Komi Science Centre of Russian Academy of Sciences, personally Dr. Oleg Mikhaylov and Dr. Michail Miglovets, for invaluable help in field studies and logistics. The study was supported by DFG Emmy Noether Programm (Wi 2680/2-1) and a Sofja Kovalevskaja Award (M. Wilmking) of the Alexander von Humboldt Foundation.

References

Beer, J., and C.Blodau. 2007. Transport and thermodynamics constrain belowground-carbon turnover in a northern peatland. *Geochim. Cosmochim. Acta* 71: 2989-3002.

Chanton, J.P., L.S. Chasar, Glaser P., and D.I. Siegel. 2005.Carbon and hydrogen isotopic effects in microbial methane from terrestrial environments.In *Stable Isotopes and Biosphere-Atmosphere Interactions*, ed. L.B. Flanagan, J.R. Ehleringer, and D.E. Pataki, 85–105. Elsevier. Amsterdam.

Chasar, L.S., J.P. Chanton, P.H. Glaser, and D.I. Siegel. 2000. Methane concentration and stable isotope distribution as evidence of rhizospheric processes: comparison of a fen and bog in the glacial lake Agassiz peatland complex. *Ann. Bot.* 86(3): 655–663.

Clarens, M., N. Bernet, J.F. Delgenейs, and R. Moletta. 1998.Effects of nitrogen oxides and denitrification by *Pseudomonas stutzeri*onacetotrophicmethanogenesis by *Methanosarcinamazei*. *Microbiol. Ecology* 25: 271-276.

Coleman, D.D., J.B. Risatti, and M. Schoell. 1981.Fractionation of carbon and hydrogen isotopes by methane-oxidizing bacteria. *Geochim. Cosmochim. Acta* 45: 1033–1037.

Conrad, R. 2005. Quantification of methanogenic pathways using stable carbon isotopic signatures: A review and proposal. *Org. Geochem.* 36:739–752.

De Visscher, A., I. De Pourcq, and J. Chanton. 2004. Isotope fractionation effects by diffusion and methane oxidation in landfill cover soils. *J. Geophys. Res.* 109, D18111, doi:10.1029/2004JD004857

Dorodnikov, M., M. Marushchak, C. Biasi and M. Wilmking. 2013. Effect of microtopography on isotopic composition of methane in porewater and efflux at a boreal peatland. *Boreal Env. Res.* 18: 269-279.

Eriksson, T., M.G. Oquist, and M.B. Nilsson. 2010. Production and oxidation of methane in a boreal mire after a decade of increased temperature and nitrogen and sulfur deposition. *Global Change Biol.*16: 2130–2144.

Hornibrook, E.R.C., F.J. Longstaffe, W.S. Fyfe. 1997. Spatial distribution of microbial methane production pathways in temperate zone wetland soils: Stable carbon and hydrogen isotope evidence. *GeochimCosmochimActa* 61:745– 753, doi:10.1016/S0016-7037(96)00368-7

Knorr K.-H., B. Glaser, and C. Blodau 2008. Fluxes and ^{13}C isotopic composition of dissolved carbon and pathways of methanogenesis in a fen soil exposed to experimental drought. *Biogeosciences* 5: 1457-1473.

Liptay, K., J. Chanton, P. Czepiel, and P. Mosher. 1998. Use of stable isotopes to determine methane oxidation in landfill cover soils. *J. Geophys. Res.* 103:8243–8250.

Popp, T.J., J.P. Chanton, G.J. Whiting, and N. Grant. 1999. Methane stable isotope distribution at a *Carex* dominated fen in north central Alberta. *Global Biogeochem. Cycl*es 13:1063 – 1077.

Preuss, I., C.Knoblauch, J. Gebert, and J.-M. Pfeifer. 2013. Improved quantification of microbial CH_4 oxidation efficiency in arctic wetland soils using carbon isotope fractionation. *Biogeosciences* 10: 2539–2552.

Reeburgh, W.S., J.Y. King, S.K. Regli, G.W. Kling, N.A. Auerbach, and **D.A. Walk**er. 1998. A CH_4 emission estimate for the Kupurak River basin. *Alaska J. Geophys. Res.* 103 (D22): 29005-29013.

Smemo, K.A., and J.B. Yavitt 2011. Anaerobic oxidation of methane: an underappreciated aspect of methane cycling in peatland ecosystems. *Biogeosciences* 8 :779-793.

Steinmann, P., B. Eilrich, M. Leuenberger, and S.J. Burns. 2008. **Stable carbon isotope composition and concentrations of CO_2 and CH_4 in deep catotelm of a peat bog.** *Geochim.Cosmochim.Acta*72:6015-6026.

Turunen, J., E. Tomppo, K. Tolonen, and A. Reinikainen. 2002. Estimating carbon accumulation rates of undrained mires in Finland – application to boreal and subarctic regions. *Holocene* 12: 69–80.

Tyler, S.C., P.M. Crill, and G.W. Brailsford. 1994. $^{13}C/^{12}C$ fractionation of methane during oxidation in a temperate forested soil. *Geochim. Cosmochim. Acta* 58: 1625-1633.

Valentine, D. L. 2002. Biogeochemistry and microbial ecology ofmethane oxidation in anoxic environments: a review. *A. Van. Leeuw.* 81: 271–282.

Whiticar, M.J., E. Faber, and M. Schoell. 1986. Biogenic methane formation in marine and freshwater environments: CO_2 reduction vs. acetate fermentation - Isotope evidence. *Geochim. Cosmochim. Acta* 50: 693-709.

Whiticar, M.J. 1999. Carbon and hydrogen isotope systematics of bacterial formation and oxidation of methane. *Chem. Geol.* 161: 291-314.

Chapter 13
SURFACE ENERGY BALANCE AND ITS DRIVERS IN A BOREAL PEATLAND

Peatland hydrology, ecological functioning, and development are largely dependent on the local energy balance and whether precipitation is balanced by evapotranspiration (ET). Additional considerations include the effects of sensible (H) and ground (G) heat flux on the soil or moss surface temperature, which are critical for regulating bacterial activity and CO_2 or CH_4 production (Frolking et al., 2011).

The primary driver of latent energy fluxes (LE) in wetlands is generally seen to be net radiation (R_n), with wetland LE/R_n ratios generally exceeding 0.5 and fen values generally higher than bog values (Lafleur, 2008). The effect of the water table position is often of lesser importance though it does help determine canopy conductance (g_c) as it controls the relative contributions of different ground components such as bare soil, mosses, or vascular plants (Lafleur et al., 2005; Sonnentag et al., 2010). Other studies have found some positive effect from lower water tables on ET, but these impacts may be confounded by the coupling to the synoptic meteorological conditions driving the water table conditions (i.e., less precipitation and higher vapor pressure deficit – VPD) (Wu et al., 2010). Tests of the peatland energy balance in land surface modeling schemes have estimated more accurate fluxes for fens than for bogs, in part due to the complexities of moss evaporation and its link to water table height, which often varies irregularly through a site (Comer et al., 2000).

The European part of Russia includes approximately 200,000 km^2 of peatlands, mostly in its boreal regions, thus composing more than 50% of the world's boreal peatland landscapes (Apps et al., 1993; Joosten et al., 2012). The potential of these sites for long-term carbon uptake is not assured due to a variety of climatic and biological factors ranging from increased temperature to carbon saturation in the sink mechanisms. While most research on northern peatlands focuses on Alaska, Canada, and Scandinavia, some energy flux research has been performed in the Russian taiga wetlands (Kurbatova et al., 2002). Their water relations and energy balances have long been studied (Romanov, 1968a; Ivanov, 1981), but the results of this research are often under-reported or delayed in English-language literature (Masing et al., 2010). For example, one relatively recent report (Shutov, 2004) describes the water balances of boreal peatland bogs in northwest European Russia based on investigations with weighing lysimeters in the 1970s. This report found significant reductions in peatland evaporation as the summer water level dropped below the threshold where the surface peat was wetted by the capillary fringe (i.e., to −50 cm). Comparing results from relatively wet and dry years, the authors found similar rates of evapotranspiration and assume it is driven more by vegetation cover than by water availability. As a result, in the relatively wet year, the ratio between evapotranspiration (ET)

and precipitation (P), used as a climate wetness index with implications for peat growth and hydrology, was 0.38 whereas in the dry year the ET/P ratio was 0.47. In both cases, ET was 63% of global solar radiation so the change in the ET/P ratio was derived nearly entirely by the reduction in P rather than a change in ET. In contrast to the relative consistency of ET rates in different climate conditions, the authors do find spatial heterogeneity of ET across their peatland landscape, with open water and lake-filled regions evaporating more water than a hollow-ridge complex consisting of some bare peat surfaces.

There is some history of work using the eddy covariance methodology (Baldocchi, 2003) to determine the energy balance and drivers of evapotranspiration in the continental peatlands of Russia. For instance, a comparison between a European bog (Fyodorovskoye) and a central Siberian bog (Zotino) revealed strong LE fluxes relative to H, with higher Bowen ratios (H/LE) in Fyodorovskoye (the approximate mid-summer average of a 5-day running mean ratio was 0.6-0.8 vs. 0.3, respectively) (Kurbatova et al., 2002). Both sites were characterized by close surface–atmospheric coupling through the effect of surface drying, limiting the role of net radiation in driving evaporative fluxes. This finding is in contrast to other work in a western Siberia bog (Shimoyama et al., 2004) that found a strong decoupling and therefore a large role for net radiation in driving the latent energy flux. Despite these studies, however, examples of the energy balance in Russian peatlands remain rare with a relative paucity of data compared to other regions (Lafleur, 2008; Wang and Dickinson, 2012). Finally, Russia's peatlands contain a diversity of hydro-ecological forms (Minayeva and Sirin, 2012), and there seem to be no reports of Russian boreal fen energy balances in the eddy covariance literature.

Therefore the key objective of this study is to quantify and describe the diurnal and seasonal variations and drivers of the energy balance for a typical boreal peatland complex of the Russian Federation's Komi Republic. This site, like many in this region, contains both fen-like and bog-like portions. However, since the predominant wind direction at our measurement site created an average measurement footprint covering the fen portion, that region was made the focus of the study. This work compares the relative contributions of net radiation and vapor pressure deficit to controlling latent energy fluxes. It also explores drivers of canopy conductance and how these factors change over time. Finally, an 11-month energy balance is generated, and the evapotranspiration fluxes are contextualized within the water balance, including measured changes in the water table and rates of precipitation and snowfall.

METHODS

Site description and data collection

The river valley peatland Medla-Pev-Nyur is in a transitional state from fen to bog following paludification and so consists of minerogenous, ombrogenous, and transitional zones; it lies within a region of the Komi Republic that has been classified as mainly containing ombrotrophic raised bogs (Vasander, 2007) and is not underlain by permafrost. Detailed characteristic of peatland Medla-Pev-Nyur was given earlier (Schneider et al., 2012).

An eddy covariance system with a closed-path CO_2 and H_2O gas analyzer (LI-7000, LI-COR Biosciences, USA) was used to measure the turbulent fluxes of momentum, heat, CO_2 and H_2O from 1 April 2008 until 12 February 2009 (Gažovič

et al., 2010). An ultrasonic anemometer (R3-100, Gill Instruments, UK) measured wind velocity components in three dimensions and sonic temperature at 20 Hz frequency at a height of 3 m. Sample air was drawn at a rate of 8.5 L min^{-1} from the air intake close to the anemometer measurement point, through a high-density polyethylene tube of 12 m length and 4 mm inner diameter, and through the closed-path gas analyzer. At the time of the start of measurements, the tube was new, i.e. the inner tube walls were uncontaminated. The site's fetch is relatively flat and homogeneous despite the microtopographic variation in the peatland surface. Initial investigation of the CO_2 data collected in this campaign indicates a growing season length of approximately 120 days, from DOY 140 to 260, or 19 May to 16 Sept, based on positive 24-hour net ecosystem productivity (Gažovič et al., in preparation).

This site was supported by an adjacent meteorological station that collected data on relative humidity (RH) and air temperature (T_a) (CS215, Campbell Scientific Ltd., UK), air pressure (RPT410F, Druck Inc., USA) and four-component radiation (CNR 1, Kipp and Zonen, Netherlands). Surface temperature (T_s) was determined from the outgoing long-wave radiation measurement with the Stefan-Boltzmann law and an assumed emissivity of 0.98; it is used to decide when to apply the latent heat of sublimation (at $T_s < 0$ °C) in place of latent heat of evaporation in converting water vapor fluxes to latent energy fluxes. Soil temperature at 1 cm and 5 cm below the peat surface was measured by CS-107 temperature probes (Campbell Scientific Ltd., UK) and heat flux plates (HFP01, Hukseflux, NL) measured at two nearby positions at a depth of 5 cm. Rainfall was measured by a HOBO RG2 tipping bucket rain gauge (Onset Computer Corporation Inc., USA), water level in the fen was measured by MDS Dipper groundwater loggers (SEBA Hydrometrie GmbH, Germany), and photosynthetically active radiation (PAR) was measured by an SKP215 sensor (Skye Instruments Ltd., UK). Vapor pressure deficit (*VPD*) was determined from *RH* and T_a using a vapor pressure saturation curve (Bolton, 1980). Water level fluctuations are compared to precipitation and evapotranspiration in the vertical (land–atmosphere) water balance by assuming a specific yield (S_y) of 0.60, which has been estimated for the upper layers of other boreal peatlands (Petrone et al., 2008). Snow cover and water content was determined through a series of seven vertical profile measurements in a transect line through the peatland over eight days between 27 March and 10 April 2008 and again during the period between 3 February and 10 February 2009. These data were supplemented by snow and precipitation data from the meteorological station at Syktyvkar, approximately 50 km to the southeast. All data are reported in local time, which is UTC+4 hours.

Eddy covariance data processing

Our flux data processing and correction routine is similar to one used in previous studies at this site (Runkle et al., 2012), and includes data screens based on stationarity and integral turbulence characteristics (Foken and Wichura, 1996). The processing routine uses a peak-detection algorithm in order to more accurately capture the delayed lag time possible under higher humidity and low-flux conditions and applies it in the flux data-processing routine after coordinate rotation of the wind velocity vectors. Corrections for tube attenuation of water vapor, based on cospectral similarity to the heat flux signal, are applied on the data until 15 October 2008 because a inlet tube heating cable installed at that time changed and largely eliminated this response (Runkle et al., 2012). Calculations

have been performed using EdiRe v1.5 (R. Clement, University of Edinburgh, UK) for flux data processing and Matlab v7.13 2011b (Mathworks, Inc., USA) for other numerical analyses.

Gap-filling on the time series of the turbulent energy fluxes (H and LE) was performed using an automated moving window, semi-empirical look-up method based on the response of these fluxes with VPD, T_a, and incoming solar radiation (R_s) (Falge et al., 2001; Reichstein et al., 2005). Once screened for wind direction to remove the non fen-like segments, gap-filling was required for 50% of LE measurement intervals and 40% of H measurement intervals. For certain months, the gap-filling requirements were higher; i.e., October's dataset required 78% of the half-hour periods to be filled, January required 71% and February required 91%. The other measured months required 38-53% of time periods to be gap-filled. The LE flux was further gap-filled using several modeling techniques described below. Footprint modeling was performed using an analytical model that assumes height-independent crosswind dispersion and that the vertical turbulent mixing process is stationary and behaves as a gradient analogous to diffusion (Kormann and Meixner, 2001). This approach has been applied to other boreal peatland sites (Forbrich et al., 2011) and is used primarily to distinguish between the fen-like and bog-like portions of the site.

Energy balance and modeling evapotranspiration

The surface energy balance is composed of net radiation (R_n), ground heat flux (G), the turbulent sensible heat flux (H), the turbulent latent heat flux (LE), the energy used to melt snow (Q_m), and a closure term or residual to account for an incomplete balance through measurement error or missing terms (C):

$$R_n = G + LE + H + Q_m + C \quad (1)$$

The sign convention used is that R_n and G are positive downward and H and LE are positive upward. Q_m is positive when the snow melts.

Q_m is modeled using the specific latent heat of fusion of water (L_f, 0.33 MJ kg^{-1}). For the April 2008 period, the snowpack's water equivalent (SWE) was measured on site and used with L_f. For the following winter SWE was derived from the Syktyvkar weather station's precipitation data. A degree-day snowmelt model was then applied using a 0 °C reference temperature and an open-area melt-rate factor of 4 mm $°C^{-1}$ d^{-1} (Rango and Martinec, 1995). This modeled melt water amount is then converted to the energy term Q_m using L_f. A sensitivity analysis of this factor conducted by shifting it between 3 and 5 mm $°C^{-1}$ d^{-1} revealed only slight impact (3-5 days) on the timing of snowmelt and a statistically indistinguishable effect on the 30-minute energy balance closure. As a diagnostic indicator of the performance of the eddy covariance technique, the energy balance closure is evaluated by using the half-hourly measurements and finding the least-squares linear regression slope $EB\text{-}C_{30}$ and intercept $EB\text{-}C_{30i}$, of the equation $(LE + H) = EB\text{-}C_{30} \cdot (R_n - G - Q_m) + EB\text{-}C_{30i}$ (as presented in Wilson and Baldocchi, 2000).

LE (i.e., ET $L_e r_w$) is modeled and gap-filled using the Penman-Monteith equation:

$$ET = \frac{1}{L_e \rho_w} \cdot \frac{sR_a + c_p \rho_a VPD g_a}{s + \gamma\left(1 + g_a / g_c\right)} \quad (2)$$

where R_a is the available energy and is approximated from the sum of H and LE. Alternatively and perhaps more traditionally, $R_n - G - Q_m$ is used, but the potential mismatch in their footprints and the difficulty of a good spatial estimate of G across the site's microtopography preclude this option here. The other terms are aerodynamic conductance (g_a), surface or canopy conductance (g_c), the slope of the saturation vapor pressure curve against temperature (s), the psychrometric constant (g), the density of water (r_w) and dry air (r_a), the latent energy of evaporation (L_e), the heat capacity of air (c_p), and the vapor pressure deficit (VPD). This model can be modified to estimate the potential evapotranspiration rate (PET) by setting g_c to infinity. The model is inverted to create estimates of g_c based on measured LE.

When the sonic anemometer provided quality-controlled estimates of u_*, a formula for g_a is computed to include excess boundary resistance to heat and water vapor transport. This approach has been used in previous studies of peatland landscapes (Kim and Verma, 1996; Humphreys et al., 2006), referencing work describing flow over irregular surface elements (Wesely and Hicks, 1977; Verma, 1989):

$$g_a = \left(\frac{kB^{-1}}{ku_*} \left(\frac{d_h}{d_v} \right)^{2/3} + \frac{u}{u_*^2} \right)^{-1} \quad (3)$$

where u_* is the friction velocity, u is the mean wind speed, k is the von Karman constant with a value of 0.4, and d_h/d_v is the ratio of thermal diffusivity (d_h) to molecular diffusivity of water vapor (d_v) and is set to 0.89 at 20 °C. The kB^{-1} term, using the dimensionless parameter B^{-1}, is an estimate of the logarithmic ratio between the roughness length of momentum and the roughness length for mass or sensible heat fluxes (Owen and Thomson, 1963). A kB^{-1} value of 2 is used for comparison to a recent review of the peatland energy balance (Humphreys et al., 2006), though slightly lower (1.6) and higher (2.3) values have also been used in peatland studies (Campbell and Williamson, 1997; Shimoyama et al., 2004). The two conductance terms are determined on a half-hourly basis but are presented using monthly and diurnal average values; they are also determined separately for wet or dry periods as defined as the presence (or absence) of rainfall in the preceding 12 hours (Brümmer et al., 2012).

The surface roughness length z_0 is determined from the sonic anemometer's 30-min estimate of u_* and mean wind speed, similar to Sonnentag et al. (2011):

$$z_0 = \frac{z - d_0}{\exp(k * u/u_*)} \quad (4)$$

where, z is the measurement height (3 m), d_0 is the zero-displacement height (assumed to be 0.66*h) and z_0 is assumed to be 0.1*h (Foken, 2008), where h is the vegetation canopy height. Therefore, z_0 and h can then be derived from the other terms. This z_0 parameter is derived under near-neutral conditions ($|z/L| < 0.025$) and high mean horizontal wind speeds ($u > 3$ m s^{-1}) to ensure minimal correlation between z_0 and u. A seasonal evolution of z_0 is then developed based on the monthly mean z_0 estimates, interpolated through time, and used to generate estimates of u_* from the meteorological wind sensor when the sonic anemometer's performance failed quality control.

Measured and modeled evapotranspiration can also be compared to equilibrium evaporation E_{eq} (McNaughton, 1976). This rate represents the vapor flux expected from an extensive moist surface in the absence of advective influences (as it is missing the u, VPD, and conductance terms of the Penman-Monteith equation):

$$ET_{eq} = \frac{1}{L_e \rho_w} \cdot \frac{sR_a}{s+\gamma} \tag{5}$$

where R_a is the available energy, which is defined either as ($R_n - G - Q_m$) or as (H + LE). Both terms are used in the literature and offer a chance to explore the effect of the incomplete energy balance closure on the Priestley-Taylor (1972) relationship, which uses ET_{eq} in the formula $ET = a_{PT} ET_{eq}$, where a_{PT} is fit through linear regression against measured ET. Some researchers consider the Priestley-Taylor a_{PT} of 1.26 as a truer representation of equilibrium conditions (Eichinger et al., 1996). In either case, a_{PT} can be a useful indicator of the drivers of evaporation, as the fitted value can vary substantially among different wetlands (Roulet and Woo, 1986; Souch et al., 1996).

Canopy conductance modeling

The canopy conductance is modeled by the following relationship, which modifies relationships used in other wetland studies (Kellner, 2001; Wu et al., 2010) and is fit for the inverted g_c estimates on a monthly basis by minimizing the root-mean-square error of modeled output:

$$g_c = \frac{a \times R_s + b}{1 + c \times VPD} \tag{6}$$

where R_s is the incoming shortwave radiation and a (mm s^{-1} W^{-1} m^2), b (mm s^{-1}), and c (kPa^{-1}) are the best-fit parameters. This modeled value is used with the Penman-Monteith equation (where $R_a = R_n - G - Q_m$) to gap-fill the full time series of LE fluxes. At a daily time scale, the daytime mean g_c is compared to daytime mean VPD through a relationship used in other peatland energy balance studies (Humphreys et al., 2006; Sottocornola and Kiely, 2010):

$$g_c = \frac{g_{c,\max}}{1 + b_D \times VPD} \tag{7}$$

In this relationship, $g_{c,max}$ (mm s^{-1}) and b_D (kPa^{-1}) are best-fit parameters similar to b and c in the previous equation. This relationship is fit for daytime intervals with PAR > 400 mmol m^{-2} s^{-1}, which is a lower light threshold than used in comparative studies, but allows more data from a wider portion of the growing season to be examined.

The decoupling coefficient can also be used to quantify the degree of interaction between the evaporating surface and the atmosphere outside of the leaf boundary layer (McNaughton and Jarvis, 1983; Jarvis and McNaughton, 1986):

$$\Omega = \frac{s/\gamma + 1}{s/\gamma + 1 + g_a/g_c} \tag{8}$$

An Ω value near 0 implies a strong coupling between atmosphere and vegetation so that VPD in the region of the leaf (or otherwise evaporating surface) is negligibly distinct from VPD in the atmosphere. In these cases, $g_c << g_a$ and E is primarily controlled by g_c and VPD. Alternatively, a Ω of 1 implies complete de-

coupling of LE and the atmospheric moisture budget, as R_n is the only contributor to E ($g_c >> g_a$) and changes in evaporation tend to have no effect on VPD in the region of the evaporating surface. Such decoupled conditions may develop in the moist microclimates within a forest canopy or a wet landscape, while coupling tends to be stronger in drier, more water-limited ecosystems, including peatlands if the moss surface dries out.

Ground heat flux

The ground heat flux plate measurements (G_5) at 5 cm depth (Dz) were corrected for changes in heat storage in the overlying peat layers using the combination method of C.B. Tanner (Brutsaert, 1982; Drexler et al., 2004). This method uses the difference of the average peat temperature measured at both 1 cm and 5 cm over a 30-min interval ($dT_{1\text{-}5}$), assumes a constant heat capacity (C_h) in time (t) and space (z), and uses dt set to 1800 s (the measurement interval of the ground heat flux plate):

$$G = G_5 + C_h \frac{dT_{1-5}}{dt} \Delta z \qquad (9)$$

A weighted heat capacity was used by assuming continuously saturated peat conditions and porosity 0.8. This value (3.54 MJ m^{-3} K^{-1}) assumes constant heat capacities of dry peat soil (2.3 MJ m^{-3} K^{-1}) and of water (4.2 MJ m^{-3} K^{-1}). The mean corrected ground heat flux from each plate measurement for each 30-minute interval was used to average the effects of spatial heterogeneity in heat conduction.

RESULTS

Site energy balance

The site's observed meteorological conditions reflected its position in the boreal zone, with cold, extended freezing conditions in winter and warm summer months in June and July (Fig. 1). At the Syktyvkar meteorological station, the study year of 2008 was both warmer and wetter than long term annual average conditions with a mean annual temperature of 3.4 °C and a precipitation of 687 mm (water equivalent) from April 2008 to February 2009 (though the installed station at the study site measured only 486 mm precipitation). Relative to long-term conditions, the study year had higher than average temperatures in July and the winter months and more rainfall in August largely due to a single storm event.

Near the start of field measurements, on 6 April 2008, the peatland surface was completely covered with a snow layer of approximately 40 cm depth (with average volumetric water content of 29%, representing 36 MJ m^{-2} cumulative melt energy or one-third of April's net radiation). This time was followed soon after by rain events and higher temperatures, melting all snow and contributing to a rise in the water table. From 16 April, the water table was near the surface on hummock locations and from +5 to +17 cm over the peat surface in transitional to minerogenic regions, respectively. These water surfaces dropped by 3 to 9 cm from 21 April to 3 May, during a period with pronounced daily temperature fluctuation and nighttime freezing of the water and peat surfaces (Gažovič et al., 2010). Despite punctuation by small precipitation events, the water table continued on a general decline to −14 cm until a large (36 mm) rain event 19-20

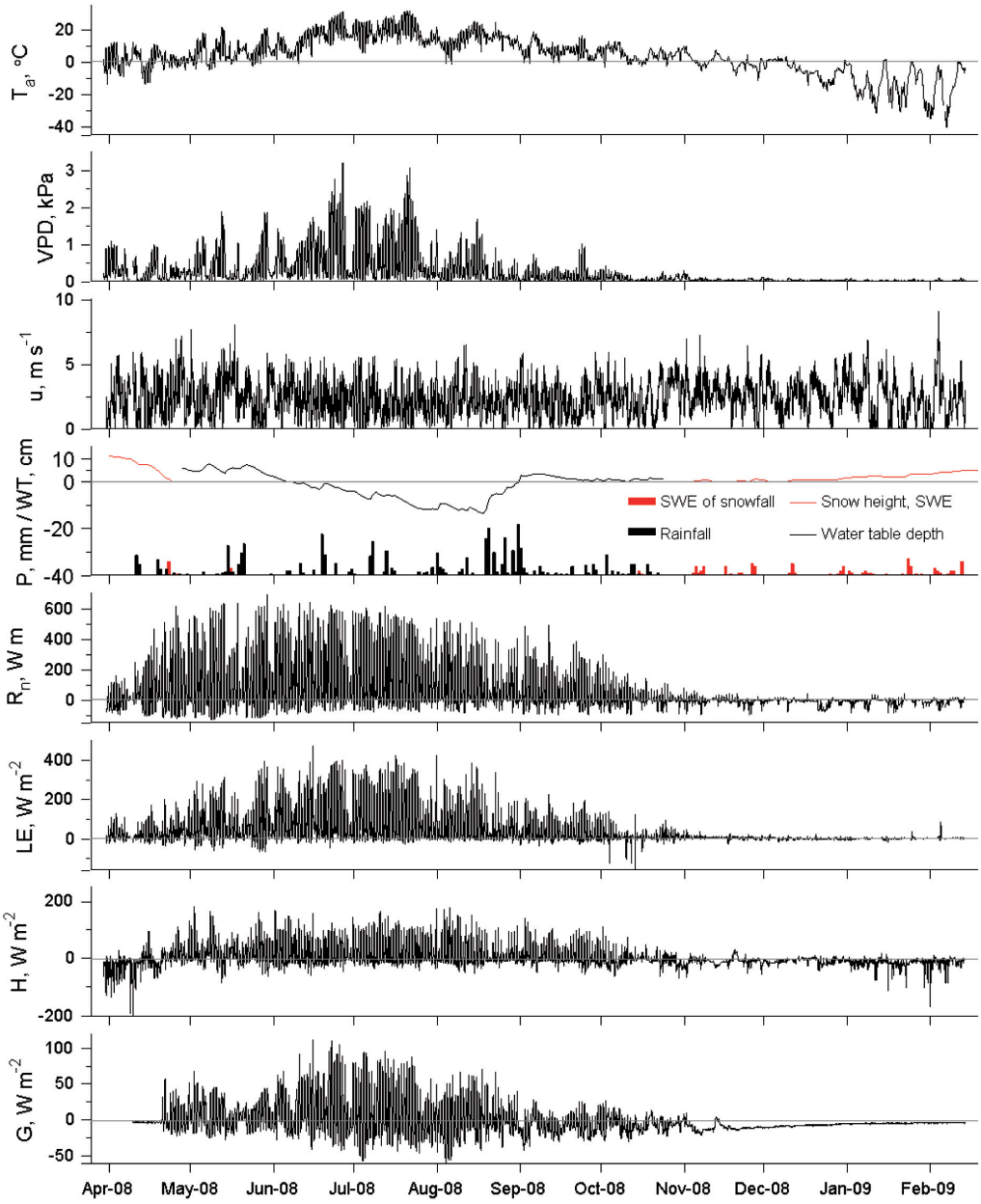

Fig. 1: Meteorological conditions and gap-filled energy fluxes derived from the eddy-covariance methodology (or ground heat flux modeling) for 2008-09 field year, measured or modeled on a half-hourly frequency. Measured meteorological terms include air temperature (T_a), vapor pressure deficit (VPD), horizontal wind speed (u), and precipitation (P), which represents rainfall (in black) and the water-equivalent of snow (in red). The water table depth (WT) is the mean of two wells in the fen region of the peatland site. Note the changing y-axis limits on the heat fluxes-net radiation (R_n), latent energy (LE), sensible heat (H), and ground heat flux (G).

August and subsequent rainfall brought the mean water table up toward the surface. Examining solar albedo from the 4-component radiometer suggests a first winter snowfall on 5 November 2008, followed by a brief melt event one week later, and then near continuous site snow cover until the end of the measurement campaign.

The eddy covariance measurements were screened for quality and footprint to generate time series for LE and H. As a diagnostic of the half-hourly flux measurements, the site achieved a 75% closure slope (i.e., $EB\text{-}C_{30}$ at of the full dataset), though closure was much higher in the summer months ($EB\text{-}C_{30}$ of 0.73 in September to $EB\text{-}C_{30}$ of 0.97 in July and August). Moreover, the gap-filled cumulative annual energy balance was 86% of incoming radiation (Table 1 and Table 2). The dominant wind direction generated a seasonal eddy flux footprint weighted toward the site's fen-like portions, with much less data representing the mire's bog regions. Of the 30-minute eddy flux intervals that passed data-screening and technical concerns, 78% were from wind directions (124-327°) where 50% or more of the flux-contributing areas were within the fen region. No consistent changes to the energy partition were found to differentiate the bog and fen contributing regions during meteorologically similar data collection intervals. The result of these screens was that 50% of the measurement period's half-hourly data was kept for further analysis. The footprint model additionally demonstrated that in 96% of the flux measurement periods, 80% of the flux footprint was within 500 m of the eddy tower, thus largely avoiding the patches of forest on the mire's outskirts. The remainder of flux measurements occurred during stable, night-time conditions with low fluxes and so had little effect on the total energy balance, and the region of maximum contribution to the overall flux at these times was still well within the open peatland's boundaries. The lookup-table method was successful in generating gap-filled H fluxes with root-

Table 1

Monthly cumulative surface energy balance terms* with units MJ m^{-2}

Month	R_n	H	LE	G	Q_m	C	LE_{pot}	LE_{eq}	LW_{in}	LW_{out}	SW_{in}	SW_{out}
Apr.08	108	–27	63	1	39	31	125	37	669	803	380	134
May.08	278	51	183	20	1	23	272	143	766	936	497	50
Jun.08	355	49	252	36	0	17	378	210	860	1004	580	78
Jul.08	360	64	260	19	0	18	424	242	942	1091	620	111
Aug.08	193	34	140	0	0	19	212	121	938	1023	343	66
Sep.08	98	21	75	–21	0	24	122	64	816	900	216	34
Oct.08	12	–19	23	–15	1	22	50	12	840	889	73	12
Nov.08	–20	–24	11	–25	7	11	26	–1	775	805	19	9
Dec.08	–32	–20	3	–18	3	1	15	–3	741	774	11	9
Jan.09	–33	–42	2	–10	1	16	5	–5	613	647	33	32
**Feb.09	–9	–11	2	–3	0	3	3	–1	250	261	22	20
Total	1310	77	1014	–16	52	183	1630	819	8211	9134	2794	554

* Sensible heat flux (H) is derived from a look-up approach gap-filling tool on eddy covariance data. Latent energy (LE) is gap-filled with the Penman-Monteith model described in the text. Net radiation (R_n) and incoming and outgoing short- and long-wave radiation (SW_{in}, SW_{out}, LW_{in}, LW_{out}) are measured using a net radiometer and 4-component radiometer, respectively. Ground heat flux (G) is measured with heat flux plates and corrected for changes in heat storage in the overlying peat layers, the energy required for snow melt (Q_m) is modeled based on measured snow height and density, and C indicates the residual. Potential (LE_{pot}) and equivalent (LE_{eq}) latent energy fluxes are modeled as described in the text.

** The measurement campaign concluded 12 Feb 2009, so February is presented as a partial month.

Table 2

Monthly ratios of key energy balance terms, where "Annual" implies ratios derived from the study period's total radiation components. $B_{r,mid\text{-}day}$ refers to the average half-hourly Bowen ratio (H/LE) for the mid-day period (10:00-14:00 h), and the standard deviation is given as the uncertainty range; the "Annual" value given for this term only refers to the growing season, defined as between 19 May and 16 September. EB-C_{30} and EB-C_{30i} refer to the diagnostic energy balance closure slope and intercept, respectively, from the 30-minute measurement intervals. Other abbreviations are the same as in Table 1 and the text

Month	LE/R_n	H/LE	H/R_n	G/R_n	C/R_n	LE/LE_{pot}	R_n/SW_{in}	SW_{out}/SW_{in}	$B_{r,mid\text{-}day}$	EB-C_{30}	EB-C_{30i}, W m^{-2}
Apr.08	0.59	–0.43	–0.25	0.01	0.29	0.50	0.28	0.35	0.01 ± 2.48	29.2 ± 1.4	0.23 ± 0.06
May.08	0.66	0.28	0.18	0.07	0.08	0.67	0.56	0.10	0.53 ± 0.33	61.5 ± 0.9	0.50 ± 0.03
Jun.08	0.71	0.20	0.14	0.10	0.05	0.67	0.61	0.13	0.35 ± 0.20	82.6 ± 0.8	0.77 ± 0.04
Jul.08	0.72	0.25	0.18	0.05	0.05	0.61	0.58	0.18	0.37 ± 0.19	96.5 ± 0.7	0.97 ± 0.04
Aug.08	0.72	0.25	0.18	0.00	0.10	0.66	0.56	0.19	0.47 ± 0.18	96.9 ± 0.9	0.97 ± 0.04
Sep.08	0.76	0.28	0.21	–0.21	0.24	0.61	0.45	0.16	0.68 ± 0.24	72.9 ± 0.8	0.70 ± 0.04
Oct.08	1.95	–0.83	–1.61	–1.22	1.81	0.47	0.16	0.16	0.27 ± 1.39	64.9 ± 2.2	0.69 ± 0.08
Nov.08	–0.57	–2.09	1.19	1.28	–0.54	0.43	–1.04	0.47	–0.47 ± 2.82	41.9 ± 2.3	0.41 ± 0.10
Dec.08	–0.09	–6.98	0.64	0.56	–0.03	0.20	–2.98	0.87	1.84 ± 6.15	41.9 ± 1.8	0.38 ± 0.07
Jan.09	–0.05	–27.06	1.28	0.31	–0.49	0.33	–0.98	0.95	9.11 ± 12.76	49.5 ± 2.1	0.33 ± 0.10
Feb.09	–0.22	–5.47	1.18	0.36	–0.31	0.67	–0.41	0.91	21.63 ± 58.98	39.4 ± 5.8	0.39 ± 0.23
Annual	0.77	0.08	0.06	–0.01	0.14	0.62	0.47	0.20	0.47 ± 0.25	75.2 ± 0.4	0.72 ± 0.02

mean-square error (rmse) of 13.6 W m^{-2}, determined by comparing measured data to the modeled values estimated from the gap-filling technique. Compared to the measured data points, modeled LE fluxes had rmse of 23.0 W m^{-2} using the lookup-table method and improved to rmse of 12.2 W m^{-2} using the Penman-Monteith model with parameters presented below.

The magnitude of the energy fluxes closely followed net radiation (Table 1 and Table 2), which during the unfrozen months was largely partitioned into latent energy flux (>60%). Because of substantial winter-time negative sensible heat fluxes, LE represented 77% of the measurement period energy balance. During the growing season, H reached nearly 20% of the monthly energy balance and G approached 10% (in June). Compared to potential evapotranspiration, total actual evapotranspiration during the summer was in the range 61-67% and often exceeded total equilibrium evapotranspiration. The monthly averaged growing season shortwave albedo was between 10% and 19%, and the summer R_n/SW_{in} ratio was in the range 0.56-0.61. The cumulative monthly Bowen ratio (i.e., H/LE including both night and day values) had high values of 0.28 in September and May but was as low as 0.20 in June and was 0.08 for the complete 11-month measurement period (lowered by strongly negative sensible heat fluxes during the snow-covered months). Monthly average mid-day Bowen ratios were in the range 0.35-0.68 during the growing season months.

The monthly mean diurnal cycle of the primary energy flux terms revealed the dominance of the latent energy flux within the partition of net radiation at nearly all points of the diurnal cycle for the months with significant incoming net radiation (Fig. 2). While LE generally rose in concert with morning increases in net radiation, it declined more slowly in the late afternoon, as T_a and VPD remained high during this period. During the afternoon and into the evening, LE often met or exceeded R_n. The ratio H/R_n was more constant during daytime hours relative to LE/R_n. This pattern is made explicit through plotting the Bowen ratio's average diurnal cycle in Fig. 4, which demonstrates that early-morning peaks in the H/LE ratio approached 0.85 in some months and then declined during the day. Modelled G peaked approximately 1 hour later in the day than R_n and took a higher proportion of R_n earlier in the year than later. During wintertime, latent energy was negligible, and the ground and sensible heat fluxes, which were generally negative, left larger relative energy imbalances in the budget.

The relative strength of R_n and VPD in driving latent energy fluxes changed through the months (see Supplemental Data table). From April through November R_n, was a stronger influence than VPD, with greater coefficient of determination (r^2) on a regression of half-hourly data (up to 0.88 in July; $p < 0.001$). During the months June-August, a regression line determining this control has a slope of 0.56 or greater, though at other times the slope is lower (0.23 ± 0.02 in April, 0.42 ± 0.04 in October, and insignificant during the winter months). The maximum explanatory power of VPD alone on LE was in August ($r^2 = 0.62$, $p < 0.001$) with September sharing a similarly high slope in a regression line between VPD and LE (i.e., 210 W m^{-2} kPa^{-1}). The strong temporal correlation between R_n and VPD (Pearson correlation coefficient $r = 0.64$, $p < 0.001$, across the whole measurement period) precludes determining from these regressions alone whether either's relationship with LE was solely causal.

The parameters and indicators describing different portions of the controls on LE changed over the season and generally tracked vegetation growth as expressed by vascular plant GAI (Table 3).

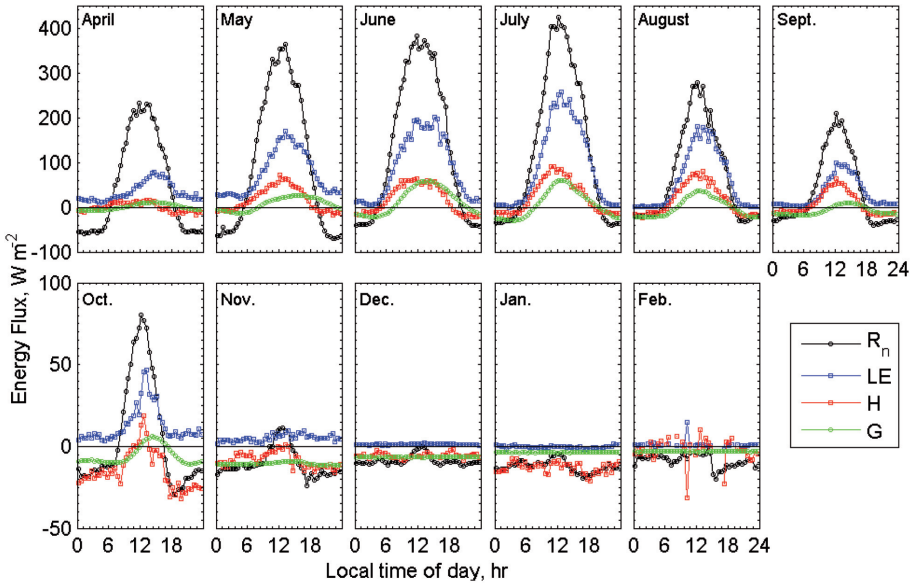

Fig. 2: Monthly mean diurnal pattern of the study site's energy fluxes — net incoming radiation (R_n), latent energy (LE), sensible heat (H), and ground heat flux (G) – during the study period (April 2008–February 2009). The energy required for snowmelt is not shown, but follows the diurnal course of air temperature. Note the change in y-axis scaling between the two rows of plots.

The estimated roughness length z_0 reached a maximum 46 ± 12 mm in August and was 3 ± 2 mm in February. The decoupling coefficient, W, had a daytime average value of 0.65 ± 0.16 during the full measurement period but was slightly higher during the growing season, with a monthly average range of 0.65-0.73 and a standard deviation of approximately 0.14 in each month. This higher decoupling indicates more direct influence of R_n on LE fluxes. The imperfect energy closure has considerable influence on the a_{PT} parameter. During June-August, a_{PT} was in the range 0.97-1.06 when assuming available radiation is equivalent to $R_n - G - Q_m$, whereas these values climbed to 1.06 to 1.17 when using gap-filled H + LE. During these summer months, the Priestley-Taylor relationship is an effective model of LE, with r^2 values between 0.78 and 0.87 (using R_n–G), though monthly rmse can exceed 50 W m^{-2}. As a descriptive model using H + LE for available energy, r^2 rises above 0.95, and rmse is more than halved. Additionally, the residuals of this relationship skew positive, for instance when available radiation is negligible or negative, LE_{eq} was also negative but actual LE was positive. This bias along with the energy imbalance helps to explain why the monthly total LE is often 10-30% higher than monthly LE_{eq}, yet a_{PT} remains around 1.0. Over the whole measurement period, the two methods generate a_{PT} values of 0.93 and 1.14 (when $R_a = R_n - G - Q_m$ or $R_a = H + LE$, respectively).

Conductance terms and their drivers

On a monthly basis, mean g_a and g_c were generally of similar magnitude, and both increased during the growing season (Table 4). The uncertainties around these values are substantial when averaging across different time periods within either the diurnal or seasonal cycle, driven as they are by quickly chang-

Table 3

Monthly parameters governing and describing conductance and LE fluxes. Vascular plant green area index (GAI) is determined via leaf size and number estimates (Schneider et al., 2012); the roughness length (z_0); decoupling coefficient (W), determined when PAR > 20 mmol m^{-2} s^{-1}; and the Priestley-Taylor coefficient (a_{PT}) and its fit statistics are presented. The a_{PT} coefficient and other Priestley-Taylor model terms are determined twice, with different assumptions for the available radiation (R_a), but in both cases use only daytime intervals with PAR > 20 mmol m^{-2} s^{-1}. This model's root-mean-square error (rmse) from measured latent energy flux is used as a fit-statistic and has units of W m^{-2}. Annual values are derived from the full measurement dataset

Month	GAI	z_0 (mm)	Ω (day)	$R_a = R_n - G - Q_m$			$R_a = H + LE$		
				α_{PT} (day)	r^2, p-value	rmse	α_{PT} (day)	r^2, p-value	rmse
Apr.08	0	18 ± 10	0.53 ± 0.17	0.54 ± 0.05	0.26, p < 0.001	36.24	1.45 ± 0.05	0.76, p < 0.001	25.02
May.08	0.08	26 ± 10	0.67 ± 0.12	0.82 ± 0.03	0.69, p < 0.001	52.85	1.34 ± 0.03	0.95, p < 0.001	18.8
Jun.08	0.43	32 ± 13	0.70 ± 0.13	0.97 ± 0.03	0.78, p < 0.001	48.24	1.17 ± 0.03	0.96, p < 0.001	21.37
Jul.08	1.54	45 ± 12	0.65 ± 0.12	1.02 ± 0.02	0.87, p < 0.001	38.86	1.06 ± 0.02	0.98, p < 0.001	15.92
Aug.08	1.41	46 ± 12	0.67 ± 0.14	1.06 ± 0.03	0.82, p < 0.001	36.73	1.08 ± 0.03	0.98, p < 0.001	14.33
Sep.08	0.33	38 ± 12	0.73 ± 0.14	0.84 ± 0.03	0.58, p < 0.001	29.32	1.16 ± 0.03	0.91, p < 0.001	13.78
Oct.08	0.03	38 ± 11	0.49 ± 0.16	0.82 ± 0.10	0.58, p < 0.001	17.88	1.14 ± 0.10	0.83, p < 0.001	15.39
Nov.08	0	30 ± 12	0.69 ± 0.17	0.18 ± 0.15	0.01, p = 0.35	9.57	0.60 ± 0.15	0.21, p < 0.001	8.92
Dec.08	0	16 ± 8	0.44 ± 0.34	0.06 ± 0.14	0.06, p = 0.02	3.9	0.35 ± 0.14	0.50, p < 0.001	3.63
Jan.09	0	4 ± 3	0.28 ± 0.20	0.12 ± 0.07	0.08, p = 0.01	2.03	0.24 ± 0.07	0.17, p < 0.001	1.98
Feb.09	0	3 ± 2	0.39 ± 0.18	–0.68 ± 0.18	0.89, p < 0.001	1.59	–1.41 ± 0.18	0.45, p < 0.001	2.75
Annual	0.35	28 ± 13	0.65 ± 0.16	0.93 ± 0.01	0.77, p < 0.001	42.64	1.14 ± 0.01	0.95, p < 0.001	20.62

Table 4

The aerodynamic and canopy resistance terms (g_a and g_c, respectively) are monthly averages of data determined from modeling eddy covariance measurements of water vapor flux. Annual values are derived from the full measurement dataset. Wet values are the mean of time intervals within 12 hours of a rain event or on days with snow cover; dry values average other periods

Month	g_a, mm s^{-1}	g_c, mm s^{-1}	Wet g_c, mm s^{-1}	Dry g_c, mm s^{-1}	Wet g_a, mm s^{-1}	Dry g_a, mm s^{-1}
Apr.08	11.2 ± 6.8	12.0 ± 2.3	11.9 ± 2.4	12.4 ± 1.4	10.6 ± 6.5	14.2 ± 7.9
May.08	14.1 ± 8.2	18.6 ± 5.3	20.7 ± 3.9	17.7 ± 5.7	17.8 ± 6.7	12.5 ± 8.2
Jun.08	14.2 ± 7.4	15.7 ± 5.9	18.6 ± 6.2	14.5 ± 5.4	16.4 ± 7.0	13.3 ± 7.5
Jul.08	14.2 ± 9.1	12.6 ± 6.8	16.0 ± 6.6	10.9 ± 6.2	14.1 ± 8.5	14.2 ± 9.3
Aug.08	15.4 ± 8.5	20.2 ± 4.9	21.2 ± 4.1	18.1 ± 5.6	15.1 ± 8.2	15.9 ± 9.0
Sep.08	14.8 ± 8.5	28.0 ± 5.7	28.4 ± 5.8	27.3 ± 5.5	16.0 ± 8.6	13.4 ± 8.0
Oct.08	15.7 ± 8.7	10.9 ± 1.0	11.0 ± 1.0	10.8 ± 0.9	17.2 ± 8.1	14.8 ± 8.9
Nov.08	17.0 ± 6.7	10.5 ± 0.3	10.5 ± 0.3	10.5 ± 0.3	16.1 ± 6.8	18.0 ± 6.5
Dec.08	12.7 ± 5.7	10.5 ± 0.2	10.5 ± 0.2	10.5 ± 0.1	13.2 ± 5.7	11.3 ± 5.7
Jan.09	7.9 ± 6.6	10.6 ± 0.6	10.6 ± 0.6	–	7.9 ± 6.6	–
Feb.09	7.4 ± 4.7	10.8 ± 0.8	10.8 ± 0.8	–	7.4 ± 4.7	–
Annual	13.5 ± 8.1	14.8 ± 6.8	14.8 ± 6.7	14.8 ± 6.9	13.0 ± 7.9	14.1 ± 8.3

ing synoptic factors. Comparing wet to dry data intervals, defined by the presence rainfall in the preceding 12 hours, wetter periods generated higher canopy conductance, with reduced resistance to surface water availability and more direct evaporation. There were negligible differences between wet and dry periods in the aerodynamic conductance. During the growing season 43% of the time was classified as "wet". The mid-summer average canopy conductance during wet periods (16-21.2 mm s^{-1}) exceeded dry-period canopy conductance (10.9-18.1 mm s^{-1}) as well as wet-period aerodynamic conductance (14.1-16.4 mm s^{-1}). The peak monthly mean g_a occured in November (17.0 ± 6.7 mm s^{-1}) and the peak monthly mean g_c occurred in September (28.0 ± 5.7 mm s^{-1}).

Similarly to their monthly average values, the canopy conductance and aerodynamic conductance were of similar magnitude to each other throughout the diurnal cycle (Fig 3), particularly in the summer months. The drivers of canopy conductance vary substantially during the diurnal course and also within a given month. The time-course of VPD closely followed that of temperature, and both lag incoming radiation (expressed either as PAR or R_g). The conductance terms both tended to reach their maximum between the daily peaks of PAR and VPD (at approximately 14:00, compared to approximately 12:00 or 17:00, respectively). Mean diurnal wind speed (u) peaked around 14:30 in April, peaked earlier in July (12:00) and then peaked around 13:00 for the remainder of the growing season. This timing is consistent with creating an aerodynamic conductance value that varied relatively synchronously with canopy conductance. For gap-filling during cases when the sonic anemometer failed, g_a was determined using a derived estimate of u_* from the assumed logarithmic profile of wind speed. The g_a estimates from this model have a root-mean-square error (rmse) of 4.6 mm s^{-1} ($r^2 = 0.71$, $p < 0.001$) when compared to periods with valid sonic anemometer estimates of friction velocity.

The wide diurnal peaks of VPD, T_a, and u contributed to similarly broad diurnal peaks in the decoupling coefficient Ω (Fig. 4). This parameter changed little during daytime and only declined in the evening hours when the contribution of R_n to ET was minimal. During the main summer growing season, the mid-day

Ω varied little, with monthly mean values in the range 0.65-0.73 (and standard deviation < 0.2). The small but inconsistent scatter across each month's mean diurnal pattern prevented detecting a clearly defined peak, but most months seemed to have peak Ω at around 12:00 followed by a gentle decline into the late afternoon and evening hours, reflecting the general shift of influence from R_n at mid-day towards VPD later on.

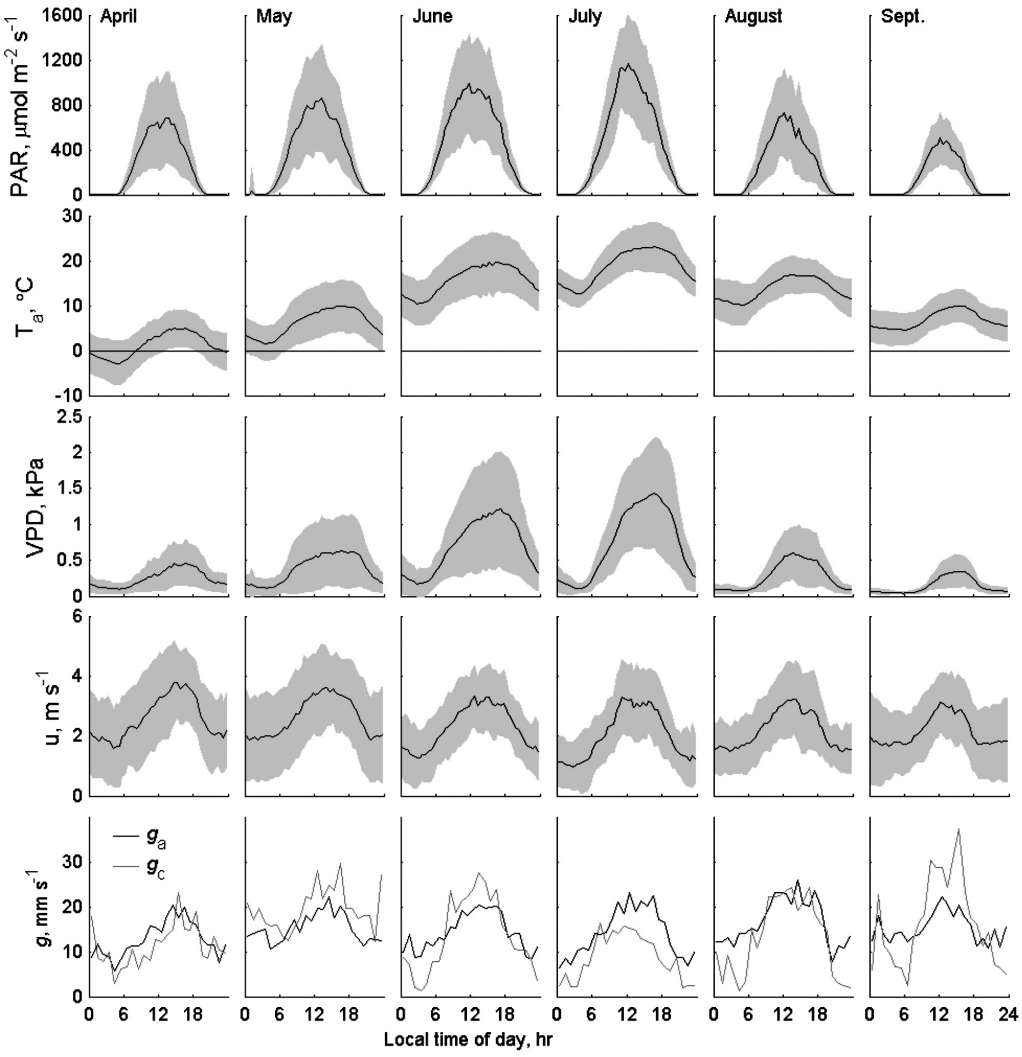

Fig. 3: Diurnal patterns of aerodynamic conductance g_a and canopy conductance g_c and their drivers by month during the growing season; values are the mean of all measurements for each data-collection interval. No gap-filling data were used for the conductance terms. The shading around the driver variables represents one standard deviation. The drivers are presented at half-hourly intervals; the conductance terms are presented at hourly intervals.

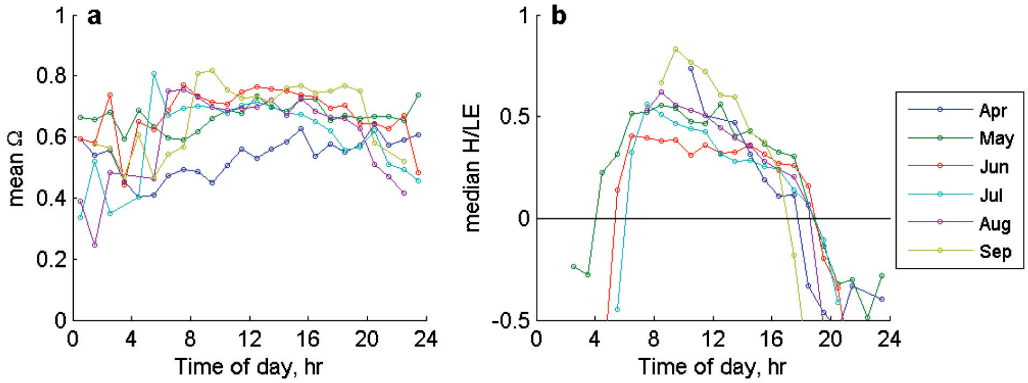

Fig. 4: Monthly mean diurnal evolution of (a) the decoupling factor Ω and (b) the Bowen ratio (H/LE), calculated by binning data into hourly intervals during periods with valid eddy covariance measurements of the sensible heat (H) and latent energy (LE) fluxes. The mid-day standard deviation for is always less than 0.2; the mid-day standard deviation for the Bowen ratio (in May-Sep) is always less than 0.25.

The surface canopy conductance was reduced in response to increasing VPD (Fig. 5 and Table 5). This response appears to be stronger later in the growing season, as indicated by higher values of the *c* parameter (Table 5) and reduced g_c under similar VPD conditions relative to earlier in the year (Fig. 5). The parameter estimates for the terms in equation 8 (Table 5) reveal the uncertainty inherent in this approach, with relatively high error bars (ranging from 10-50 % of the parameter estimates) and low r^2 (maximum monthly explanatory power in July of 0.35; $p < 0.01$). Day of year explained 24% of the variation in the modeled g_c residuals ($p \sim 0.001$), while water table depth (insignificantly) explained 4% ($p = 0.16$), with higher water tables associated with higher g_c values. The g_c residuals switched from likely positive to likely negative on 9 July, which roughly coincides with maximum vegetation cover (i.e., the completion of the main plant growth period).

The relationship between daily mean g_c and VPD (Fig. 5) has relatively high uncertainty bounds on the parameter estimates. The extent of this uncertainty is made clearer by the changes in these parameters given different PAR thresholds. When more data are included by relaxing the PAR threshold, more low-VPD periods are included that have much higher g_c values. This inclusion increases

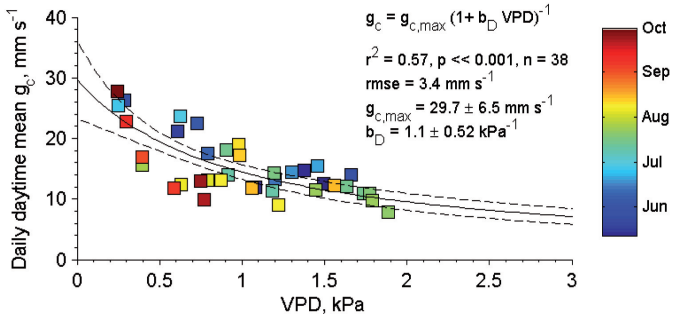

Fig. 5: Daily average canopy conductance g_c plotted against vapor pressure deficit (VPD), where daily values are only calculated when GAI > 0.05, there are six hours or more since last rain, PAR exceeds 400 μmol m^{-2} s^{-1}, and < 50% gaps within daytime (10:00-17:00 local time). Points are colored by day of year; the model is fit via nonlinear ordinary least squares regression.

Table 5

Monthly fit parameters for g_c model, i.e., eqn. 8 (values from October were used for gap-filling in later months, when low PAR conditions and more frequent measurement errors precluded new parameterizations)

Month	a, mm s^{-1} W^{-1} m^2	b, mm s^{-1}	c, kPa^{-1}	rmse, mm s^{-1}	r^2
Apr.08	0.015 ± 0.012	13.8 ± 3.7	1.37 ± 0.93	9.2	0.11, p << 0.01 (n=297)
May.08	0.052 ± 0.019	21.4 ± 2.8	2.03 ± 0.72	11.2	0.22, p << 0.01 (n=554)
Jun.08	0.062 ± 0.020	23.7 ± 3.7	2.66 ± 0.84	8.8	0.31, p << 0.01 (n=438)
Jul.08	0.180 ± 0.103	34.1 ± 10.5	10.28 ± 5.70	7.2	0.35, p << 0.01 (n=473)
Aug.08	0.049 ± 0.026	27.3 ± 4.2	3.21 ± 1.38	9.4	0.23, p << 0.01 (n=400)
Sep.08	0.014 ± 0.023	36.9 ± 5.7	3.10 ± 1.29	11.2	0.24, p << 0.01 (n=341)
Oct.08	0.018 ± 0.036	10.4 ± 5.4	-0.48 ± 1.57	7.9	0.08, p = 0.08 (n= 38)

the apparent sensitivity of g_c to VPD by raising b_D, without much demonstrable change in the g_c-VPD relationship at the region of real interest (i.e., high VPD). For half-hourly intervals with VPD > 1 kPa, the g_c-VPD slope was -5.7 ± 1.3 mm s^{-1} kPa^{-1} ($r^2 = 0.18$, $p < 0.001$, $n = 316$).

Evapotranspiration in the water cycle

In addition to its role in the surface energy balance, water vapor fluxes expressed as ET can be related to other terms in the hydrological cycle (Table 6).

Table 6

Monthly surface water balance terms including the residual term R (positive residual implies a net inflow; negative residual implies a net outflow). Snowfall was measured at the Syktyvkar weather station approximately 50 km from the field site and is presented in terms of its water equivalent. All terms have units of mm

Month	Rain	Snow	ET	Δ WT (n=2)	R (if S_y = 0.6)
Apr.08	29.2	8.1	23.8	–32.5 ± 28.5	–14.1
May.08	48.8	3.3	73.5	–26.4 ± 2.2	–40.5
Jun.08	48.6	0	101.1	–58.9 ± 4.4	–87.8
Jul.08	49.4	0	105.2	–88.4 ± 19.7	–108.8
Aug.08	134.4	0	56.4	141.1 ± 11.0	162.6
Sep.08	45.4	0	30.1	–13.9 ± 2.2	7
Oct.08	32.8	2.6	9.3	1.5 ± 2.2	24.4
Nov.08	0	27.9	4.3	–	–4.3
Dec.08	0	15.3	1.1	–	–1.1
Jan.09	0	22.4	0.5	–	–0.5
Feb.09	0	18.6	0.7	–	–0.7
sum	388.6	98.2	406.0	–77.5	–63.9

While the water budget is incomplete due to the lack of in- and outflow measurements, this analysis reveals that ET (406 mm in the period April to October) was roughly in balance with rainfall (389 mm). ET exceeded precipitation during May, June, and July, and was a much less substantial water balance term in the later months. As well as ET exceeding rainfall in these early months, the relatively large drop in the water table indicates additional net outflows of surface or near-surface water in the months through July. This period is followed by net inflow in August and October, with September's lateral water fluxes nearly in balance. The pattern of P – ET generally controlled the behavior of the water table,

which declined until its large increase following a rain event in August. During the growing season (DOY 140-260), ET averaged 2.5 mm d^{-1}, with a maximum daily rate of 5.6 mm d^{-1} on 6 July 2008.

DISCUSSION

Recent ecological work in this region has described the territory of the Komi Republic as characterized by surplus moisture, i.e., that the annual rainfall significantly exceeds mean annual evapotranspiration (Lopatin et al., 2006). Previous work has also characterized the water balance of bogs in the oligotrophic zones of European Russia and suggested that bogs in the study region fit within 225-250 mm y^{-1} evaporation isolines, with evaporation in "unbogged parts" in the range 275-300 mm y^{-1} (Romanov, 1968b). This study's site had significantly higher annual evapotranspiration (408 mm) than these previous estimates, though during this study year more precipitation was recorded at the Syktyvkar meteorological station than the long-term average. The general lack of high-precision estimates of the latent energy fluxes, and conflicting descriptions of these mires' behavior, allow the current study to suggest some functional overview to the energy balance terms of the fen portion of one of these mires. By many indicators of wetland evapotranspiration, including the Priestley-Taylor a_{PT} term, atmospheric decoupling term W, Bowen ratio, and the vertical water balance, the studied fen site in the Medla-Pev-Nyur river valley peatland behaved similarly to open fens in other boreal zones. The site's ample water supply (and high water table) allowed an evapotranspiration flux primarily driven by net radiation.

In its general energy balance characteristics, the Medla-Pev-Nyur fen site is similar to other wetlands. The mid-summer shortwave radiation albedo (monthly mean values from 0.10 in June, peaking at 0.19 in August) and the radiation efficiency ratio (R_n/SW_{in}; with mid-summer monthly mean values ranging from 0.45 to 0.61) are similar to those found in other boreal wetlands (den Hartog et al., 1994; Lafleur et al., 1997). Even more so than other wetlands surveyed (Lafleur, 2008), the Medla-Pev-Nyur latent energy fluxes are the most significant component of its energy budget (with summer monthly averages greater than 70%). Modeled Q_m is significant in the late spring snowmelt period while it has a similar (and low) magnitude to LE throughout the winter months. On a monthly and daily basis, H is generally of higher magnitude than G. The method to derive G has some error in its assumed heat capacity, which may change over time but is given a static value in the current study. Additionally, the two heat flux plates may not adequately cover the range of microtopographic sites within the fen. Such caveats aside, however, G composes a sizeable portion of the summer energy balance (greater than 10% on a cumulative basis in June, and greater than 15% on selected days' cumulative energy flux). We are therefore hesitant to support the presumption (Peichl et al., 2013) that on the daily time scale G may be neglected as a small contributor to the energy balance. The challenge of measuring available radiation as $R_n - G - Q_m$ has also introduced different methods for determining the Priestley-Taylor factor a_{PT}, which is discussed next.

The a_{PT} at the site explored in this study (0.95-1.05 in the peak growing season assuming R_a is composed of $R_n - G - Q_m$) was similar to other open boreal fens, but higher than other boreal peatland types (both treed fens and open bogs). Determining this value involved some uncertainty deriving from the incomplete

energy budget closure, a problem similarly explored elsewhere in relationship to the derived canopy conductance (Wohlfahrt et al., 2009). If a_{PT} was estimated using the sum of H and LE for available energy, rather than ($R_n - G - Q_m$), a_{PT} was 3-65% higher (depending on the month), and had a growing season monthly average always greater than 1.06 (up to 1.34). Previous reviews and studies have used each strategy: some use $R_n - G - Q_m$ (Brümmer et al., 2012; Roulet and Woo, 1986), while others use H+LE (Humphreys et al., 2006; Sonnentag et al., 2010; Souch et al., 1996). The first method is probably better for modeling purposes when the turbulent fluxes are unavailable, but the second is probably better for describing the behavior of the measured LE fluxes given its reduction in the measurement footprint's mismatch. Additional considerations should be made for the corrections necessary for tube-wall adsorption on closed-path sensors (Massman and Ibrom, 2008; Runkle et al., 2012; Nordbo et al., 2013). For two peatlands in Canada (Brümmer et al., 2012), the annual average (daytime, dry-foliage) Priestley-Taylor a_{PT} was in the range 0.55-0.57 (Alberta Western Peatland, a treed, moderately rich fen, 54°57′ N, 112°28′ W) and 0.74-0.92 (Ontario Eastern Peatland, or Mer Bleue, an ombrotrophic, nutrient-poor bog with more non-vascular ground cover, 45°25′ N, 75°31′ W). Mid-summer daily peaks of a_{PT} at this latter site may be as high as 1.5 (Admiral et al., 2006). A third Canadian peatland (53°48′ N, 104°37′ W), the open, moderately rich Sandhill fen site in Saskatchewan, had mean daily mid-day a_{PT} values between 0.99 and 1.04 in three wet years and 0.79 during dry conditions (Sonnentag et al., 2010). A survey of seven Canadian peatlands found mid-summer a_{PT} values in a range from 0.82 to 1.05, used to suggest some physiological limitations to LE flux (Humphreys et al., 2006). In this survey, the two poor fens (a part of Mer Bleue and one near Lac La Biche, Alberta, 55°54′ N, 112°33′ W) had the highest estimates of a_{PT}, in comparison to the bog part of Mer Bleue, two wooded fens and two extreme-rich fens. Finally, the Swedish carpet-lawn fen Degerц Stormyr had a five-year, growing-season average a_{PT} of 0.98, ranging from 0.86 to 1.17, and derived from ignoring G as relatively insignificant (Peichl et al., 2013).

The relatively high a_{PT} values for the study site imply a stronger control by radiation than vapor pressure deficit in driving evapotranspiration. This characteristic is also implied by the atmospheric decoupling term W, which may be higher for open fens than for either treed fens or bog sites. A recent survey of Canadian sites also evaluated their decoupling coefficients, which were 0.16 for three years at the treed fen and in the range 0.29-0.34 for the eastern bog (Brümmer et al., 2012). Our site had higher W values in the range around 0.65 in the growing season. This value was relatively insensitive to small changes in formulating g_a or g_c (e.g., which value of kB^{-1} to use). These values are similar to an open fen in Minnesota (Kim and Verma, 1996), but higher than some other open fen sites (Table 7). The values at the study site are also higher than those at the Fyodorovskoye peat bog in Western Russia (56°27′ N, 32°55′ E), which ranged between 0.2 and 0.5 and were shown to be reduced as the peat surface dried and as vascular plants contributed a proportionately larger amount of measured water vapor fluxes, relative to open-water and moss-dominated surfaces (Kurbatova et al., 2002). They also exceed reported values (0.3-0.5) from three years of eddy covariance measurements at the Zotino bog, a 5 km^2 mixed *Sphagnum*-vascular landscape surrounded by a *Pinus sylvestris* forest in Western Siberia (60°45′ N, 89°23′ E) (Kurbatova et al., 2002). Higher values indicating strong decoupling and near complete evaporative control by net radiation ($W > 0.82$, approaching

Table 7

Comparative review of energy balance indicators for different boreal fen sites. The Bowen ratio is defined as H/LE, the decoupling coefficient is defined in the text (equation 10), the canopy and aerodynamic conductance terms are given as g_c and g_a, respectively

Site name	Peatland description	Latitude	Longitude	Location	Bowen ratio	Decoupling coefficient, Ω	Conductance terms, g_c or g_a	Reference
Medla-Pev-Nyur	Fen	61° 56' N	50° 13' E	Komi, Russia	summer cumulative value 0.24, but mid-day averages 0.33-0.63	around 0.65 in the growing season and less (to 0.27) in the winter	g_a and g_c in range 12-26 mm s^{-1} (similar magnitude)	This study
Kaamanen	open flark fen	69° 08' N	27° 17' E	N. Lapland, Finland	mid-day, summer-time, 0.74	n/a	n/a	(Aurela et al., 2001)
Degerö Stormyr	oligotrophic fen	64° 11' N	19° 33' E	Västerbotten, Sweden	five-year average, midday growing season as 0.86 ± 0.08	low (qualitative estimate from g_a/g_s relationship)	g_a 20 mm s^{-1}, g_c 5 mm s^{-1}	(Peichl et al., 2013)
Salmisuo	Fen/bog mire	62° 46′ N	30° 58′ E	N. Karelia, Finland	drier year 2006 (Bowen ratio 0.2-0.3) cf. wetter 2007 season (Bowen ratio ~0.5)	n/a	g_c mean was 7.8 mm s^{-1} (range 4-20 mm s^{-1}), g_a not reported	(Wu et al., 2010)
Churchill sedge fen	permafrost sedge fen	58° 40' N	94° 40' W	Manitoba, Canada	0.48 (average annual); 0.2-0.3 (mid-summer cumulative value)	n/a	g_c (daily mean ~11 mm s^{-1}; noontime values up to 59 mm s^{-1}). g_a daily mean in range from 7-35 mm s^{-1}, noontime values ~18 mm s^{-1}	(Rouse, 2000; Eaton et al., 2001; Raddatz et al., 2009)
Thompson, Northern Study Area	Rich fen	55° 54' N	98° 24' W	Manitoba, Canada	Cumulative, 0.46 during green period; day-time values are closer to 1	n/a	n/a	(Lafleur et al., 1997)
Near Lac La Biche	Poor fen	55° 54' N	112° 33' W	Alberta, Canada	Mid-day mid-summer, 0.25-0.4	n/a	$g_{a,noon}$ ~20 mm s^{-1} $g_{c,noon}$ ~12-13 mm s^{-1}	(Glenn, 2005; Glenn et al., 2006; Humphreys et al., 2006)
Alberta Western Peatland / Tony's Fen	Treed, moderately rich fen	54° 57' N	112° 28' W	Alberta, Canada	Approximately 1, lower from late spring values exceeding 2 as the growing season progressed and the sedge canopy density increased	0.16 for three years	$g_{a,noon}$ ~40 mm s^{-1} $g_{c,noon}$ ~9 mm s^{-1}	(Glenn, 2005; Glenn et al., 2006; Humphreys et al., 2006; Brümmer et al., 2012)
Sandhill fen	Fen	53° 48' N	104° 37' W	Saskatchewan, Canada	n/a	n/a	g_c in range 3.9-4.6 mm s^{-1} (very weak or no response between g_c and VPD), g_a not reported	(Sonnentag et al., 2010)
Bog Lake Peatland	oligotrophic, open *Sphagnum* fen	47° 32' N	93° 28' W	Minnesota, USA	0.3-0.4 (AM), 0.6-1.0 (PM)	ranged from 0.55 to 0.89	g_c in range 2-15 mm s^{-1} g_a most often greater than g_c	(Kim and Verma, 1996)

0.99 in the growing season) were found in a freshwater marsh in northeastern China (Sun and Song, 2008). The higher W values at the study site are related to the similar magnitude between g_c and g_a through the year. Many of the other boreal fen sites reviewed in Table 7 show g_c less than g_a, implying a relatively low W value. This difference may derive from the study site's relatively high water table (always higher than 20 cm below surface) allowing capillary and root transport from the mire groundwater. This connection is slightly strengthened when considering the month of July at the site, when g_c reaches its mid-summer low. Unfortunately the synchronicity of the relatively low water table and highest VPD rates preclude a clear interpretation of the drivers of this low g_c, though the statistical look at residuals of equation 9 suggests a larger role for VPD than the water table. Phenological factors may also play a role in this reduced g_c, as the reduction starts following the peak in vegetation cover. Three of the Canadian peatlands surveyed by Humphreys et al. (2006), two wooded fens and a rich fen, showed a stronger ($b_D > 1$ kPa^{-1}) response of canopy conductance to VPD, though the other sites had a weaker relationship ($b_D < 0.3$ kPa^{-1}) than this study's data indicate ($b_D < 1.1 \pm 0.52$ kPa^{-1}). The Glencar Atlantic blanket bog in Ireland (51°55′ N, 9°55′ W) had a stronger response ($b_D = 8.6$ kPa^{-1}) though as in the current study, the relationship had a relatively weak fit ($r^2 < 0.40$) and indicates more of a qualitative than exact control by VPD (Sottocornola and Kiely, 2010).

A recent study of errors in ET models finds higher predictive uncertainty in landscapes with low W or high controls by surface conductance on ET (Polhamus et al., 2013). This finding implies that it may be easier to make ET predictions of these landscapes using well-defined radiation terms rather than more difficult biophysical parameterizations of the transpiring surface vegetation. The implication for modeling studies on these boreal fen landscapes is that they require less detail on the surface scale and interactions between VPD, g_c, surface wetness, and ET.

The site's Bowen ratio (a summer average via total cumulative fluxes of 0.24, but mid-day averages in the range 0.33-0.63) was relatively low compared to other peatland field sites. In particular, two relatively nearby northern European fens (Aurela et al., 2001; Peichl et al., 2013), which may otherwise be considered as analogous to the study site, showed higher average mid-day summer-time Bowen ratios (Table 7). The Bowen ratios of two other poor fens (Kim and Verma, 1996; Glenn et al., 2006) and a Finnish fen/bog mire (Wu et al., 2010) are more comparable to the study site. The study site's Bowen ratios may also be comparable to low values found at some Russian peatland bogs: for the two Russian bogs mentioned previously (Kurbatova et al., 2002) mid-summer values of approximately 0.3 (Zotino) and 0.4-0.8 (Fyodorovskoye) were reported. At another West Siberian continental bog (56°51′ N, 82°50′ E), the summer Bowen ratio ranged from 0.57 during the early growing season and up to 0.78 in the peak growing season (Shimoyama et al., 2003), so the similarities to Russian bogs may not be universal. Similarly, the Stormossen bog in central Sweden (60°07′N, 17°05′ E) had a reported mid-summer minimum Bowen ratio of 0.6 (Kellner, 2001). A recent review of wetland evaporation found higher summer median (cumulative flux) values in both fens (0.46) and bogs (0.6) and roughly similar values for marshes (0.25), though with a fairly small number of studies in each group (n from 5 to 7) (Lafleur, 2008). In the study site, at least, the comparatively low Bowen ratio appears to be driven by the relatively high water table and the associated high surface conductance values.

The study site's mean daily growing season ET rate (2.5 mm d^{-1}; peak 5.8 mm d^{-1}) is comparable to some of the wetland sites in its latitude band, as reviewed by Lafleur (2008, Fig. 10). In particular, these evapotranspiration rates are similar in magnitude to the Danish riparian wetland (56°22′ N, 9°41′ E) studied by Andersen et al. (2005), who found average ET rates of 3.6 mm d^{-1} (peak of 5.6 mm d^{-1}), accounting for 82% of daytime net radiation. These evaporation rates are also similar to those found in the Bog Lake Peatland of Minnesota (47°32′ N, 93°28′ W), an oligotrophic, open *Sphagnum* fen with growing season average 3.0 mm d^{-1} (peak 4.8 mm d^{-1}) and with fen ET 85-115% of potential ET (Kim and Verma, 1996). Similarly, a *Carex lasiocarpa* marsh in China's Sanjiang Plain (47°35′ N, 133°31′ E) showed daily ET rates averaging 2.3 mm d^{-1} (peak 4.8 mm d^{-1}) and a_{PT} of 1.01 (using R_n–G for R_a) (Sun and Song, 2008; Guo and Sun, 2011). The previously mentioned Finnish site, Salmisuo, had comparable growing season daily ET rates of 2.23 mm d^{-1} and 1.59 mm d^{-1} for its dry and wet years, respectively, with a peak rate of 5.0 mm d^{-1} (Wu et al., 2010).

Finally, the study site's roughness length changed with season more than stability or wind direction, and so was presented as a monthly mean (Table 3). The roughness length estimate (peaking at 46 ± 12 mm) is comparable to a Quebec natural bog with *Sphagnum* hummocks and low ericaceous (i.e., acid-loving) shrubs, where z_0 was modeled from wind profile data as 40.9 mm (Campbell et al., 2002). Average z_0 estimates of 18.6 mm (ranging from 10-30 mm) have been determined for a Swedish bog named Ryggmosen (Mölder and Kellner, 2002). During the snow-free period in Canada's Mer Bleue bog, a constant z_0 value of 77 ± 1 mm was derived from sonic anemometer data (Lafleur et al., 2005). Other estimates of z_0 for peatlands are in the range 20-70 mm for a Siberian bog (Shimoyama et al., 2004), or 21-32 mm for a Swedish mire nearby Ryggmosen (Kellner, 2001). The northern Finnish flark fen Kaamanen had z_0 of 80 mm (Aurela et al., 2001), and the Swedish carpet-lawn fen Degerц Stormyr had z_0 up to 30 mm (Peichl et al., 2013). This range of values is indicative of the variety of peatland types and vegetation cover, and places the Medla-Pev-Nyur site studied here, with its low vegetation and slight hummock features, in the mid-range of the peatlands surveyed.

CONCLUSION

We have generated an 11-month energy balance for the oligotrophic fen portion of a mixed bog-fen river valley peatland in the boreal zone of European Russia by supplementing eddy covariance measurements with gap-filling models and in situ measurements of non-turbulent energy fluxes and associated meteorological terms. The evapotranspiration flux may reasonably be estimated using the Priestley-Taylor method, provided adequate assumptions about the energy balance closure can be provided. The growing season energy balance (April through September) was dominated by evapotranspiration, which seemed largely governed by net radiation at the surface with a lower-level control provided by vapor pressure deficit in its role in restricting the canopy conductance. The canopy conductance was higher earlier in the growing season than later in the season, with the reduction starting roughly coincident with the peak vegetation cover. Canopy conductance was higher than at other similar sites in the boreal zone, perhaps due to the relatively high water table. During the period April-October 2008, evapotranspiration (399.4 mm) nearly balanced rainfall (402.6 mm). High

snowfall (84.2 mm water equivalent) and limited evapotranspiration (6.6 mm) during the rest of the year generated an annual atmospheric water budget with excess incoming water. On a monthly basis, the growing season months of May-July had nearly twice the evapotranspiration as precipitation. Disentangling the roles of vascular plant cover and water table height in controlling the energy balance, and particularly the latent energy flux term, is challenging to do for the dataset in this study and should be encouraged as a target of future studies. However, the higher decoupling coefficient and predominance of R_n in driving ET lend encouragement to relatively simplistic modeling approaches for this landscape.

ACKNOWLEDGEMENTS

B. Runkle, C. Wille, and L. Kutzbach are supported by the Cluster of Excellence "CliSAP" (EXC177; Integrated Research Activity 08/2-034) of the University of Hamburg, as funded by the German Research Foundation (DFG). Field work was conducted by the Emmy Noether Independent Research Group led by M. Wilmking and funded by the German Research Foundation (Wi 2680/2-1). Infrastructure and field work was partially supported by the CARBO-North Project (6th FP of the EU, Contract number 36993). In addition, we thank and acknowledge Svetlana Zagirova and other members of the Komi Science Centre for their logistical support. We appreciate the field data collection and logistical support of Peter Schreiber, Julia Schneider, and Oleg Mikhaylov, and the footprint modeling by Inke Forbrich. We appreciate suggestions from Armine Avagyan that helped improve the manuscript and assistance in mapping from Sebastian Zubrzycki. We thank the two anonymous reviewers for their useful suggestions.

References

Admiral, S.W., P.M. Lafleur, and N.T. Roulet. 2006. Controls on latent heat flux and energy partitioning at a peat bog in eastern Canada. *Agricultural and Forest Meteorology* 140: 308–321.

Andersen, H.E., S.Hansen, and H.E. Jensen. 2005. Evapotranspiration from a riparian fen wetland. *Nordic Hydrology* 36: 121–135.

Apps, M.J., W.A. Kurz, R.J. Luxmoore, L.O. Nilsson, R.A. Sedjo, , R. Schmidt, L.G. Simpson, and T.S. Vinson. 1993. Boreal forests and tundra. *Water, Air, & Soil Pollution* 70: 39–53.

Aurela, M., T. Laurila, and J.-P.Tuovinen. 2001. Seasonal CO_2 balances of a subarctic mire. *Journal of Geophysical Research: Atmospheres* (1984–2012) 106: 1623–1637.

Baldocchi, D.D., 2003. Assessing the eddy covariance technique for evaluating carbon dioxide exchange rates of ecosystems: past, present and future. *Global Change Biology* 9: 479–492.

Billett, M.F., S.M. Palmer, D. Hope, C. Deacon, R. Storeton-West, K.J. Hargreaves, C. Flechard, and D. Fowler. 2004. Linking land-atmosphere-stream carbon fluxes in a lowland peatland system. *Global Biogeochemical Cycles* 18.

Bolton, D., 1980. The computation of equivalent potential temperature. *Monthly weather review* 108: 1046–1053.

Brümmer, C., T.A. Black , R.S. Jassal, N.J. Grant, D.L. Spittlehouse, B. Chen, Z. Nesic, B.D. Amiro, M.A. Arain, A.G. Barr, C.P.-A. Bourque, C. Coursolle, A.L. Dunn, L.B. Flanagan, E.R. Humphreys, P.M. Lafleur, H.A. Margolis, J.H. McCaughey, and S.C. Wofsy. 2012. How climate and vegetation type influence evapotranspiration and water use efficiency in Canadian forest, peatland and grassland ecosystems. *Agricultural and Forest Meteorology* 153: 14–30.

Brutsaert, W. 1982. Evaporation into the atmosphere: theory, history, and applications. Reidel Dordrecht.

Campbell, D.I., and J.L. Williamson. 1997. Evaporation from a raised peat bog. *Journal of Hydrology* 193: 142–160.

Campbell, D.R., C. Lavoie, and L. Rochefort. 2002. Wind erosion and surface stability in abandoned milled peatlands. *Canadian Journal of Soil Science* 82: 85–95.

Comer, N.T., P.M. Lafleur, N.T. Roulet, M.G. Letts, M. Skarupa, and D. Verseghy. 2000. A test of the Canadian land surface scheme (CLASS) for a variety of wetland types. *Atmosphere-Ocean* 38: 161–179.

Couwenberg, J., and H. Joosten. 2005. Self-organization in raised bog patterning: the origin of microtope zonation and mesotope diversity. *Journal of Ecology* 93: 1238–1248.

Den Hartog, G., H.H. Neumann, K.M. King, and A.C. Chipanshi. 1994. Energy budget measurements using eddy correlation and Bowen ratio techniques at the Kinosheo Lake tower site during the Northern Wetlands Study. *J. Geophys. Res.* 99: 1539–1549.

Drexler, J.Z., R.L. Snyder, D. Spano, and U.K.T. Paw. 2004. A review of models and micrometeorological methods used to estimate wetland evapotranspiration. *Hydrol. Process.* 18: 2071–2101.

Eaton, A.K., W.R. Rouse, P.M. Lafleur, P. Marsh, and P.D. Blanken. 2001. Surface energy balance of the western and central Canadian subarctic: Variations in the energy balance among five major terrain types. *Journal of climate* 14: 3692–3703.

Eichinger, W.E., M.B. Parlange, and H. Stricker. 1996. On the concept of equilibrium evaporation and the value of the Priestley-Taylor coefficient. *Water resources research* 32: 161–164.

ESA, 2010. GlobCover 2009 (Global Land Cover Map) Released on 21 December; http://due.esrin.esa.int/globcover/.

Falge, E., D. Baldocchi, R. Olson, P. Anthoni, M. Aubinet, C. Bernhofer, G. Burba, R. Ceulemans, R. Clement, H. Dolman, A. Granier, P. Gross, T. Grьnwald, D. Hollinger, N.-O. Jensen, G. Katul, P. Keronen, A. Kowalski, C. Ta Lai, B.E. Law, T. Meyers, J. Moncrieff, E. Moors, J. William Munger, K. Pilegaard, Ь. Rannik, C. Rebmann, A. Suyker, J. Tenhunen, K. Tu, S. Verma, T. Vesala, K. Wilson, and S. Wofsy. 2001. Gap filling strategies for long term energy flux data sets. *Agricultural and Forest Meteorology* 107: 71–77.

Foken, T. 2008. Micrometeorology. Springer-Verlag, Berlin Heidelberg.

Foken, T., and B. Wichura. 1996. Tools for quality assessment of surface-based flux measurements. *Agric For Meteorol* 78: 83–105.

Forbrich, I., L. Kutzbach, C. Wille, T. Becker, J. Wu, and M. Wilmking. 2011. Cross-evaluation of measurements of peatland methane emissions on microform and ecosystem scales using high-resolution landcover classification and source weight modelling. *Agricultural and Forest Meteorology* 151: 864–874.

Frolking, S., J. Talbot, M.C. Jones, C.C. Treat, J.B. Kauffman, E.S. Tuittila, and N. Roulet. 2011. Peatlands in the Earth's 21st century climate system. *Environmental Reviews* 19: 371–396.

Gažovič, M., L. Kutzbach, I. Forbrich, J. Schneider, C. Wille, M. Wilmking, n.d. Temperature and plant phenology control the seasonal variability of CO_2 and CH_4 fluxes from a boreal peatland in North-West Russia. in preparation.

Gažovič, M., L. Kutzbach, P. Schreiber, C. Wille, and M. Wilmking. 2010. Diurnal dynamics of CH_4 from a boreal peatland during snowmelt. *Tellus* B 62: 133–139.

Glenn, A.J. 2005. Growing season carbon dioxide exchange of two contrasting peatland ecosystems. Lethbridge, Alta.: University of Lethbridge, Faculty of Arts and Science.

Glenn, A.J., L.B. Flanagan, K.H. Syed, and P.J. Carlson. 2006. Comparison of net ecosystem CO_2 exchange in two peatlands in western Canada with contrasting dominant vegetation, *Sphagnum* and *Carex*. *Agricultural and Forest Meteorology* 140: 115–135.

Guo, Y., and L. Sun. 2011. Surface energy fluxes and control of evapotranspiration from a *Carex lasiocarpa* mire in the Sanjiang Plain, Northeast China. *Int J Biometeorol*: 1–12.

Humphreys, E.R., P.M. Lafleur, L.B. Flanagan, N. Hedstrom, K.H. Syed, A.J. Glenn, and R. Granger. 2006. Summer carbon dioxide and water vapor fluxes across a range of northern peatlands. J. *Geophys. Res.* 111: 16

Ivanov, K.E. 1981. Water movement in mirelands (Vodoobmen v bolotnykh landshaftakh). Academic Press London.

Jarvis, P.G., and K.G. McNaughton. 1986. Stomatal control of transpiration: Scaling up from leaf to region. *Adv. Ecol. Res* 15: 1–49.

Joosten, H., M.-L. Tapio-Biström, and S. Tol. 2012. Peatlands-guidance for climate change mitigation through conservation, rehabilitation and sustainable use. FAO.

Kellner, E., 2001. Surface energy fluxes and control of evapotranspiration from a Swedish *Sphagnum* mire. *Agricultural and Forest Meteorology* 110: 101–123.

Kim, J., and S.B. Verma. 1996. Surface exchange of water vapour between an open *sphagnum* fen and the atmosphere. *Boundary-Layer Meteorology* 79: 243–264.

Kormann, R., and F.X. Meixner. 2001. An analytical footprint model for non-neutral stratification. *Boundary-Layer Meteorology* 99: 207–224.

Kurbatova, J., A. Arneth, N.N. Vygodskaya, O. Kolle, A.V. Varlargin, I.M. Milyukova, N.M. Tchebakova, E.D. Schulze, and J. Lloyd. 2002. Comparative ecosystem-atmosphere exchange of energy and mass in a European Russian and a central Siberian bog I. Interseasonal and interannual variability of energy and latent heat fluxes during the snowfree period. *Tellus* B 54: 497–513.

Lafleur, P.M. 2008. Connecting Atmosphere and Wetland: Energy and Water Vapour Exchange. *Geography Compass* 2: 1027–1057.

Lafleur, P.M., R.A. Hember, S.W. Admiral, N.T. Roulet. 2005. Annual and seasonal variability in evapotranspiration and water table at a shrub-covered bog in southern Ontario, Canada. *Hydrol. Process.* 19: 3533–3550.

Lafleur, P.M., J.H. McCaughey, D.W. Joiner, P.A. Bartlett, and D.E. Jelinski. 1997. Seasonal trends in energy, water, and carbon dioxide fluxes at a northern boreal wetland. *J. Geophys. Res.* 102: 29009–29020.

Limpens, J., F. Berendse, C. Blodau, J.G. Canadell, C. Freeman, J. Holden, N. Roulet, H. Rydin, and G. Schaepman-Strub. 2008. Peatlands and the carbon cycle: from local processes to global implications- a synthesis. *Biogeosciences* 5: 1475–1491.

Lopatin, E., T. Kolstrom, H. Spiecker. 2006. Determination of forest growty trends in Komi Republic (northcoestern Russia): combination of tree-ring analysis and remote sensing data. *Boreal Ewironment Recearch* 11: 341–353.

Masing, V., M. Botch, and A. Läänelaid. 2010. Mires of the former Soviet Union. Wetlands *Ecology and Management* 18: 397–433.

Massman, W.J., and A. Ibrom. 2008. Attenuation of concentration fluctuations of water vapor and other trace gases in turbulent tube flow. *Atmos Chem Phys* 8: 6245–6259.

McNaughton, K.G.. 1976. Evaporation and advection I: evaporation from extensive homogeneous surfaces. *Quarterly Journal of the Royal Meteorological Society* 102: 181–191.

McNaughton, K.G., and P.G. Jarvis. 1983. Predicting effects of vegetation changes on transpiration and evaporation. *Water deficits and plant growth* 7: 1–47.

Minayeva, T.Y., and Sirin, A.A., 2012. Peatland biodiversity and climate change. *Biology Bulletin Reviews* 2: 164–175.

Mölder, M., and E. Kellner. 2002. Excess resistance of bog surfaces in central Sweden. *Agricultural and Forest Meteorology* 112: 23–30.

Nordbo, A., P. Kekäläinen, E. Siivola, R. Lehto, T. Vesala, and J. Timonen. 2013. Tube transport of water vapor with condensation and desorption. *Applied Physics Letters* 102: 194101–194101–5.

Owen, P.R., and W.R. Thomson. 1963. Heat transfer across rough surfaces. *Journal of Fluid Mechanics* 15: 321–334.

Peichl, M., J. Sagerfors, A. Lindroth, I. Buffam, A. Grelle, L. Klemedtsson, H. Laudon, and M.B. Nilsson. 2013. Energy exchange and water budget partitioning in a boreal minerogenic mire. *Journal of Geophysical Research: Biogeosciences* 118: 1–13.

Petrone, R.M., K.J. Devito, U. Silins, C. Mendoza, S.C. Brown, S.C. Kaufman, and J.S. Price. 2008. Transient peat properties in two pond-peatland complexes in the subhumid Western Boreal Plain, Canada. *Mires and peat* 3: 1–13.

Polhamus, A., J.B. Fisher, and K.P. Tu. 2013. What controls the error structure in evapotranspiration models? *Agricultural and Forest Meteorology* 169: 12–24.

Priestley, C.H.B., and R.J. Taylor. 1972. On the assessment of surface heat flux and evaporation using large-scale parameters. *Monthly weather review* 100: 81–92.

Raddatz, R.L., T.N. Papakyriakou, K.A. Swystun, and M. Tenuta, 2009. Evapotranspiration from a wetland tundra sedge fen: Surface resistance of peat for land-surface schemes. *Agricultural and Forest Meteorology* 149: 851–861.

Rango, A., and J. Martinec. 1995. Revisiting the Degree-Day Method for Snowmelt Computations1. *Journal of the American Water Resources Association* 31: 657–669.

Reichstein, M., E. Falge, D. Baldocchi, D. Papale, M. Aubinet, P. Berbigier, C. Bernhofer, N. Buchmann, T. Gilmanov, A. Granier, T. Grunwald, K. Havrankova, H. Ilvesniemi, D. Janous, A. Knohl, T. Laurila, A. Lohila, D. Loustau, G. Matteucci, T. Meyers, F. Miglietta, J.-M. Ourcival, P. J. Rumpanen, S. Rambal, E. Rotenberg, M., J. Tenhunen, G. Seufert, F. Vaccari, T. Vesala, D. Yakir, and R. Valentini. 2005. On the separation of net ecosystem exchange into assimilation and ecosystem respiration: review and improved algorithm. *Global Change Biol* 11:1424–1439.

RIHMI-WDC, 2013. Hydrometeorological data, Baseline Climatological Data Sets, Syktyvkar Site # 23804, http://meteo.ru/english/data/.

Romanov, V.V. 1968a. Evaporation from Bogs in the European Territory of the USSR. Israel Program for Scientific Translation, Jerusalem.

Romanov, V.V., 1968. Hydrophysics of Bogs (Gidrofizika bolot). Israel Program for Scientific Translation.

Roulet, N.T., and M. Woo. 1986. Wetland and Lake Evaporation in the Low Arctic. *Arctic and Alpine Research* 18: 195–200.

Rouse, W.R. 2000. The energy and water balance of high-latitude wetlands: controls and extrapolation. *Global Change Biology* 6: 59–68.

Runkle, B.R.K., C. Wille, M. Gažovič, and Kutzbach, L.. 2012. Attenuation Correction Procedures for Water Vapour Fluxes from Closed-Path Eddy-Covariance Systems. *Boundary-Layer Meteorology* 142 :401–423.

Schneider, J., L. Kutzbach, and M. Wilmking. 2012. Carbon dioxide exchange fluxes of a boreal peatland over a complete growing season, Komi Republic, NW Russia. *Biogeochemistry* 111: 485–513.

Shimoyama, K., T. Hiyama, Y. Fukushima, and G. Inoue. 2003. Seasonal and interannual variation in water vapor and heat fluxes in a West Siberian continental bog. *J. Geophys. Res.* 108: 4648, doi: 10.1029/2003JD003485, D20.

Shimoyama, K., T. Hiyama, Y. Fukushima, and G. Inoue. 2004. Controls on evapotranspiration in a west Siberian bog. *J. Geophys. Res.* 109: D08111, doi: 10.1029/2003JD004114.

Shutov, V. 2004. Extensive studies in boreal wetland watersheds in northwestern Russia. (Proceedings of a workshop held at Victoria, Canada, March 2004). IAHS Publ. 290: 103–110.

Sonnentag, O., M. Detto, B.R.K. Runkle, Y.A. Teh, W.L. Silver, M. Kelly, and D.D. Baldocchi. 2011. Carbon dioxide exchange of a pepperweed (*Lepidium latifolium* L.) infestation: How do flowering and mowing affect canopy photosynthesis and autotrophic respiration? *J. Geophys. Res.*: 116. G01021, doi:10.1029/2010JG001522.

Sonnentag, O., G. van der Kamp, A.G. Barr, and J.M. Chen. 2010. On the relationship between water table depth and water vapor and carbon dioxide fluxes in a minerotrophic fen. *Global Change Biology* 16: 1762–1776.

Sottocornola, M., and G. Kiely. 2010. Energy fluxes and evaporation mechanisms in an Atlantic blanket bog in southwestern Ireland. Water Resour. Res. 46, W11524, doi:10.1029/2010WR009078.

Souch, C., C.P. Wolfe, and C.S.B. Grimmtind. 1996. Wetland evaporation and energy partitioning: Indiana Dunes National Lakeshore. *Journal of Hydrology* 184: 189–208.

Sun, L., and C. Song. 2008. Evapotranspiration from a freshwater marsh in the Sanjiang Plain, Northeast China. *Journal of Hydrology* 352: 202–210.

Vasander, H. 2007. Peatlands. In *On the European Edge: Journey through Komi Nature and Culture*, ed. M. Pearson, P. Ojanen, M. Havimo, T. Kuuluvainen, and H. Vasander. 103–112. Helsinki: University of Helsinki.

Verma, S.B.. 1989. Aerodynamic resistances to transfers of heat, mass and momentum. In *Estimation of Areal Evapotranspiration*, ed. T.A. Black. 13–20. Int. Assoc. Hydrol. Sci.

Wang, K., and R.E. Dickinson. 2012. A review of global terrestrial evapotranspiration: Observation, modeling, climatology, and climatic variability. *Rev. Geophys*: 50, RG2005, doi:10.1029/2011RG000373.

Wesely, M.L., and B.B. Hicks. 1977. Some factors that affect the deposition rates of sulfur dioxide and similar gases on vegetation. J*ournal of the Air Pollution Control Association* 27: 1110–1116.

Wilson, K.B., and D.D. Baldocchi. 2000. Seasonal and interannual variability of energy fluxes over a broadleaved temperate deciduous forest in North America. *Agricultural and Forest Meteorology* 100: 1–18.

Wohlfahrt, G., A. Haslwanter, L. Hörtnagl, R.L. Jasoni, L.F. Fenstermaker, J.A. Arnone III, and A. Hammerle. 2009. On the consequences of the energy imbalance for calculating surface conductance to water vapour. *Agricultural and Forest Meteorology* 149: 1556–1559.

Wu, J., L. Kutzbach, D. Jager, C. Wille, and M. Wilmking. 2010. Evapotranspiration dynamics in a boreal peatland and its impact on the water and energy balance. *J. Geophys. Res*. 115. G04038, doi:10.1029/2009JG001075.

Supplemental Data Table: Monthly dependence of LE on R_n or VPD

Month	Slope, LE vs R_n (W m^{-2} W^{-1} m^2)	Slope, LE vs VPD (W m^{-2} kPa^{-1})
Apr.08	0.23 ± 0.02, r^2 0.32, p < 0.001, rmse 33.0	94 ± 9, r^2 0.06, p < 0.001, rmse 39.3
May.08	0.44 ± 0.01, r^2 0.67, p < 0.001, rmse 50.8	169 ± 6, r^2 0.56, p < 0.001, rmse 57.0
Jun.08	0.56 ± 0.01, r^2 0.80, p < 0.001, rmse 44.6	167 ± 7, r^2 0.48, p < 0.001, rmse 69.5
Jul.08	0.64 ± 0.01, r^2 0.88, p < 0.001, rmse 38.5	150 ± 6, r^2 0.50, p < 0.001, rmse 76.2
Aug.08	0.61 ± 0.02, r^2 0.81, p < 0.001, rmse 38.1	213 ± 8, r^2 0.62, p < 0.001, rmse 53.5
Sep.08	0.45 ± 0.02, r^2 0.60, p < 0.001, rmse 28.5	210 ± 10, r^2 0.44, p < 0.001, rmse 34.4
Oct.08	0.42 ± 0.04, r^2 0.63, p < 0.001, rmse 16.4	173 ± 18, r^2 0.53, p < 0.001, rmse 16.8
Nov.08	0.01 ± 0.07, r^2 0.02, p = 0.142, rmse 9.8	120 ± 17, r^2 0.32, p < 0.001, rmse 5.8
Dec.08	0.01 ± 0.04, r^2 0.12, p < 0.001, rmse 3.9	55 ± 12, r^2 0.53, p < 0.001, rmse 2.8
Jan.09	0.03 ± 0.01, r^2 0.10, p = 0.005, rmse 2.0	–2 ± 13, r^2 0.26, p < 0.001, rmse 2.2
Feb.09	–0.20 ± 0.06, r^2 0.83, p < 0.001, rmse 1.6	64 ± 45, r^2 0.51, p = 0.004, rmse 3.0
mean	0.51 ± 0.01, r^2 0.72, p < 0.001, rmse 46.5	164 ± 3, r^2 0.57, p < 0.001, rmse 57.3

Relationships are determined for half-hour measurement intervals with PAR > 20 μmol m^{-2} s^{-1}. All rmse values have units W m^2. The 95% confidence intervals around the slope terms are derived using the Jacobian computed during the nonlinear fitting procedure used to find the slope.

SUMMARY AND CONCLUSIONS

The observed and potential effects of climate warming and possible feedbacks of these processes on boreal peatland ecosystems were actively investigated over the past two decades in various parts of the world. Key questions of peatland studies remain the turnover of organic substance and the emissions of greenhouse gases as carbon dioxide and methane.

In this book we tried to show the whole variety of the investigations conducted at the Medla-Pev-Nyur peatland including not only the biogeochemical studies but also those on biology and development of the peatland. In the following, we present the main results.

The development of the peatland Medla-Pev-Nyur was initiated during the early Holocene, approximately 9600 years ago, with expansion rate of ca 3 m per century (Chapter 5). Presence of wooden plant rests at the bottom of the peat deposits confirms the development of peatland Medla-Pev-Nyur through paludification of the forests (Chapter 1). Paludification of forest landscapes was followed by decreasing carbon storage in vegetation and increasing carbon storage in soil. At the present time the general stock of carbon makes 13.5 kg C m^{-2} on margin and more than 100 kg C m^{-2} in the center of the peatland.

The microscopic fungi (micromycete) composition of peat in the investigated boreal peatland is dominated by microbe communities. 73 species of soil micromycetes were found in the upper layer of peat in Medla-Pev-Nyur (Chapter 4). The highest diversity in micromycete community was obtained in hollows. The number of micromycetes was changing over the vegetative season.

The vegetation of the peatland is mosaic, plant communities are formed in different ecological habitats. About 120 species of plants were found in the peatland, including 15 species of mosses (Chapter 2). The most numerous of higher plants species presents families Ceperaceae (17), Rosaceae (9), Ericaceae (8). Many plants are used by local inhabitants as medical plants and food. Sphagnum mosses were dominant species regarding the carbon sequestration of the peatland Medla-Pev-Nyur. The fraction of *Sphagnum* in different habitats varied from 70 to 86%. The photosynthetic uptake (sequestering) of carbon calculated on the basis of chlorophyll index varied from 162 to 212 g C m^{-2} $year^{-1}$, the contribution of mosses to this process makes between 45 and 70% (Chapter 7). The same estimation was made by using the classification of satellite images combined with land cover specific data (Chapter 3). The annual sink of carbon increased up to 2.3 kg m^{-2} on peatland margins which are coved by trees and up to 6.8 g m^{-2} on the forest plots adjoining the peatland.

Slow decomposition of the plant residues leads to an accumulation of large amounts of dead organic material in boreal peatland. Growth rate of peat on different microforms of peatland Medla-Pev-Njur were estimated by using dendrochronology methods (Chapter 6). Peat growth rate was on average 35.8 mm $year^{-1}$ and did not differ significantly in the centre and margin of the peatland. A positive correlation between the growth of trees in height and the peat growth rate was detected.

The annual carbon sink in peatland ecosystem measured by eddy-covariance in 2012-2013 years was 123 g m^{-2} (Chapter 8). Over the course of a season, the CO_2 exchange was influenced by temperature, in combination with changes in PPFD and in plant phenology (Chapter 10). The seasonal trend of CH_4 exchange was strongly influenced by changes in soil temperature and plant phenology, and no clear relationship with water table was detected on a landscape scale, but only on the microform scale by using chamber method (Chapter 11). Highest methane fluxes were observed in July in mesotrophic plant communities, where *Carex* was dominant.

Stable carbon isotopic composition of pore water CH_4 and CO_2 showed that most active methanogenesis took place between 1.5 and 2.0 m of peat profile. Peat layer between 0.5 and 1.0 m was found to be most active regarding CH_4 oxidation, presumably through the occurrence of oxygen in the rhizosphere of aerenchymatous plants and/or anaerobic methane oxidation (Chapter 12).

NEE of a boreal peatland Medla-Pev-Nyur measured by closed chambers, eddy-covariance and modeled by LPJ-GUESS were compared. The estimation NEE on the basis of measurements by eddy-covariance was higher, than by using the static chambers (Chapter 9). The cumulative NEE varied from 15 to −800 g CO_2 m^{-2} for the investigation period between the different model runs. One of the main error sources could be the averaging of CO_2 fluxes, received from chamber measurement on different microforms of the peatland which are characterized by high variability and the other is the calculation of the area occupied by the different microform types. Therefore for an estimation of the net ecosystem exchange of a peatland in mathematical models it is recommended to use values of LAI or biomass.

For the first time the surface energy balance was determined for the boreal peatland Medla-Pev-Nyur for an 11-month period in 2008-09 using the eddy covariance method (Chapter 12). Latent energy fluxes exceeded 70% of net radiation and 60% of potential evapotranspiration. The growing season months of May-July had nearly twice the amount of evapotranspiration as precipitation. Close relation was established between surface conductivity of land cover and water vapor deficit.

The given book is the first attempt to synthesize the results of investigations on development, structure and functioning of one ecosystem out of numerous and poorly investigated peatlands in Komi Republic. It became possible, first of all, thanks to cooperation of experts from the different countries and with financial support of the international projects Carbonorth and UNDP/GEF Komi PA. Despite a variety of the presented actual material, many questions of functioning of peatland Medla-Pev-Nyur remained unanswered. In the future research, more effort should be made to intensify the cooperation between the researchers in order to reach a higher level of data integration. Authors hope that the current collection of studies will be useful to the future researchers of boreal peatland ecosystems and the data can serve as a baseline for future comparisons as climate and perharps other environmental conditions change

The peatland Medla-Pev-Nyur is now one of the best investigated peatlands in Komi Republic and it would be great if we could develop this investigation site as a long-term monitoring site for evaluating carbon pools and their dynamics in relation to vegetation and peat properties, and climatic factors.

ЗАКЛЮЧЕНИЕ

Проблема потепления климата и возможные его последствия для болотных экосистем активно исследуется в последние два десятилетия во многих странах мира. Ключевыми вопросами в изучении болотных экосистем остаются нетто-продукция и разложение органического вещества и факторы, регулирующие эти процессы. Особое внимание при этом уделяется роли болот в глобальном углеродном цикле.

В монографии мы попытались обобщить основные результаты исследований, посвященные эволюции, разнообразию растительного покрова и биогеохимическим процессам на болоте Медла-Пэв-Нюр.

Начало формирования болота Медла-Пэв-Нюр датируется ранним Голоценом, примерно 9600 лет назад, а скорость его экспансии составляла 3 м за столетие (Chapter 5). Присутствие остатков древесных растений в самых нижних слоях торфяной залежи подтверждает развитие болота Медла-Пэв-Нюр через заболачивание покрытой лесом территории (Chapter 1). Заболачивание лесных ландшафтов сопровождалось снижением запасов углерода органического вещества в фитомассе и увеличением запасов почвенного углерода. На современном этапе развития болота общий запас углерода составил 13.5 кг С $м^{-2}$ на его окрайке и более 100 кг С $м^{-2}$ в центральной части.

В микробном сообществе в верхнем горизонте торфа на исследованном болоте доминируют микромицеты. Было описано 73 вида микромицетов, наиболее высокое разнообразие этих организмов выявлено в мочажинах (Chapter 4). Выявлено изменение разнообразия почвенных микромицетов в течение вегетационного сезона.

Современный растительный покров болота мозаичный, сообщества растений формируется в разных условиях минерального питания и увлажнения. На болоте произрастает около 120 видов растений, в том числе 15 видов мхов (Chapter 2). По видовому богатству высших растений отличаются семейства *Ceperaceae* (17), *Rosaceae* (9), *Ericaceae* (8). Многие виды растений являются лекарственными и пищевыми, которые использует местное население. Доля сфагновых мхов в фитомассе на разных участках составила 70-86 %. Фотосинтетический сток (секвестрация) углерода, рассчитанный по хлорофилльному индексу, на открытых участках болота варьировал в пределах 162-212 г С $м^{-2}$, вклад мхов в этот процесс составил 45-70%, в зависимости от типа сообщества (Chapter 7). Сходные данные были получены с использованием космоснимков и классификации растительного покрова болота (Chapter 3). На залесенных окрайках болота сток углерода достигал 2.3 кг $м^{-2}$, а на лесных участках, примыкающих к болоту – 6.8 г С $м^{-2}$.

Медленная скорость разложения растительных остатков приводит к накоплению значительных запасов мертвого органического вещества в болотах бореальной зоны. Использование дендрологического метода позволило уста-

новить, что вертикальная скорость накопления торфа составляет на разных участках болота Медла-Пэв-Нюр в среднем 35.8 мм год$^{-1}$ и достоверно не различается в центре болота и на его окрайке (Chapter 6). Установлена положительная корреляция роста деревьев в высоту и приростом торфа.

Величина стока углерода из атмосферы в болотные экосистемы определяется погодными условиями в период вегетации. Измерения CO_2 газообмена методом эдди-ковариянс в течение 2012-2013 гг. показали, что на болоте Медла-Пэв-Нюр ежегодный сток углерода из атмосферы составляет около 123 г С м$^{-2}$ (Chapter 8). Сезонная динамика вертикальных потоков CO_2 газообмена между болотным ландшафтом и атмосферой зависела от температуры, сочетания потока света и фенологии растений (Chapter 10). Суммарный поток CH_4 из болота в атмосферу, измеренный методом эдди-ковариянс в течение одного сезона, также определялся температурой и фенологией растений, но слабо зависел от уровня болотных вод. Однако, тесная зависимость скорости эмиссии метана от уровня залегания болотных вод отмечена при использовании камерного метода (Chapter 11). В сезонной динамике максимальный поток метана с поверхности болота в атмосферу наблюдался в июле. Наиболее высокие значения эмиссии метана за четыре года наблюдений отмечены с мезотрофных участковх, где в растительном покрове доминировали осоки.

Использование изотопного метода для измерения концентрации CH_4 и CO_2 в болотной воде на разной глубине позволило установить, что наиболее активно метан образуется в слое 1.5-2.0 м, а процесс окисления метана - в слое торфа 0.5-1.0 м. Предполагается, что кислород для окисления поступает из атмосферы в болотные воды через корни растений (Chapter 12). Не были выявлены достоверные различия в концентрации метана в воде на соответствующих глубинах торфяной залежи на разных участках болота.

Оценка нетто-обмена CO_2 на болоте Медла-Пэв-Нюр на ландшафтом уровне была выполнена с использованием данных одного года измерений методом камер, эдди-ковариянс и модели LPJ-GUESS. Кумулятивное значение NEE варьировало от 15 до -800 г CO_2 при использовании разных методов. Расчеты на основе данных, полученных методом эдди-ковариянс, дали более высокие значения NEE, чем при использовании данных камерных измерений (Chapter 9). Авторы считают, что причиной этих различий могло быть усреднение результатов измерений нетто-обмена, полученных методом камер на разных микроформах, которые могут существенно различаться по величине и направленности потоков CO_2. Поэтому для оценки нетто-обмена на болоте рекомендовано вводить в математические модели характеристики LAI или биомассы.

Впервые для болота Медла-Пэв-Нюр были получены характеристики энергообмена в приземном слое атмосферы методом эдди-ковариянс за 11 месяцев наблюдений 2008-2009 гг., включая зимний период (Chapter 13). Затраты тепла на испарение (*LE*) составили 77% радиационного тепла и 60% потенциальной евапотранспирации. В период с мая по июль эвапотранспирация превышала сумму осадков в два раза, в то же время с апреля по октябрь эти показатели имели близкие значения. Установлена тесная связь проводимости растительного покрова с дефицитом влаги в атмосферном воздухе. По мнению авторов актуальным остается изучение роли растительного покрова и уровня болотных вод в контроле энергообмена болотной экосистемы.

Монография представляет собой первую попытку обобщить результаты изучения эволюции, структуры и функционирования экосистемы одного из многочисленных и мало исследованных болот на территории Республики Коми. Это стало возможным, прежде всего, благодаря кооперации специалистов из разных стран при финансовой поддержке международных проектов Carbonorth и ПРООН/ГЭФ Коми ООПТ. Несмотря на разнообразие представленного фактического материала, многие вопросы функционирования болота Медла-Пэв-Нюр остались пока за рамками представленной монографии и требуют дальнейших исследований. Авторы выражают надежду, что книга будет полезной для будущих исследователей болотных экосистем.

Болото Медла-Пэв-Нюр является одним из наиболее детально изученной болотной экосмистемой в Республике Коми, и мы бы хотели продолжать исследования на данном природном объекте в будущем для оценки запасов углерода и его динамики в связи с развитием растительного покрова и климатическими факторами.

Annex

Class - Equisetopsida

Family 1. Equisetaceae

Equisetum fluviatile L. (= *Equisetum limosum* L.)

Polyzonal Holarctic species. Hygrophyte. Not rare. Transitional swamps, streams, peat edge: wet mixed dwarf shrub-sphagnum forest. Perennial grass.

Equisetum palustre L.

Polyzonal Holarctic species. Hygrophyte. Rare. Peat edge: wet mixed dwarf shrub-sphagnum forest. Perennial grass.

Equisetum sylvaticum L.

Boreal Holarctic species. Mesophyte. Not rare. Peat edge: wet mixed dwarf shrub-sphagnum forest, spruce dwarf shrub-green moss forest. Perennial grass.

Class - Polypodiopsida

Family 2. Athyriaceae

Gymnocarpium dryopteris (L.) Newm.

Boreal Holarctic species. Mesophyte. Rare. Peat edge: spruce dwarf shrub-green moss forest. Perennial grass.

Class - Pinopsida

Family 3. Pinaceae

Picea obovata Ledeb.

Boreal mainly Siberian species. Mesophyte. Frequent. Peat edge: wet mixed dwarf shrub-sphagnum forest, spruce dwarf shrub-green moss forest. Tree.

Pinus sylvestris L.

Boreal Eurasian species. Hygromesophyte. Frequent. Oligotrophic, mesotrophic sites in the peat centre: pine-dwarf shrub-sphagnum, pine-dwarf shrub-cloudberry-sphagnum communities. Peat edge: wet mixed dwarf shrub-sphagnum forest. Tree.

Family 4. Cupressaceae

Juniperus communis L.

Boreal Holarctic species. Xeromesophyte. Not rare. Peat edge: wet mixed dwarf shrub-sphagnum forest, spruce dwarf shrub-green moss forest. Shrub.

Class - Liliopsida

Family 5. Scheuchzeriaceae

Scheuchzeria palustris L.

Boreal Holarctic species. Hygrophyte. Frequent. The central peat part, oligotrophic hollows, transition swamps: *Scheuchzeria palustris*-sphagnum, *Scheuchzeria palustris*-mossy, sedge-sphagnum communities in microrelief depressions. Dominant or co-dominant in peat communities. Perennial grass.

Family 6. Poaceae (= Gramineae)

Calamagrostis purpurea (Trin.) Trin.

Boreal mainly Asian species. Hygromesophyte. Not rare. Peat edge: wet mixed dwarf shrub-sphagnum forest. Perennial grass.

Family 7. Cyperaceae

Carex aquatilis Wahlenb.

Boreal Holarctic species. Hygrophyte. Rare. Peat edge: wet mixed dwarf shrub-sphagnum forest. Perennial grass.

Carex cespitosa L.

Boreal Eurasian species. Hygrophyte. Not rare. Peat edge: wet mixed dwarf shrub-sphagnum forest. Perennial grass.

Carex chordorrhiza Ehrh.

Boreal Holarctic species. Hygrophyte. Rare. Transitional swamps: sedge-sphagnum, grassy-mossy communities. Perennial grass.

Carex cinerea Poll.

Boreal Holarctic species. Hygrophyte. Rare. Peat edge: wet mixed dwarf shrub-sphagnum forest. Perennial grass.

Carex disperma Dew.

Boreal Holarctic species. Hygrophyte. Rare. Peat edge: wet mixed dwarf shrub-sphagnum forest. Perennial grass.

Carex globularis L.

Boreal Eurasian species. Hygrophyte. Not rare. Peat edge: wet mixed dwarf shrub-sphagnum forest, spruce dwarf shrub-green moss forest. Perennial grass.

Carex juncella (Fries) Th. Fries

Boreal Eurasian species. Hygrophyte. Rare. Peat edge: wet mixed dwarf shrub-sphagnum forest. Perennial grass.

Carex lasiocarpa Ehrh.

Boreal Holarctic species. Hygrophyte. Not rare. Mesotrophic peat part: dwarf shrub-sedge-sphagnum communities. Perennial grass.

Carex limosa L.

Boreal Holarctic species. Hygrophyte. Not rare. The central peat part, ologotrophic hollows: dwarf shrub-sedge-sphagnum communities. Perennial grass.

Carex pauciflora Ligtf.

Boreal Holarctic species. Hygrophyte. Not rare. The central peat part, ologotrophic hillocks: dwarf shrub-sphagnum and dwarf shrub-cotton grass-sphagnum communities. Peat edge: wet mixed dwarf shrub-sphagnum forest. Perennial grass.

Carex paupercula Michx. (= *Carex magellanica* Lam. ssp. *irrigua* (Wahlenb.) Hiit)

Boreal Holarctic species. Hygrophyte. Not rare. The central peat part, mesotrophic mats and swamps: sedge-sphagnum and grassy-sphagnum communities. Perennial grass.

Carex rostrata Stokes

Boreal Holarctic species. Hygrophyte. Not rare. The central peat part, mesotrophic mats and swamps: sedge-sphagnum and dwarf shrub-sedge-sphagnum communities. Peat edge: wet mixed dwarf shrub-sphagnum forest. Frequent dominant in wet communities. Perennial grass.

Carex tenuiflora Wahlenb.

Boreal Holarctic species. Hygrophyte. Rare. Peat edge: wet mixed dwarf shrub-sphagnum forest. Perennial grass.

Carex vaginata Tausch

Boreal Holarctic species. Mesophyte. Rare. Peat edge: wet mixed dwarf shrub-sphagnum forest, spruce dwarf shrub-green moss forest. Perennial grass.

Eriophorum gracile Koch.

Boreal Holarctic species. Hygrophyte. Not rare. The central peat part, transition swamps: grassy-mossy communities. Perennial grass.

Eriophorum polystachion L.

Boreal Holarctic species. Hygrophyte. Not rare. The central peat part, transition swamps: dwarf shrub-sedge-sphagnum and grassy-sphagnum communities. Perennial grass.

Eriophorum vaginatum L.

Boreal Holarctic species. Hygrophyte. Frequent. The central peat part, oligotrophic mats: cotton grass-sphagnum, dwarf shrub-cotton grass-sphagnum, and dwarf shrub-sedge-sphagnum communities. Peat edge: pine-cotton grass-sphagnum communities. Dominant in wet communities. Perennial grass.

Family 8. Araceae Juss.

Calla palustris L.

Boreal Holarctic species. Hygrophyte. Not rare. Peat edge: wet mixed dwarf shrub-sphagnum forest. Perennial grass.

Family 9. Juncaceae

Luzula pilosa (L.) Willd.

Boreal Eurasian species. Mesophyte. Rare. Peat edge: wet mixed dwarf shrub-sphagnum forest, spruce dwarf shrub-green moss forest. Perennial grass.

Family 10. Convallariaceae

Maianthemum bifolium (L.) F.W.Schmidt.

Boreal Eurasian species. Mesophyte. Rare. Peat edge: wet mixed dwarf shrub-sphagnum forest, spruce dwarf shrub-green moss forest. Perennial grass.

Family 11. Orchidaceae

Corallorhiza trifida Chatel.

Boreal Holarctic species. Hygromesophyte. Very rare, single specimens. Peat edge: wet mixed dwarf shrub-sphagnum forest. Perennial grass.

Dactylorhiza hebridensis (Wilmott) Aver.

Boreal Eurasian species. Hygrophyte. Rare. The central peat part: dwarf shrub-sedge-sphagnum communities. Perennial grass.

Dactylorhiza incarnata (L.) Soo

Boreal Eurasian species. Hygromesophyte. Very rare, single specimens. The central peat part: dwarf shrub-sedge-sphagnum communities. Perennial grass. It is included into the Red Databook of the Komi Republic under the protection category 3.

Dactylorhiza maculata (L.) Soo

Boreal Eurasian species. Hygromesophyte. Rare. The central peat part: dwarf shrub-sedge-sphagnum communities. Perennial grass.

Hammarbia paludosa (L.) O. Kuntze

Boreal Eurasian species. Hygrophyte. Very rare, single specimens. Peat edge: wet mixed dwarf shrub-sphagnum forest. Perennial grass. It is included into the Red Databook of the Komi Republic under the protection category 3.

Class - Magnoliopsida

Family 12. Salicaceae

Salix aurita L.

Boreal European species. Hygromesophyte. Not rare. Peat edge: wet mixed dwarf shrub-sphagnum forest. Shrub.

Salix lapponum L.

Hypoarctic Eurasian species. Hygrophyte. Not rare. Peat edge: wet mixed dwarf shrub-sphagnum forest. Shrub.

Salix myrsinifolia Salisb.

Boreal European species. Hygrophyte. Not rare. Peat edge: wet mixed dwarf shrub-sphagnum forest. Shrub.

Salix myrtilloides L.

Boreal Eurasian species. Hygrophyte. Not rare. Peat edge: wet mixed dwarf shrub-sphagnum forest. Shrub.

Salix phylicifolia L.

Hypoarctic European species. Hygromesophyte. Frequent. The central peat part: dwarf shrub-sedge-sphagnum communities. Peat edge: wet mixed dwarf shrub-sphagnum forest. Shrub.

Family 13. Betulaceae

Alnus incana (L.) Moench

Boreal European species. Hygromesophyte. Not rare. Peat edge: wet mixed dwarf shrub-sphagnum forest, spruce dwarf shrub-green moss forest. Tree.

Betula nana L. s.l.

Hypoarctic almost holarctic species. Hygrophyte. Frequent. The central peat part: dwarf shrub-sedge-sphagnum communities. Peat edge: wet mixed dwarf shrub-sphagnum forest. Shrub, dwarf shrub.

Betula pubescens Ehrh.

Boreal Eurasian species. Mesophyte. Frequent. Transition swamps: grassy-mossy communities. Peat edge: wet mixed dwarf shrub-sphagnum forest, spruce dwarf shrub-green moss forest. Tree.

Family 14. Polygonaceae

Bistorta major S.F. Gray (= *Polygonum bistorta* L.)

Boreal holarctic species. Hygromesophyte. Not rare. Peat edge: wet mixed dwarf shrub-sphagnum forest. Perennial grass.

Family 15. Ranunculaceae

Caltha palustris L.

Boreal holarctic species. Hygrophyte. Not rare. Peat edge: wet mixed dwarf shrub-sphagnum forest. Perennial grass.

Ranunculus lapponicus L.

Hypoarctic holarctic species. Hygrophyte. Very rare. Peat edge: wet mixed dwarf shrub-sphagnum forest. Perennial grass.

Ranunculus propinquus C.A. Mey (= *Ranunculus borealis* Trautv.)

Hypoarctic Eurasian species. Hygromesophyte. Not rare. Peat edge: wet mixed dwarf shrub-sphagnum forest. Perennial grass.

Family 16. Droseraceae

Drosera rotundifolia L.

Boreal holarctic species. Hygrophyte. Not rare. The central peat part: dwarf shrub-sedge-sphagnum communities. Perennial grass.

Family 17. Saxifragaceae

Chrysosplenium alternifolium L.

Boreal holarctic species. Hygromesophyte. Not rare. Peat edge: wet mixed dwarf shrub-sphagnum forest. Perennial grass.

Family 18. Grossulariaceae

Ribes hispidulum (Jancz.) Pojark.

Boreal Siberian species. Hygromesophyte. Rare. Peat edge: spruce dwarf shrub-green moss forest. Shrub.

Family 19. Rosaceae

Comarum palustre L.

Boreal holarctic species. Hygrophyte. Not rare. Transition swamps: bog bean-grassy-mossy and grassy-mossy communities. Peat edge: wet mixed dwarf shrub-sphagnum forest. Perennial grass.

Filipendula ulmaria (L.) Maxim.

Boreal Eurasian species. Hygrophyte. Not rare. Peat edge: wet mixed dwarf shrub-sphagnum forest, spruce dwarf shrub-green moss forest. Perennial grass.

Geum rivale L.

Boreal Eurasian species. Hygrophyte. Not rare. Peat edge: wet mixed dwarf shrub-sphagnum forest. Perennial grass.

Rosa acicularis Lindl.

Boreal holarctic species. Mesophyte. Not rare. Peat edge: wet mixed dwarf shrub-sphagnum forest, spruce dwarf shrub-green moss forest. Shrub.

Rubus arcticus L.

Hypoarctic holarctic species. Hygromesophyte. Not rare. Peat edge: wet mixed dwarf shrub-sphagnum forest, spruce dwarf shrub-green moss forest. Perennial grass.

Rubus chamaemorus L.

Hypoarctic holarctic species. Frequent. The central peat part, oligotrophic hillocks: (pine)-dwarf shrub-cloudberry-sphagnum and dwarf shrub-sphagnum communities. Peat edge: wet mixed dwarf shrub-sphagnum forest. Frequent dominant or co-dominant. Perennial grass.

Rubus humilifolius C.A. Mey

Boreal Siberian species. Hygromesophyte. Rare. Peat edge: wet mixed dwarf shrub-sphagnum forest. Perennial grass.

Rubus saxatilis L.

Boreal Eurasian species. Mesophyte. Rare. Peat edge: spruce dwarf shrub-green moss forest. Perennial grass.

Sorbus aucuparia L.

Boreal European species. Mesophyte. Rare. Peat edge: spruce dwarf shrub-green moss forest. Tree.

Family 20. Fabaceae

Lathyrus pratensis L.

Boreal Eurasian species. Mesophyte. Rare. Peat edge: wet mixed dwarf shrub-sphagnum forest. Perennial grass.

Lathyrus vernus (L.) Bernh.

Boreal-nemoral Eurasian species. Hygromesophyte. Not rare. Peat edge: wet mixed dwarf shrub-sphagnum forest, spruce dwarf shrub-green moss forest. Perennial grass.

Vicia sepium L.

Boreal Eurasian species. Mesophyte. Not rare. Peat edge: wet mixed dwarf shrub-sphagnum forest, spruce dwarf shrub-green moss forest. Perennial grass.

Family 21. Geraniaceae

Geranium sylvaticum L.

Boreal Eurasian species. Mesophyte. Not rare. Peat edge: wet mixed dwarf shrub-sphagnum forest, spruce dwarf shrub-green moss forest. Perennial grass.

Family 22. Oxalidaceae

Oxalis acetosella L.

Boreal holarctic species. Mesophyte. Not rare. Peat edge: wet mixed dwarf shrub-sphagnum forest, spruce dwarf shrub-green moss forest. Perennial grass.

Family 23. Empetraceae

Empetrum hermaphroditum (Lange) Hagerup

Hypoarctic Eurasian species. Hygromesophyte. Frequent. The central peat part, oligotrophic hillocks: (pine)-dwarf shrub-cloudberry-sphagnum and dwarf shrub-sphagnum communities. Peat edge: wet mixed dwarf shrub-sphagnum forest. Dwarf shrub.

Family 24. Violaceae

Viola epipsila Ledeb.

Boreal European species. Hygrophyte. Not rare. Peat edge: wet mixed dwarf shrub-sphagnum forest. Perennial grass.

Viola palustris L.

Boreal European species. Hygrophyte. Rare. Peat edge: wet mixed dwarf shrub-sphagnum forest. Perennial grass.

Family 25. Onagraceae

Chamaenerion angustifolium (L.) Scop.

Boreal holarctic species. Mesophyte. Not rare. Peat edge: wet mixed dwarf shrub-sphagnum forest, spruce dwarf shrub-green moss forest. Perennial grass.

Epilobium palustre L.

Boreal holarctic species. Hygromesophyte. Rare. Transition swamps: grassy-mossy communities. Peat edge: wet mixed dwarf shrub-sphagnum forest. Perennial grass.

Family 26. Apiaceae

Angelica sylvestris L.

Boreal Eurasian species. Mesophyte. Rare. Peat edge: wet mixed dwarf shrub-sphagnum forest. Perennial grass.

Cicuta virosa L.

Boreal Eurasian species. Hygrophyte. Rare. Transition swamps: grassy-mossy communities. Perennial grass.

Family 27. Pyrolaceae

Moneses uniflora (L.) A. Gray

Boreal holarctic species. Mesophyte. Rare. Peat edge: wet mixed dwarf shrub-sphagnum forest. Perennial grass.

Ortilia secunda (L.) House (= *Ramischia secunda* (L.) Garcke)

Boreal holarctic species. Mesophyte. Rare. Peat edge: wet mixed dwarf shrub-sphagnum forest, spruce dwarf shrub-green moss forest. Perennial grass.

Pyrola rotundifolia L.

Boreal holarctic species. Mesophyte. Not rare. Peat edge: wet mixed dwarf shrub-sphagnum forest, spruce dwarf shrub-green moss forest. Perennial grass.

Family 28. Ericaceae

Andromeda polifolia L.

Boreal holarctic species. Hygrophyte. Frequent. The central peat part, oligotrophic hillocks: dwarf shrub-sphagnum and dwarf shrub-cloudberry-sphagnum communities. Peat edge: wet mixed dwarf shrub-sphagnum forest. Dwarf shrub.

Chamaedaphne calyculata (L.) Moench.

Boreal Eurasian species. Hygrophyte. Frequent. The central peat part, oligotrophic hillocks: (pine)-dwarf shrub-cloudberry-sphagnum and dwarf shrub-sphagnum communities. Peat edge: wet mixed dwarf shrub-sphagnum forest. Frequent dominant or co-dominant. Dwarf shrub.

Ledum palustre L.

Boreal holarctic species. Hygrophyte. Frequent. The central peat part, oligotrophic hillocks: (pine)-dwarf shrub-cloudberry-sphagnum and dwarf shrub-sphagnum communities. Peat edge: wet mixed dwarf shrub-sphagnum forest. Dwarf shrub.

Oxycoccus microcarpus Turcz. ex Rupr.

Hypoarctic Eurasian species. Hygrophyte. Frequent. The central peat part, oligotrophic hillocks: (pine)-dwarf shrub-cloudberry-sphagnum and dwarf shrub-sphagnum communities. Peat edge: wet mixed dwarf shrub-sphagnum forest. Dwarf shrub.

Oxycoccus palustris Pers. (= *Oxycoccus quadripetalus* Gilib.)

Boreal holarctic species. Hygrophyte. Frequent. The central peat part: most oligotrophic and mesotrophic communities. Peat edge: wet mixed dwarf shrub-sphagnum forest. Dwarf shrub.

Vaccinium myrtillus L.

Boreal holarctic species. Mesophyte. Frequent. Peat edge: wet mixed dwarf shrub-sphagnum forest, spruce dwarf shrub-green moss forest. Dwarf shrub.

Vaccinium uliginosum L.

Hypoarctic holarctic species. Hygrophyte. Frequent. The central peat part, oligotrophic hillocks: (pine)-dwarf shrub-cloudberry-sphagnum and dwarf shrub-sphagnum communities. Peat edge: wet mixed dwarf shrub-sphagnum forest, spruce dwarf shrub-green moss forest. Dwarf shrub.

Vaccinium vitis-idaea L.

Boreal holarctic species. Hygrophyte. Frequent. Peat edge: wet mixed dwarf shrub-sphagnum forest, spruce dwarf shrub-green moss forest. Dwarf shrub.

Family 29. Primulaceae

Trientalis europaea L.

Boreal Eurasian species. Mesophyte. Not rare. Peat edge: wet mixed dwarf shrub-sphagnum forest, spruce dwarf shrub-green moss forest. Perennial grass.

Family 30. Menyanthaceae

Menyanthes trifoliata L.

Boreal holarctic species. Hygrophyte. Frequent. Transition swamps: bog bean, bog bean-sphagnum, and grassy-mossy communities. Peat edge: wet mixed dwarf shrub-sphagnum forest. Dominant. Perennial grass.

Family 31. Boraginaceae

Myosotis palustris L.

Boreal Eurasian species. Hygrophyte. Rare. Peat edge: wet mixed dwarf shrub-sphagnum forest. Perennial grass.

Family 32. Scrophulariaceae

Melampyrum pratense L.

Boreal Eurasian species. Mesophyte. Frequent. The central peat part: (pine)-dwarf shrub-cloudberry-sphagnum and dwarf shrub-sphagnum communities. Peat edge: wet mixed dwarf shrub-sphagnum forest, spruce dwarf shrub-green moss forest. Annual grass.

Family 33. Lentibulariaceae

Utricularia intermedia Hayne

Boreal holarctic species. Hydatophyte. Not rare. The central peat part: dwarf shrub-sedge-sphagnum communities. Perennial grass.

Family 34. Rubiaceae

Galium boreale L.

Boreal Eurasian species. Mesophyte. Not rare. Peat edge: wet mixed dwarf shrub-sphagnum forest, spruce dwarf shrub-green moss forest. Perennial grass.

Galium palustre L.

Boreal holarctic species. Hygrophyte. Rare. Transition swamps: grassy-mossy communities. Peat edge: wet mixed dwarf shrub-sphagnum forest. Perennial grass.

Family 35. Caprifoliaceae

Linnaea borealis L.

Boreal holarctic species. Mesophyte. Not rare. Peat edge: spruce dwarf shrub-green moss forest. Dwarf shrub.

Lonicera pallasii Ledeb.

Boreal Siberian species. Mesophyte. Rare. Peat edge: spruce dwarf shrub-green moss forest. Shrub.

Family 36. Adoxaceae

Adoxa moschatellina L.

Boreal holarctic species. Hygromesophyte. Rare. Peat edge: spruce dwarf shrub-green moss forest. Perennial grass.

Family 37. Asteraceae

Cirsium heterophyllum (L.) Hill.

Boreal European species. Hygromesophyte. Rare. Peat edge: spruce dwarf shrub-green moss forest. Perennial grass.

Cirsium oleraceum (L.) Scop.

Boreal European species. Hygromesophyte. Rare. Peat edge: wet mixed dwarf shrub-sphagnum forest. Perennial grass.

Crepis paludosa (L.) Moench.

Boreal-nemoral European species. Hygromesophyte. Not rare. Peat edge: wet mixed dwarf shrub-sphagnum forest. Perennial grass.

Petasites frigidus (L.) Fries. (= *Nardosmia frigida* (L.) Hook.)

Hypoarctic holarctic species. Hygrophyte. Rare. Peat edge: wet mixed dwarf shrub-sphagnum forest. Perennial grass.

Научное издание

Коллектив авторов

ECOSYSTEM OF A MESOOLIGOTROPHIC PEATLAND IN NORTHWESTERN RUSSIA:
development, structure, and function

Рекомендовано к изданию Ученым советом Института биологии Коми НЦ УрО РАН

Оригинал-макет Е.А. Волкова

Фото на обложке В.А. Канева

Лицензия № 0047 от 10.01.99

Подписано в печать 22.12.2016. Формат 70x100 1/16. Бумага офсетная.
Печать офсетная. Усл. печ. л. 13.98. Тираж 300 экз. Заказ № 15646.

Отпечатано с готового оригинал-макета заказчика
в полном соответствии с предоставленными материалами
в ООО «Кировская областная типография»
610004, г. Киров, ул. Ленина, д. 2.
Тел.: (8332) 38-34-34